

Mobility and hydrodynamic implications of the long neck in plesiosaurs

PERNILLE V. TROELSEN

A thesis submitted in partial fulfilment of the requirements of Liverpool
John Moores University for the degree of Doctor of Philosophy

December 2018

Contents

Acknowledgements	7
List of Tables.....	10
List of Figures	11
Abstract	17
Institutional abbreviations.....	18
Chapter 1 - Introduction	19
1.1 Part A: Plesiosaur palaeobiology.....	19
1.1.1 Introduction.....	19
1.1.2 Overview of the history of plesiosaur research	19
1.1.3 Plesiosaurian diversity and morphology.....	24
1.1.4 Phylogeny, taxonomy and ecological categorisation.....	47
1.1.5 Foraging and feeding strategies	52
1.2 Part B: Long necks in extant vertebrates	59
1.2.1 Introduction.....	59
1.2.2 Neck morphology in extant vertebrates	59
1.2.3 Main differences between terrestrial and aquatic necks	76
1.3 Conclusion.....	78
Chapter 2 – Range of motion in ostrich necks	79
2.1 Introduction	79
2.1.1 Range of motion studies of necks in extant animals.....	80
2.1.2 Long necks in extant animals.....	87
2.2 Materials and methods.....	89
2.2.1 Physically manipulated neck	89
2.2.2 Digitally manipulated neck.....	92
2.3 Results	93
2.4 Discussion	99

2.4.1 Physically manipulated neck	99
2.4.2 Digitally manipulated neck	101
2.4.3 Comparing the two methods	101
2.5 Conclusions	103
Chapter 3 – Range of motion in plesiosaur necks.....	104
3.1 Introduction	104
3.1.1 Plesiosaur neck morphology.....	104
3.1.2 Previous studies on neck flexibility in plesiosaurs	111
3.1.3 Rationale of the present study.....	114
3.2 Materials and methods.....	115
3.2.1 Specimens	115
3.2.2 Photogrammetry.....	115
3.2.3 Attaining range of motion data	116
3.3 Results	118
3.4 Discussion	128
3.4.1 Neck movement in plesiosaurs	128
3.4.2 Plesiosaur ecology and other aspects of biology	132
3.5 Conclusions	133
Chapter 4 – Fluid dynamics	134
4.1 Introduction	134
4.1.1 Fluid dynamics.....	134
4.1.2 Computational Fluid Dynamics	143
4.2 Validation experiments.....	156
4.2.1 Methods	156
4.2.2 Results with respective approaches	157
4.3 Conclusions	175

Chapter 5 – The hydrodynamic implications of neck elongation and thickness in plesiosaur necks.....	177
5.1 Introduction	177
5.1.1 Soft tissue in plesiosaurs.....	177
5.1.2 Hydrodynamics	179
5.1.3 Computational Fluid Dynamics	179
5.2 Materials and methods.....	180
5.2.1 Selected plesiosaur species	180
5.2.2 Modelling the plesiosaur.....	181
5.2.3 Computational fluid dynamics simulations	182
5.3 Results	184
5.4 Discussion	186
5.4.1 Neck elongation and thickness	186
5.4.2 Ecology and behaviour of plesiosaurs	188
5.5 Conclusions	190
Chapter 6 – Hydrodynamic effects of plesiosaurs bending the neck during forward motion	191
6.1 Introduction	191
6.2 Methods	193
6.2.1 Building the plesiosaur models.....	193
6.2.2 Characteristic length for a plesiosaur model with bent neck.....	198
6.2.3 Computational fluid dynamics.....	199
6.3 Results	201
6.3.1 Effect of bending location and distribution using primitives	201
6.3.2 Effects of bending the neck in idealized plesiosaur models	202
6.4 Discussion	206
6.4.1 Effect of bending location and distribution using primitives	206
6.4.2 Effects of bending the neck in idealized plesiosaur models	206

6.4.3 Comparing the two studies	206
6.4.4 Turning performance	206
6.4.5 Plesiosaur ecology	208
6.5 Conclusions	211
Chapter 7 – Discussion	212
7.1 Summary of preceding chapters	212
7.1.1 Range of motion in ostrich necks	212
7.1.2 Range of motion in plesiosaur necks	212
7.1.3 Fluid dynamics.....	213
7.1.4 The hydrodynamic implications of neck elongation and thickness in plesiosaur necks	213
7.1.5 Hydrodynamic effects of plesiosaurs bending the neck during forward motion	213
7.2 Wider implications of this work.....	214
7.2.1 Digitisation of specimens.....	214
7.2.2 Plesiosaur palaeobiology	214
7.2.3 Evolution of the long neck in plesiosaurs – Body proportions.....	222
7.3 CFD as a method for studying the hydrodynamics of plesiosaur necks	226
7.3.1 Advantages.....	226
7.3.2 Limitations	227
7.3.3 Other simulation software and experimental methods	227
Chapter 8 - Conclusions and further work	229
8.1 Conclusions and significance of work undertaken.....	229
8.2 Future work	230
8.2.1 FEA.....	230
8.2.2 Geometric morphometrics	230
8.2.3 Improvement of models	230
8.2.4 Free body motion in CFD	230

References231

Acknowledgements

First, I would like to thank Liverpool John Moores University for funding this PhD by giving me a Faculty of Science PhD Scholarship. I would not have been able to neither start nor finish the PhD without this funding, and I am deeply grateful for this opportunity. I would like to give my greatest appreciations and gratitude to my Director of Studies / main supervisor Dr Peter L. Falkingham who gave me encouragement and great advice at even the hardest and darkest times of the PhD. Falkingham also taught me a lot about various helpful software I needed for the PhD, which I am deeply grateful for. My co-supervisor's Dr Carlo Meloro and Dr David Wilkinson are additionally thanked for their great advice, comments and suggestions given during my PhD, helping me to extend my point of view of my PhD and its importance. Ryan Marek is also thanked for the collaboration on ostrich necks and for fruitful and helpful discussions about necks in general. This collaboration has taught me a lot of how to use the strengths and expertise across fields to get data needed for a project and how to interpret the data in order to finish the project.

Computational fluid dynamics (CFD) can be really hard to understand, and Dr David Allanson and Dr Mehdi Seddighi helped me out in this matter. Both made sure I understood all the basics of computational fluid dynamics before moving on to more complex work on plesiosaurs, and I would like to thank both for doing so. Great discussions on CFD were also made with Dr Sam Van Wassenbergh during the Society of Experimental Biology (SEB) conferences in 2016 and 2017. A specialist in CFD and animal biomechanics, like Van Wassenberg, to give feedback on my work during these conferences has helped me improve my thinking of CFD and biomechanics in general. Thank you for this!

The advice and comments on my CFD work from Falkingham, Wilkinson, Allanson and Seddighi has made me able to produce a manuscript for a scientific journal in collaboration within the field of engineering which I am so thankful for. The manuscript contained the work I did for two chapters of my PhD, and reviewing of this manuscript has been read and commented by several people. I would like to thank the two anonymous reviewers from Royal Society Interface, Robin O'Keefe (editor in Journal of Vertebrate Paleontology), and two anonymous reviewers from Journal of Vertebrate Paleontology for great suggestions and comments that helped improve both the manuscript, but particularly improve the two chapters of the PhD.

The help to understand plesiosaurs which I got during my PhD was certainly needed for studying their palaeobiology and ecology. This expertise came exclusively from three plesiosaur specialists of the UK; Richard Forrest, Dr Mark Evans, and Dr Adam Smith. I thank you all for your advice, suggestions and comments on the work I achieved in this PhD, as well as fruitful discussions during the annual Symposium of Vertebrate Palaeontology and Comparative Anatomy (SVPCA) conferences in 2016, 2017 and 2018. Furthermore, data collection of plesiosaur specimens from various museums could not have been done without the help of Dr Hilary Ketchum (Oxford Museum), The Oxford Clay Working Group, Dr Neil Clark (Glasgow Museum), Dr David Gelsthorpe (Manchester Museum), Sarah King and Stuart Ogilvy (York Museum), Dr Sandra Chapman (London NHM), Dr Aubrey Jane Roberts and Dr Jørn Harald Hurum (both from Oslo Museum). Thank you all for great assistance when handling the specimens, and particularly Stephanie Wright (intern at Oxford Museum) for producing a 3D model of the atlas-axis complex from the specimen examined during my visit to Oxford Museum, which has been used as part of my data collection.

In connection with SEB 2017 in Gothenburg, I was also fortunate to receive a travel grant from SEB, which helped me financially to attend the conference. I would therefore like to thank SEB for awarding me the travel grant. Regarding SVPCA 2018 in Manchester, I would like to thank the Jones-Fenleigh Fund for the award that I was given to financially support my attendance at the conference, in order to present my most recent PhD work.

Finally, I would like to thank my family and friends for their understanding and encouragement of why I started this PhD, and why I moved abroad in order to follow and pursue my dream of becoming a palaeontologist. The most supportive person I have had during the PhD is my dear partner, Mustafa Nasufovic. Without you I would have quit the PhD long ago, so thank you for your understanding even at the most frustrating times. I know it has been hard on you, especially with my extensive mood swings. Nonetheless, you never stopped believing in me, you remained by my side and most importantly you waited for me to finish the PhD, which I am forever grateful for. Thank you, Musse!

*“Human subtlety will never devise an invention more beautiful,
more simple or more direct than does nature, because in her
inventions nothing is lacking, and nothing is superfluous.”*

— Leonardo da Vinci

*“It is not the strongest of the species that survives,
not the most intelligent that survives.
It is the one that is the most adaptable to change.”*

— Charles Darwin

List of Tables

Table 1: Terms and definitions of plesiosaurians.....	49
Table 2: Division of plesiosaurians as only two morphotypes and their variances.....	51
Table 3: Gastroliths found in different plesiosaur specimens and one shark.....	56
Table 4: Muscle groups and their origin in the cervical musculature of ostriches.....	72
Table 5: Range of motion in some reptilian necks.....	81
Table 6: Range of motion in some avian necks.....	85
Table 7: Range of motion in some mammalian necks.....	86
Table 8: Range of motion data from previous studies on plesiosaur necks.....	113
Table 9: Total maximum flexion in four cryptoclodid specimens.....	118
Table 10: The 10 available turbulence models in Autodesk Simulation CFD.....	151
Table 11: Average rotation between neck joints.....	196
Table 12: Reynolds numbers for plesiosaur models with straight and bent neck.....	199

List of Figures

Figure 1: Illustrations of some plesiosaurs.....	22
Figure 2: Phylogenetic relationships of Sauropterygia.....	24
Figure 3: Ventral view of colour coded skeletal outline of <i>Meyerasaurus victor</i>	25
Figure 4: Sauropterygian skulls without mandibles.....	26
Figure 5: Views of the skull of <i>Nichollsia borealis</i>	28
Figure 6: The seven feeding guilds of Mesozoic marine reptiles.....	29
Figure 7: Vertebral column of <i>Plesiosaurus dolichodeirus</i> divided in three sections.....	31
Figure 8: Dorsal, ventral, lateral, and posterior view of C23 in <i>Muraenosaurus</i> sp.....	32
Figure 9: Cervical vertebrae from plesiosaurs illustrating ontogenetic changes.....	33
Figure 10: Lateral view of adjacent cervical vertebrae from various plesiosaur families...34	
Figure 11: VLI values through geological age for various plesiosaur families.....	35
Figure 12: Number of cervical vertebrae in plesiosaur families through geological ages...38	
Figure 13: Plesiosaurian morphology of the shoulder girdle, trunk and pelvic girdle.....	40
Figure 14: Reconstruction of the shoulder muscle M. clavodeltoideus.....	41
Figure 15: Shoulder girdles from <i>Cryptoclidus eurymerus</i>	42
Figure 16: Pelvic girdles of <i>Cryptoclidus eurymerus</i>	42
Figure 17: Evolution of sauropterygian forelimbs.....	43
Figure 18: Body proportions (neck/trunk ratio) in plesiosaurs.....	47
Figure 19: Simplified phylogenetic relationship of diapsid marine reptile lineages.....	48
Figure 20: Phylogenetic tree of plesiosaurians.....	50
Figure 21: Life reconstruction of <i>Morturneria seymourensis</i> presenting its oral cavity....	52
Figure 22: Gastrolith mass frequency.....	55
Figure 23: Gastroliths from KUVF 129744.....	57

Figure 24: General shapes of vertebral centra.....	60
Figure 25: Vertebral centra shapes indicating structural variation in neck movement.....	61
Figure 26: Example of a dorsal vertebra from a teleost.....	62
Figure 27: Atlas of caecilian <i>Dermophis mexicanus</i>	63
Figure 28: General outline of the skeleton of salamanders.....	63
Figure 29: Neck vertebrae and osteological neck posture of various reptiles.....	64
Figure 30: Muscles and tendons in the spine of various reptiles.....	66
Figure 31: Selected muscles in the m. transversospinalis group of various reptiles.....	67
Figure 32: Osteological neck posture for various birds.....	68
Figure 33: Ostrich C14 in various views.....	69
Figure 34: Cross-section through middle of an ostrich neck	70
Figure 35: Muscles and tendons in cervical vertebrae in ostriches	70
Figure 36: Selected muscles of the m. transversospinalis group in the neck of an ostrich..	71
Figure 37: Examples of skeletal mammalian necks.....	73
Figure 38: Anterior part of skeleton of balaenopterid and sperm whales.....	74
Figure 39: Neck from a young juvenile giraffe in various dissection stages.....	76
Figure 40: Dorsal flexion of a camel neck.....	88
Figure 41: ONP of cervical vertebrae in an alligator and ostrich.....	89
Figure 42: The setup for the study of Chapter 2.....	90
Figure 43: Lego calibration object showing the whole frame for each raspberryPi cam....	90
Figure 44: Pins inserted into 10 articulated ostrich cervical vertebrae.....	91
Figure 45: Position of joint axes between two adjacent cervical vertebrae.....	91
Figure 46: Screenshot of the Graph Editor in Autodesk Maya.....	92
Figure 47: Alignment of digitised ostrich cervical vertebrae in Autodesk Maya.....	93

Figure 48: Example of rotation axes for straight and maxi right lateral bent ostrich neck..	94
Figure 49: Dorsoventral and lateral rotation measurements from physical manipulation...	95
Figure 50: Dorsoventral and lateral rotation measurements from digital manipulation.....	96
Figure 51: Dorsoventral and lateral rotation visualisations.....	98
Figure 52: Examples of photos/illustrations of preserved articulated plesiosaur necks....	105
Figure 53: Intervertebral distance as % of centrum length vs. cervical vertebra joint.....	109
Figure 54: Intervertebral distances found in articulated plesiosaur necks.....	110
Figure 55: Visualisation of method applied for measuring range of motion.....	117
Figure 56: Max. osteological range of motion with 5 % CID vs. cervical vertebrae.....	120
Figure 57: Max. osteological range of motion with 10 % CID vs. cervical vertebrae.....	121
Figure 58: Max. osteological range of motion with 20 % CID vs. cervical vertebrae.....	122
Figure 59: Max. osteological lateral flexion of GLAHM V1091 with different CID's....	124
Figure 60: Max. osteological lateral flexion of OUNHM J.95000 with different CID's...	125
Figure 61: Max. osteological lateral flexion of PMO 224.248 with different CID's.....	126
Figure 62: Max. osteological lateral flexion NHMUK R2863 with different CID's.....	127
Figure 63: Geological age of plesiosaurs used in RoM studies + predominant flexion....	132
Figure 64: Force acting on a surface.....	134
Figure 65: Laminar and turbulent flow.....	135
Figure 66: Simplified flow patterns around a sphere at different Reynolds numbers.....	137
Figure 67: Velocity distribution and flow pattern of boundary layer development.....	139
Figure 68: Moving sphere and the three forces acting on it.....	140
Figure 69: Cd and corresponding Re based on frontal area for three shapes.....	141
Figure 70: Reynolds number vs. drag coefficients.....	142
Figure 71: Diagram of air-/hydrofoil cross-section with effects from angle of attack.....	143

Figure 72: A simplified flow diagram of a generalised iterative solver.....	144
Figure 73: Before and after applying domain to a 1m sphere.....	146
Figure 74: Structured grids.....	147
Figure 75: Example of an unstructured grid around a sphere and in its wake.....	148
Figure 76: Region refinement in domain behind a sphere.....	149
Figure 77: Wall layers and the mesh around a cylinder.....	150
Figure 78: Example of Convergence Monitor result.....	153
Figure 79: Plane visualisation in Autodesk Simulation CFD	154
Figure 80: Particle traces visualized in Autodesk Simulation CFD	155
Figure 81: Static pressure on sphere showing iso volume + iso volume w/ surface.....	155
Figure 82: Example of Wall Calculator.....	156
Figure 83: Frontal and side view of cylinder in domain	157
Figure 84: Flow velocity around sphere and cylinder with a diameter of 0.1m and 1.0m	158
Figure 85: Re vs. Cd with and without slip/symmetry boundary conditions for sphere ...	159
Figure 86: Re vs. Cd with and without slip/symmetry boundary conditions for cylinder	159
Figure 87: Domain vs. Cd w/without slip/symmetry boundary conditions for sphere	160
Figure 88: Domain vs. Cd w/without slip/symmetry boundary conditions for cylinder ..	160
Figure 89: Re vs. Cd with and without walls set to velocity at 0m/s for a sphere	161
Figure 90: Re vs. Cd with and without walls set to velocity at 0m/s for a cylinder	161
Figure 91: Domain vs. Cd with and without walls set to velocity 0m/s for a sphere	162
Figure 92: Domain vs. Cd with and without walls set to velocity 0m/s for a cylinder	162
Figure 93: Change in mesh size of a sphere causing difference in flow velocity pattern .	164
Figure 94: Mesh size of sphere vs. Cd and computation time.....	164
Figure 95: Change in mesh size of cylinder causing difference in flow velocity pattern .	165

Figure 96: Mesh size of cylinder vs. Cd and computation time.....	165
Figure 97: Mesh size of the sphere and cylinder domain vs. Cd	167
Figure 98: Region refinement mesh size with sphere and cylinder inside vs. Cd	167
Figure 99: Number of wall layers added to the mesh of sphere and cylinder vs. Cd	168
Figure 100: Layer factor for wall layers of sphere and cylinder vs. Cd	169
Figure 101: Layer gradation for wall layers of sphere and cylinder vs. Cd	169
Figure 102: Cycles w/ enabling adaption w/without FSL for sphere and cylinder vs. Cd	170
Figure 103: Refinement limit for sphere and cylinder vs. Cd	171
Figure 104: Sphere with mesh sizes applied with different turbulence models vs. Cd	172
Figure 105: Cylinder with mesh sizes applied with different turbulence models vs. Cd...	172
Figure 106: Turbulence models for sphere applied at different Re vs. Cd	173
Figure 107: Turbulence models for cylinder at different Re vs. Cd	174
Figure 108: Re vs. Cd for sphere and cylinder	175
Figure 109: Variables to test in CFD.....	176
Figure 110: Soft tissue preservation in <i>Mauriciosaurus fernandezii</i>	178
Figure 111: Soft tissue preservation in SMNS 51945.....	179
Figure 112: Modelling the plesiosaur	181
Figure 113: 3D flow velocity pattern surrounding plesiosaur models at 1m/s	185
Figure 114: Simulation results using the five plesiosaur models	186
Figure 115: Plesiosaur model made using primitives	193
Figure 116: Example of the rigging for the idealized plesiosaur models	194
Figure 117: Organisation of joints and connections with respective NURBs circles	195
Figure 118: Three idealized plesiosaur models with various curvature	197
Figure 119: Three idealized plesiosaur models with joints for each cervical vertebra	198

Figure 120: Determination of the characteristic length of a plesiosaur model	199
Figure 121: Results from plesiosaur model made of primitive shapes.....	201
Figure 122: Flow velocity pattern for plesiosaur model made of primitives	202
Figure 123: Frontal Cd with increase in neck bending for idealized plesiosaur models....	203
Figure 124: Lateral forces w/ increase in neck bending for idealized plesiosaur models..	204
Figure 125: Flow velocity patterns and pressure distributions for plesiosaur models	205
Figure 126: Potential feeding envelopes in lateral movements for plesiosaur models	210
Figure 127: Paired foramina found in the four cryptoclidid specimens from Chapter 3...	218
Figure 128: Various ratios plotted against neck length	224
Figure 129: Various ratios plotted against neck length and geological age	225

Abstract

Plesiosaurs are extinct marine reptiles that lived during the Mesozoic, well-known for their unique body plan with two pairs of flippers and an elongated neck. What this long neck was used for is unclear. Various hypotheses have been proposed regarding its use, however biomechanical implications of these scenarios remain untested. Even the effects on locomotion are poorly understood. This thesis sets out to explore biomechanical implications of long-necked plesiosaurs.

Interpreting results on range of motion (RoM) in extant taxa can help suggest biomechanical and ecological restrictions of the neck in extinct animals, such as plesiosaurs. RoM in digitized plesiosaur necks was calculated by digital manipulation using a method validated against physical and digital manipulation of an ostrich neck. Neck vertebrae from the posterior-most half of an ostrich neck were manipulated to determine dorsoventral and lateral RoM at successive stages of dissection. Neck vertebrae from four plesiosaur specimens were digitised to study RoM, and showed plesiosaurs potentially had large ranges of motion in the neck, highly dependent on the number of cervical vertebrae. Extreme examples need only small rotation between each bone to produce large overall rotation, even accounting for a reduction in flexibility due to soft tissue. Results showed the largest motions occurred laterally, rather than dorsoventrally.

Computational fluid dynamics was used to investigate the hydrodynamics of plesiosaurs. Sensitivity analyses and validation of the software were carried out in a virtual flume using a sphere and cylinder with known flow responses. The virtual flume was then used for idealized plesiosaur models (three neck lengths and two neck thicknesses). The long-necked plesiosaur model did not meaningfully increase drag, implying no disadvantage to the hydrodynamic performance during forward swimming speeds of 1-10 m/s. Additionally, at low speeds, the feeding envelope would have increased greatly in long-necked forms. Neck thickness did alter drag, as the thick-necked plesiosaur model experienced lower drag compared with the thin-necked model at swimming speeds from 1-10 m/s. This could indicate thick-necked plesiosaurs reduced overall drag, and spend less energy on straight, forward swimming compared with thin-necked forms. In conjunction with soft tissue evidence, this would provide support for a more sea lion-like morphology. Bending the neck evenly in lateral flexion showed greatest turning radius and drag in long-necked plesiosaurs and least in short-necked forms, demonstrating short-necked plesiosaurs were more likely to make faster neck turns and have shorter turning radius, compared with long-necked forms.

Institutional abbreviations

AM	Australian Museum, Sydney, Australia
BRSUG	Bristol University Geology Museum, Bristol, UK
CIT	California Institute of Technology, California, USA
FMNH	Field Museum of Natural History, Chicago, Illinois, USA
GLAHM	The Hunterian Museum, University of Glasgow, Glasgow, UK
GPMM	Geomuseum of the Westfälische Wilhelms University, Münster in Westfalen, Germany
KUVP	Kansas University (Museum of Natural History) of Vertebrate Palaeontology, Kansas, USA
MLP	Museo de La Plata, Buenos Aires Province, Argentina
MMUM	Manchester Museum, The University of Manchester, Manchester, UK
MNA	Museum of Northern Arizona, Arizona, USA
NHMUK	Natural History Museum, London, UK
NJSM	New Jersey State Museum, New Jersey, USA
OUNHM	Oxford University Museum of Natural History, Oxford, UK
PMO	The Paleontological Museum of the Natural History Museum Oslo, Norway
QMF	Queensland Museum, Brisbane, Australia
RMF	Richmond Marine Fossil Museum, Richmond, Australia
SAM	South Australian Museum, Adelaide, Australia
SDSM	South Dakota School of Mines and Technology, South Dakota, USA
SMNS	Staatliches Museum für Naturkunde, Stuttgart, Germany
SGO	Museo Nacional de Historia Natural, Santiago, Chile
TMP	Royal Tyrell Museum of Palaeontology, Drumheller, Canada

Chapter 1 – Introduction

This thesis combines the range of motion in plesiosaurs and extant taxa, found via three-dimensional modelling and digitisation of neck vertebrae, with computational fluid dynamics simulations of plesiosaur models, to explore the functional and biomechanical implications of the long neck in plesiosaurs.

1.1 Part A: *Plesiosaur palaeobiology*

1.1.1 Introduction

Plesiosaurs (vernacular name “plesiosaurs” from the Greek “almost lizard” (Callaway and Nicholls, 1997)) were a clade of marine reptiles living in the Mesozoic (Late Triassic to Late Cretaceous) (Ketchum and Benson, 2010; Bardet *et al.*, 2014; Wintrich *et al.* 2017a). First discovered 300 years ago (Stukely, 1717), their long necks and unique morphology are iconic to palaeontologists and the public alike. Plesiosaurs have no modern analogues - thus, it is difficult to reconstruct their mode of life. Understanding how plesiosaurs behaved and fed, may have wider implications as it will allow us to identify the limits and constraints of vertebrate morphological evolution in relation to an aquatic lifestyle. Additionally, investigating plesiosaur biomechanics might help us understand morphological diversity in extant taxa, whose aquatic adaptations never achieved such an extreme phenotypic change. What were the biomechanical implications of the plesiosaur neck for moving? What would it mean for a plesiosaur if it bent its neck while swimming? Despite the strong research focus into plesiosaur ecomorphology and biomechanics (e.g. O'Keefe, 2001b; Araújo and Polcyn, 2013; Muscutt *et al.*, 2017) these questions remain unanswered. Here, an overview of the current knowledge on the functional anatomy and phylogeny of plesiosaurs is provided as a solid background to biomechanical studies on the hydrodynamics of the plesiosaur neck.

1.1.2 Overview of the history of plesiosaur research

Plesiosaurs were one of the first groups of fossil reptiles to be recognised and scientifically described (Conybeare, 1824), and they have been excavated worldwide ever since (Chatterjee and Small, 1989; Gasparini *et al.*, 2003; Kear, 2004; Smith, 2008; Ketchum and Benson, 2010). After the first plesiosaur species description was completed, the number of plesiosaur species described each year has increased steadily, from a total of five descriptions per year in 1840 to 117 descriptions per year in 2016 (Tutin and Butler, 2017). The major milestones in the scientific history of plesiosaurs including the first discoveries and restorations through time, especially of their long necks, are summarised below.

1717: William Stukely provides the oldest known published illustration (Figure 1A) of what is now known to be a plesiosaur, which is a partial specimen of an unknown species from Nottinghamshire, UK (Stukely, 1717; Smith, 2007). The specimen comprises parts of the pelvic girdle, parts of the trunk including 16 dorsal vertebrae, and parts of the limbs (Figure 1A). At the time Stukely (1717) interpreted the remains as being from a crocodile or porpoise, and therefore he thought it had to be either amphibious or marine.

1821: Henry De la Beche and William Conybeare identified miscellaneous bones from Early Jurassic of Southern England (Benton and Taylor, 1984; Smith, 2007) and they recognised partial skeletons as belonging to a new form, which they name *Plesiosaurus* (Brown 1981; Callaway and Nicholls, 1997). Conybeare considered this new form as an intermediate between ichthyosaurs and lizards (Brown, 1981; Rudwick, 2008).

1822: The first plesiosaurs from Yorkshire are reported (Benton and Taylor, 1984).

1823: First complete plesiosaur skeleton (Figure 1B) is found on the Dorset shoreline in the Lias Formation at Lyme Regis in England by fossil hunter Mary Anning (Torrens, 1995; Rudwick, 2008). This specimen (NHMUK 22656), a young adult of moderate size (Callaway and Nicholls, 1997) is the lectotype of all plesiosaurs because of its completeness (Conybeare, 1824).

1824: Conybeare names and describes the discovery of the complete plesiosaur skeleton from 1823 as *Plesiosaurus dolichodeirus* (Figure 1B) (Brown, 1981).

1829: Mary Anning discovers her second *Plesiosaurus* (Torrens, 1995).

1830: Henry De la Beche illustrates a painting titled "Duria Antiquior" or "A More Ancient Dorset" (Figure 1C) which features plesiosaurs, ichthyosaurs and other fossils found in Lyme Regis in Dorset (Buckland, 1903). It has been regarded as the first attempt to accurately reconstruct the Mesozoic world, and was sold in aid of the Anning family who was in financial trouble at the time (Rudwick, 2008). In the painting the plesiosaurs are illustrated with different neck postures including a swan-like appearance.

1834: Thomas Hawkins makes a restoration drawing of a plesiosaur (Figure 1D) having a rather irregular 'wavy' looking neck (Shuler, 1950). There is a similarity in the reconstruction of the plesiosaur neck between the drawing by Hawkins and the painting by Henry De la Beche in 1830.

1835: Henri Marie Ducrotay de Blainville proposes and defines Plesiosauria as a taxonomical order (Brown, 1981), and more than 180 years later the order still remains with the original name.

1840: Richard Owen describes a plesiosaur specimen as *Plesiosaurus macrocephalus*, named by Buckland in 1836 (Torrens, 1995).

1841: Richard Owen makes the first major division of the order Plesiosauria by introducing the name *Pliosaurus* as a subgenus (Brown, 1981).

1847: Mary Anning dies (Torrens, 1995).

1855: G. F. Richardson illustrates Mesozoic fossils (Figure 1E) including a plesiosaur having a swan-like neck posture feasting on a pterodactyl, and this sketch has a strong influence on later restorations of plesiosaurs (Shuler, 1950).

1861: Richard Owen introduces *Pliosaurus* as a genus on its own (Brown, 1981) and not just a subgenus as he stated 20 years earlier.

1869: Edward Drinker Cope illustrates an elasmosaur (Figure 1F) with an extremely long tail (Shuler, 1950). Later it is found that the reason for this reconstruction is that Cope incorrectly identified the anterior and posterior vertebrae, placing the skull as the tip of the tail (Ellis, 2003; Everhart, 2017).

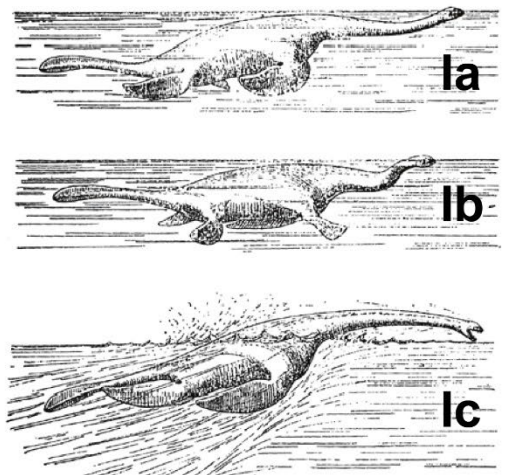
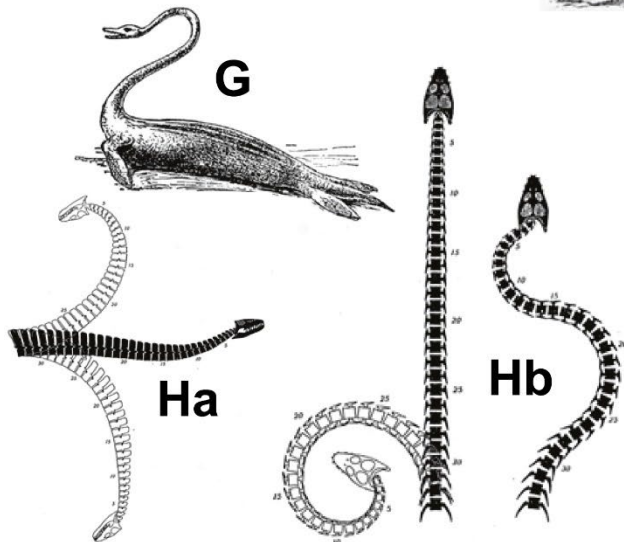
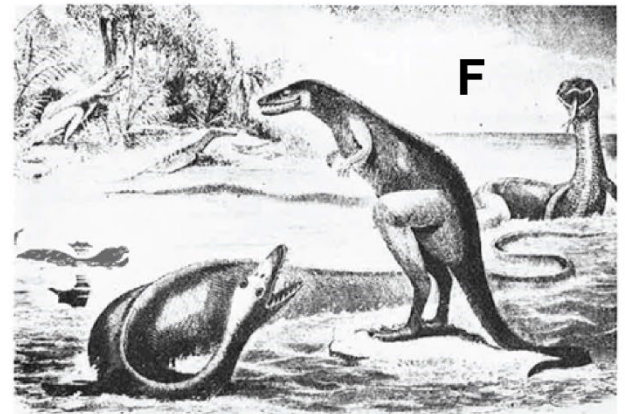
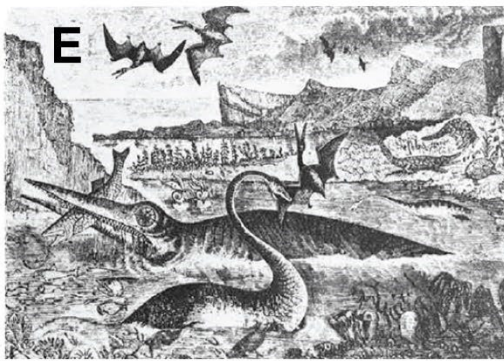
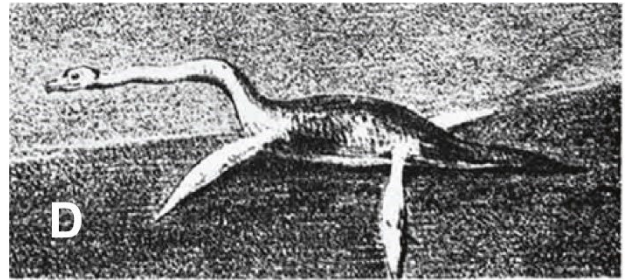
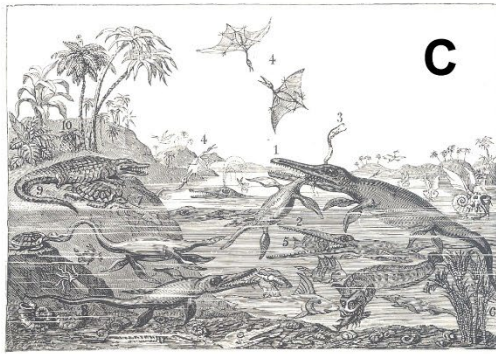
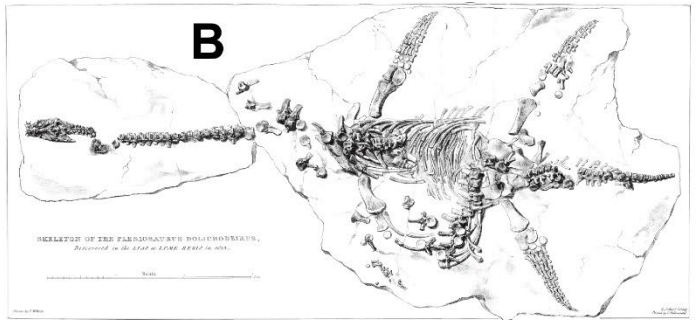
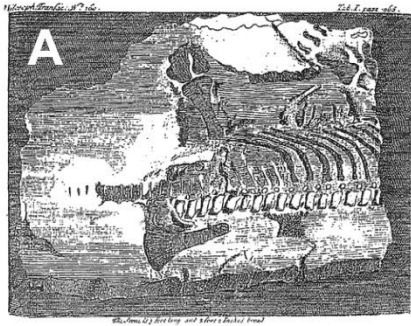
1890: Frederick Starr makes a rather abstract drawing of a plesiosaur (Figure 1G) with the swan-like neck posture and a new idea of the hind flippers and the tail being more similar to that of a sea lion instead of using the morphological features of the plesiosaur (Shuler, 1950).

1925: The first study on plesiosaur neck flexibility is published. Zarnik (1925) reconstructs neck flexibility of plesiosaurs based on a comparison with modern crocodiles and snakes (Figure 1H) and proposes neck positions and movements at the water surface based on this comparison (Figure 1I). Future studies following Zarnik's on plesiosaur neck flexibility are included in this thesis and are therefore not part of the summary stated here.

The long scientific history of plesiosaurs goes back to the early eighteenth century (Conybeare, 1824), a time when systematic approaches differed significantly from the methods of today (Tutin and Butler, 2017). As a consequence, plesiosaur classification is particularly confused – not least because in the 1800s the taxonomic level ‘genus’ was roughly equivalent to the ‘ordinal’ level as understood today (Smith, 2007). It is therefore

unsurprising that hundreds of plesiosaur species from strata worldwide, ranging in age throughout the Mesozoic, were arbitrarily positioned into De la Beche's and Conybeare's single genus *Plesiosaurus* (Conybeare, 1824; Owen, 1840; Andrews, 1910). To some extent, this confusion remains today. Although many species of *Plesiosaurus* have now been allocated new generic names, many more remain not assigned to any known taxon, reflecting our changed attitude towards systematics (Brown, 1981; O'Keefe, 2006). As seen in the historical and modern illustrations, the restoration approaches of plesiosaurs vary between artists, and not until the 1940s did the necks of plesiosaurs start to seem more realistic, due to neck flexibility studies of various plesiosaur species (Welles, 1943; Evans, 1993; Zammit *et al.*, 2008; Nagesan *et al.*, 2018).

Figure 1 (over page): Illustrations of plesiosaurs. A) First published plesiosaur skeleton illustration of the specimen found in Nottinghamshire, UK from Stukely (1717). B) Illustration of *Plesiosaurus dolichodeirus* found in England by Mary Anning in 1823 from Conybeare (1824). C) The painting "Duria Antiquior" by Henry De la Beche in 1830 illustrating the Mesozoic life from Buckland (1903). D) Plesiosaur restoration by Thomas Hawkins in 1834 from Shuler (1950). E) Illustration of Mesozoic fossils by G. F. Richardson in 1855 from Shuler (1950). F) The incorrect elasmosaur restoration by Cope in 1869 from Shuler (1950). G) Swan-like posture of a plesiosaur by Frederick Starr in 1890 from Shuler (1950). H) Neck vertebrae flexibility of *Plesiosaurus Guilelmi imperatoris* in various flexions; Ha (lateral view): Normal position (black) and dorsoventral flexion (white). Hb (dorsal view): Normal position (black in middle), extreme lateral flexion (white), and zig-zagging maximum lateral flexion (black to the right) from Zarnik (1925). I) Reconstructions of *Plesiosaurus Guilelmi imperatoris* in three swimming modes: a) Swimming quietly, b) getting ready for attack, and c) moment of attack from Zarnik (1925).



1.1.3 Plesiosaurian diversity and morphology

Plesiosaurs are part of a larger clade given they are placed within the group sauropterygians (Figure 2), consisting of placodonts, pachypleurosaurs, nothosaurs, pistosaurs, and finally, the plesiosaurians containing plesiosaurs and pliosaurs (Motani, 2009; Klein, 2010; Sobral *et al.*, 2016; Soul and Benson, 2017). Plesiosaurs are diapsid reptiles and are more closely related to ichthyosaurs than archosaurs and lepidosaurs.

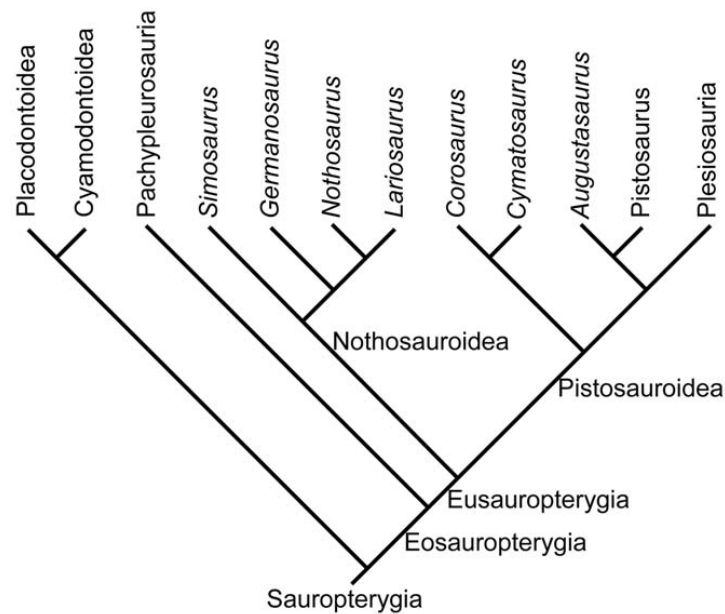


Figure 2: Phylogenetic relationships of Sauropterygia. From Klein (2010).

Plesiosaurs and pliosaurs used to be classified depending on the number of neck vertebrae (Williston, 1907). Today they are placed within two morphotypes: plesiosauromorphs (small head, long neck) and pliosauromorphs (large head, short neck) (O'Keefe, 2001a, 2002; Ketchum and Benson, 2010; Druckenmiller and Knutsen, 2012; Knutsen *et al.*, 2012b; Benson and Druckenmiller, 2014), with an intermediate body plan between the two included in recent phylogenetic studies (Fischer *et al.*, 2017; Tutin and Butler, 2017; Smith and Benson, 2018). Plesiosaur phylogenetics are described in further detail in a subsequent section of this chapter.

Plesiosaurians vary in size, from around 1.5m long (e.g. *Thalassiodracon* from the Early Jurassic of the UK, 205 Ma) to 15m long giants (e.g. *Pliosaurus* from the Middle Jurassic Oxford Clay Formation of the UK, 149-159 Ma) (Smith, 2007). The largest forms tend to be found in younger strata (Brown 1981), indicating a possible evolutionary trend towards large size – apparently conforming to Cope's rule (Hone and Benton, 2005). The base anatomy of plesiosaurians is considered to have originated with the Rhomaleosauridae family, especially

the pliosaur *Meyerasaurus victor* (Smith and Vincent, 2010). This species is a good template for understanding the anatomy of plesiosaurs (Figure 3), mainly because of its skeletal completeness (Smith and Vincent, 2010).

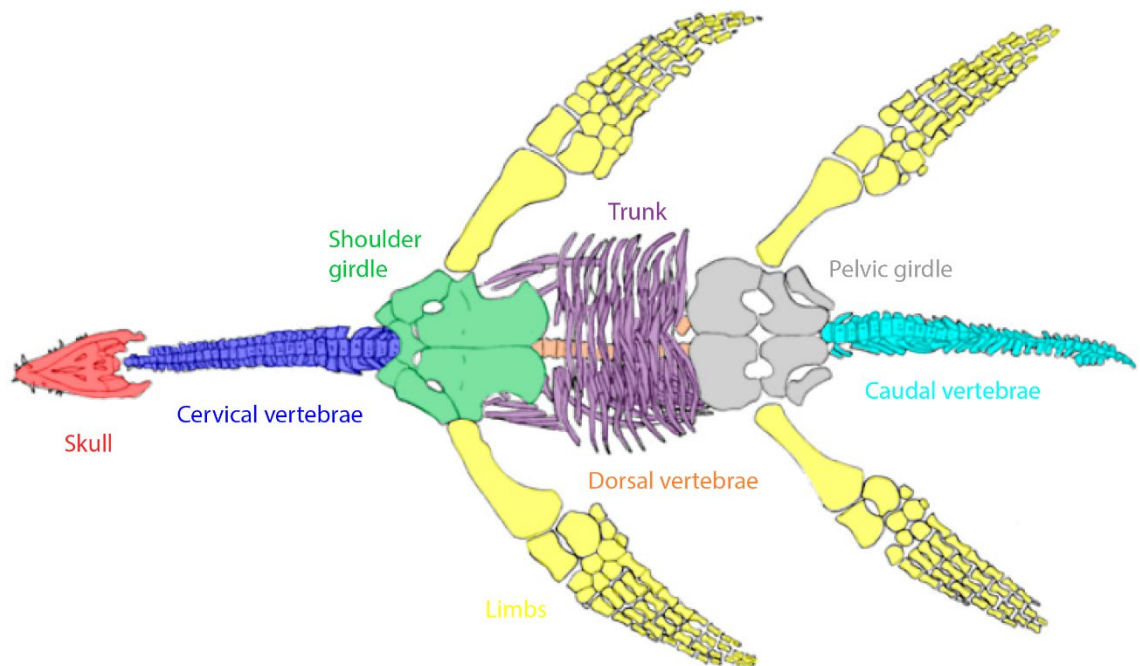


Figure 3: Ventral view of the colour coded skeletal outline of *Meyerasaurus victor*. Modified from Smith (2007).

In proportion, the skull greatly varies in size relative to the cervical region, while the shoulder girdle is generally larger than the pelvic girdle (Brown, 1981; O'Keefe, 2002). Front limbs equally tend to be bigger than hind limbs while the cervical region is as long – or even longer – than the caudal region (Brown, 1981; O'Keefe, 2002). This basic bauplan characterises the two main plesiosaurian groups – with skull generally shorter than the cervical region in plesiosauromorphs – and a skull characterised by a larger rostrum being proportionally bigger than the cervical region in pliosauro-morphs (e.g. Brown, 1981; Chatterjee and Small, 1989; Taylor, 1992). The plesiosaurian anatomy reviewed in the following is important for understanding their behaviour and lifestyle.

1.1.1.1 Skull

The sauropterygian skull changed significantly from Late Triassic to Late Cretaceous genera (Figure 4). Simplified, the cranium contains a skull roof, palate, braincase and mandibles (Brown and Cruickshank, 1994). The plesiosaurian skull is small with respect to the trunk (Brown, 1981), and it is streamlined and lightly built (Taylor, 1987; Noè *et al.*, 2017). An example of the dorsal, ventral and lateral view of a plesiosaur skull is shown in Figure 5. The difference in orbit size is clear when comparing nothosaurs (small orbit) and cryoclidids

(large orbit) (Figure 4), and could be due to simultaneous selection for both sensitivity to low light and visual acuity (Humphries and Ruxton, 2002), as plesiosaurs would have lived in different parts of the water column depending on taxa. Furthermore, the rostrum changes significantly in size from early forms to more derived forms with an increase in length of the premaxilla (Figure 4), indicating a clear change in lifestyle and habitat.

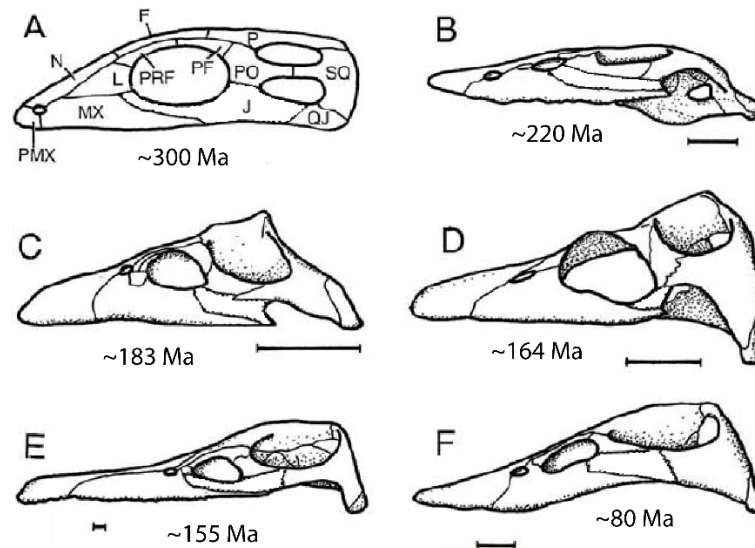


Figure 4: Sauropterygian skulls without mandibles. Scale bars = 50 mm. **A:** Generalised early diapsid ~ 300 Ma. **B:** Nothosaurid (*Simosaurus*) ~220 Ma. **C:** Microcleidid (*Microcleidus brachypterygius*) ~183 Ma. **D:** Cryptocleidid (*Cryptocleidus eurymerus*) ~ 164 Ma. **E:** Pliosaurid (*Pliosaurus brachyspondylus*) ~155 Ma. **F:** Elasmosaurid (*Styxosaurus snowii*) ~80 Ma. Abbreviations: F = frontal, J = jugal, L = lacrimal, N = nasal, MX = maxilla, P = parietal, PF = postfrontal, PMX = premaxilla, PO = postorbital, PRF = prefrontal, QJ = quadratojugal, and SQ = squamosal. Modified from Brown and Cruickshank (1994).

The first reconstruction of the muscles attached to a plesiosaur skull was made by Taylor (1992). In that study, the musculature of the skull of *Rhomaleosaurus zetlandicus* was combined with skeletal functions ascribed to aquatic tetrapods, making it possible to study different functions of the skull of this species e.g. maximal structural strength, maximal swimming speeds and feeding efficiency (Taylor, 1992). Taylor (1992) found that the skull of *R. zetlandicus* would functionally be a compromise of the need to maximize swimming ability and strength of the skull to allow feeding efficiency. In addition, Araújo and Polcyn (2013) used 3D finite element analysis to assess cranial performance and feeding models based on a detailed reconstruction of the adductor chamber musculature in long necked plesiosaurs. In their study, Araújo and Polcyn (2013) estimated stress, strain distributions and bite force by varying the morphology of the anatomical structures of the skull of the Late Cretaceous plesiosaur *Libonectes morgani*. The study also used morphometric data from the literature of different skulls in various eosauroptrygians to compare with *L.*

morgani and found that across the sauropterygian evolution, morphological changes of the adductor chamber would have functioned to accommodate increased mass of the jaw adductor muscles, without reduction of the skull's mechanical performance (Araújo and Polcyn, 2013).

Among plesiosaurians there has been a suggestion that a specialised underwater olfactory system has been part of a common adaptation (Cruickshank *et al.*, 1991; Brown and Cruickshank, 1994; Smith, 2007). As the internal nostrils of plesiosaurs are situated near the orbits (Swinton, 1965), they are associated with palatal grooves, which have been interpreted as adaptations to channel water into the internal nares (Cruickshank *et al.*, 1991). The flow of water through the nasal passage would thus have been maintained by hydrodynamic pressure over the retracted external nares during locomotion (Smith, 2007). During its passage through the nasal ducts water would have been intercepted by the olfactory epithelia (Smith, 2007), which is a specialized tissue inside the nasal cavity involved in smelling.

A recent study in plesiosaur histology by Fleischle *et al.* (2018) has suggested that plesiosaurs were endothermic based on fast bone growth and fast metabolism. It has also been suggested that the internal and external nostrils of *Rhomaleosaurus* would have been partially shut by soft tissue during normal swimming/diving (Cruickshank *et al.*, 1991). The placement of nostrils would have hindered respiratory air flow, meaning that this group of plesiosaurs would instead have breathed through the mouth and water would have been excluded from the trachea by a glottal valve and a large muscular tongue (Cruickshank *et al.*, 1991).

Unlike anisodont teeth (regionalised size variation), which have been found in one elasmosaurid (Kear *et al.*, 2017), and heterodont teeth (variety in shape) found in e.g. mammals (Osborn, 1893) and one known pliosaur (Sassoon *et al.*, 2015), plesiosaurs mostly possess homodont teeth (equally sized) (Figure 5) (Persson, 1959; Brown, 1981; Sørensen *et al.*, 2013). The number of pairs of homodont teeth in plesiosaurs range from 24-30 in Lower Jurassic species to 14-58 in Late Cretaceous species (Brown, 1981), indicating an increase in the diversity of teeth among species from the Jurassic to the Cretaceous. The tooth form for plesiosaurs possessing large skulls are generally observed with large roots, and the crown is short, wide, and slightly curved (Brown, 1981). Small-skulled plesiosaurs have smaller roots compared with large-skulled plesiosaurs with proportionally slimmer crowns (Brown, 1981). The tooth ornament has numerous longitudinal ridges with a distinct

pattern and there is some ontogenetic variation as the ridges in older individuals are more prominent than in juvenile specimens (Brown, 1981). Generally, plesiosaurs possess five pairs of premaxillary teeth carried in each premaxilla, and large-skulled species always retain this number, with only cryptoclidids and elasmosaurids bearing more than this (six and eight, respectively) (Brown, 1981; Brown and Cruickshank, 1994).

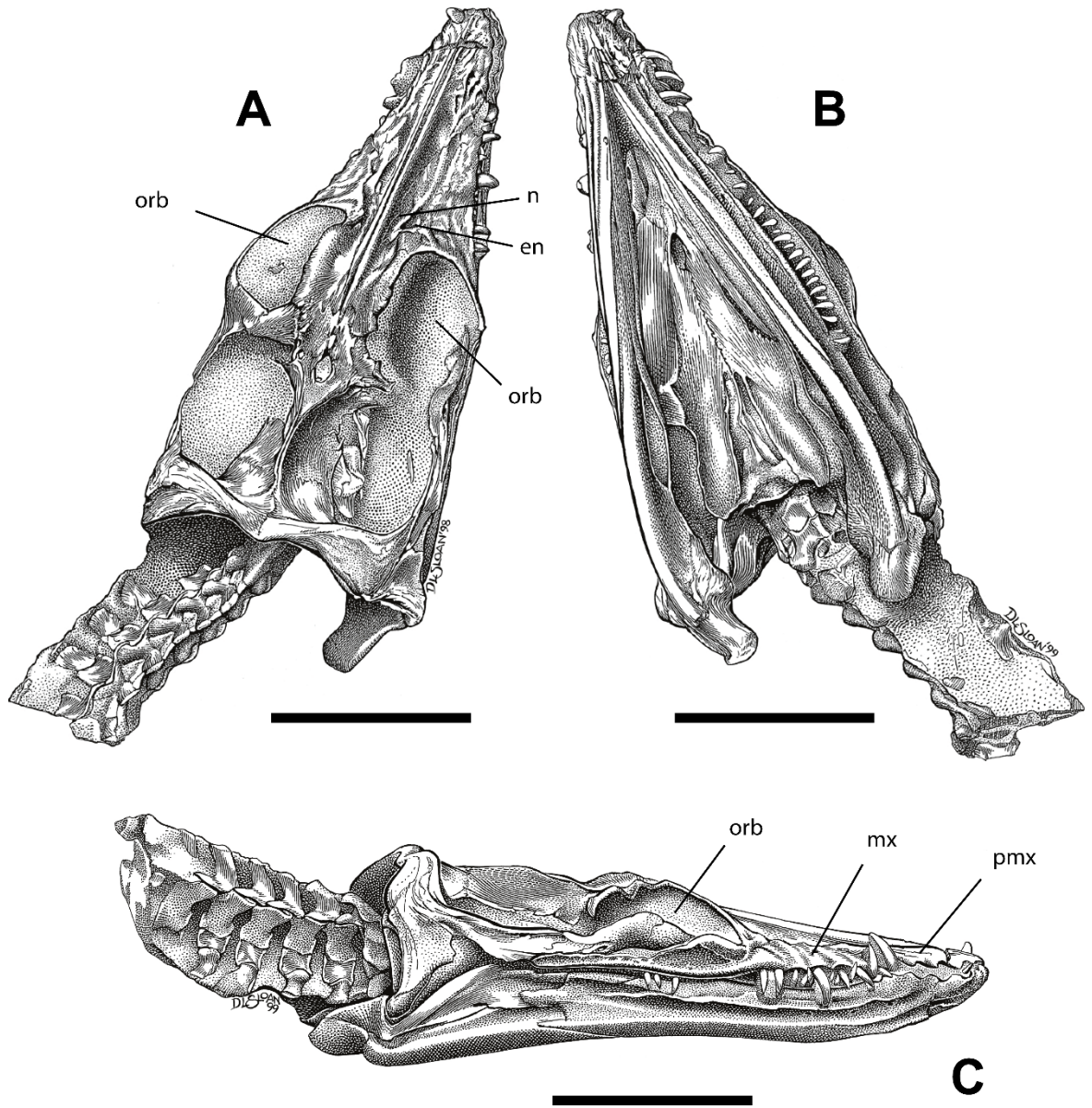


Figure 5: Dorsal (A), ventral (B), and right lateral (C) view of the skull of the leptocleidid *Nichollisia borealis*, TMP 94.122.01. This specimen possesses homodont teeth. Scale bars = 10 cm. Abbreviations: en: external naris; mx: maxilla; n: nasal; orb: orbit; pmx: premaxilla. Modified from Druckenmiller and Russell (2008b).

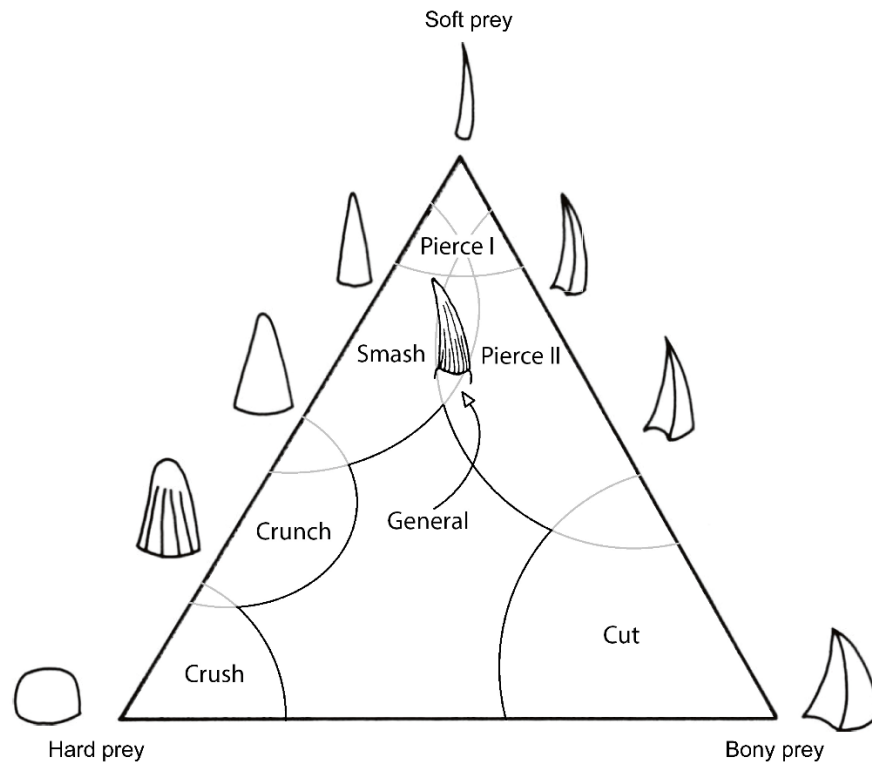


Figure 6: The seven predator types/feeding guilds (crush, crunch, smash, pierce I, pierce II, cut and general) of Mesozoic marine reptiles based on tooth crown morphology. Corners also indicate prey preferences (hard, soft and bony prey) corresponding to tooth form. The guilds overlap each other, some more than others, with crush and crunch overlapping the least, as the difference between the two types are very distinctive compared with the others. Notice the general guild is placed in between smash and pierce II. Modified from Massare (1987).

Defined by Root in 1967, a predator type/guild is “a group of species that exploit the same class of environmental resources in a similar way”, allowing grouping of species without regards to taxonomy (Massare, 1987). A total of seven feeding guilds have been assigned to Mesozoic marine reptiles (Massare, 1987) with prey preferences indicated by three distinctive types of prey in each corner of the ternary diagram shown in Figure 6.

Generally Jurassic plesiosaurian teeth are placed into the “Pierce I guild”, meaning that their teeth are long, slender, delicate, sharply pointed, rarely showing wear (Massare, 1997). Such teeth would be used for piercing very soft prey or very small, bony prey (Massare, 1987, 1997). For Middle Jurassic genera, such as e.g. *Muraenosaurus*, *Cryptoclidus*, and *Tricleidus* (Brown, 1981), the top of the crown is slightly compressed, creating two distinct, fairly sharp keels at the tip (Massare, 1987), thus placing these species in between the “General guild”. Cretaceous elasmosaurs have more robust teeth compared with Jurassic plesiosaurs and shift from “Pierce I guild” to being either “General guild” or “Pierce II guild” depending on the species, as the teeth are getting more curved and moderate in length (Massare, 1997). “Pierce II guild” differ from “Pierce I guild” in shape and kind of wear

which is rare, and teeth placed in the “Pierce II guild” are smaller in size compared with teeth placed in the “Pierce I guild”. We therefore see a change over time in tooth morphology and associated predator types among plesiosaurs represented by the shift in feeding guilds in some plesiosaur families.

1.1.1.2 Vertebral column

The plesiosaurian vertebral column can be subdivided into cervical-, dorsal-, and caudal vertebrae (neck, back and tail, respectively) (Figure 7), with the post-cervical vertebral column being nearly straight. Generally, in vertebrates, arches protrude from the top and bottom of each centra along with vertebral processes (common types are transverse processes and zygapophyses). If an arch is protruding from the top of the centrum it is called a neural arch (Taylor and Wedel, 2013a), while when protruding from underneath the centrum of the arch is called either haemal arch or chevron (McGowan, 1999). In plesiosaurs, the vertebrae possess neural arches as well as anterior and posterior zygapophyses, overlapping one another (Andrews, 1910). Some authors have further subdivided the posterior part of the cervical region/anterior part of the dorsal region to include pectoral vertebrae (Sachs *et al.*, 2013, 2016; Sachs and Kear, 2017a, 2017b), being either part of the cervical series or the dorsal series depending on the specific vertebra found. However, this subdivision is not widely accepted (Carpenter, 1999; O’Gorman and Fernandez, 2016; Noè *et al.*, 2017).

In all plesiosaurs the first (atlas) and second (axis) cervical vertebrae are fused into an atlas-axis complex, which is attached to the occipital condyle bone in the skull (VanBuren and Evans, 2016; Frey *et al.*, 2017). The morphology of the occipital condyle is circular and the cotyle of the atlas is cup-shaped allowing for enhanced mobility in dorsoventral and lateral rotations at the cranio-cervical joint (VanBuren and Evans, 2016). Proceeding from the atlas-axis complex the neck is then comprised of numerous cervical vertebrae ranging from 16-76, transitioning into dorsal vertebrae in the region around the trunk and girdles, shifting into caudal/tail vertebrae in the posterior end of the skeleton (Figure 7). The caudal vertebrae are generally flat and wide, especially the anterior-most caudal vertebrae, as the neural spines are lower than the dorsal vertebrae (Sennikov, 2015).

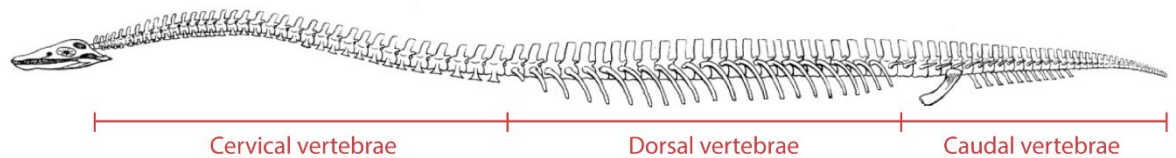


Figure 7: The vertebral column of *Plesiosaurus dolichodeirus* divided in three sections (cervical-, dorsal-, and caudal vertebrae). Modified from Conybeare (1824).

The central part of each vertebra is called the centrum which consists of a solid cylindrical body (Kardong, 2012). The proportions of the centra (Figure 8) vary ontogenically; centra are relatively shorter in younger individuals (Brown, 1981). It has also been observed that the centrum breadth is always greater than the height (or almost equal to height in dorsal vertebrae) (Brown, 1981; Murray, 1987). Cervical centra show similarities across plesiosaur families being mostly circular, and the centra are recognised as amphicoelous (similar to modern amphibians and reptiles) in shape being concave at both ends (Grossmann, 2007; Ketchum and Smith, 2010; Sachs *et al.*, 2016; Sachs and Kear, 2017a; Marzola *et al.*, 2018) but these tend to become flat in long-necked species and especially in some Cretaceous genera (Brown, 1981). In all plesiosaurs, regardless of the age of the individual, the mid-dorsal vertebrae are the largest vertebrae with equivalently longest neural spines (Brown, 1981). The longer neural spines in the dorsal vertebrae could imply a slight increase in the mechanical advantage of the muscles in this region compared with the rest of the vertebral column (Kardong, 2012).

1.1.1.2.1 Dimensions of the cervical vertebrae

The axis has a short neural spine (VanBuren and Evans, 2016). The neck vertebrae following the atlas-axis complex consist of centra forming the base of each vertebra, with neural spine attached on the top and ribs attached on both sides of the centrum (Figure 8). The pre- and post-zygapophyses are attached to each side of the base of the neural spine. A neural canal is positioned between the spine and centrum going from the anterior to the posterior part of the vertebra. Neuro-central sutures (only visible in juvenile specimens) are positioned at the top of each side of the centrum, creating a clear path between the muscles which are thought to be positioned between the lower part of the spine and the centrum, and the muscles would have attached to each side of the vertebra.

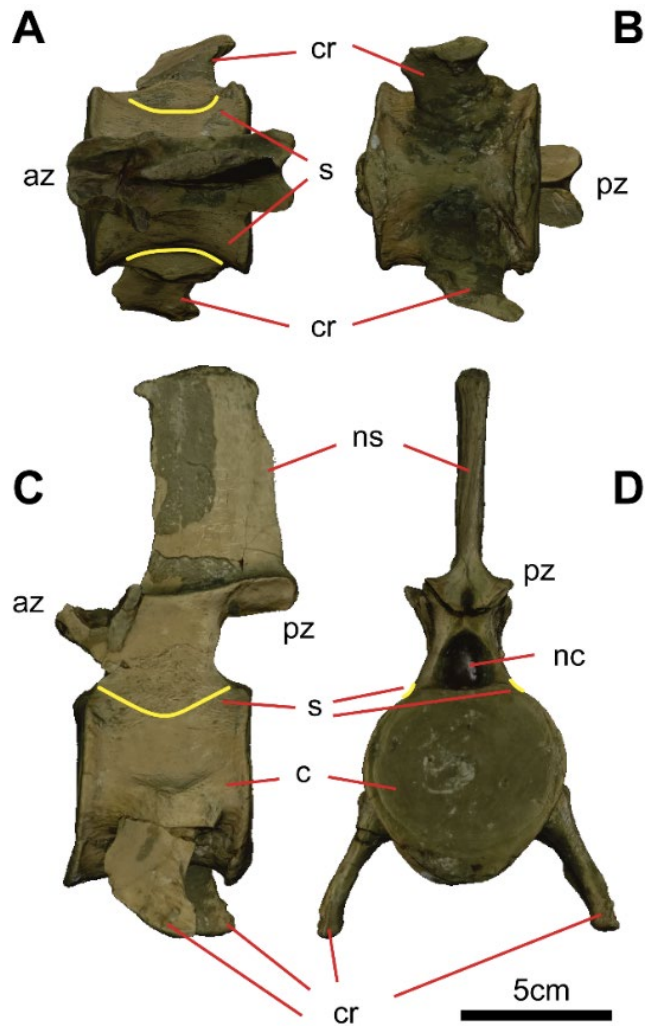


Figure 8: Dorsal (A), ventral (B), lateral (C), and posterior (D) view of C23 in *Muraenosaurus* sp. (OUNHM J.95000). az = anterior-zygapophyses, c = centrum, cr = cervical rib, nc = neural canal, ns = neural spine, pz = post-zygapophyses, s = neuro-central sutures (here visualised by yellow lines due to the specimen being adult).

The cervical ribs are small but prominent crests of bone which (if they occur) divide the lateral surface of the cervical centrum into almost equal upper and lower concave areas (Figure 8 and Figure 9A-F) (Brown, 1981). These ribs are correlated with neck length, and are almost consistently present on anterior cervical vertebrae of long-necked species from Late Jurassic and Cretaceous (Brown, 1981). The development of cervical ribs is thought to be associated with the strengthening of neck muscles (Brown, 1981). All Early Jurassic plesiosaurs have double headed cervical ribs, and consequently the cervical centra bear paired facets (Brown, 1981). Otero et al. (2014a) illustrated the cervical ribs of *Aristonectes quiriquinensis* as pointing in the anterior direction, unlike the normal arrangement where cervical ribs point in the posterior direction (e.g. Andrews, 1910; Brown, 1981; Druckenmiller and Russell, 2008b; Sachs *et al.*, 2016).

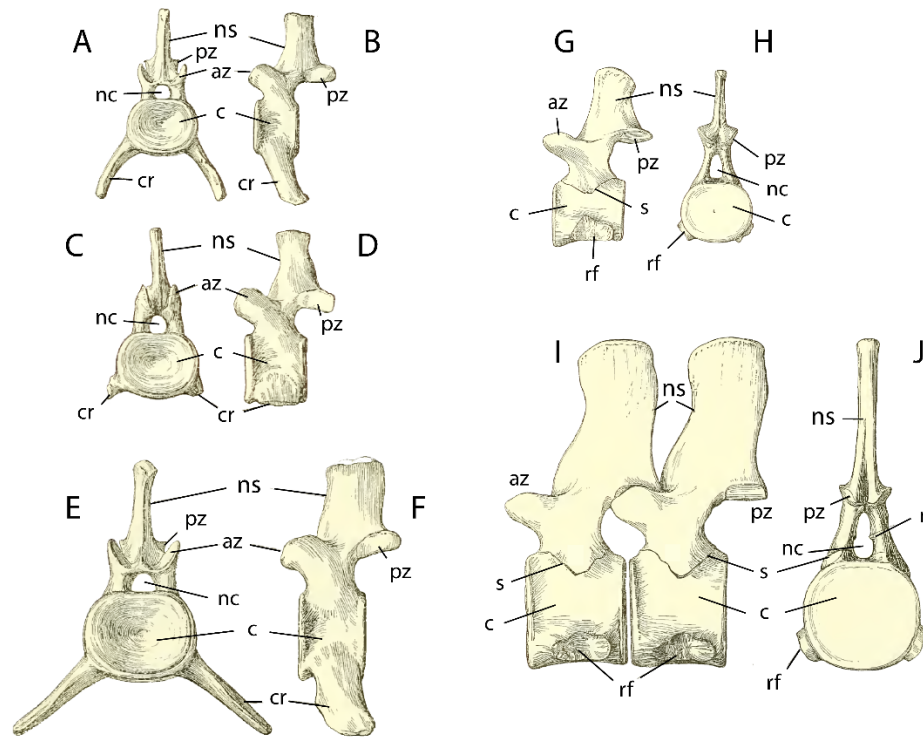


Figure 9: Cervical vertebrae from plesiosaur specimens illustrating ontogenetic changes. A-F: Adult *Cryptoclidus eurymerus* (R2412); A-D is anterior cervical vertebrae and E-F is a posterior cervical. G-J: Juvenile *Muraenosaurus leedsii* (R2863); G-H is an anterior cervical and I-J is a posterior cervical. A, C, and E in frontal view. B, D, F, G, and I in lateral view. H and J in caudal view. All cervical vertebrae scaled to each other. Abbreviations: az: anterior zygapophyses; c: centrum; cr: cervical rib; nc: neural canal; ns: neural spine; r: ridge on inner face of neural arch; rf: facet for cervical rib; pz: posterior zygapophyses; s: neuro-central suture. Modified from Andrews (1910).

The dimension and curvature of each part of the vertebra varies among plesiosaur families. In cryptoclidids (Figure 10A) the spine is high and narrow, and the zygapophyses align at a higher distance from the centrum, creating a gap between the zygapophyses and the centrum. Jurassic cryptoclidids (e.g. *Cryptoclidus*) are significantly different from any of the Cretaceous taxa in exhibiting a nearly circular centrum shape (Brown, 1981; Brown *et al.*, 1986; Chatterjee and Small, 1989; O'Keefe, 2001a; Kear, 2006). In leptoclidids (Figure 10B) and elasmosaurids (Figure 10C) the spine is relatively short and thick, and the zygapophyses align close to the centrum allowing little space between the zygapophyses and the centrum. In leptocleidids the neural spines curve backwards (Figure 10B), whereas in elasmosaurids the neural spines are almost squared in lateral view, creating little space of movement between each vertebra. This could indicate that cryptoclidids and leptocleidids would have greater dorsal range of motion compared with elasmosaurids.

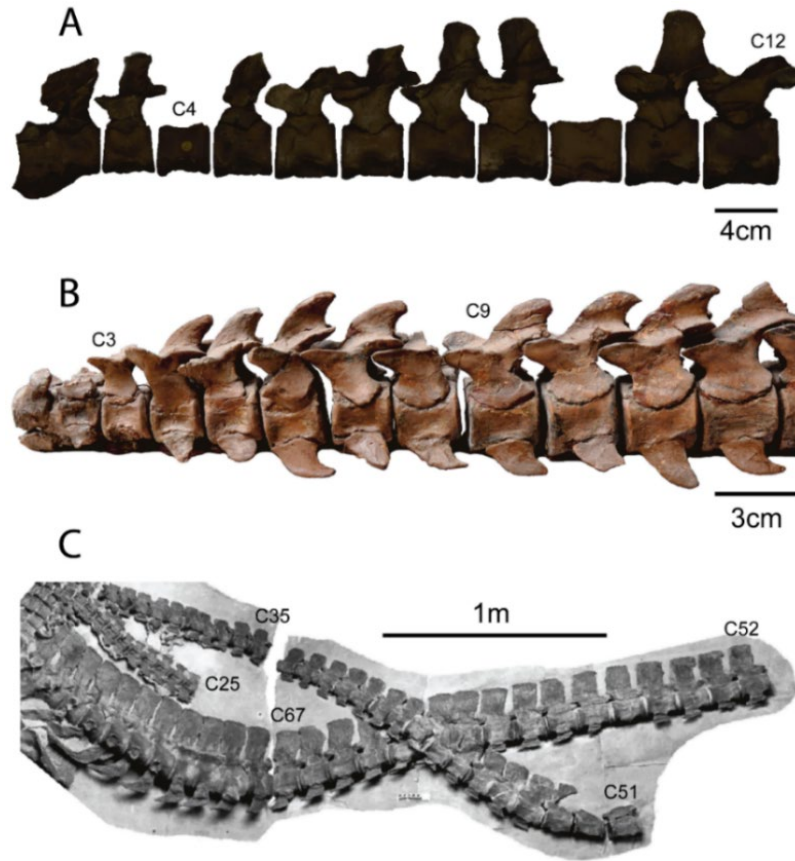


Figure 10: Lateral view of adjacent cervical vertebrae from various plesiosaur families. A) The anterior part of the neck (atlas-axis-C12) from the cryptocleidid *Muraenosaurus leedsii* (NHMUK R2863) used in this chapter. B) The anterior part of the neck (atlas-axis-C12) from the leptocleidid *Brancasaurus brancai* (GPMM A3.B4) (Sachs *et al.*, 2016). C) Middle and posterior part of the neck from the elasmosaurid *Albertonectes vanderveldei* (TMP 2007.011.0001) (Kubo *et al.*, 2012). Notice the difference in the shape of the neural spines and position of zygapophyses among the three families.

Using a metric allows easy comparison of vertebrae. Estimating a vertebral length index for plesiosaur centra can help reveal the rate of vertebral elongation (O'Keefe and Hiller, 2006; Otero *et al.*, 2014b; O'Gorman *et al.*, 2016b) as well as variation of proportions in the centra with an evolutionary aspect. In 1981, Brown came up with the Vertebral Length Index (VLI) (Equation 1) including all vertebrae in the vertebral column. The VLI (stated as %) is depended on the three dimensions of the centrum: length, height and width. The main reason for using these three dimensions is because plesiosaur vertebrae are usually only found with the centrum preserved; the neural spines, ribs and zygapophyses break off easily during fossilisation.

$$VLI = \frac{l}{(w+h)/2} * 100 \%$$

Equation 1: Vertebral length index (VLI); l = vertebral length, w = posterior central width, and h = posterior central height From Brown (1981) and Brown *et al.* (1986).

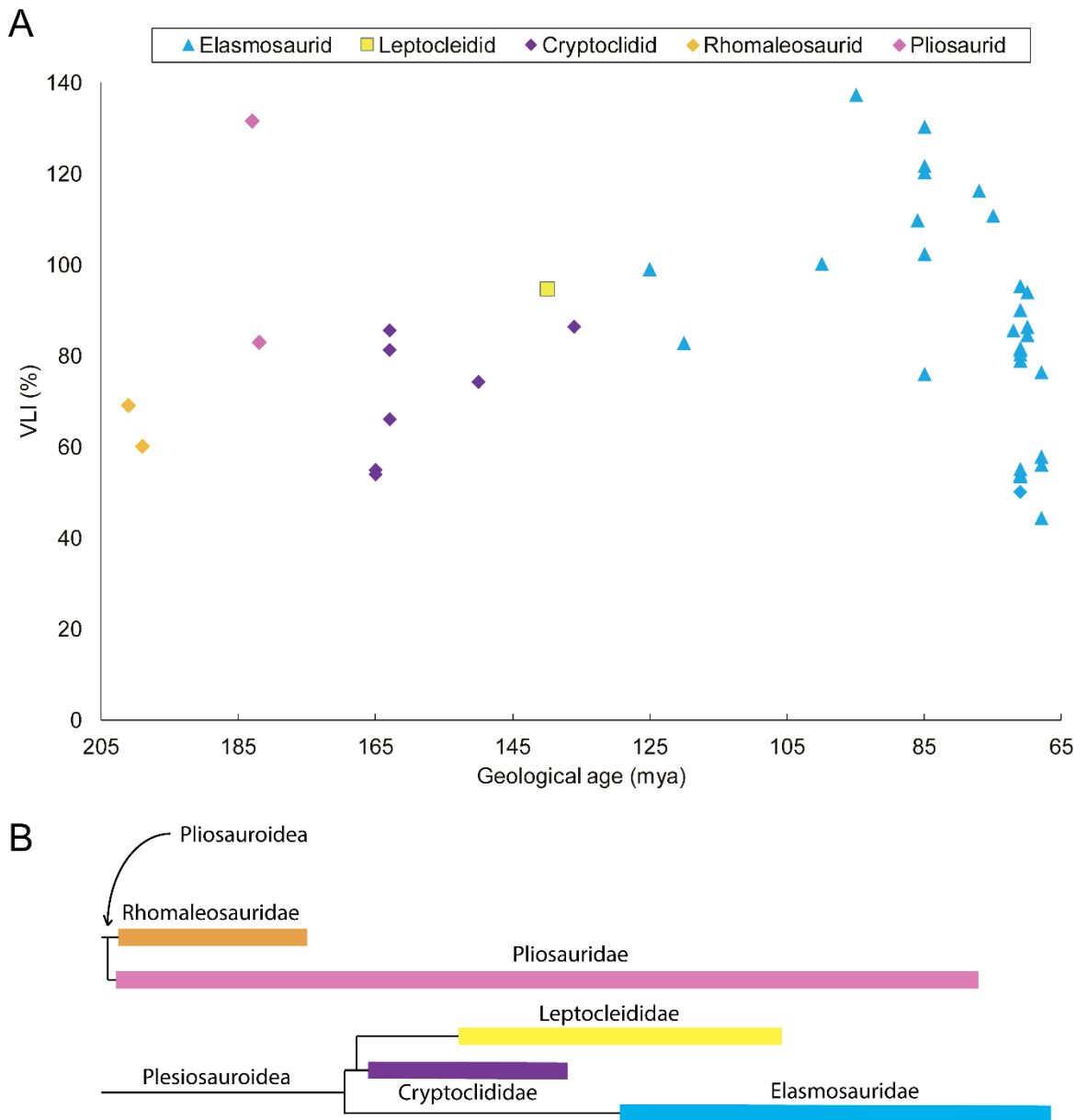


Figure 11: VLI values (%) as average of the whole neck through geological age (million years ago) for various plesiosaur families: blue: elasmosaurid; yellow: leptocleidid; purple: cryptocleidid; orange: rhomaleosaurid, pink: pliosaurid. Geological time span (A) and phylogeny (B) for each family used in this survey indicated by solid horizontal lines in matching colour with data points. Data collected from Andrews (1910), Smellie (1917), Brown (1981), Brown et al. (1986), Evans (1993), O’Keefe and Hiller (2006), Sato et al. (2006), Ketchum and Smith (2010), Benson et al. (2011), Berezin (2011), Vincent (2011), Kubo et al. (2012), O’Gorman et al. (2013, 2014, 2016a, 2016b, 2017, 2018a), Otero et al. (2014b), Otero (2016), and Smith and Araújo (2017).

VLI has been calculated for various plesiosaur specimens, and the average of VLI for the whole neck in each specimen shows that VLI varies slightly across families, but especially within the elasmosaurids (Figure 11). The higher the VLI the longer the centra are compared with height and width, and vice versa for the lowest VLI values. Elasmosaurids are characterised by having the highest and lowest VLI values among plesiosaurs making them

achieve long necks from both an increase in- and elongation of the cervical vertebrae, and vice versa for the elasmosaurids with the shortest neck lengths (Figure 11: light blue). In contrast, rhomaleosaurids tend to have the lowest VLI values due to the short and limited number of cervical vertebrae (Figure 11: orange). A common pattern in long-necked plesiosaurs, like elasmosaurids, is the increase in centrum length which only occurs in the anterior two-thirds of the neck, whereas the centra in the posterior third possess a relatively constant absolute length, after which the length shortens over the last 10 % of the cervical series (O'Keefe and Hiller, 2006; Vincent *et al.*, 2017a). Generally, the average VLI for the whole neck does not go below 40 % or above 140 % in any plesiosaur family, and the VLI varies greatly in especially elasmosaurids (Figure 11) due to their great variety of neck lengths and difference in centra which in Jurassic forms are relatively thinner and lower compared to Cretaceous species (Welles, 1943).

$$HI = \frac{h}{l} * 100 \%$$

Equation 2: Height index (HI); h = central height, l = vertebral length. From Welles (1952).

The centrum shape affects range of motion (Buchholtz and Schur, 2004), and plesiosaurs had a variety of centra lengths, widths and heights, potentially creating differences in range of motion of their necks. The longer the centra, the less flexible the neck would be, and vice versa for shorter centra (Buchholtz and Schur, 2004), indicating that elasmosaurids could have had stiffer necks in comparison with especially rhomaleosaurids. However, the flexibility of the neck in elasmosaurids could ultimately be higher than what is seen in other families if the number of cervical vertebrae is higher.

$$BI = \frac{b}{l} * 100 \%$$

Equation 3: Breadth index (BI); b = central breadth, and l = vertebral length. From Welles (1952).

Other indices considering vertebral centrum proportions to describe external morphologies are the height (Equation 2) and breadth indices (Equation 3) stated by Welles (1952). O'Gorman and colleagues recently (2013, 2014, 2016b) applied similar ratios using a breadth/height index (Equation 4) and Brown's (1981) VLI and Welles' (1952) two indices. O'Gorman *et al.* (2013, 2014, 2016b) showed that BHI was significantly higher than the VLI and HI ratios, but similar or lower than the BI ratio, indicating that species like the elasmosaurids have much broader than high cervical vertebrae. The indices provide more

detailed descriptions of the vertebrae, often used in descriptions of new specimens in more recent literature though not as often used as the VLI.

$$BHI = \frac{b}{h} * 100 \%$$

Equation 4: Breadth/height index (BHI); b = central breadth, and h = central height. From O'Gorman et al. (2013, 2014, 2016b).

1.1.1.2.2 Cervical vertebrae count

Plesiosaurs vary in the quantity of cervical vertebrae (Figure 12). Rhomaleosaurids have between 27-30 cervical vertebrae (Figure 12: orange), and pliosaurids only exceed this interval a little by having up to 37 (Figure 12: pink). The range increase in microcleidids being 29-41 (Figure 12: green), and leptocleidids have 24-32 cervical vertebrae (Figure 12: yellow). Cryptocleidids vary greatly in cervical vertebrae count, from 25 to 60 (Figure 12: purple), and in contrast polycotylids only vary from 19 to 30 (Figure 12: red). Placed in no particular family but being similar in range with pliosaurids, plesiosaurids range from 18 to 42 cervical vertebrae (Figure 12: dark blue). Elasmosaurids vary the most in number of cervical vertebrae ranging from 26-76 (Figure 12: light blue). In cryptocleidids, the highest number of cervical vertebrae is found in the species *Spitrasaurus wensaasi*, with a total of 60 cervical vertebrae. This significantly exceeds that described for plesiosaur specimens from the Late Triassic to Late Jurassic, but is comparable to some Cretaceous elasmosaurids (Figure 12).

(1943) used the designation based on Seeley's (1874) definition to include pectoral vertebrae in the vertebral column of elasmosaurids. Carpenter (1999) excluded pectoral vertebrae completely and only included cervical and dorsal vertebrae, with the last cervical defined as a vertebra where the rib facets extend across the centrum-spine boundary. In recent years, the decision of whether use the term pectoral vertebrae into descriptions of plesiosaurs has not been consistent. Sachs et al. (2013; 2016) and O'Gorman et al. (2017) included pectoral vertebrae in their descriptions of specimens, whereas Sato (2002), Druckenmiller and Russell (2006) and Kubo et al. (2012) did not include pectoral vertebrae. Sato (2002) mentioned pectoral vertebrae as cervical vertebrae and in contrast Druckenmiller and Russell (2006) defined pectoral vertebrae as dorsal vertebrae, which changes the total cervical count even in the same species and creates confusion. Whether pectoral vertebrae should be included as part of the vertebral column in plesiosaurs is an ongoing debate. Classifying a vertebra as either cervical or dorsal will always be challenging as the vertebral column of plesiosaurs is rarely complete when excavated and therefore the transition from cervical to dorsal vertebrae can be difficult to identify. Compared with the approach used with modern animals, identifying cervical or dorsal vertebrae in plesiosaurs as pectoral vertebrae appears rather atypical as no modern animals are classified as possessing pectoral vertebrae, and there is therefore no solid argument for plesiosaurs to be exclusive and possess pectoral vertebrae.

Plesiosaurs exhibited a great variety of neck lengths (Carpenter, 1999; Sachs *et al.*, 2013; O'Gorman and Fernandez, 2016; Otero, 2016). Neck elongation in plesiosaurs is known throughout their evolutionary history, from the Late Triassic to the Late Cretaceous (Knutsen *et al.*, 2012b; Soul and Benson, 2017). The elongation of the plesiosaur neck can be explained by the elongation of the cervical vertebrae, increase in the count of cervical vertebrae, and cervicalisation of dorsal vertebrae, or as a combination of the three (Soul and Benson, 2017). Neck length estimation of plesiosaurs is calculated as the sum of the length of each cervical vertebra (Otero, 2016).

Elasmosaurids show the most variable neck length among plesiosaurs (Carpenter, 1999; O'Keefe and Hiller, 2006; Sachs *et al.*, 2013; O'Gorman and Fernandez, 2016; Otero, 2016; Serratos *et al.*, 2017) and the most extreme case is the elasmosaurid *Albertonectes vanderveldei* (Kubo *et al.*, 2012). *A. vanderveldei* possess 76 cervical vertebrae having a neck length nearly 400 % of the length of its trunk (Soul and Benson, 2017). The neck length of *A. vanderveldei* (7 m according to Taylor and Wedel, 2013b) is the longest among all

plesiosaurs (Kubo *et al.*, 2012). The neck elongation of elasmosaurids seem to have occurred during an early stage of their evolution (Kubo *et al.*, 2012).

1.1.1.2.3 Dorsal and caudal vertebrae

The dorsal vertebrae have single-headed ribs attached and the centra are higher than long (Smith, 2007; Sachs *et al.*, 2016). During the transition from cervical to dorsal, the rib facets move from the centrum to the neural arch and become more elongate (Andrews, 1910). Caudal vertebrae decrease in size posteriorly, and the straight and laterally directed caudal ribs almost disappear completely around the last caudal (Smith, 2007).

1.1.1.3 Trunk and girdles

The trunk is situated between the shoulder girdle and pelvic girdle (Figure 13). The trunk consists of ribs found in the ventral body wall, usually with five interlocking elements per row closely packed and probably bound by tendons and muscles linking to the shoulder- and pelvic girdles (Noè *et al.*, 2017). The tightly bound trunk, combined with a ventral expansion of the shoulder and pelvic girdle plates would make the trunk relatively stiff and inflexible (Robinson, 1977).

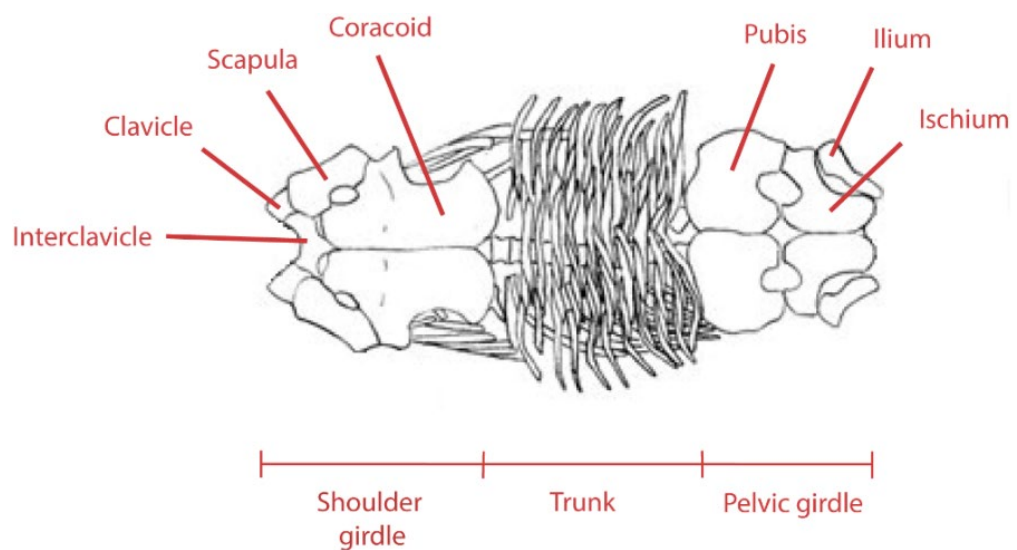


Figure 13: Ventral view of plesiosaurian morphology (*Meyerasaurus victor*) with trunk and shoulder- and pelvic girdle. Modified from Smith (2007).

The plesiosaur shoulder girdle includes an interclavicle, and a pair of clavicles, scapulae, and coracoids (Andrews, 1910; Brown, 1981), of which the latter form a surface to the forelimbs. Araújo and Correia (2015) reconstructed the shoulder musculature in plesiosaurs using basal eosauropterygian taxa and the muscles known from the extant phylogenetic bracket (Witmer, 1995) – in this case squamates and crocodiles. The study by Araújo and

Correia (2015) showed a clear variation in muscle size across the phylogenetic bracket, especially noticeable for the muscles attached to the coracoid as they tend to increase in size in more derived species (Figure 14). The disparity in the shoulder muscle over time seems to be caused by morphological limb change.

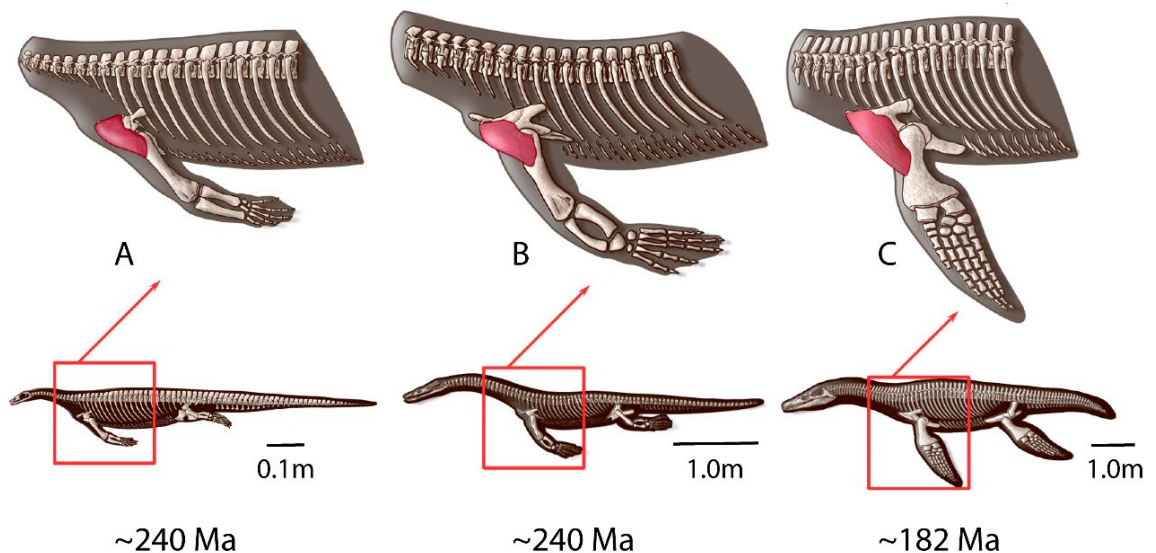


Figure 14: Reconstruction of the shoulder muscle *M. clavodeltoideus* in A) the nothosaur *Neusticosaurus* (~240 Ma), B) the lariosaur *Ceresiosaurus* (~240 Ma), and C) the pliosaur *Rhomaleosaurus* (~182 Ma). Modified from Araújo and Correia (2015).

Many Early Jurassic plesiosaurs do not develop the shoulder girdle further in juvenile specimens going into adult stage, but in Late Jurassic genera its development is typically ontogenetic with ossification being completed in the adult specimens and frequently followed by fusion of the scapulae and coracoids in old adult specimens (Brown, 1981). In several Late Cretaceous genera (e.g. *Thalassomedon*) the clavicles and interclavicle are retained in a moderately well-developed state (Brown, 1981). The species *Cryptoclidus eurymerus* exhibits such development of the shoulder girdle, with juvenile specimens possessing smaller, less ossified bones than the adults (Figure 15) (Sato *et al.*, 2018).

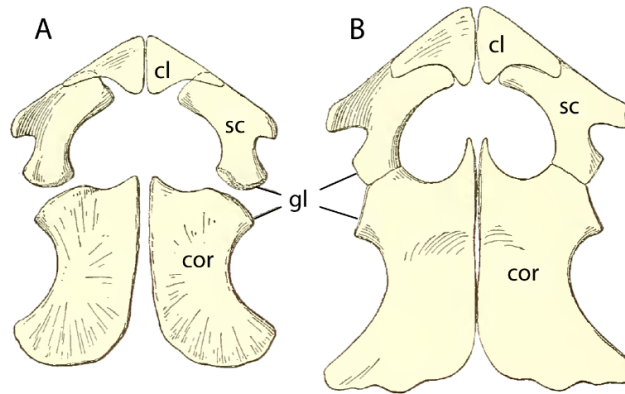


Figure 15: Ventral view of shoulder girdles from *Cryptoclidus eurymerus* (Late Jurassic). A) juvenile specimen (NHMUK R2416) and B) adult specimen. Abbreviations: cl: clavicle; cor: coracoid; gl: glenoid cavity; sc: scapula. Modified from Andrews (1910).

The pelvic girdle is composed of pairs of pubes, ischia, and ilia (Sato, 2002). In the pelvic girdle the ischium is relatively short in long-necked species and relatively long in short-necked large-skulled species (Brown, 1981). The ilium can become narrow proximally, or remain broad, and no evolutionary trends in ilium development have been demonstrated (Brown, 1981). The connection between the pelvic girdle and the vertebral column is generally reduced in plesiosaurs (Vincent *et al.*, 2017a), and ontogenetic development is also visible in the pelvic girdle (Figure 16).

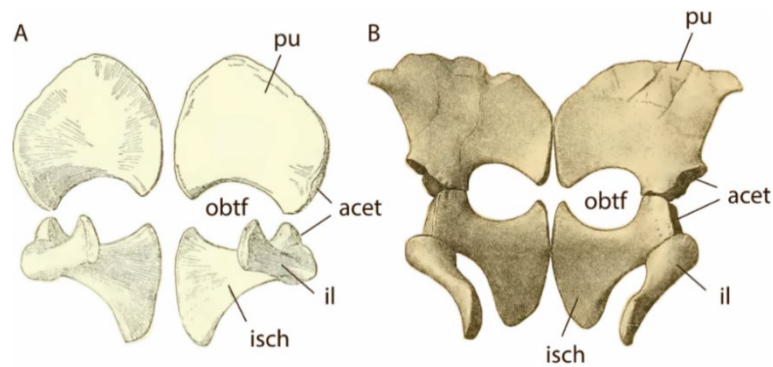


Figure 16: Ventral view of pelvic girdles of *Cryptoclidus eurymerus* (Late Jurassic). A) juvenile specimen (NHMUK R2417) and B) adult specimen (NHMUK R2616). Abbreviations: acet: acetabulum; il: ilium; isch: ischium; obtf: obturator foramen; pu: pubis. Modified from Andrews (1910).

1.1.1.4 Limbs

The basic tetrapod limbs can be observed in the earliest plesiosaurs, and the transition from plesio-pedal limbs to hydro-pedal limbs (so-called flippers) can be seen with the modification into paddles (Carpenter *et al.*, 2010; Benson, 2013). The transition shows a clear increase in the number of phalanges (Figure 17), and connective tissue between digits were lost over time (Welles, 1943; Caldwell, 2002). The transition to a fully aquatic mode of life would

therefore have occurred sometime before the Late Triassic (Benson and Druckenmiller, 2014).

The front flippers are generally slightly larger than the hind flippers (Sachs and Kear, 2015). The four flippers share a hydrofoil-shaped form and possess propodials (humerus in front flippers and femur in hind flippers), epipodials (radius and ulna in front flippers and tibia and fibula in hind flippers), mesopodials, metapodials, and phalanges (Figure 17). Unlike ichthyosaurs, plesiosaurs did not alter the metapodial rows, and maintained five metapodials throughout their lineage (Caldwell, 2002).

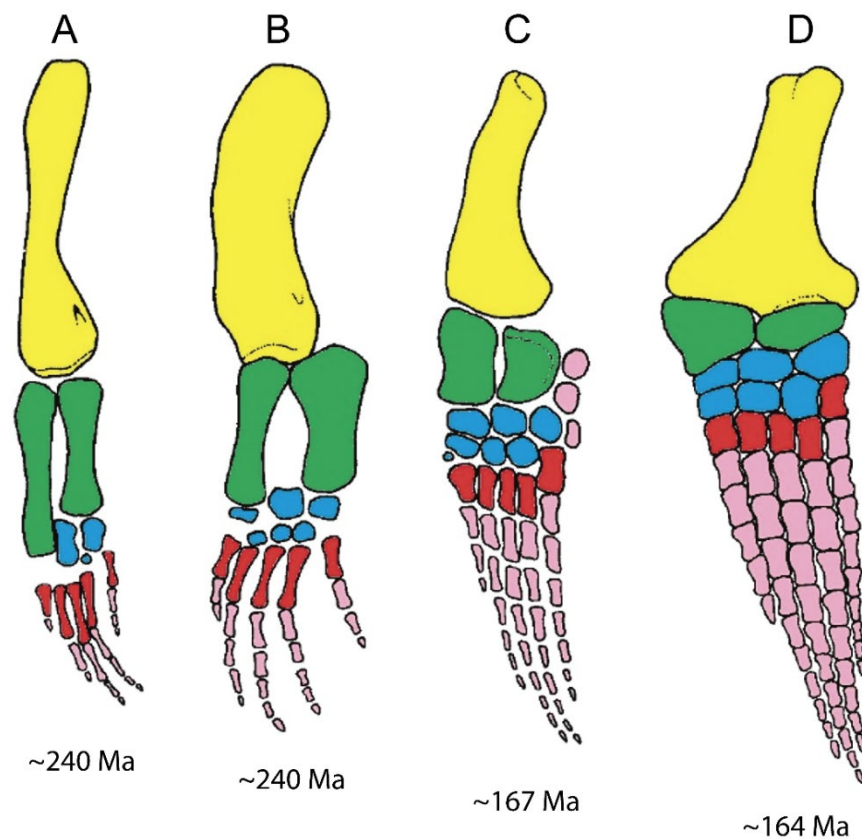


Figure 17: Evolution (in the order left to right) of sauropterygian forelimbs. Not to scale. (A) The pachypleurosaur *Neusticosaurus* (~240 Ma); (B) The nothosaurid *Ceresiosaurus* (~240 Ma); (C) The Early Jurassic plesiosaur *Thaumatosaurus* (~167 Ma); (D) The Late Jurassic plesiosaur *Cryptoctidus eurymerus* (~164 Ma). Yellow = propodials (humerus bone), green = epipodials (left: radius bone, right: ulna bone), blue = mesopodials, red = metapodials, pink = phalanges and accessory ossicles. Modified from Storrs (1993).

In short-necked, large-skulled species (which also have elongated ischia), the femur is larger than the humerus, and both propodials tend to have a slim and elongated appearance (Brown, 1981). In all other species the propodials are either equal in size or the humerus is slightly larger than the femur, and these propodials have a more short and stout appearance (Brown, 1981). The epipodials of early species are elongate and dumb-bell shaped, recalling the shape

of the epipodials of a terrestrial ancestor (Brown, 1981; Storrs, 1993). There is a trend throughout the entire order for the epipodials to shorten and widen until they resemble mesopodials in shape, and they are considerably broader than long (Brown, 1981).

Early Jurassic plesiosaur species show hyperphalangy, with up to about ten phalanges in the longest digit, and this is increased to a maximum of nineteen phalanges in the longest digit in Late Jurassic species (Brown, 1981; Storrs, 1993; Caldwell, 2002). The characteristic feature starts in early plesiosaurs for both fore- and hindlimbs (Storrs, 1993; Caldwell, 2002). Ancestral pachypleurosaurs and nothosaurids from the Triassic possessed a forelimb phalangeal count of 1-2-3-4-3 (Figure 17A) and 2-4-5-5-3 (Figure 17B), respectively. The Early Jurassic plesiosaur *Thaumatosauros* had a forelimb count of 3-6-8-8-10 (Figure 17C), while the Late Jurassic *Cryptoclidus eurymerus* (Figure 17D) possessed a 5-10-11-9-9 phalangeal count (Storrs, 1993; Caldwell, 2002).

With the reduction of intralimb flexibility, having hyperphalangy and interlocking phalanges, and the appearance of extra ossification in the limbs, allowed plesiosaurs to effectively perform forward locomotion by using the limbs for propulsion (Andrews, 1910; Storrs, 1993; Benson *et al.*, 2012b). Using limbs as the dominant way to achieve forward locomotion is also seen in turtles (Storrs, 1993; Callaway and Nicholls, 1997; Caldwell, 2002). Early work in this area suggested that plesiosaurs used single forward-and-backward rowing strokes (Watson, 1924) while later studies argued a subaqueous flight movement was more likely (Robinson, 1975; Massare, 1994) which is also seen in modern sea lions and penguins (Godfrey, 1985). However, the most recent study indicates a four-flipper swimming style which would also be a very effective system to apply for plesiosaurs (Muscutt *et al.*, 2017). Thus, plesiosaurs could have applied several swimming styles (analogue to the gait of horses), but how the animals essentially swam has been, and is still being, heavily debated (Taylor, 1981, 1986; Halstead, 1989; Massare, 1994; O'Keefe, 2002; Liu *et al.*, 2015; Sennikov, 2015). Additionally, another recent study has suggested a specific elasmosaurid specimen discovered in Antarctica to be a slow swimmer due to the presence of osteosclerosis in its bones, which can also be seen in modern manatees (Ossa-Fuentes *et al.*, 2017). Osteosclerosis is a lack of central cavity in the bone as the bone tissue herein has been replaced with calcified cartilage, making it hard for the animal to move rapidly (Ossa-Fuentes *et al.*, 2017). This finding indicates a likely diversity in the locomotion, speed, and subsequently ecology of plesiosaurs.

1.1.1.5 Ontogeny

Young plesiosaur specimens have been found in great numbers (Welles and Gregg, 1971; Brown, 1981; Cruickshank, 1994; Carpenter, 1999; Gasparini *et al.*, 2003; Kear, 2006; Martin *et al.*, 2007; Knutsen, 2012b; O'Gorman *et al.*, 2013, 2016b, 2018a; Otero *et al.*, 2014a, 2017; Frey *et al.*, 2017; O'Keefe *et al.*, 2017; Ossa-Fuentes *et al.*, 2017; Vincent *et al.*, 2017a; O'Keefe *et al.*, 2019), and characters such as small overall size, and a lack of fusion between certain significant bones are indications of a juvenile plesiosaur (Brown, 1981; Cruickshank, 1994). Neural arches and cervical/caudal ribs are fused in adult specimens (Figure 9A-F), but free in juvenile specimens (Figure 9G-J) (Brown, 1981; Evans, 1999). Neural spines tend to be relatively higher in juvenile specimens than adults, and the bony part of the neural spines is proportionally shorter in juvenile specimens since they are terminated in cartilage (Brown, 1981). Usually skull and girdle elements are not fused in juveniles (Andrews, 1910; Brown, 1981; Cruickshank, 1994; Otero *et al.*, 2017) and their pubes seem to be rounded (Brown, 1981). Concerning age, juvenile individuals of *C. eurymerus* has a length approximately 20 % less than the corresponding centra of an old adult individual of the same species (Brown, 1981). Generally, the vertebrae of juvenile specimens are smoother in appearance compared to older individuals, which have a more rough and wrinkled surface (Brown, 1981). Furthermore, the total neck length comparison between juvenile and adult plesiosaurs has previously been studied by Brown (1981) by comparing VLI (Equation 1) of the vertebral column. The study by Brown (1981) showed that the vertebral column of *C. eurymerus* had a correspondingly growing tendency, indicating that plesiosaurs increased in length of the cervical vertebrae as they aged. For elasmosaurids, the ontogenetic changes of cervical proportions that have been recorded seems mostly related to vertebral elongation (O'Keefe and Hiller, 2006).

A recent study (O'Gorman *et al.*, 2016b) analysed specimen MLP 14-I-20-8 using the VLI to test whether the specimen was of juvenile or adult age. O'Gorman *et al.* (2016b) found that the specimen corresponds to a juvenile of *Aristonectes quiriquinensis*. The adult stage of this species would have been around 8 m (Otero *et al.*, 2014a) and the estimated body length of the juvenile would be around 3.7-5.7 m (O'Gorman *et al.*, 2016b). Another issue surrounding the aristonectines is the explanation for the large quantity of specimens that show juvenile morpho-osteological features (O'Gorman *et al.*, 2014). Some specimens from this taxon show relatively large sized elements compared to other juvenile elasmosaurids (Otero *et al.*, 2012; O'Gorman *et al.*, 2013). One explanation for this pattern is that the

aristonectines retain juvenile features until they reach larger sizes relative to other elasmosaurids (O'Gorman *et al.*, 2014, 2016b), which makes sense comparing with statements made previously in the study by Martin *et al.* (2007).

1.1.1.6 Body proportions

The great diversity in body proportions among plesiosaurs is unlike the early Triassic forms such as the placodonts, pachypleurosaurs, nothosaurs and pistosaurs (Soul and Benson, 2017), and plesiosaurian morphology and size was made possible through their aquatic lifestyle. Large body sizes and long necks that would be problematic on land were supported in the water through buoyancy. However, following the worldwide increase in diversity of plesiosaurs in the Early Jurassic (e.g. Brown, 1981; Callaway and Nicholls, 1997), they did not deviate far from the basic structural and adaptive framework from the earliest forms found in the Late Triassic (e.g. O'Keefe, 2002).

The definition of neck length is, according to Benson *et al.* (2012a), the length from the atlas-axis complex to the last cervical vertebrae. Additionally, defined by Benson and colleagues (2012a), trunk length is the distance between the anterior surface of the anterior-most vertebrae with an elongate “dorsalised” rib and the posterior surface of the posterior-most dorsal vertebrae. The ratio between neck and trunk can, according to Benson and colleagues (2012a) be used as a representation for overall body proportions, and is adopted in Figure 18 to illustrate the diversity of neck/trunk ratios among plesiosaurians.

The neck/trunk ratio is the main feature that increased in diversity in plesiosaurs from Late Triassic to Late Cretaceous (Figure 18), especially in members of the Elasmosauridae family. The Late Triassic and Early Cretaceous plesiosaurian fossil record are generally scarce (Sachs *et al.*, 2017; Wintrich *et al.*, 2017a) and therefore missing in the plesiosaur fossil record in Figure 18. The second most dominant body proportion that change in plesiosaurs is the head size, and pliosaurs generally possess larger skulls than plesiosaurs (Storrs, 1993; O'Keefe, 2002).

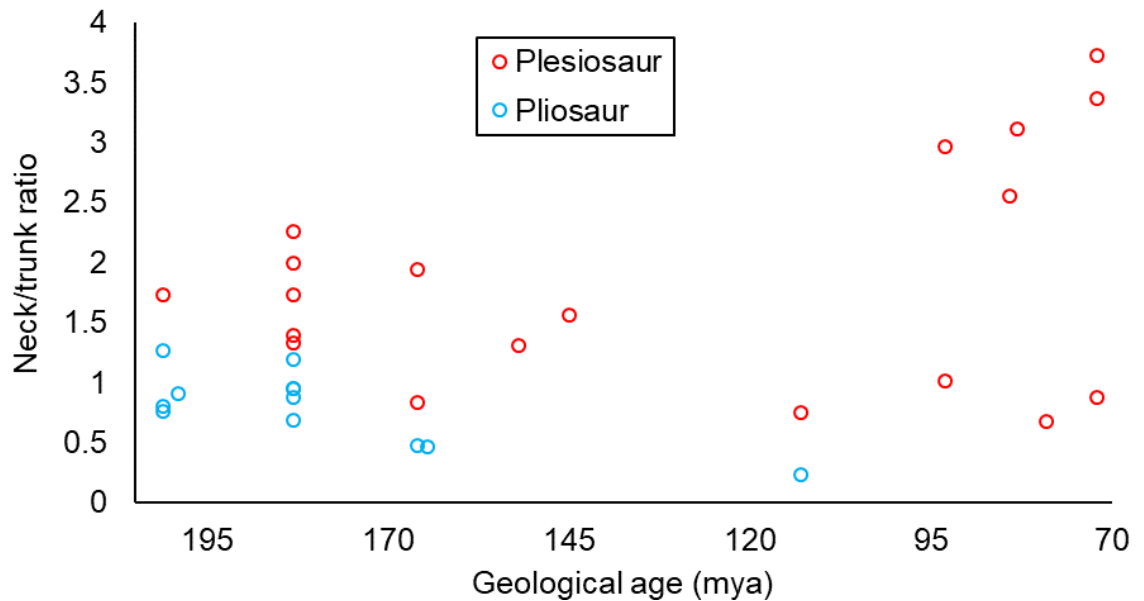


Figure 18: Body proportions (neck/trunk ratio) in plesiosaurs from different geological ages from Late Triassic to Late Cretaceous. Data from Conybeare (1824), Stutchbury (1846), Owen (1865), Cope (1869), Seeley (1874), Dames (1895), Williston (1904, 1906), Andrews (1910, 1913), Fraas (1910), Smellie (1917), Huene (1923), White (1940), Welles (1943, 1952, 1962), Welles and Bump (1949), Brown (1981), Sciau et al. (1990), Taylor (1992), Cruickshank (1994), Callaway and Nicholls (1997), Bardet et al. (1999), Carpenter (1999), O'Keefe (2001b, 2002, 2004), Cruickshank and Fordyce (2002), Sato (2002, 2003), Buchy et al. (2005), Everhart (2005), Druckenmiller and Russell (2006, 2008b), Sato et al. (2006), Grossmann (2007), Smith (2007), Smith and Dyke (2008), Ketchum and Smith (2010), Smith and Vincent (2010), Vincent and Taquet (2010), Benson et al. (2011), Ketchum and Benson (2011), Vincent (2011), Benson et al. (2012a), Evans (2012), Knutsen et al. (2012b), Kubo et al. (2012), Otero et al. (2014a), Sachs et al. (2016), Frey et al. (2017), Soul and Benson (2017), Vincent et al. (2017a), Fischer et al. (2018), and Otero et al. (2018).

The distribution of body proportions among plesiosaurs (Figure 18) from the earliest to the latest forms (Welles and Bump, 1949; Welles, 1952; O'Keefe and Carrano, 2005; Benson *et al.*, 2012a) have been studied and have shown the largest ratio to be among elasmosaurids (Welles and Bump, 1949; Welles, 1952; Benson *et al.*, 2012a). Indeed, Late Cretaceous elasmosaurids have necks representing up to 2/3 of their total body length (Bardet *et al.*, 2014) making them the most extreme cases of neck elongations amongst plesiosaurs.

1.1.4 Phylogeny, taxonomy and ecological categorisation

Plesiosaur genera and species names have changed a lot in the last 50 years, as more specimens have been discovered (Tutin and Butler, 2017) helping to solve many previous taxonomic issues. This difference is especially clear when comparing the lists of valid plesiosaur species in the studies by Welles (1962) and Smith (2007) created 45 years apart, and our understanding of the systematics of plesiosaurs has developed through a number of phases, reflecting changes in evolutionary thought and methodologies (Smith, 2007).

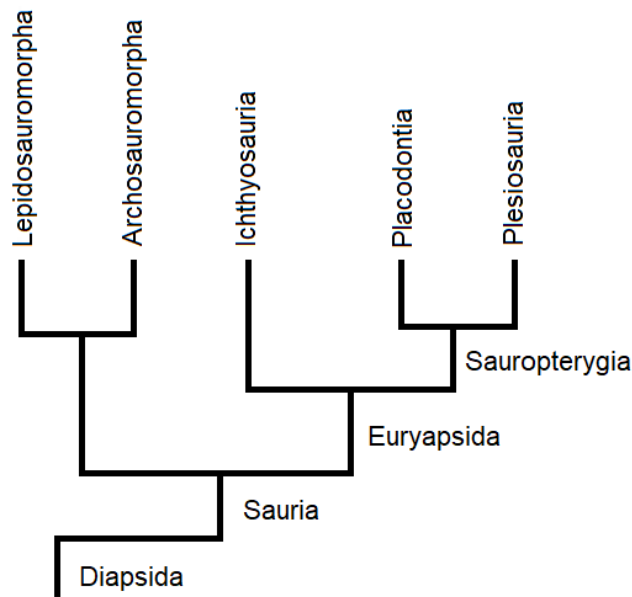


Figure 19: Simplified phylogenetic relationships of diapsid marine reptile lineages. Modified from Sobral et al. (2016).

Plesiosaurs are diapsid reptiles, more closely related to ichthyosaurs than archosaurs and lepidosaurs (Figure 19). The order Plesiosauria derives from Sauropterygia that contain two clades; the Placodontiforms and the Eosauropterygia, both appearing in the Early Triassic (Sobral *et al.*, 2016). In total, Sauropterygia includes more than 110 genera and more than 170 species (Benson, 2013; Bardet *et al.*, 2014), being the largest and most diverse group of ancient marine reptiles to have lived through nearly the entire Mesozoic Era (Cheng *et al.*, 2004; Smith and Vincent, 2010; Sobral *et al.*, 2016). Eosauropterygians include pachypleurosaurs, nothosaurs, pistosaurs, and plesiosaurs (Sobral *et al.*, 2016). The clade experienced its greatest diversity in the Triassic with only plesiosaurs making it to the Triassic-Jurassic boundary (Sobral *et al.*, 2016). The order Plesiosauria appears in the Late Triassic (Taylor, 1992; Sobral *et al.*, 2016).

The earliest classifications of plesiosaurs placed considerable weight upon the number of cervical rib facets, the length of the neck, and the number of vertebrae comprising the cervical series (Williston, 1907; Brown, 1981). In 1994, Brown and Cruickshank then offered a classification of plesiosaurs based on skull characters.

Table 1: Terms and definitions of plesiosaurians. From Ketchum and Benson (2010).

Term	Definition
<p>plesiosaurian</p> <p>(All taxa more closely related to <i>Plesiosaurus dolichodeirus</i> and <i>Pliosaurus brachydeirus</i> than to the piosaur <i>Augustasaurus hagdorni</i>).</p>	A member of plesiosauria.
<p>plesiosauroid</p> <p>(All taxa more closely related to <i>Plesiosaurus dolichodeirus</i> than to <i>Pliosaurus brachydeirus</i>).</p>	A member of plesiosauroidea.
<p>pliosauroid</p> <p>(All taxa more closely related to <i>Pliosaurus brachydeirus</i> than to <i>Plesiosaurus dolichodeirus</i>).</p>	A member of pliosauroidea.
‘plesiosauromorph’	A plesiosaurian with the ‘plesiosauromorph’ body plan, showing a relatively long neck and small head, short coracoids, short ischia and high aspect ratio limbs.
‘pliosauromorph’	A plesiosaurian with the ‘pliosauromorph’ body plan, showing a relatively short neck and large head, long coracoids, long ischia and low aspect ratio limbs. Some ‘pliosauromorphs’ (Polycotyliidae) may be plesiosauroids.

Later studies suggested the plesiosaurians should be divided into two general morphotypes; pliosauromorphs and plesiosauromorphs (Table 1 and Table 2) (O’Keefe, 2001b, 2002; Ketchum and Benson, 2010), because of the size of the skull (Taylor, 1992) which reflects ecological differences (Massare, 1987, 1988). Other dissimilarities in the two types include the neck, as well as teeth, head, scapula and limbs. Both morphotypes share the feature of the trunk and tail both being relatively short (Callaway and Nicholls, 1997), with the body plan of pliosauromorphs evolving two times (Rhomaleosauridae and Pliosauridae) and the long necks of plesiosauromorphs evolving in three clades (Leptocleididae, Plesiosauroidea and Elasmosauridae) (O’Keefe, 2001a, 2002; Ketchum and Benson, 2010; Druckenmiller and Knutsen, 2012; Knutsen *et al.*, 2012b; Benson and Druckenmiller, 2014).

Several genera in Leptocleididae, such as *Leptocleidus*, *Nichollssaura* and *Vectocleidus*, exhibit intermediate body plans between plesiosauromorph and pliosauromorph (Benson *et al.*, 2012b). However, this intermediate placement of plesiosaurs is to date still under debate as to which specific species are intermediates and which are within plesiosauromorph and pliosauromorph.

Table 2: The recognised division of plesiosaurians as two morphotypes and their variances in body characters; neck, teeth, skull, scapula, limbs, and ischium.

Body	Plesiosauromorph	Pliosauromorph
<i>Neck</i>	<ul style="list-style-type: none"> - Long (Taylor, 1992) and slender (Chatterjee and Small, 1989) - Number of cervical vertebrae: between 16 and 76 (Williston, 1906; Brown, 1981; Callaway and Nicholls, 1997; Druckenmiller and Russell, 2008b; Otero, 2016; Fischer <i>et al.</i>, 2018) - Dimensions of cervical vertebrae: As long as or longer than wide (Brown, 1981; O'Keefe, 2002) 	<ul style="list-style-type: none"> - Short (Chatterjee and Small, 1989; Taylor 1992; O'Gorman <i>et al.</i>, 2018b) - Number of cervical vertebrae: 13 to 28 (Brown, 1981; O'Keefe, 2002; Sato, 2002; Ellis, 2003; Smith and Vincent, 2010) - Dimensions of cervical vertebrae: Shorter than wide (Brown, 1981; O'Keefe, 2002)
<i>Teeth</i>	<ul style="list-style-type: none"> - Numerous fine-pointed recurved teeth serving as trap for small fish and cephalopods (Smellie, 1917; Halstead, 1989; Taylor, 1992) - Filter or straining feeders on smaller fish and crustaceans (Brown, 1981; Chatterjee and Small, 1989) - Slim crowns not showing wear on their tips (Cruickshank, 1994) 	<ul style="list-style-type: none"> - Enlarged, massive and stubby with characteristics of cephalopod feeders (Halstead, 1989; Cruickshank, 1994) - Fed on a wider range of prey sizes (Taylor, 1992) - Sometimes showing wear on their tips (Cruickshank, 1994)
<i>Skull</i>	<ul style="list-style-type: none"> - Relatively small (Brown, 1981; Chatterjee and Small, 1989; Taylor, 1992; Cruickshank, 1994; O'Keefe, 2002) - Short mandibular symphysis (Chatterjee and Small, 1989; Druckenmiller, 2002) 	<ul style="list-style-type: none"> - Relatively large (Brown, 1981; Chatterjee and Small, 1989; Taylor, 1992; O'Keefe, 2002; Knutsen, 2012a; O'Gorman <i>et al.</i>, 2018b) - Long mandibular symphysis (Chatterjee and Small, 1989)
<i>Scapula</i>	<ul style="list-style-type: none"> - Relatively long (Brown, 1981; O'Keefe, 2002) - Median contact of scapulae with associated lengthening of these bones along the anterior-posterior axis (O'Keefe, 2002). 	<ul style="list-style-type: none"> - Relatively short (Brown, 1981; O'Keefe, 2002) - Ischium tends to be relatively long when compared with the pubis (O'Keefe, 2002).
<i>Limbs</i>	<ul style="list-style-type: none"> - Longer forelimbs than hind (Brown, 1981; O'Keefe, 2002) - Specialized for speed (Halstead, 1989). 	<ul style="list-style-type: none"> - Hind limbs longer than forelimbs (Brown, 1981; O'Keefe, 2002) - Specialized for power (Halstead, 1989).
<i>Ischium</i>	<ul style="list-style-type: none"> - Relatively short (Brown, 1981; O'Keefe, 2002) 	<ul style="list-style-type: none"> - Relatively long (Brown, 1981; O'Keefe, 2002)

1.1.5 Foraging and feeding strategies

Aquatic tetrapods use their head, neck and body in a combination to catch and eat their prey (Taylor, 1987) and the same was true for plesiosaurs. As head characters determine the drag exerted by the surrounding water during sideways sweeps, plesiosaur heads are slender, and particularly shallow in depth presenting a minimum cross-sectional area to the oncoming water (Taylor, 1987). The small head relative to the body size of plesiosaurs could therefore allow fast acceleration of the mouth for capturing elusive prey, as observed in today's fish-eating long-necked birds (Wilkinson and Ruxton, 2012). Another advantage of the long neck could be that it enabled the head to encounter groups of small prey before the large body could be detected (Callaway and Nicholls, 1997). Cryptoclidids have revealed a palate and cheek regions showing no adaptations for resisting torsional forces upon the jaws meaning that cryptoclidids were only capable of eating small soft-bodied prey (Brown and Cruickshank, 1994).

A study by Rothschild and Storrs (2003) found evidence of decompression syndrome in plesiosaur humeri and femora which could indicate a deep-diving lifestyle. Decompression syndrome (also called avascular necrosis) is a pathology which includes the lack of blood supply to the bone and the bone tissue therefore dies (Rothschild, 1982). The evidence of decompression syndrome is seen in some of the basal plesiosaurs (Plesiosauridae) but also in some of the later forms (Elasmosauridae and Polycotylidae) (Rothschild and Storrs, 2003). Thus, it appears that some plesiosaurs did not develop any specific physiological adaptation to deep diving (Rothschild and Storrs, 2003).

By studying the teeth of plesiosaurs, and comparing them with modern animals such as crocodiles, it has been proposed that pliosauromorphs would have had the ability to feed on large prey (Taylor, 1987). Due to their large skulls, jaws and deeply rooted teeth, pliosauromorphs would have been capable of biting pieces of the prey before swallowing it whole (Taylor, 1987).

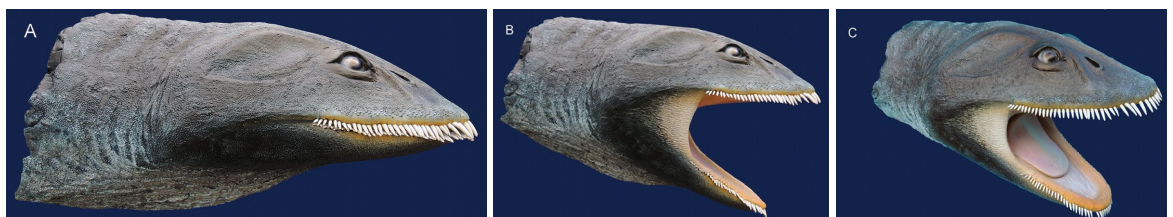


Figure 21: Life reconstruction of *Morturneria seymourensis* by Stephen J. Godfrey presenting the oral cavity of this species A = mouth closed, B = mouth open, C = oblique view with mouth open. From O'Keefe et al. (2017).

The adaptation to filter feeding (as seen in whales and birds) is generally rare in Mesozoic marine reptiles (O'Keefe *et al.*, 2017) and was previously thought to be anatomically impossible for plesiosaurs due to the lack of a secondary palate (Sanderson and Wassersug, 1993; Collin and Janis, 1997). However, a recent study by O'Keefe *et al.* (2017) found the aristonectine elasmosaur *Morturneria seymourensis* to have lower and upper dentition that formed an oral battery. This trait could plausibly function like a sieve by removing food particles from substrate excluded from the oral cavity (Figure 21), indicating that this plesiosaur had a whale-like filter-feeding behaviour (Noè, 2006) which is the first of its kind found among all plesiosaurs (O'Keefe *et al.*, 2017). In fact, the evolution of filter feeding in Late Cretaceous elasmosaurs mirrors that of baleen whales living 30 million years after the elasmosaurs went extinct (O'Keefe *et al.*, 2017). Furthermore, elasmosaurs have also been stated to possess replacement teeth as seen in sharks (Kear *et al.*, 2017), indicating elasmosaurs adapted to other feeding styles than earlier forms, e.g. by feeding on harder prey which was swallowed whole and processed by gastroliths in the gut.

Foraging preferences have been identified for numerous plesiosaurs from stomach contents of various kinds, including fragments of fish bone, cephalopods (squid, belemnites and ammonites) (Cope, 1869; Brown, 1904; Callaway and Nicholls, 1997; Sato and Tanabe, 1998; Curimurri and Everhart, 2001), bivalve shells, gastropods, pieces of crinoid (McHenry *et al.*, 2005), and even an ichthyosaur embryo (O'Keefe *et al.*, 2009) has been discovered in association with the abdomen of a plesiosaur skeleton. In elasmosaurids the prey was probably swallowed whole, as elasmosaurian teeth were not suitable for crushing shells (Brown, 1904; Sato and Tanabe, 1998). This could indicate that some plesiosaurs were not only specialised in capturing free-swimming prey but also feed on nekton and bottom-dwelling invertebrates (McHenry *et al.*, 2005; Otero *et al.*, 2018). Furthermore, Cope (1872) reported the remains of a juvenile mosasaur inside an elasmosaur, and even a pterodactyl bone has been discovered inside the stomach area of an elasmosaurid (Cope, 1869; Massare, 1987). This could indicate that at least elasmosaurids were able to catch prey from above water. However, it could also indicate a drowning pterodactyl ending up dying in the same spot as this elasmosaurid's foraging area, making it an easy meal for the animal. The stomach content of elasmosaurs also raises the possibility of a dietary shift occurring in the history of the elasmosaurid family, suggesting that the long elasmosaurid neck does not indicate a narrow feeding ecology (McHenry *et al.*, 2005).

Due to their long neck, plesiosaurs would most likely have used ambush to catch their prey, as the potential prey would not be able to spot the long neck if the plesiosaur approached its prey directly from the front (Massare, 1988; Callaway and Nicholls, 1997; Zammit *et al.*, 2008; Wilkinson and Ruxton, 2012). Massare (1994) calculated the relative swimming speed of plesiosaurs by using estimated values of drag coefficient and surface area of a prolate spheroid of 2 m³, and hypothesized the speed to be relatively slow, around 3-5m/s. If this was the case, it is reasonable to imagine that plesiosaur relied more on surprise or stealth than pursuit (Callaway and Nicholls, 1997; Wilkinson and Ruxton, 2012).

Besides the vertebrate and invertebrate remains found in the stomach region of several elasmosaurids and other plesiosaurs, a number are also found with gastroliths preserved, which includes adults as well as juveniles (Welles and Bump, 1949; Shuler, 1950; Darby and Ojakangas, 1980; Taylor, 1981; Taylor and Cruickshank, 1993; Curimurri and Everhart, 2001; Martin *et al.*, 2007; Druckenmiller and Russell, 2008b; O'Gorman *et al.*, 2012; Otero *et al.*, 2014a; Vincent *et al.*, 2017a). When present, the gastroliths are usually found in quite small numbers (O'Gorman *et al.*, 2012). In an extreme case a staggering 2626 gastroliths were found in one elasmosaurid specimen (Thompson *et al.*, 2007). The diversity in the number of stones could correspond to a temporal, behavioural or physiological difference among plesiosaurs, as the two elasmosaurids with the most stones found have been discovered in Antarctica (high-latitude) and thus might differ from those at lower latitudes (Thompson *et al.*, 2007; O'Gorman *et al.*, 2012).

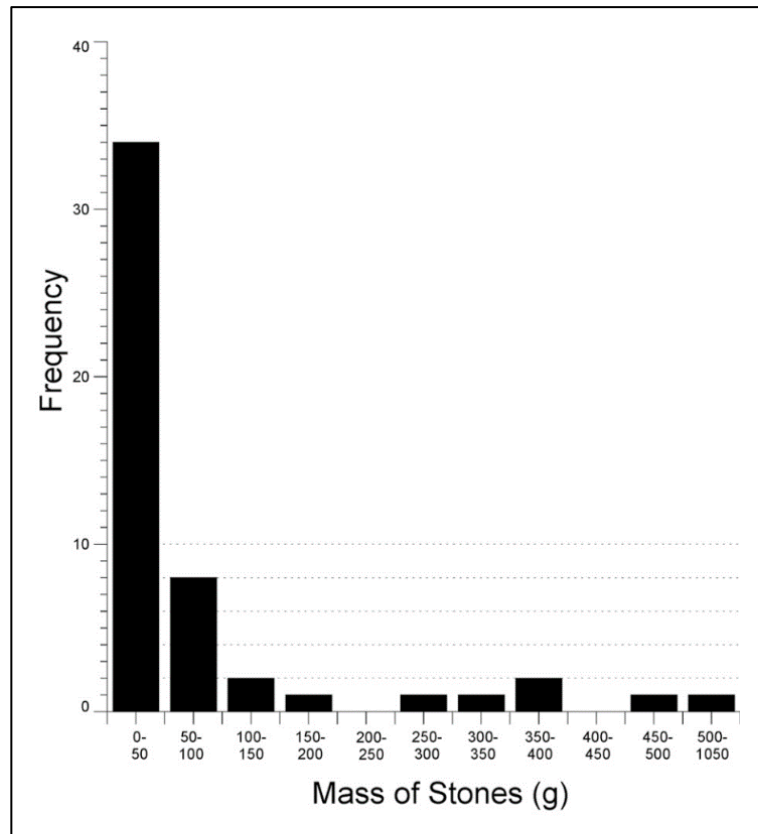


Figure 22: Gastrolith mass frequency; here shown with the gastroliths found in *Albertonectes vanderveldei* as an example. From Kubo et al. (2012).

Considering the generally small weight of the stones (Table 3; Figure 22) it is not surprising that so many specimens contain them (Brown, 1904). A total weight of 13 kg in gastroliths has been found in one specimen with an average weight of 313g per stone (Everhart, 2000). However, it seems that the normal mass frequency for these stone is in between 0-50g in general, and only a few stones would exceed this (Figure 22). The maximum diameter is around 170 mm and the maximum weight for one stone is around 1500g (Table 3). These dimensions seem reasonable as plesiosaurs were generally quite large animals: a mass of 7500 kg for a plesiosaur of 14 m in total body length (Alexander, 1989), about 2000 kg for a plesiosaur of 2.8-3.7 m in total body length (Massare 1994) and 2800 kg for a plesiosaur of 9 m in total body length (Everhart, 2000). Furthermore, Everhart (2000) concluded the total mass of the stones would only be around 1 % of the mass of the plesiosaur and therefore insignificant with respect to using the stones as ballast for buoyancy. Gastroliths have mainly been found in elasmosaurids (Table 3) which are the largest plesiosaurians.

Table 3: Number of gastroliths found in different plesiosaur specimens and one shark including (where possible) maximum diameter (mm), average diameter (mm), maximum weight (g), average weight (g), total weight (g), and their respective references.

Specimen no. and species	Family	Number of gastroliths	Max diameter (mm)	Max weight (g)	Average weight (g)	Total weight (g)	References
<i>Aristonectes quiriquinensis</i>	Elasmosaurid	5	70	N/A	N/A	N/A	Otero et al. (2014a)
<i>Tuarangisaurus keyesi</i>	Elasmosaurid	23	30	N/A	N/A	N/A	Otero et al. (2017)
Unknown	Elasmosaurid	40	N/A	N/A	N/A	N/A	Sato et al. (2006)
KUVP 129744	Elasmosaurid	47	170	1490	313	13078	Everhart (2000)
<i>Elasmosaurus/Libonectes morgani</i>	Elasmosaurid	70	N/A	N/A	N/A	N/A	Shuler (1950)
NJSM 15435 (<i>Styxosaurus</i> sp.)	Elasmosaurid	95	151	1060	79	6800	Carpenter (1999); Everhart (2000); Curimurri and Everhart (2001); Thompson et al. (2007)
TMP 2007.001.0001 (<i>Albertonectes vanderveldei</i>)	Elasmosaurid	97	135	1095	N/A	9050	Kubo et al. (2012)
SAM P24560 (<i>Opallionectes andamookaensis</i>)	Elasmosaurid	107	129.55	N/A	N/A	2762	Kear (2006)
<i>Nichollsia</i>	Leptocleidid	120	25	N/A	N/A	N/A	Druckenmiller and Russell (2008b)
SDSM 77499 (<i>Styxosaurus</i>)	Elasmosaurid	124	N/A	183	N/A	2218	Thompson et al. (2007)
KUVP 1318	Elasmosaurid	125	68	170	N/A	N/A	Williston (1893); Everhart (2000)
<i>Styxosaurus</i> sp.	Elasmosaurid	197	114	662	45	8841	Darby and Ojakangas (1980); Carpenter (1999)
FMNH 12009 (<i>Hydralmosaurus serpentinus</i>)	Elasmosaurid	206	102	417	N/A	N/A	Riggs (1939); Carpenter (1999)
SDSM 451 (<i>Styxosaurus snowii</i>)	Elasmosaurid	253	128	580	33	8249	Welles and Bump (1949); Carpenter (1999)
MNA V10046 (<i>Dolichorhynchops</i> sp.)	Polycotylid	289	34.5	18.5	N/A	518	Schmeisser and Gillette (2009)
Unknown	Elasmosaurid	389	N/A	N/A	N/A	N/A	Cerda and Salgado (2008); Schmeisser and Gillette (2009)
<i>Aristonectes</i> sp.	Elasmosaurid	560	N/A	N/A	N/A	N/A	O'Gorman et al. (2012)
MLP 98-I-10-9	Elasmosaurid	2626	N/A	46	N/A	3021	Thompson et al. (2007)

The gastroliths generally tend to be smooth and well rounded (Figure 23) (Curimurri and Everhart, 2001), and some even exhibit a high degree of polish while others appear dull or waxy (Everhart, 2000). Gastroliths mostly appear oval and it is inferred that they must have resided in the stomach for a long time to get this shape (Everhart, 2000). The polish of the stones may have been the result of internal scratching within the plesiosaurs, as the stones are usually found in the abdominal region (e.g. Welles and Bump, 1949; Shuler, 1950; Darby and Ojakangas, 1980; Martin *et al.*, 2007; O'Gorman *et al.*, 2012; Otero *et al.*, 2014a).



Figure 23: Gastroliths from KUV 129744. Scale bar = 10 cm. From Everhart (2000).

Various purposes regarding the use of gastroliths have been proposed in the literature: grinding food (Seeley, 1877; Brown, 1904; Williston, 1904; Andrews, 1910; Moodie, 1912; Shuler, 1950; Darby and Ojakangas, 1980; Martin and Kennedy, 1988; Everhart, 2000; Curimurri and Everhart, 2001; Ellis, 2003; McHenry *et al.*, 2005; Kear, 2006), neutralization of upward buoyancy (Brown, 1904; Darby and Ojakangas, 1980; Storrs, 1981, 1993; Taylor, 1981, 1994; Taylor and Cruickshank, 1993; Ellis, 2003; Kear, 2006), swallowed accidentally (lithophagy) while feeding on prey living at the bottom of the ocean (Darby and Ojakangas, 1980; Everhart, 2000; Kubo *et al.*, 2012), or even ingested for the minerals that they contain (geophagy) (Everhart, 2000). If the stones were swallowed it could provide an idea of the cross-sectional area of the largest prey that could have been ingested by the plesiosaur (Curimurri and Everhart, 2001). Because most documented gastroliths consist of granite, quartz, or other insoluble minerals, it seems unlikely that geophagy is a valid explanation (Everhart, 2000). Alternatively, the stones could simply be a matter of current transport carrying the stones to the site of the plesiosaur corpse. However, Darby and Ojakangas

(1980) tested this possibility by observing beach and river pebbles, and found that the stones did not get as smooth as the gastroliths found preserved inside plesiosaur fossils.

The use of gastroliths for buoyancy regulation can be seen in modern crocodiles (Darby and Ojakangas, 1980; Curimurri and Everhart, 2001), and the buoyancy depends in part on the animal's contained gas, and therefore on the surrounding pressure and depth (Taylor, 1994). However, the hypothesis that gastroliths consumed by plesiosaurs were used for neutralization of upward buoyancy has been rejected by Henderson (2006) by performing a computational study of the effects of gastroliths in plesiosaurs. The study showed that the necks of plesiosaur would not have been able to be maintained above water because of unbalanced centre of buoyancy acting on the body (Henderson, 2006). In addition, the amount of gastroliths needed to make an impact on plesiosaur buoyancy showed to be more than 10 % of the animal's total body mass, and this does not seem possible as the number of stones found associated with plesiosaurs is not this great in most cases (Everhart, 2000; Henderson, 2006; Richards, 2011). More analyses of the functional morphology of neck and head are needed before any confirmation can be drawn about the appliance of plesiosaurian gastroliths, although with grinding or accidental swallowing as the most reasonable functional explanations to date.

1.2 Part B: Long necks in extant vertebrates

1.2.1 Introduction

The majority of vertebrates possess a vertebral column, varying in size, shape, and number of vertebrae (Rockwell *et al.*, 1938; Swinton, 1965; Ward *et al.*, 2018). Part of the vertebral column are the neck vertebrae, which are a feature in tetrapods with a number of functions including feeding, locomotion, sexual display and behaviour (Rockwell *et al.*, 1938; Böhmer and Werneburg, 2017).

Through evolution, the neck of vertebrates has both shortened and extended in size, shape and the number of vertebrae (Rockwell *et al.*, 1938), and some extant animals like giraffes and birds exhibit relatively long necks related to their total body length. In the majority of cases, long necks can be explained in terms of foraging requirements (Wilkinson and Ruxton, 2012). To understand the neck morphology and range of motion in extinct animals, we need to understand the neck morphology of long necked modern animals. By looking at e.g. muscle attachment, tendons, and ligaments in the necks of extant animals we are far better suited to interpret the same structures for extinct marine reptiles such as plesiosaurs. This part of the chapter introduces neck morphology as a comparative study of long necks in extant species found in the literature.

1.2.2 Neck morphology in extant vertebrates

The vertebral column is made of cylindrical centra with intervertebral discs positioned in between (Rockwell *et al.*, 1938; McGowan, 1999; Taylor and Wedel, 2013a). The intervertebral disc has been a very important adaptation to moving on land (Rockwell *et al.*, 1938) allowing greater movement of the head and neck (Shapiro and Risbud, 2014). Arches protrude from the top and bottom of each centra along with vertebral processes (common types are transverse processes and zygapophyses). If an arch is protruding from the top of the centrum it is called a neural arch (Taylor and Wedel, 2013a), while when protruding from underneath the centrum of the arch is called either haemal arch or chevron (McGowan, 1999).

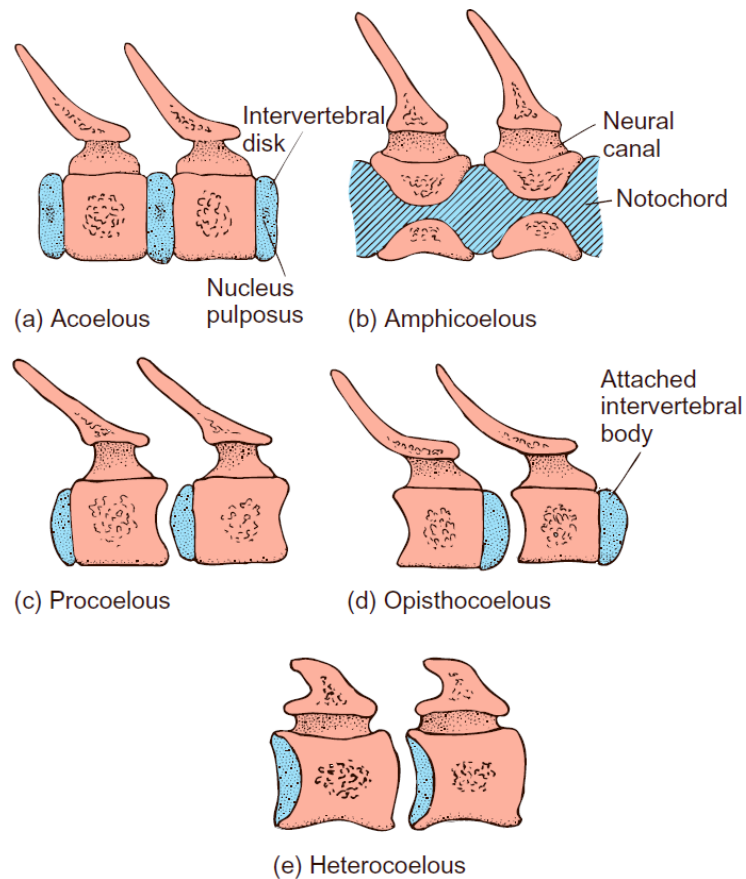


Figure 24: General shapes of vertebral centra in lateral view. (a) acoelous; centrum has flat ends, (b), amphicoelous; centrum has concave ends, (c) procoelous; centrum has concave end anteriorly and convex end posteriorly, (d) opisthocoelous; centrum has convex end anteriorly and concave end posteriorly, and (e) heterocoelous; centrum has saddle-like ends. Anterior to the right and posterior to the left. From Kardong (2012).

Vertebrae are shaped differently depending on the type of animal, and there are five common shapes of vertebra (Figure 24) with the procoelous centra being the most common (Tihen, 1965). The centra of plesiosaurs are recognised as amphicoelous in shape being concave at both ends (Grossmann, 2007; Ketchum and Smith, 2010; Sachs and Kear, 2017a; Marzola *et al.*, 2018). The shape of the vertebra centrum is different for various groups of animals and the vertebral shape is also dependent on the position in the vertebral column. The shape of the centra affects the possible angle of rotation, as well as intervertebral distance (Buchholtz and Schur, 2004). The cumulative effects of curvature and length of individual centra are demonstrated in Figure 25. Low curvature and short centra allow little rotation and elastic stability, while high curvature and short centra allow more rotation but low displacement (Buchholtz and Schur, 2004). Low curvature and long centra produce a rigid vertebral column, while high curvature with long centra means more rotation and displacement (Buchholtz and Schur, 2004). The reason for the higher total rotation is due to the increase in degrees between each centra creating a higher total movement in the vertebral

column. Thus, for optimal movement of the vertebral column, an animal would apply high curvature and relatively low centra length.

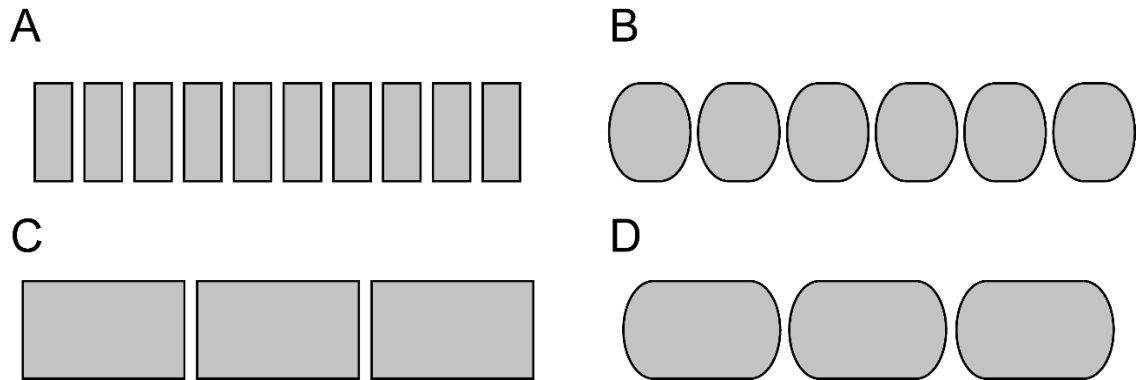


Figure 25: Diagram of vertebral centra shapes in lateral view, indicating structural variation in neck movement depending upon centra shapes. A) Low curvature and short centrum length, creating elastic stability. B) High curvature and short centrum length, creating rotation with low displacement, allowing optimal movement and the highest flexibility. C) Low curvature and long centrum length, creating rigidity. D) High curvature and long centrum length, creating rotation with high displacement. Modified from Buchholtz and Schur (2004).

Adjacent vertebrae articulate in different ways, and the vertebral centra are joined together by the intervertebral discs and ligaments (McGowan, 1999). Moreover, the articulated vertebrae connect with the pre- and post-zygapophyses (McGowan, 1999; Taylor and Wedel, 2013a). Muscles are attached around the vertebrae helping to form the overall shape of the vertebral column (McGowan, 1999). The cervical vertebrae bearing the head are surrounded by an extensive and compliant ligament, called the nuchal ligament, which extends all the way down the neck (McGowan, 1999). Lowering the head makes the ligament stretch, storing a great deal of elastic energy, which is released when the depressor muscles of the head are relaxed during the raise of the head (McGowan, 1999). The compliance of ligaments, and the storage of elastic energy is dependent upon the amount of elastin in the ligament, which is variable between and within animals. The attachments of the various muscles and tendons of the neck in different animal groups are reviewed below. Each muscle region/group is here abbreviated as “mm.” and each muscle as “m.” Furthermore, it is reviewed how the neck vertebrae of fish, lissamphibians (all modern amphibians), reptiles, birds (primarily ostriches) and mammals differ, forming the basis for understanding the neck morphology in extant vertebrates to compare with plesiosaurs in the following chapter.

1.2.2.1 Fish

The vertebrae in bony fish, with the only exception being the genus *Lepidosteus*, are amphicoelous in form (Figure 26) being concave on ends of the vertebrae (Rockwell *et al.*,

1938). The intervertebral space between articulated centra is filled with the notochord (Rockwell *et al.*, 1938). In all fish, no cervical region is distinguished (Galis, 1999), and instead they only exhibit dorsal (trunk) and caudal (tail) vertebrae (Clothier, 1950). The head and anterior abdominal region is stiffened in most bony fish which is a unique feature within vertebrates (Schnell and Johnson, 2017) as flexibility of the vertebral column is part of the locomotion in most tetrapods. The tail region of bony fish is very flexible, with the most extreme being seahorses capable of bending their tails ventrally over more than 800° (Neutens *et al.*, 2017).

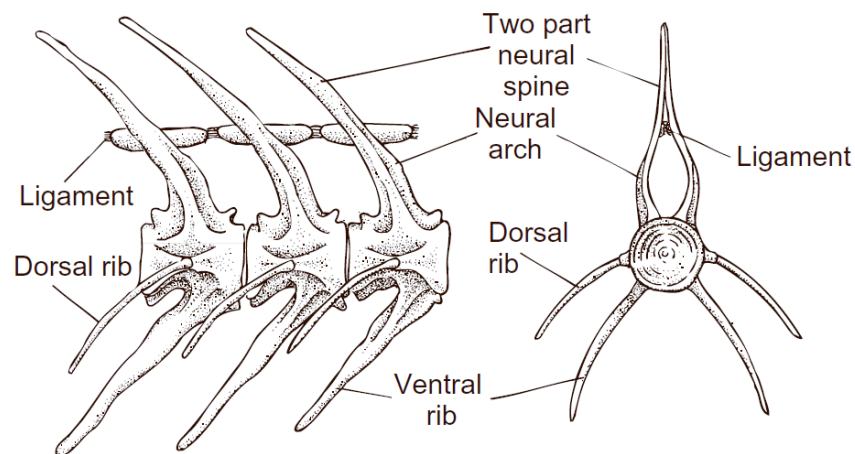


**Figure 26: Example of dorsal vertebrae from a teleost (bony fish) in lateral view (left) and cross section (right).
Modified from Kardong (2012).**

1.2.2.2 Lissamphibians

Lissamphibians consist of three groups: Salientia (frogs and toads), Caudata (salamanders and newts), and Gymnophiona (limbless caecilians) (Heiss *et al.*, 2018). Lissamphibians have either amphicoelous (Asian salamanders, early frogs and toads, and caecilians), procoelous (advanced frogs and toads) or opisthocoelous (true salamanders and newts) shaped centra depending if the animal is fully aquatic, semi-aquatic, or mostly terrestrial. Asian salamanders and lesser siren salamanders are fully aquatic, whereas some frogs and toads, caecilians, true salamanders and newts are semi-aquatic, and various toads and tree frogs are (mostly) terrestrial (Stephenson, 1951; Tihen, 1965; Duellman and Trueb, 1986; Ratnikov and Litvinchuk, 2007). This demonstrates that various centra shapes can be appropriate for a semi-aquatic lifestyle, and therefore the centra shape in lissamphibians is more reliant on locomotion rather than lifestyle.

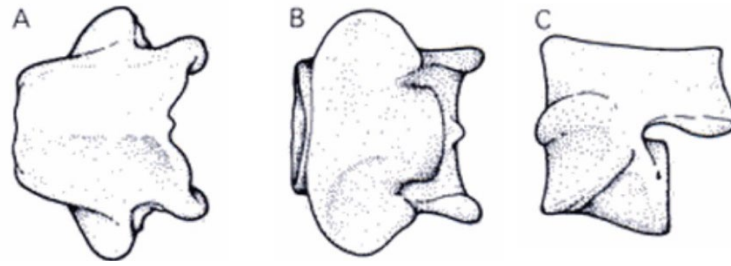


Figure 27: Atlas of the caecilian *Dermophis mexicanus* – (A) dorsal, (B) ventral, and (C) lateral view. Modified from Duellman and Trueb (1986).

In lissamphibians (with the exception of caecilians) only one cervical is present; the atlas (Figure 27; Figure 28), and it is modified anteriorly to articulate with the skull (Gadow, 1896; Duellman and Trueb, 1986; Shapiro and Risbud, 2014). Caecilians possess 19 or 20 cervical vertebrae other than the atlas (Duellman and Trueb, 1986). The neck region in amphibians is surrounded by the muscle *m. intertransversarius* which is divided into three muscles attaching to the back of the skull (Duellman and Trueb, 1986): The *mm. trancersarius capitis superior, posterior, and inferior* (Duellman and Trueb, 1986). The rest of the vertebral column consist of dorsal vertebrae, sacral, caudal-sacral (only in salamanders), and caudal vertebrae (only in salamanders and newts) or urostyle (only in frogs and toads) (Ratnikov and Litvinchuk, 2007).

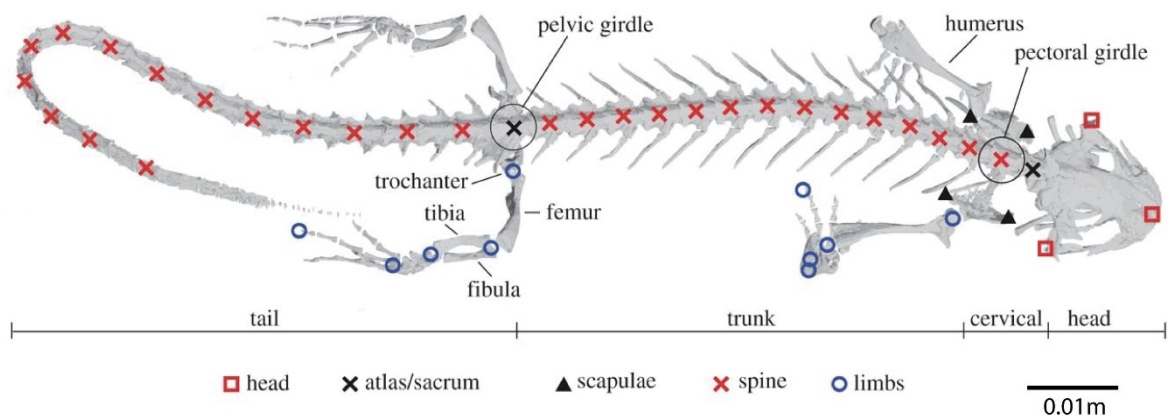


Figure 28: General outline of the skeleton of salamanders in top view, with indications of head, atlas, scapulae, spine, and limbs. Modified from Karakasiliotis et al. (2016).

1.2.2.3 Reptiles

Extant reptiles are divided into six groups: turtles/tortoises, crocodilians, snakes, worm lizards (amphisbaenians), lizards, and tuatara (Khanna, 2004). Reptiles generally have procoelous shaped centra (Figure 29), with exceptions being the tuatara having amphicoelous shaped centra (Gadow, 1896; Salisbury and Frey, 2001), and turtles that have a variety of shapes in cervical vertebrae (Figure 29) as each cervical centrum has a specific

purpose in movement. C2-C4 are opisthocoelous in cryptodirans (hidden-neck turtles), C5 and C8 are biconvex in cryptodirans, C1 in cryptodirans and pleurodirans (side-necked turtles) is biconcave or amphicoelous, C7 is biconcave or amphicoelous in cryptodirans, and C2-C8 are opisthocoelous in pleurodirans (Zarnik, 1925; Herrel *et al.*, 2007).

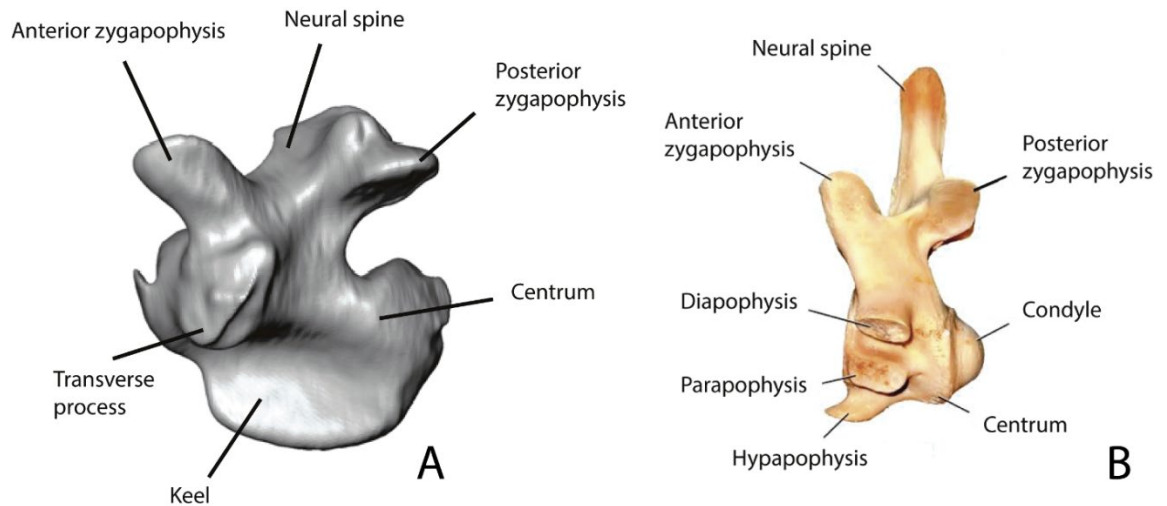


Figure 29: Examples of neck vertebrae (top: A and B) and osteological neck posture of various reptiles (bottom). **A)** Left lateral view of C4 in the cryptodire sea turtle *Lepidochelys kempii* – modified from Jones *et al.* (2012). **B)** Left lateral view of C6 in the crocodylian *Alligator mississippiensis* - modified from Böhmer (2013). **Bottom:** Head and neck region in **A)** The Nile Monitor *Varanus niloticus*, **B)** the crocodylian *Alligator mississippiensis*, **C)** Komodo Dragon *Varanus komodoensis*, **D)** the crocodylian *Crocodylus acutus*, **E)** the Seychelles tortoise *Testudo elephantina*, and **F)** the cryptodiran snapping turtle *Chelydra serpentina* – from Stevens (2013). Not to scale.

The vertebral column of reptiles is either distinguished as four or five regions: 1) cervical, 2) dorsal/thoracic and 3) lumbar, 3/4) sacral, 4/5) caudal vertebrae (Molnar *et al.*, 2014). The cervical vertebrae in reptiles consist of a series of eight (except for snakes) including

atlas (C1) and axis (C2) (Zarnik, 1925; Herrel *et al.*, 2007; Molnar *et al.*, 2014; Böhmer and Werneburg, 2017). Crocodylians and the tuatara have a proatlas anterior to the atlas (Tsuihiji, 2005), supplying additional support and stability to the head-neck region, and making it a total of nine cervical vertebrae in these two reptilian groups (Böhmer, 2013).

Reptiles with procoelous shaped centra stabilise their vertebral column against dorsoventral and transverse shear loads by the limited movement between articulated adjacent vertebrae (Salisbury and Frey, 2001). In contrast, the tuatara having amphicoelous shaped centra are not capable of the same amount of stability in the neck region. This is due to the increased intervertebral spacing which allows a greater flexibility compared with the cartilage/intervertebral disc found in other centra shapes (Rockwell *et al.*, 1938; Salisbury and Frey, 2001). In reptiles, the cervical vertebrae are higher than they are wide and long, due to the neural spine which remain constant in height with present ribs (Figure 29, top right and bottom: A-D) (Böhmer, 2013). The maximum ratio in height and length of reptilian cervical vertebrae is observed in the second cervical, slightly decreasing towards the middle part of the neck and from hereon remain constant to the base of the neck (Böhmer, 2013). In turtles, the cervical vertebrae are about 1.5 – 2 times longer than wide (Figure 29, top left and bottom: E-F) (Zarnik, 1925; Herrel *et al.*, 2007) and cervical ribs are lacking (Böhmer and Werneburg, 2017). The zygopophyses in turtles are positioned in a way that makes movement possible (Zarnik, 1925). The neural arch rises and covers the neural spine, and is reduced in height in most turtles (Herrel *et al.*, 2007). In snakes the articular surfaces of the zygopophyses are horizontal (Zarnik, 1925).

The muscles of snakes, worm lizards, lizards and tuatara necks consist of *m. spinalis capitis* (attached to the tips of the neural spine in anterior cervical vertebrae), *m. spinalis et semispinalis cervicis* (attached to the neural spine and zygopophyses in anterior cervical vertebrae), and *m. longissimus cervico-capiti pars articulo-parietalis* (attached to zygopophyses in anterior cervical vertebrae) (Figure 30A; Figure 31A) (Tsuihiji, 2005). For turtles (Figure 30C), the cervical musculature vary between the two groups, cryptodirans and pleurodirans, as the longissimus muscle system in cryptodiran is strongly developed whereas in pleurodirans it appears to be completely absent (Herrel *et al.*, 2007). This is due to the difference in neck retraction in the two groups, as cryptodirans move their head and neck dorsoventrally and pleurodirans move their head and neck laterally (Herrel *et al.*, 2007; Werneburg *et al.*, 2014; Anquetin *et al.*, 2017). Furthermore, leatherback turtles have

additional insulating fat in the neck region, which is a unique character among turtles (Davenport *et al.*, 2009).

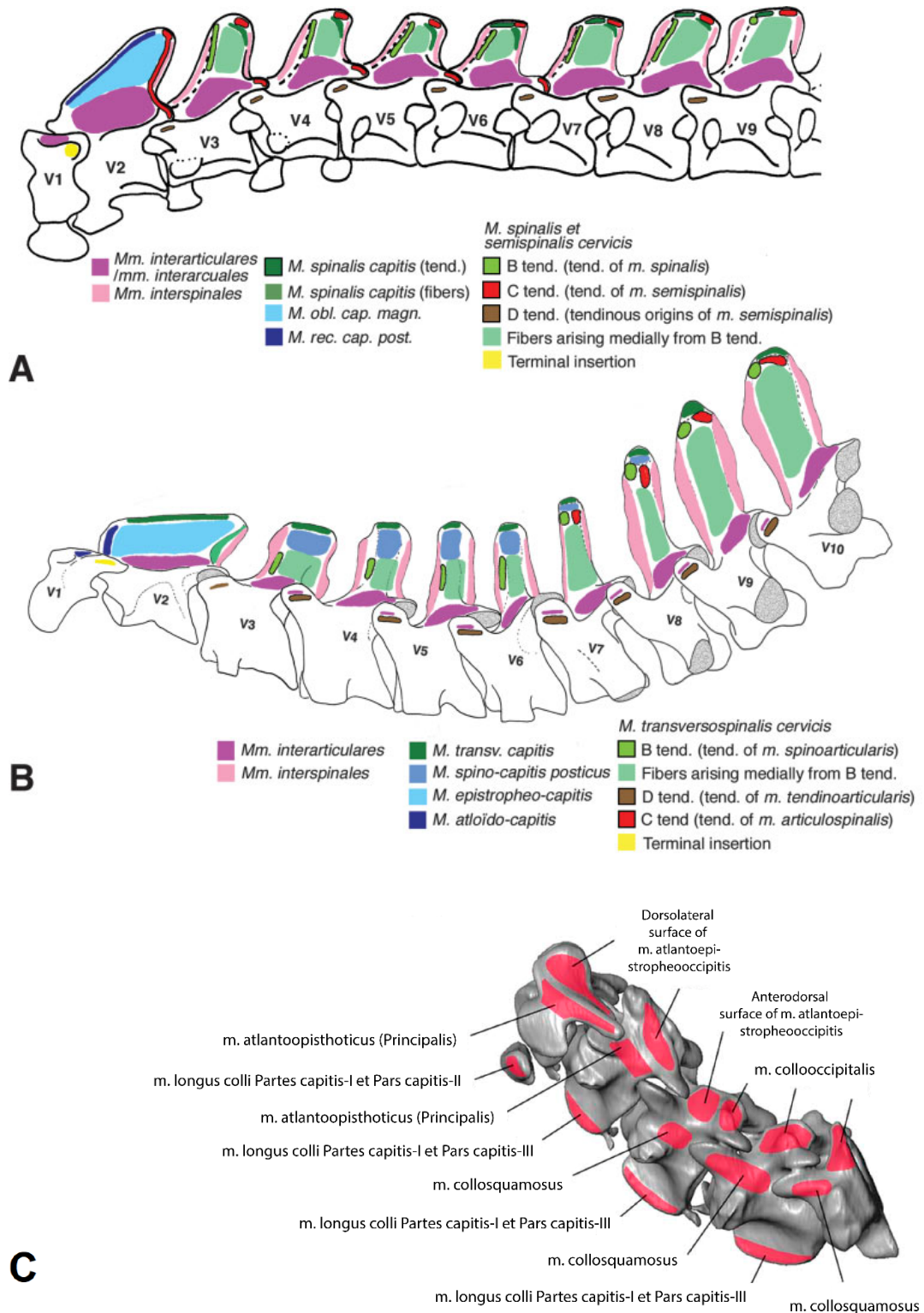


Figure 30: Muscles and tendons along the spine with respective positions in the neck of A) Green iguana, B) American alligator where V1 represents the atlas, V2 the axis, and V3 the first cervical vertebrae, and C) *Lepidochelys kempii* showing atlas to C4. Abbreviation: obl. cap. magn.: obliquus capitis magnus; rec. cap. post.: rectus capitis posterior; tend: tendons. A) and B) from Tsuihij (2005), and C) modified from Jones *et al.* (2012).

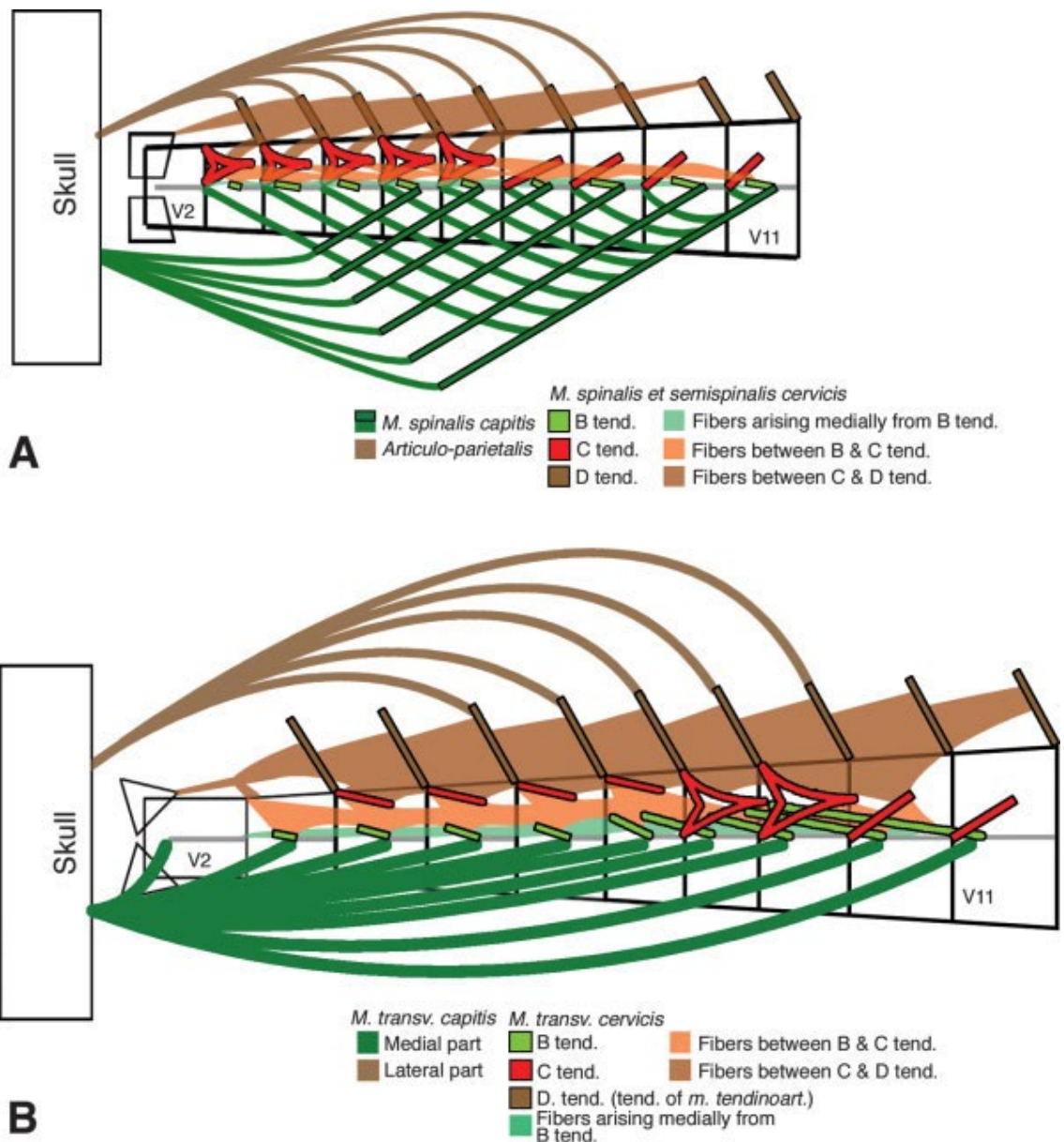


Figure 31: Diagram of selected muscles in the m. transversospinalis group in dorsal view of A) Green iguana, and B) American alligator. V1 represents the atlas, V2 the axis, and V3 the first cervical vertebrae. Abbreviations: tend: tendons; tendinoart: tendinoarticularis; transv: transversospinalis. From Tsuihiji (2005).

The diameter of crocodile necks is three or four times the diameter of the cervical vertebrae (Taylor and Wedel, 2013b). The crocodilian neck muscles are comprised of a medial and lateral m. transversospinalis capitis (attached to tips of the neural spine), m. spino-capitis posticus (attached to the lateral surface of the neural spine), and m. transversospinalis cervicis (attached to the lateral surface of the neural spine and zygapophyses) (Figure 30B; Figure 31B) (Tsuihiji, 2005). The muscles and tendons in the neck overlap with each other in order to interact with the skull (Figure 31). The cartilage:bone ratio between cervical vertebrae in American alligators is 14.90 % of the centra length (Taylor and Wedel, 2013a).

1.2.2.4 Birds

The avian neck is highly complex both anatomically and functionally compared with reptiles (Leeuw *et al.*, 2001), and the general morphology of bird cervical vertebrae (Figure 32) is similar to the morphology of reptilian cervical vertebrae (Figure 29: bottom).

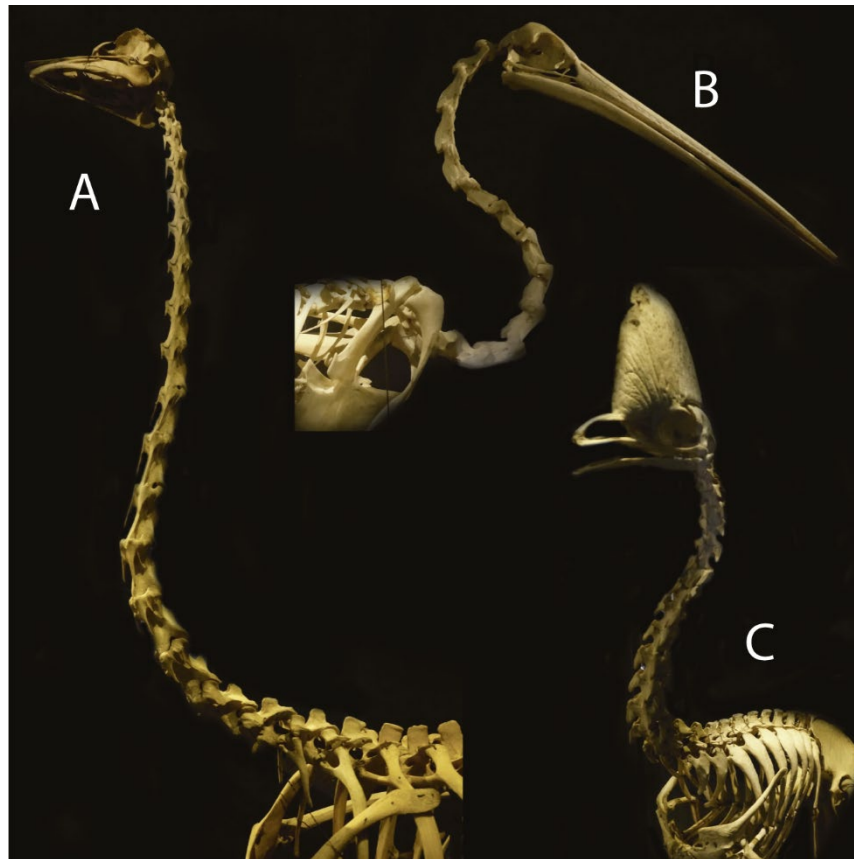


Figure 32: Osteological neck posture for various birds. A) ostrich, B) pelican, C) cassowary. Specimens on display at Manchester Museum.

All birds have heterocoelous shaped vertebra centra (Figure 24) (Zweers *et al.*, 1987; Samman, 2006; Böhmer, 2013; Stevens, 2013), a great variety of neck lengths (Leeuw *et al.*, 2001) and a diverse number of cervical vertebrae (e.g. 10-15 in Tinamiformes, 13 in pigeons and swifts, and 25 in swans) (Starck, 1979; Burke *et al.*, 1995; Apostolaki *et al.*, 2015). The avian cervical vertebrae are followed by dorsal/thoracic vertebrae (depending on literature), sacral vertebrae, caudal vertebrae and a pygostyle (Böhmer, 2013; Apostolaki *et al.*, 2015). Furthermore, avian cervical ribs are incomplete to some degree (Leeuw *et al.*, 2001) while dorsal vertebrae possess fully complete ribs (Gadow, 1896; Samman, 2006; Böhmer, 2013). Ribs are not present on the atlas (Böhmer, 2013). The cervical ribs are not long enough to overlap from one cervical to another, yet the tendons inserted on the ribs do overlap and are free to slide past each other longitudinally (Taylor and Wedel, 2013b).

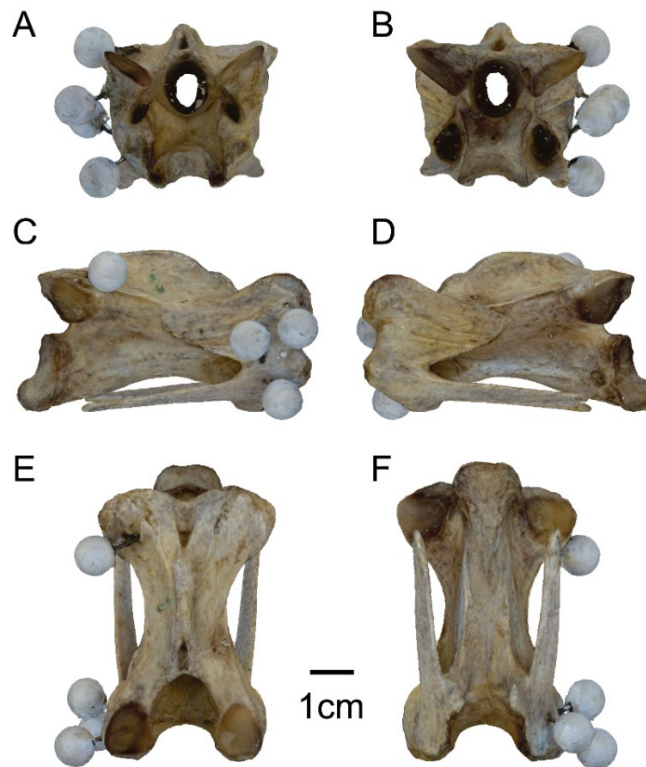


Figure 33: Ostrich (*Struthio camelus*) C14 in A) anterior view, B) posterior view, C) right lateral view, D) left lateral view, E) dorsal view, and F) ventral view. Pins were used to mark the bones for the study in Chapter 2. All to scale.

For most birds, cervical vertebrae are longer than their width and height (Landolt and Zweers, 1985; Samman, 2006; Dzemski and Christian, 2007). The opposite is the case for owls (Krings *et al.*, 2014). In ostriches, the length of cervical vertebrae varies from ~1-7cm, width ~2-5cm, height ~2-5cm, and the centra in ostriches range in length from ~1-6cm (Dzemski and Christian, 2007). The total length of the cervical series in ostriches is over two times higher than that of the dorsal series (Böhmer, 2013). The zygapophyses resemble those of turtles as the processes are in lateral position above the centra (Figure 33) (Zarnik, 1925). The articular surface of the pre-zygapophyses face upwards and post-zygapophyses face downwards (Zarnik, 1925). The neural spine in birds is reduced with the highest spine occurring around in the middle region of the neck (Zarnik, 1925).

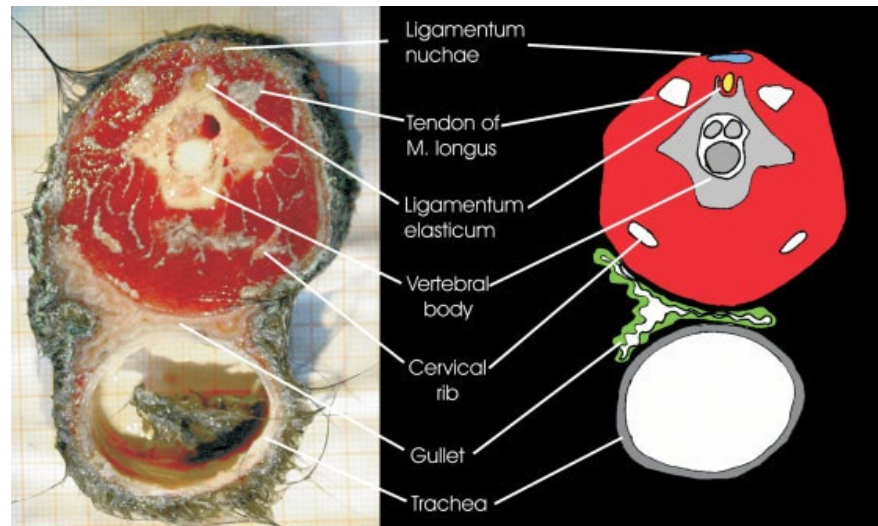


Figure 34: Cross-section of the middle of an ostrich (*Struthio camelus*) neck. From Dzemski and Christian (2007).

Despite the variety in cervical numbers, a basic design has been recognized in bird necks (Leeuw *et al.*, 2001). The increase in the number and dimensions of the cervical vertebrae when comparing reptiles to birds is visible (Figure 29 and Figure 32), and the muscular system in birds differs from that of reptiles (Leeuw *et al.*, 2001; Tsuihiji, 2004, 2005). The diameter of a bird neck is three or four times the diameter of the cervical vertebra (Figure 34) (Taylor and Wedel, 2013b).

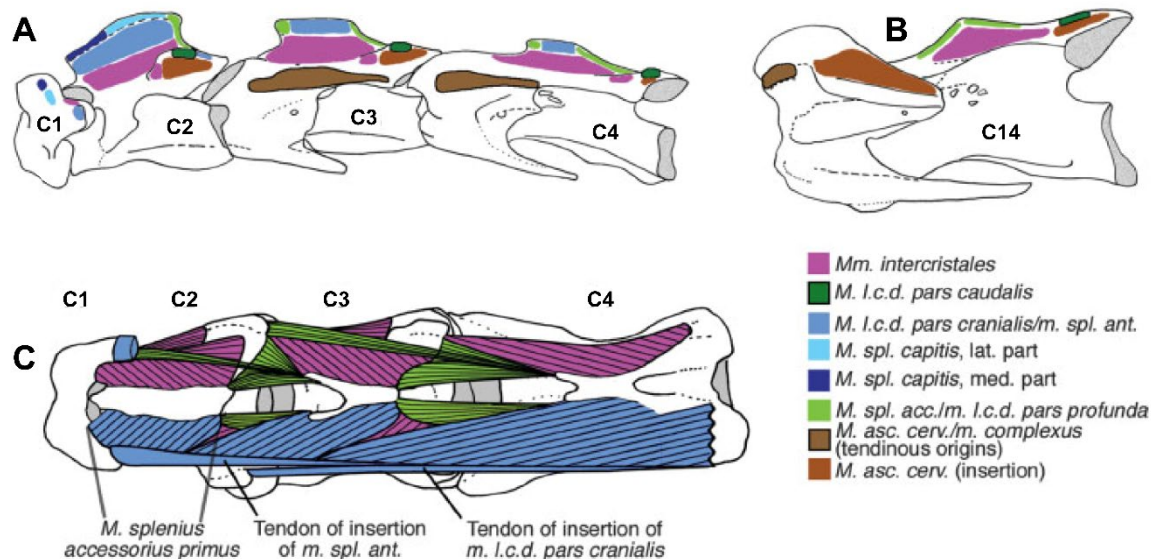


Figure 35: Muscles and tendons in the left side of three anterior-most cervical vertebrae in the ostrich (*Struthio camelus*). A) Muscle attachments in lateral view of C1-C4. B) Muscle attachments in C14 in lateral view. C) Muscle attachments of C1-C4 in dorsal view. Abbreviations: asc. cerv.: ascendens cervicalis; lat.: lateral; l.c.d.: longus colli dorsalis; med.: medial; spl. acc.: splenius accessorius; spl. ant.: splenius anticus. Modified from Tsuihiji (2005).

In birds the cervical musculature is the most complex among all animals (Kuroda, 1962). The muscles in bird necks are divided into four regions: 1) mm. craniocervicales (attached to skull and cervical vertebrae), 2) mm. cervicales dorsalis (attached to dorsal surface of cervical vertebrae), 3) mm. cervicales laterales (attached to lateral surface of cervical vertebrae), and 4) mm. cervicales ventrales (attached to ventral surface of cervical vertebrae) (Boumans *et al.*, 2015). For ostriches, the regions/groups, respective muscles, and their origin are listed in Table 4. The muscles and tendons in the neck vary in size and overlap with each other in order to interact with the skull (Figure 35 and Figure 36) (Boumans *et al.*, 2015). The amount of musculature surrounding the vertebrae and joints limits the amount of flexibility in the neck (Cobley *et al.*, 2013).

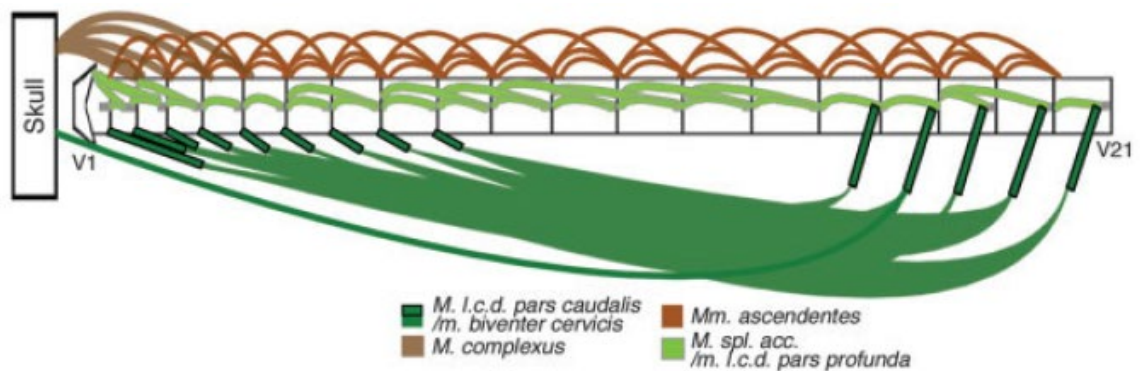


Figure 36: Diagram of selected muscles of the m. transversospinalis group in dorsal view in the neck of an ostrich (*Struthio camelus*). V1 represents the atlas, and V21 the 21st cervical vertebrae. Abbreviations: l.c.d.: longus colli dorsalis; spl. acc.: splenius accessories. From Tsuihiji (2005).

In some birds such as the turkey (*Meleagris gallopavo*) and the rhea (*Rhea americana*) the intervertebral disc is absent (Taylor and Wedel, 2013a). In ostriches (*Struthio camelus*), swans (*Cygnus atratus*) and king penguins (*Aptenodytes patagonicus*) among others, the intervertebral disc is replaced by articular cartilage (Taylor and Wedel, 2013a). This cartilage is thinner than the disc of crocodilians, and has been estimated as approximately 1-2mm thick (Taylor and Wedel, 2013a), and according to Dzemski and Christian (2007) it is even less than 1mm in ostriches. Generally, the cartilage is placed on the zygapophyses and central faces in birds (Samman 2006). The cartilage:bone ratio between cervical vertebrae is 4.56 % of the centra length in turkeys, 2.59 % in rheas (Taylor and Wedel, 2013a), and 6.30 % in ostriches (Cobley *et al.*, 2013).

Table 4: Muscle groups and their origin in the cervical musculature of ostriches. Modified from Snively and Russell (2007), Cogley et al. (2013), and Boumans et al. (2015).

Muscle group	Muscle	Origin
Dorsal	m. biventer cervicis	Neural spine in posterior cervical vertebrae
	m. longus colli dorsalis	Neural spine
	m. ascendens cervicalis	Dorsal and lateral tubercles of transverse processes, ventral to prezygapophyses
Lateral	m. flexor colli lateralis	Tubercula ansae
		Cristae laterals
Ventral	m. flexor colli medialis	Processus caroticus
		Processus costalis
Single segment	mm. intercostales	Transverse oblique crests of posterior vertebra of each pair
	mm. insterspinales	Neural spine
	mm. intertransversarii	Complex multislip origins on transverse processes

1.2.2.5 Mammals

The centra shape in mammalian necks is acoelous (Ward and Mehta, 2014), although stated as opisthocoelous for horses and camels by Taylor et al. (2013a) and additionally for rhinos and horses by Stevens and Parrish (2005a, 2005b). Mammals possess five distinct vertebral regions: 1) cervical, 2) thoracic, 3) lumbar, 4) sacral and 5) caudal vertebrae (Shapiro and Risbud, 2014). Most mammals have seven cervical vertebrae (Figure 37: left) (Narita and Kuratani, 2005; Taylor and Wedel, 2013b; Böhmer, 2017) and separate atlas (C1) and axis (C2) as part of the cervical vertebrae (Graf *et al.*, 1994; McGowan, 1999; Shapiro and Risbud, 2014; Böhmer, 2017; Naish and Witton, 2017). The only mammals evolving different numbers of neck vertebrae are sloths and manatees (Figure 37: right) (Narita and Kuratani, 2005; Böhmer *et al.*, 2018). Sloths have five to ten cervical vertebrae (Bateson, 1894; Narita and Kuratani, 2005; Buchholtz and Stepien, 2009; Varela-Lasheras *et al.*, 2011; Vaughan *et al.*, 2015; Böhmer *et al.*, 2018), and manatees have six neck vertebrae (Narita and Kuratani, 2005; Fitch, 2012). The biomechanical reason why the different number of cervical vertebrae is seen in sloths and manatees is still under debate with hypotheses such as extremely low metabolic rate, primaxial/abaxial repatterning, and global homeotic changes being possible explanations for the exception (Galis, 1999; Böhmer *et al.*, 2018).

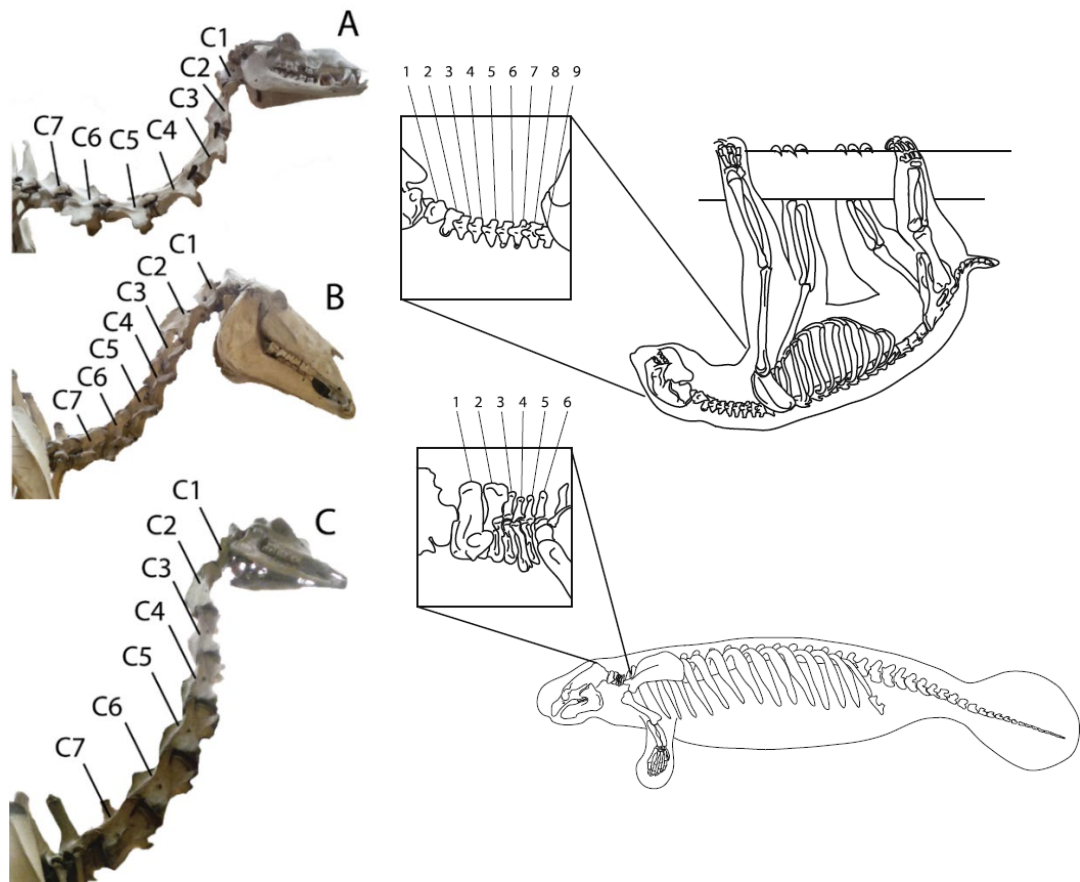


Figure 37: Examples of skeletal mammalian necks. Left: A) camel, B) horse, and C) giraffe. Right: top) Sloth and bottom) Manatee. Left modified from photos taken of specimens at Oxford University Museum of Natural History. Right modified from Fitch (2012).

Just as we see five fingers as an evolutionary constraint on digit numbers in tetrapod limbs (Galis *et al.*, 2001), the strong evolutionary conservatism of the number of cervical vertebrae in most mammals is thought to be a case of Hox gene expressions, which are genes involved in e.g. the development of the axial skeleton in embryos (Galis, 1999). Furthermore, the exceptions with fewer cervical vertebrae in manatees could also have been caused by the Hox gene expressions, making an anterior shift in the boundary of the cervical region (Narita and Kuratani, 2005). For sloths with five or six cervical vertebrae the Hox gene expression could have caused the same situation as is the case for manatees, whereas sloths possessing eight, nine or ten cervical vertebrae a posterior shift of the Hox gene expression pattern associated with the first thoracic vertebra could have caused the increase in cervical count (Böhmer *et al.*, 2018).

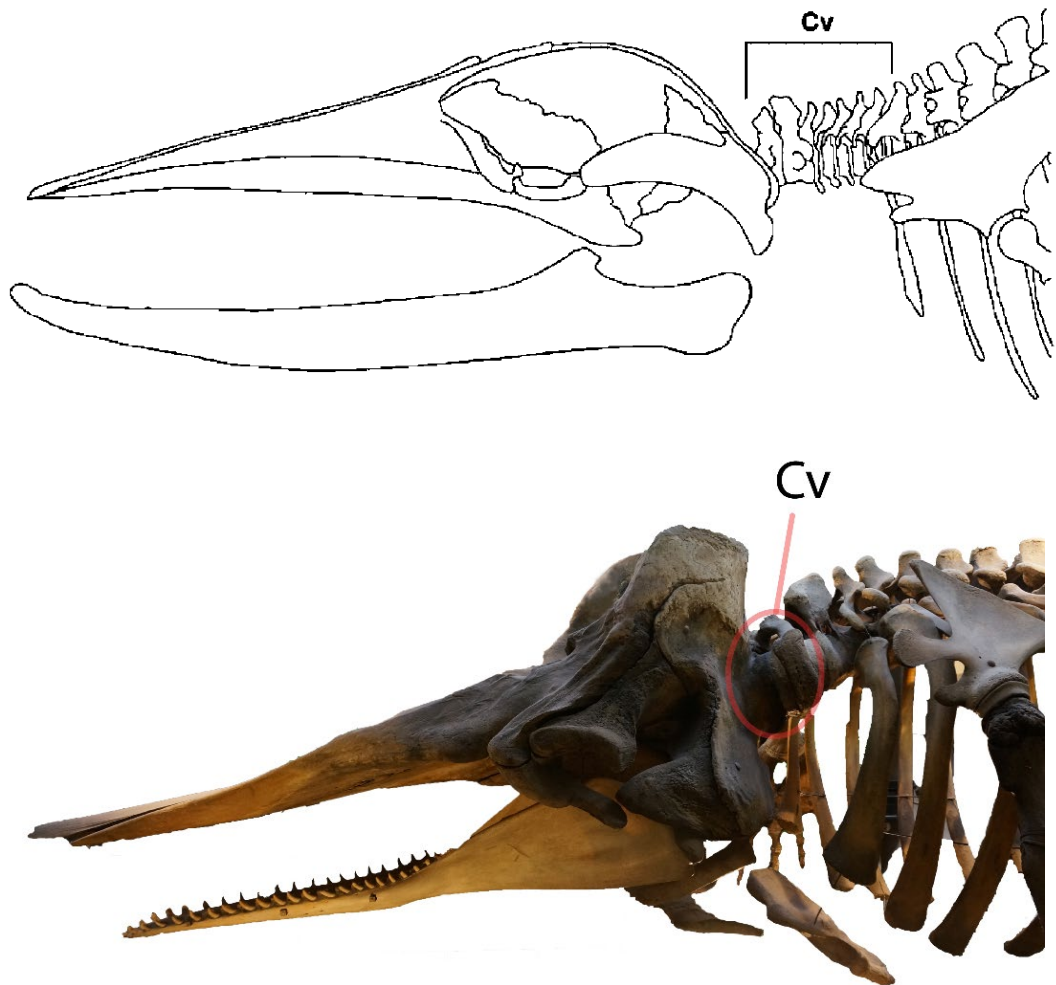


Figure 38: Anterior part of skeleton of a balaenopterid whale showing seven separate cervical vertebrae (Cv) (top). Modified from Narita and Kuratani (2005). Skeleton of the sperm whale (*Physeter macrocephalus*) showing fused cervical vertebrae forming a single bone (bottom) – edited photo from displayed specimen at Manchester Museum.

In mammals, the atlas has no anterior zygapophyses, though includes a pair of shallow concave depressions for articulation with the paired exoccipital condyles at the back of the skull (McGowan, 1999). Neural spines are short anteriorly in the neck and becomes longer posteriorly (McGowan, 1999). Given the long necks in e.g. giraffes and camels the low number of cervical vertebrae in mammals means an increase in the size of each cervical (Naish and Witton 2017). In whales the neck is foreshortened (Figure 38: top), or even fused in some species forming a single vertebra (Figure 38: bottom), and the cervical vertebrae have exceptionally short centra length (Buchholtz and Schur, 2004; Narita and Kuratani, 2005). The reduced neck length in whales causes a weakened or nearly absent function of the neck, similar to the sacrum found in humans which is made up of five vertebrae. The number of thoracic, lumbar, and sacral vertebrae vary in mammals, ranging from 9-23

thoracic, 2-9 lumbar, and 1-9 sacral vertebrae (McGowan, 1999; Narita and Kuratani, 2005; Shapiro and Risbud, 2014). The mammalian vertebral column ends with several caudal vertebrae, ranging from 2-33 (McGowan, 1999; Narita and Kuratani, 2005; Shapiro and Risbud, 2014).

The connection between muscles in the mammalian neck varies among species (Arnold *et al.*, 2017). There are five modules overall; 1) cranio-pectoral, 2) ventral, 3) mid-cervical, 4) lower cervical, and 5) thoracic. The cranio-pectoral module is represented by the muscles around the cranium, C1 and bones associated with the shoulder girdle (scapulae, clavicae, and humeri), as well as the suboccipital, cleidocephalic, atlantoscaphularis, capital longus, and capital rhomboid muscles. The ventral module consists of muscles connected to the sternum, hyoid, thyroid, mandible, and the sternocephalic and infrahyoid muscles. Of the 32 of 48 mammalian species representative of 24 orders studied by Arnold *et al.* (2017), ribs and the related scalenii muscles are also included in the ventral module. The mid-cervical module groups C2-C4, as well as the longus cervicis, spinalis, and their related interspinal, intertransversarii, and multifidii muscles. The lower cervical module embodies C5-C7 with the cervical longissimus, spinalis, and their related interspinal, intertransversarii, and multifidii muscles. The border between the mid-cervical and lower cervical modules is shifted in some species. The thoracic module consists of the thoracic spine, nuchal ligament, semi-spinalis (complexus + biventer cervicis), capital longissimus, cervical rhomboid and trapezius muscle. In sloths the organisation of neck muscles differs due to their unusual number of cervical vertebrae. In general, the morphological complexity in mammalian necks decreases from monotreme to placental mammals, regardless of the disparity in neck length and organisation in placental mammals (Arnold *et al.*, 2017).

Unlike birds, mammals have a firm intervertebral disc attached between consecutive vertebrae including high amounts of space between each cervical (Figure 39) (Taylor and Wedel, 2013a). The intervertebral distance has been estimated as 7-9mm in giraffes, 6-9mm in camels (mid-neck measurement), 4.3-5.8mm in bovine, 5.4-6.8mm in horses, and about 4mm in large dogs measured using dead specimens (Dzemeski and Christian, 2007). The lower intervertebral distance values represent the joint between second and third cervical, and higher values as the joint between the sixth and seventh cervical, with increasing values towards caudal direction (Dzemeski and Christian, 2007). The cartilage:bone ratio between cervical vertebrae has been estimated for mammals, and showed a 24 % of the centra length

in juvenile giraffes, 6.9 % in horses, 17 % in dogs, and 13 % in camels, making mammalian cartilage:bone ratios three times higher than for birds (Taylor and Wedel, 2013a).



Figure 39: Left lateral view of a neck from a young juvenile giraffe in various dissection stages. Top: Intact neck with skin stripped. Middle: Most of muscles removed from the neck. Bottom: Cervical vertebrae cleaned from soft tissue and cartilage. Modified from Taylor et al. (2013a).

In the Delphinidae, the vertebral column has been radically reorganized for axial locomotion in the aquatic environment (Buchholtz and Schur, 2004). The vertebral column of dolphins is stiff compared to other marine mammals (Maresh *et al.*, 2004) and has low flexibility of the intervertebral joints which provide stability (Long *et al.*, 1997).

1.2.3 Main differences between terrestrial and aquatic necks

Vertebrate morphology correlates with locomotor behaviour, biomechanics (Molnar *et al.*, 2014; Heiss *et al.*, 2018) and habitat (Graf *et al.*, 1994). For example, the development of the intervertebral disc has been an important adaptation to terrestrial locomotion (Rockwell *et al.*, 1938), by supporting the upright neck posture that many terrestrial vertebrates possess as part of dealing effectively with gravity (Graf *et al.*, 1994). For aquatic tetrapods, swimming style, habitual spinal loading patterns, and locomotor habits are the most noticeable changes to locomotion and biomechanics (Molnar *et al.*, 2014).

Aquatic amphibians do not share vertebral morphology with non-amphibian aquatic vertebrates, but semi-aquatic amphibians do share centra shape (opisthocoelous) with aquatic/semi-aquatic turtles. Terrestrial amphibians share centra shape (procoelous) with reptiles in general, with only terrestrial turtles (opisthocoelous) and tuatara (amphicoelous)

possessing another centra shape among reptiles. Thus, there is no clear morphological explanations as to why aquatic amphibians possess amphicoelous shaped centra. However, there is a clear link between semi-aquatic vertebrates and their centra shape, possibly due to the shape being optimal and advantageous when walking on land providing support for the vertebral column.

The variation seen in reptilian centra allows various neck movements and correlates with different lifestyles (Gadow, 1896; Salisbury and Frey, 2001; Herrel *et al.*, 2007). In cryptodiran turtles, which include both terrestrial, semi- or fully aquatic lifestyles, longer necks are observed within semi- and fully aquatic turtles compared with their terrestrial relatives (Herrel *et al.*, 2007).

Birds represent the group with the most extreme design in terms of cervical count and neck flexibility among modern vertebrates (Leeuw *et al.*, 2001). Modification of the avian cervical anatomy even occur within some species (Leeuw *et al.*, 2001). Among terrestrial birds, woodpeckers have adapted their neck muscles to pounding frequently by strengthening the base of the neck for stabilisation (Leeuw *et al.*, 2001). Rheas and chickens have similar body proportions, although rheas make relatively larger vertical neck movements compared with chickens (Leeuw *et al.*, 2001). Diving birds have short dorsal neck muscles which vary depending on the specific diving method they use, and long-flying birds have more prominent dorsal neck muscles (Leeuw *et al.*, 2001). The difference in dorsal neck muscles between diving and long-flying birds show that shorter muscles are beneficial in fast acceleration of the mouth capture elusive prey (Wilkinson and Ruxton, 2012), and longer muscles are advantageous for stabilising the neck in migration situations.

Mammals are possibly the best example to observe change between terrestrial and aquatic species because of their secondary adaptation to life in water. The transition from terrestrial to fully aquatic lifestyle meant that mammals had to adapt more extreme morphological and behavioural modifications, especially to the neck region, due to a much denser and viscous fluid (Williams, 1999). In aquatic mammals, such as pinnipeds and cetaceans, the reduction of relative centra length and width correlates with the decrease in the amount of dorsoventral flexion in the neck region during swimming (Molnar *et al.*, 2014). This is because aquatic mammals possess shorter necks compared with terrestrial mammals (Buchholtz and Schur, 2004) most likely caused by the change in habitat (air vs. water). Due to the longer and wider centra and increase in differentiation of the neck area and intervertebral disc, terrestrial

mammals have higher neck movement compared with aquatic mammals (Rockwell *et al.*, 1938; Molnar *et al.*, 2014).

1.3 Conclusion

The success of plesiosaurs may have been partly due to a combination of a versatile feeding apparatus (McHenry *et al.*, 2005) and a long neck. These two features would allow plesiosaurs to feed in all of the pelagic zone (Neenan *et al.*, 2017) and many of them would probably have adapted to a variety of the feeding styles to sustain a life avoiding being bitten or eaten by larger predators like sharks (Storrs, 1981; Everhart, 2005; Sato *et al.*, 2006), marine crocodiles (Forrest, 2003), mosasaurs (Einarsson *et al.*, 2010), or even other plesiosaurians (Rothschild *et al.*, 2018).

Chapter 2 – Range of motion in ostrich necks

2.1 Introduction

One obvious approach to understand plesiosaur necks is to study modern long-necked animals. We are able to observe how living animals move, and by using photography or high-speed video we can document and analyse external motions. If we want to understand how animals move just by looking at their bones (as is the case for extinct animals) we need an understanding of how bone and soft tissue affect one another. By physically or digitally manipulating bones, we can explore how different stages of dissection affect range of motion as muscle movement is observable from this type of experiment. A study like this can help explain what the range of motion means for the ecology of a given species because it allows us to study how the species would be able to interact with its environment. However, this kind of approach is difficult to perform as we do not have *in vivo* data to validate with.

Studying how soft tissue confines range of motion in living animals can help us constrain interpretations made from the bones of extinct animals like plesiosaurs. We can use range of motion data found in an ostrich neck to get an idea of what the flexibility would have been in plesiosaur necks.

Advances in recording three-dimensional (3D) moving morphology, such as XROMM (Brainerd *et al.*, 2010; Gatesy *et al.*, 2010; Knörlein *et al.*, 2016), have enabled an unprecedented view of how internal morphology moves, even when hidden by soft-tissue. While such methods offer exceptional levels of accuracy and precision, they are typically associated with high economic costs beyond the means of most researchers.

This chapter presents an alternative approach, namely an experimental set-up called PiROMM, consisting of three networked raspberryPi microcomputers with camera modules, which are used to record motion in a cadaveric ostrich (*Struthio camelus*) neck at progressive levels of dissection (Falkingham *et al.*, 2017). These data are compared with that derived from digital manipulation, virtually “rubbing bones together”, and the methods are then discussed. This study will help to interpret how much range of motion changes from having an intact neck to only having the clean bones. The study is a means of generally exploring how soft tissue can affect range of motion in a long neck, and a way to validate digital range of motion methods, which are the only means available for evaluating neck flexibility in extinct taxa, such as plesiosaurs. Previous studies on range of motion in the necks of extant animals are here reviewed, including factors that can lead to long necks.

2.1.1 Range of motion studies of necks in extant animals

Studies of soft tissue effects on joint mobility in extant animals can help to constrain hypotheses concerning joint mobility in extinct taxa (Manafzadeh and Padian, 2018). The variety of vertebral morphology is often related to the kinematics of an animal, with units of the vertebral column controlling range of motion (RoM) (VanBuren and Evans, 2016). Neck flexibility is constrained by the morphology of the vertebrae, intervertebral cartilage, ligaments, and musculature (Cobley *et al.*, 2013; Boumans *et al.*, 2015). Establishing the flexibility of a vertebrate neck allows estimation of the ‘feeding envelope’ of a given species, giving the maximum range over which an individual could feed while standing still (Cobley *et al.*, 2013), eventually determining ecological possibilities and adaptations for the given species. In the case of extinct species, the RoM of the neck can also tell us about palaeobiology of the given species.

2.1.1.1 Reptiles

Among reptiles, being a very diverse morphological group of vertebrates, a great variety of species have been studied in terms of neck flexibility and RoM (Zarnik, 1925; Herrel *et al.*, 2007; Zammit *et al.*, 2008; Böhmer, 2013; Werneburg *et al.*, 2015; Nagesan *et al.*, 2018). The species reviewed here include the varanid *Varanus dumerilii*, the American alligator *Alligator mississippiensis*, the snake-necked turtle *Chelodina longicollis*, the turtle genus *Emys*, species from the suborder Pleurodira, species from the suborder Cryptodira, and two snake species (*Python reticulatus* and *Diadophis punctatus*).

In the extant varanid *Varanus dumerilii*, maximum osteological RoM has recently been measured (Table 5) from a micro-CT-scan of the whole body (Nagesan *et al.*, 2018). The 3D models of the adjacent cervical bones were rotated digitally using Autodesk Maya, and the bones were bent maximally in dorsal, ventral and lateral directions until the vertebrae contacted each other. Nagesan *et al.* (2018) also used radiographed images of *V. dumerilii* post mortem placed on a flatbed to investigate its RoM. By using tape to hold the neck (which was still *in situ* and covered in soft tissue) in place when positioned in four poses (neutral and maximum dorsal, ventral and left lateral flexion) the RoM data was documented by taking screenshots of the radiographed images. Straight lines were drawn on the images in Adobe Illustrator (AI) from the base of the centrum of each vertebra and extended out beyond the length of the vertebra. The drawn lines resulted in a series of intersecting lines where the angles between each line were measured manually. Using the radiographed images Nagesan *et al.* (2018) showed that the maximum RoM increased significantly for both

dorsoventral and lateral neck flexion (45° and 27°, respectively) when comparing with the 3D models approach (30° and 17°, respectively) (Table 5) (Nagesan *et al.*, 2018), as would be expected due to the smaller amount of intervertebral distance when using radiographed images.

Table 5: Range of motion (mainly found by osteological maximum flexion but see text for others methods used) in some reptilian necks (varanid, American alligator, several turtle and snake species), including taxa, maximum dorsoventral and lateral flexion (average per cervical vertebra), number of cervical vertebrae, and respective references. Snakes only shown here using vertebrae and not specifically cervical vertebrae.

Taxa	Maximum dorsoventral flexion	Maximum lateral flexion	Number of cervical vertebrae	Reference
Varanid (<i>Varanus dumerilii</i>)	Using 3D models: 92° (dorsal) (15°) 77° (ventral) (15°)	Using 3D models: 104° (17°)	7 cervical vertebrae in total but only 5 (or 6) joints depending on rotation	Nagesan et al., 2018
	Using radiographed images: 140° (dorsal) (23°) 109° (ventral) (22°)	Using radiographed images: 136° (27°)		
American alligator (<i>Alligator mississippiensis</i>)	75° (dorsal) (11°) 54° (ventral) (8°)	57° (8°)	8	Böhmer, 2013
Cryptodiran turtle (<i>Chelodina longicollis</i>)	(10°)	(10°)	7	Zammit et al., 2008
	-	160° (23°)	8	Herrel et al., 2007
Cryptodiran turtle genus <i>Emys</i>	375° (54°)	122° (17°)	8	Zarnik, 1925
Mean of 8 Pleurodiran turtles	169° (dorsal) (24°) 170° (ventral) (24°)	378° (54°)	8	Werneburg et al., 2015
Mean of 27 Cryptodiran turtles	341° (dorsal) (49°) 158° (ventral) (23°)	212° (30°)		
Boid snake (<i>Python reticulatus</i>)	(1°)	(1°)	6	Zammit et al., 2008
Ring-necked snake (<i>Diadophis punctatus</i>)	Dorsal (8°) Ventral (14°)	(29°)	Ten measurements of two adjacent vertebrae	Zarnik, 1925

The American alligator (*Alligator mississippiensis*) has been studied in terms of maximum osteological neck flexibility by Böhmer (2013), and dorsal flexion was shown to be the greatest rotation direction in this species (Table 5). Additionally, Böhmer (2013) found that the flexion in the neck of *A. mississippiensis* is greatest in the anterior part of neck in ventral flexion and in the posterior region of the neck for dorsal flexion, whereas lateral flexion is almost even throughout the neck. The dorsal flexion in the of *A. mississippiensis* was restricted by the neural spine, ventral flexion by zygapophyses and centra, and lateral flexion by zygapophyses (Böhmer, 2013). Additionally, a study by Molnar et al. (2014) indicate that the role of the flexibility in the vertebral column in crocodylians is different from that of mammals, as the dorsoventral flexion in mammals is high and connected mostly to locomotion, whereas in crocodylians it is low and depends on joint stiffness and bending.

For the snake-necked turtle *Chelodina longicollis* and the boid snake *Python reticulatus*, dorsoventral and lateral maximum osteological flexion has been measured by Zammit et al. (2008), showing a large variance between the two taxa (Table 5: average flexion per cervical was 10° in the turtle and 1° in the snake). Lateral flexion has also been measured by Herrel et al. (2007) for *C. longicollis* post mortem with most flexion showed to occur in the middle of the neck. The difference between the results on lateral flexion in *C. longicollis* (Table 5) by Zammit et al. (2008) (10° on average per cervical) and Herrel et al. (2007) (23° on average per cervical) is probably caused by the method by which the flexion was measured, as for both studies the methodology is not clear and the results will have to be handled with circumspection. Dorsoventral and lateral osteological maximum flexion in ring-necked snakes (*Diadophis punctatus*) has been measured (Table 5) and has shown the capability of making a complete curve of 360° within only one quarter of its body length (Zarnik, 1925).

Werneburg et al. (2015) has recently made a comparative study of the neck flexibility in the two suborders of turtles (Pleurodira and Cryptodira) *in vivo*, and found that Pleurodiran turtles were more capable of lateral flexion and Cryptodiran turtles had predominantly dorsal flexion (Table 5). The results by Werneburg et al. (2015) resembles the study by Zarnik (1925) as the turtle genus *Emys* (cryptodiran) also possess a higher dorsoventral flexion compared with lateral flexion (Table 5). Zarnik (1925) also found by measuring osteological maximum flexibility, that this genus can rotate dorsoventrally with up to 74° in C7-C8, and has a lateral flexion with up to 41° in C3-C4 and has no rotation capability in C6-C8. The higher lateral flexion found in pleurodiran turtles and higher dorsoventral flexion found in cryptodiran turtles correspond with the function of the neck in the two suborders, being side-

necked and hidden-necked (cf. Chapter 1), respectively, allowing predominant flexion in the respective direction.

Clearly, the neck rotation in reptiles is diverse (Table 5). The highest maximum dorsoventral flexion is seen in cryptodiran turtles and the least in the boid snake *Python reticulatus* if we look at average per cervical vertebrae. Lateral flexion is at its maximum in pleurodian turtles when looking at average per cervical vertebrae. Snakes possess a greater total number of vertebrae in general in comparison with turtles, so the total flexion for the whole vertebral column will generally be greater in snakes. Unlike turtles, who use their legs for locomotion, snakes rely on the ability to flex their bodies in order to move.

2.1.1.2 Birds

The range of motion (RoM) in birds is just as diverse as their neck morphology. A few of them are reviewed here and especially former studies on neck flexibility in ostriches are mentioned to compare with the present study.

Leeuw and colleagues (2001) investigated the RoM in the domestic chicken *Gallus gallus domesticus*. They found that the middle part of the neck had predominant dorsal flexion and the anterior part of the neck had predominant ventral flexion. Russell and Bentley (2016) also studied the maximum RoM in cervical vertebrae of the domestic chicken (Table 6), with the largest angles measured in the posterior end of the neck. Russell and Bentley (2016) based their study on the chicken lying in a resting pose and five intermediate stations of opisthotonic posture where the neck was moved manually for each posture, whereas Leeuw et al. (2001) did not specify how exactly the flexion was measured. Opisthotonic posture is when the neck bends backwards dorsally into a hyperextended posture (Reisdorf and Wuttke, 2012). This could help explain the variation among the two studies of RoM in domestic chickens by Leeuw et al. (2001) and Russell and Bentley (2016).

According to Samman (2006), mallards (*Anas platyrhynchos*) have poor dorsiflexion in the anterior part of the neck, though with an extreme ventral flexion. The posterior part of the neck shows very limited dorsoventral flexion, and the middle region shows good dorsal flexion with some degree of ventral flexion (Samman, 2006). This finding is reinforced by the study from Leeuw et al. (2001) as they found similar results. In domesticated geese the lateral flexion has been estimated by Zarnik (1925) (Table 6), showing greatest flexibility in the anterior and posterior part of the neck and the least in the middle region.

Ostriches use their necks for a variety of purposes in terms of sanitation and foraging. When ostriches clean their plumage, they use extreme lateral turns (Dzinski and Christian, 2007). During feeding the neck usually flexes dorsally in the middle of the neck and ventrally in the posterior end of the neck, creating an S-shape which is characteristic for several avian taxa. The ventral flexion at the base of the neck allows the ostrich to strain the ligaments connected to the dorsal muscles, and thereby avoiding breakage of the elongated neck. The long necks of ostriches allow them to reach a large area without moving the trunk, and thereby saving energy. Utilization of the neck in ostriches is consequently greatly connected with the flexibility of the neck, and vice versa (Dzinski and Christian, 2007).

The maximum intervertebral flexion in ostrich cervical vertebrae has been measured by multiple authors using various cervical counts, depending upon how much of the neck was available for the specific study (Table 6). Böhmer (2013) showed that the ostrich neck has a greater amount of flexibility towards the posterior part of the neck in dorsal flexion, towards the anterior end of the neck in ventral flexion, and lateral flexion is almost even throughout the neck flexion. This contradicts the studies by Dzinski and Christian (2007) and Cobley et al. (2013). Dzinski and Christian (2007) demonstrated that dorsoventrally, the ostrich neck was slightly flexible toward the anterior, very flexible in the middle section, and stiffest posteriorly (Table 6). Lateral flexion was also investigated by Dzinski and Christian (2007) and it was measured to also vary in flexibility along the neck (Table 6). In agreement with Dzinski and Christian (2007), Cobley et al. (2013) estimated the highest amount of dorsoventral flexibility per cervical vertebra to be in the middle region of the neck and the least in the posterior end, and the same was the case for lateral flexion. Studies on range of motion in ostrich necks are variable depending on how the flexibility is measured as well as neck completeness, although the consensus is that the ostrich neck exhibits great flexibility.

Table 6: Range of motion in some avian necks (domestic chickens, domestic goose and ostriches), including taxa, maximum dorsoventral and lateral flexion (average per cervical vertebrae), number of cervical vertebrae, and respective references. Notice the diverse cervical numbers used for the chicken and ostrich due to various amounts of the neck used in the studies.

Taxa	Maximum dorsoventral flexion	Maximum lateral flexion	Number of cervical vertebrae	Reference
Domestic chicken	520° (dorsal) (35°) 271° (ventral) (18°)	-	15	Leeuw et al., 2001
	Between 163° - 210.4°/ cervical (increasing posteriorly)	-	13	Russell and Bentley, 2016
Domesticated goose	658° (44°)	183° (12°)	16	Zarnik, 1925
Ostrich	148° (dorsal) (10°) 149° (ventral) (10°)	265° (18°)	16	Böhmer, 2013
	415° (dorsal) (23°) 287° (ventral) (16°)	320° (18°)	19	Dzemski and Christian, 2007
	233° (dorsal) (18°) 121° (ventral) (9°)	224° (17°)	14	Cobley et al., 2013

In addition to the above-mentioned studies of flexibility measured using intact bird necks, Cobley et al. (2013) also measured the range of motion in ostrich necks at various stages of dissection. The change from when all tissues were present to when all muscles and ligaments were removed resulted in a greater flexibility throughout the neck, with the most extreme change happening ventrally in the anterior-most part of the neck as well as laterally at the base of the neck (Cobley *et al.*, 2013). The dissection study by Cobley et al. (2013) nicely demonstrates the extent to which muscles and ligaments contributes to the restriction of flexibility in bird necks.

2.1.1.3 Mammals

Almost all mammals possess seven cervical vertebrae (cf. Chapter 1). The strong evolutionary conservatism of the number of cervical vertebrae in most mammals is thought to be a case of Hox gene expressions, which are genes involved in the development of the axial skeleton in embryos (Galis, 1999). For sloths with five or six cervical vertebrae the Hox gene expression could have caused the same situation as is the case for manatees, whereas sloths possessing eight, nine or ten cervical vertebrae a posterior shift of the Hox

gene expression pattern associated with the first thoracic vertebra could have caused the increase in cervical count (Böhmer *et al.*, 2018).

Table 7: Range of motion (found by osteological maximum flexion) in some mammalian necks (giraffe, camel and sea lion), including taxa, maximum dorsoventral and lateral flexion (average per cervical vertebrae), number of cervical vertebrae, and respective references. Notice only five of the seven neck vertebrae in the sea lion have been measured.

Taxa	Maximum dorsoventral flexion	Maximum lateral flexion	Number of cervical vertebrae	Reference
Giraffe	86° (dorsal) (14°) 62° (ventral) (10°)	73° (12°)	7	Dzemski and Christian, 2007
Camel	143° (dorsal) (24°) 61° (ventral) (10°)	89° (15°)	7	Dzemski and Christian, 2007
Sea lion	(24°)	(15°)	5	Zammit et al., 2008

In long-necked terrestrial mammals, such as giraffes and camels, the cervico-dorsal joint (C7-D1) is the most flexible, and the rest of the neck is less-so (Dzemski and Christian, 2007). More specifically, giraffes (*Giraffa camelopardus*) have shown neck flexibility per cervical joint of up to 15° ventrally and laterally, and 27° dorsally (Table 7) (Dzemski and Christian, 2007), as well as high dorsoventral flexion in the first thoracic vertebra (Gunji and Endo, 2016). Dorsally, camels (*Camelus bactrianus*) are capable of up to 35° of flexion, ventrally up to 20°, and lateral up to 22° per cervical vertebra (Table 7) (Dzemski and Christian, 2007). In camels, dorsal flexion is lowest anteriorly and highest in the middle of neck, with ventral flexion being the least anteriorly and highest in the second joint, and lateral flexion the least anteriorly and most at the base of the neck (Dzemski and Christian, 2007).

Aquatic mammals with seven cervical vertebrae generally possess relatively short necks, and some species show significant flexibility. The range of motion per joint in the neck of sea lions (*Neophoca cinerea*) has been estimated by Zammit et al. (2008) to be 24° per cervical vertebra in dorsoventral flexion, and 15° per cervical vertebra in lateral flexion (Table 7). Generally, pinnipeds have a spine capable of considerable flexion and extension (Godfrey, 1985; Berta and Ray, 1990; Fish *et al.*, 2003; Cheneval *et al.*, 2007). Other than the dolphins (Maresh *et al.*, 2004), cetaceans show the same amount of flexibility within the whole

vertebral column as pinnipeds (Buchholtz and Schur, 2004; Cheneval *et al.*, 2007). The extensive movements of the head and neck in sea lions in a desired direction used during terrestrial progression may be viewed as compromises in adaptations both to anterior placement of the centre of gravity in the body and to overall limb shortening (English, 1976). Sea lions have also adapted to improve the catch of prey when turning, using a rapid neck extension followed by a bite (Cheneval *et al.*, 2007).

Thus, terrestrial mammals tend to have more neck flexibility compared to marine mammals. The variation in neck flexibility in mammals demonstrate the great diversity of size and shape within this group of animals, despite the (almost) consistent cervical count.

2.1.2 Long necks in extant animals

According to Taylor and Wedel (2013b), factors that correlate with long necks include: absolute body length, quadrupedal stance, a small head, numerous cervical vertebrae, elongated cervical vertebrae, and an air-sac system. The giraffe has the longest neck relative to body size among any extant animal, although only two of the above factors apply (quadrupedal stance and elongated cervical vertebrae), whereas in birds three factors apply (small head, numerous and elongated cervical vertebrae) (Taylor and Wedel, 2013b).

Giraffes, cervids, rhinocerotids and equids frequently browse holding the neck at or below shoulder height (Stevens and Parrish, 2005a). The advantage for giraffes compared with the other species is to have an elongated neck enabling them to extend their feeding envelope (Wilkinson and Ruxton, 2012).

Many seabirds possess relatively long necks. Having a long, flexible neck would seem poorly adapted for withstanding high forces, yet a subset of seabirds frequently exhibits plunge-diving at high speeds in order to catch prey and do so without sustaining injury. Work by Chang *et al.* (2016) has shown that the neck muscles act to stiffen the neck and reduce bending stresses during diving, while retaining flexibility at other times. Thus, having a long neck when foraging on aquatic prey is advantageous for seabirds (Orgeret *et al.*, 2016).

In attempting to study the motion of necks, several authors have attempted to reconstruct a 'neutral' neck posture, either through physical manipulation of vertebrae, or via 2D and 3D reconstructions (Stevens and Parrish, 1999, 2005b; Taylor *et al.*, 2009). The resulting biomechanically relaxed posture has been termed the osteological neutral pose (ONP) (Stevens and Parrish, 1999, 2005a, 2005b; Taylor *et al.*, 2009; Stevens, 2013), which allows estimation of range of motion of both extant and extinct animals while the neck is held

straight. However, depending on the morphology of the cervical, ONP will either restrict dorsoventral or lateral flexion (Taylor *et al.*, 2009). In camel necks, the neutral pose reveals a U-curved shape (Figure 40), whereas bird- (Figure 41: right) and horse necks show a S-curvature, and giraffes a sharp upturn at the base of their otherwise straight neck (Stevens and Parrish, 2005b), while alligators only bend slightly in the neck in ONP (Figure 41: left).



Figure 40: Dorsal flexion of a camel neck. The large amount of flexion for each joint is a geometric consequence of its elongated zygapophyses. Notice the catenary shape from anterior to posterior parts of the neck. From Stevens and Parrish (2005b).

By applying ONP to bird necks, Stevens and Parrish (1999) found that it was not possible to flex their neck beyond a minimum of 50 % overlap between zygapophyses of adjacent vertebrae, also referred to as ONP50. Previous studies by Christian and Dzemski (2007) and Taylor *et al.* (2009) has mainly focused on ONP as a predictor for posture. However, a study by Cogley *et al.* (2013) revealed that using ONP50 for ostrich necks resulted in a more flexible neck than by manually manipulating cadaveric material. Furthermore, if the intervertebral cartilage had been dried it allowed more dorsal flexibility (32° on average per cervical) compared with wet cartilage (23° on average per cervical) (Cogley *et al.*, 2013). This increase in flexibility is likely due to an increase in the amount of room for manoeuvrability between the joints (Cogley *et al.*, 2013). Additionally, Cogley *et al.* (2013) found that removing the intervertebral cartilage completely, allowed even greater flexibility (9.9° more compared with the intact neck), which demonstrates how soft tissue affects range of motion.

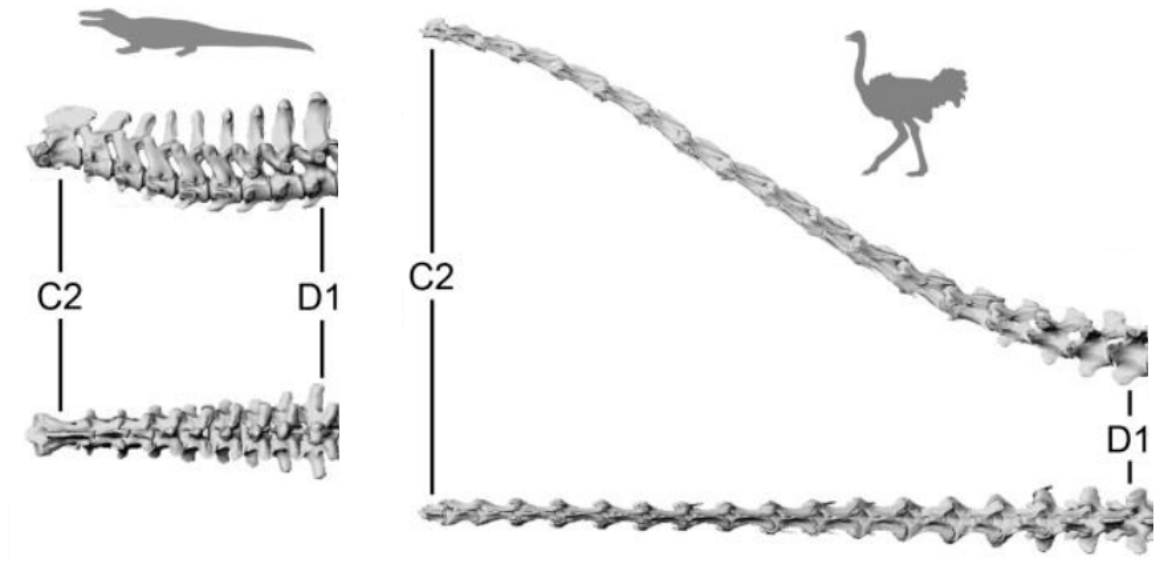


Figure 41: Osteological neutral pose of cervical vertebrae shown using digitally articulated 3D models in an alligator (left: top in lateral view and bottom in dorsal view) and ostrich (right: top in lateral view and bottom in dorsal view). C2 = second cervical vertebrae, D1 = first dorsal vertebrae. Modified from Böhmer et al. (2013).

2.2 Materials and methods

In order to quantify the effect of soft tissue on neck flexibility, and to ascertain the magnitude of error in attempting to reconstruct range of motion from bones only (as will be applied to plesiosaurs in Chapter 3), a partial ostrich neck was physically and digitally manipulated.

2.2.1 Physically manipulated neck

For this study, an ostrich neck was sourced from The Gamston Wood Farm (East Retford, United Kingdom), and the neck was supplied partial (C9-C18). Using three networked raspberryPi microcomputers with camera modules (Figure 42: left), range of motion was recorded in the ostrich neck at progressive levels of dissection. Boumans et al. (2015) and Table 1 from Copley et al. (2013) were used as guidelines for the dissection of each muscle group. Pins were inserted through the soft tissue and into the bone, and the neck was manipulated by hand. The range of motion of the neck was recorded for 8-10 seconds at three stages of dissection: (1) all muscles intact, (2) all muscles removed, and (3) bones only (ligaments removed). The neck was initially held in the same straight neutral position for each stage, except for stage three as the bones were isolated (only two cervical vertebrae were manipulated at a time), and the bones were then bent dorsoventrally and laterally. In each dissection stage, synchronized video was recorded of the moving neck using CompoundPi (Hughes, 2014; <https://compoundpi.readthedocs.io>). Bone pins were then digitized using XMALab (Knörlein *et al.*, 2016) to produce a 3D digital reconstruction of the moving bones.

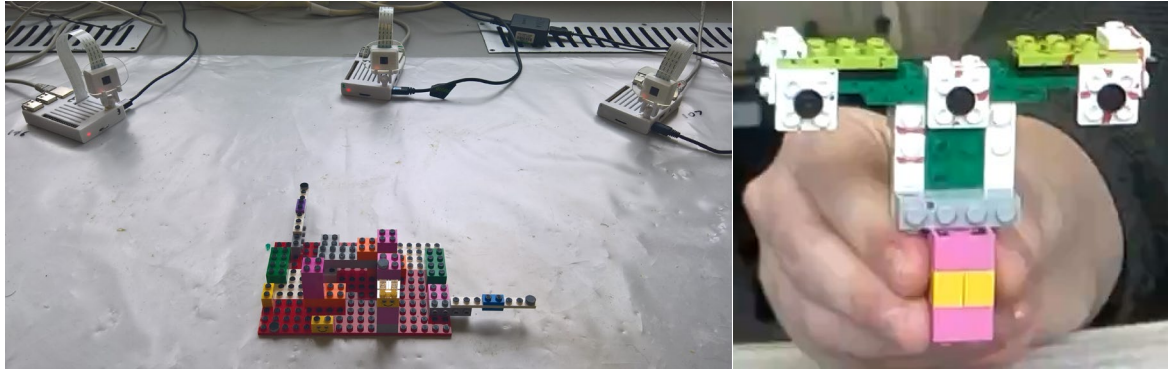


Figure 42: The setup for the study of Chapter 2. Left: The three raspberryPi computers with camera modules in 3D printed housing. Lenses from +3.00 reading glasses are mounted over the camera to focus on close objects, and the Lego calibration object in the centre of the image used to calibrate camera positions in XMALab. Right: Still image of Lego wand object used as reference to measure accuracy and precision of the actual recording of the range of motion in ostrich neck was started. Left from Falkingham et al. (2017).

2.2.1.1 Calibration

Images were taken of the calibration object by the three cameras (Figure 43) before and after each dissection step. The calibration was based on images of a 3D Lego Calibration object, and the identification of the calibration points were semi-automatically tracked in XMALab. An xyz specification file defined the world coordinates of each Lego stub.

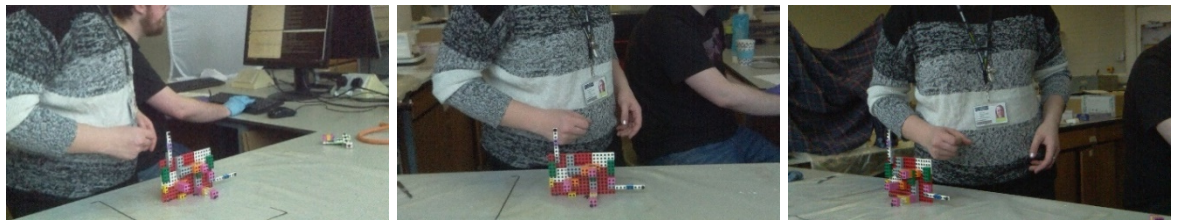


Figure 43: The Lego calibration object showing the whole frame for each raspberryPi camera. Left: Camera 1. Middle: Camera 2. Right: Camera 3.

In addition to the calibration images, recording of a Lego wand (Figure 42; right) was used as reference to measure accuracy and precision of the tracking (for 80mm in actual distance: 80.22mm and 0.756mm, respectively). Adjustments to improve tracking and calibration included factors such as available light, exposure time, camera position, lenses and synchronisation delay of cameras.

2.2.1.2 Marker tracking

White headed pins were inserted in four standard locations in each cervical vertebra, and were tracked in all three cameras in XMALab (Figure 44). Reprojection error (a measure of how well aligned the cameras are) was generally less than 2 pixels, though increased during faster movements because the camera calibration would not detect the markers correctly.

When all markers were tracked throughout the videos, rigid body transformations were calculated for each vertebra.

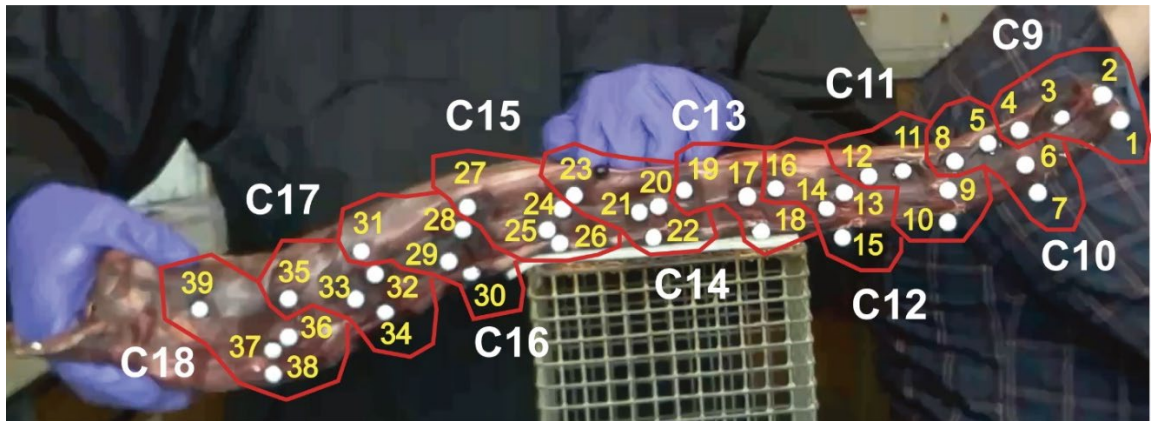


Figure 44: Pins inserted into 10 articulated ostrich cervical vertebrae in lateral view; labelled with respective pin tracking number (indicated by yellow numbers) and cervical number (indicated by red outlines).

2.2.1.3 3D reconstruction

After dissection, each separated cervical vertebrae was digitized (with pins still in place) by photogrammetry (Falkingham, 2011; Mallison and Wings, 2014) using Agisoft Photoscan (www.agisoft.com). The 3D models were imported to Autodesk Maya 2017 (www.autodesk.com) and axes were inserted between each adjacent cervical vertebra (Figure 45) at neutral pose (when cervical ribs aligned), placed in the middle of the anterior face of the centrum (edge of the *facies articularis cranialis*). This pose was similar to the anterior joint in the cervical vertebrae used in Kambic et al. (2017). The axes were made as new nodes in Autodesk Maya creating a dataset for each joint.

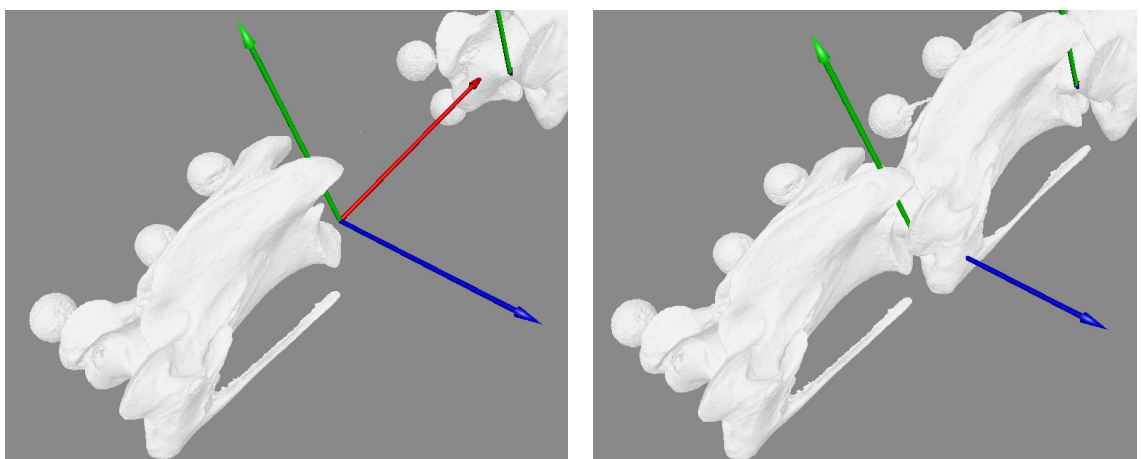


Figure 45: Position of joint axes between two adjacent cervical vertebrae. Red arrow (X-axis) pointing towards the posterior end of the neck, green (Y-axis) pointing upwards, and blue (Z-axis) pointing to the left side of the neck.

Left: Cervical vertebra is hidden to show direction of red arrow. Right: Cervical vertebra is present to demonstrate the red arrow is hidden within the cervical.

Then, rigid body transformations were imported and assigned to the respective vertebrae, resulting in a complete 3D animated scene of the neck in motion. The range of motion was documented using the Graph Editor (Figure 46) showing the rotation for the three axes.

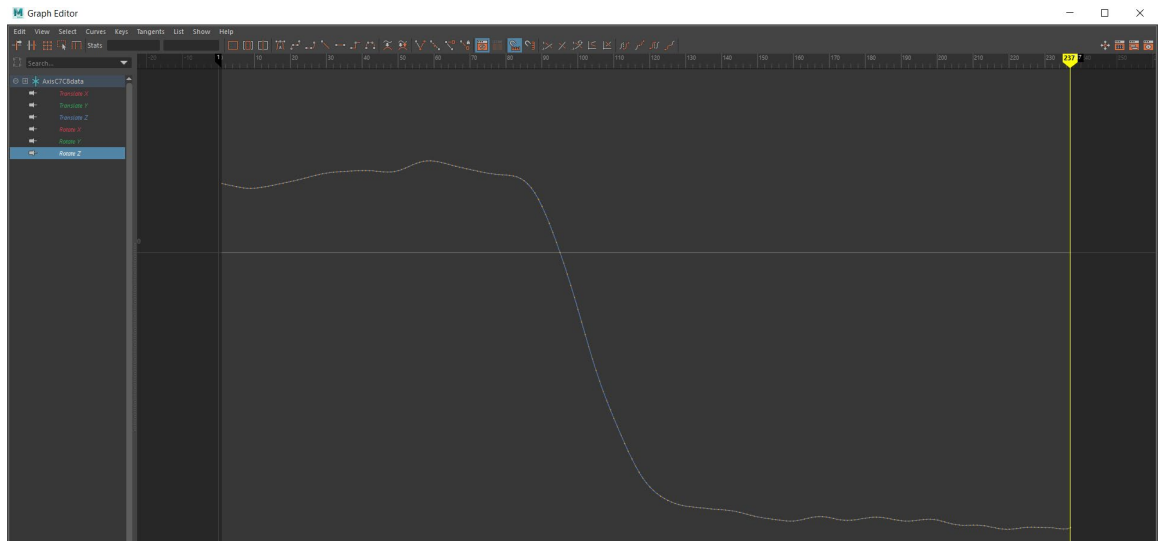


Figure 46: Screenshot of the Graph Editor in Autodesk Maya showing dorsoventral flexion for the intact ostrich neck with data for joint C7-C8. The space above the line is ventral flexion and below is dorsal flexion.

2.2.2 Digitally manipulated neck

In order to assess how accurately range of motion can be estimated from bones alone, 3D models were digitally manipulated to find the maximum osteological range of motion. First, a visibility plane was placed in the middle of the cervical vertebrae, to hide the left-lateral side in order to better visualise the morphology of the centra at the midline, allowing more precise alignment (Figure 47: black part of cervical). The cervical vertebrae were then aligned using the centra as a guideline (Figure 47A: red line). As with the dissected neck, joints were placed in the middle of the anterior face of the centrum (edge of the *facies articularis cranialis*) (Figure 47: yellow crosses) and parented with the respective cervical to allow movement in adjacent cervical vertebrae. Two intervertebral distances (5 % and 10 % of the centra length) were applied to measure how the intervertebral distance (CID = Centra as Intervertebral Distance) would affect range of motion. The CID's were based on the cartilage:bone ratio of 6.30 % previously found in an ostrich neck by Cobley et al. (2013), with a higher and lower ratio selected to investigate the difference in flexibility to the intact neck. The intervertebral distance was the percentage of the cervical vertebra anterior to the joint (e.g. joint C9-C10 used the length of the centrum from C9). Finally, the cervical vertebrae were rotated dorsally, ventrally and laterally until they visually touched to get data on maximum osteological range of motion.

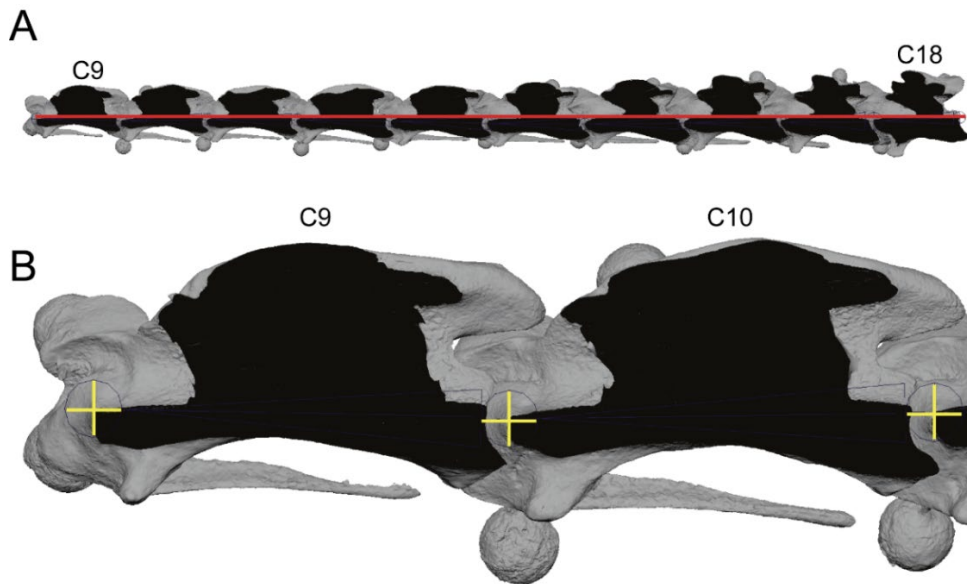


Figure 47: Lateral view of alignment of the digitised ostrich cervical vertebrae in Autodesk Maya with a plane (black part of cervical) cut midway through the cervical vertebrae with attached pins. A) All cervical vertebrae aligned with the horizontal part of the centra above the ribs indicated by a red line. B) Close-up of C9, C10 and the anterior-most part of C11 to visualise the position of joints indicated by yellow crosses.

2.3 Results

An example of the difference between the straight and maximum bent neck is illustrated in Figure 48, using rotation axes as indicators of joint angle variety for each cervical vertebra. The results for the physically manipulated neck using three dissection stages (intact, muscles removed, and bones only) showed joint angles for dorsoventral flexion (i.e. combined dorsal and ventral bending) (Figure 49A) and lateral flexion (Figure 49B) measured in the posterior part of an ostrich neck (C9-C18). For the intact stage, on average the dorsal flexion was 30° , ventral flexion 8° , and lateral flexion 20° (Figure 49A: red lines). When muscles were removed, on average the dorsal flexion was 34° , ventral flexion 13° , and lateral flexion 37° (Figure 49A: blue lines). With the bones only, on average the dorsal and ventral flexion were both 31° , and lateral flexion 35° (Figure 49A: green lines). The average dorsal flexion was higher than the ventral flexion for the intact and muscles removed stages, whereas when the bones were clean the dorsal and ventral flexion were equal. Furthermore, lateral flexion was on average higher than ventral flexion for all three stages of dissection. Total flexibility in the intact neck was 265° dorsally, 71° ventrally, and 183° laterally (right and left combined).

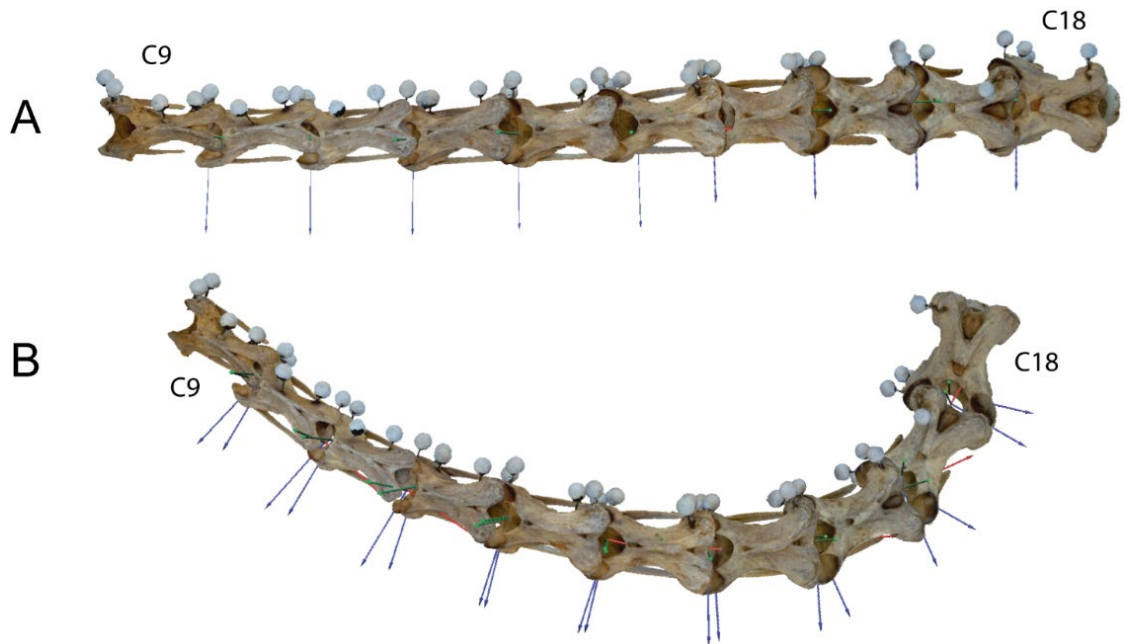


Figure 48: Example of the difference between joint angles for each cervical vertebra visualised in top view showing rotation axes for A) a straightened ostrich neck, and B) the maximum right lateral bent ostrich neck (C9-C18).

The digitally manipulated neck showed an increase in all rotations from 5 % CID to 10 % CID (Figure 46: purple and yellow dotted lines). The average for the digitally manipulated neck using 5 % CID was 28° in dorsal flexion, 26° in ventral flexion and 10° in lateral flexion. Using 10 % CID, dorsal flexion increased on average to 41°, ventral flexion to 38° and lateral flexion to 20°. For both CID's the digitally manipulated neck had a higher dorsal flexion compared with lateral flexion, and dorsal flexion was only slightly higher than ventral flexion.

The intact neck showed a maximum dorsal flexion for a single joint of 46°, and ventral flexion of 18° for a single joint (Figure 49A: red lines). Range of motion was at its greatest around the posterior part of the neck for all rotations. For a single joint the maximum dorsoventral flexion was 64° (joint C14-C15) with least movement in joint C9-C10 at 14° (Figure 49A: red lines). In lateral flexion the intact neck was capable of the most movement in the posterior part of the neck with up to 39° in joint C16-C17 and the least in joint C12-C13 at 8° (Figure 49B: red lines).

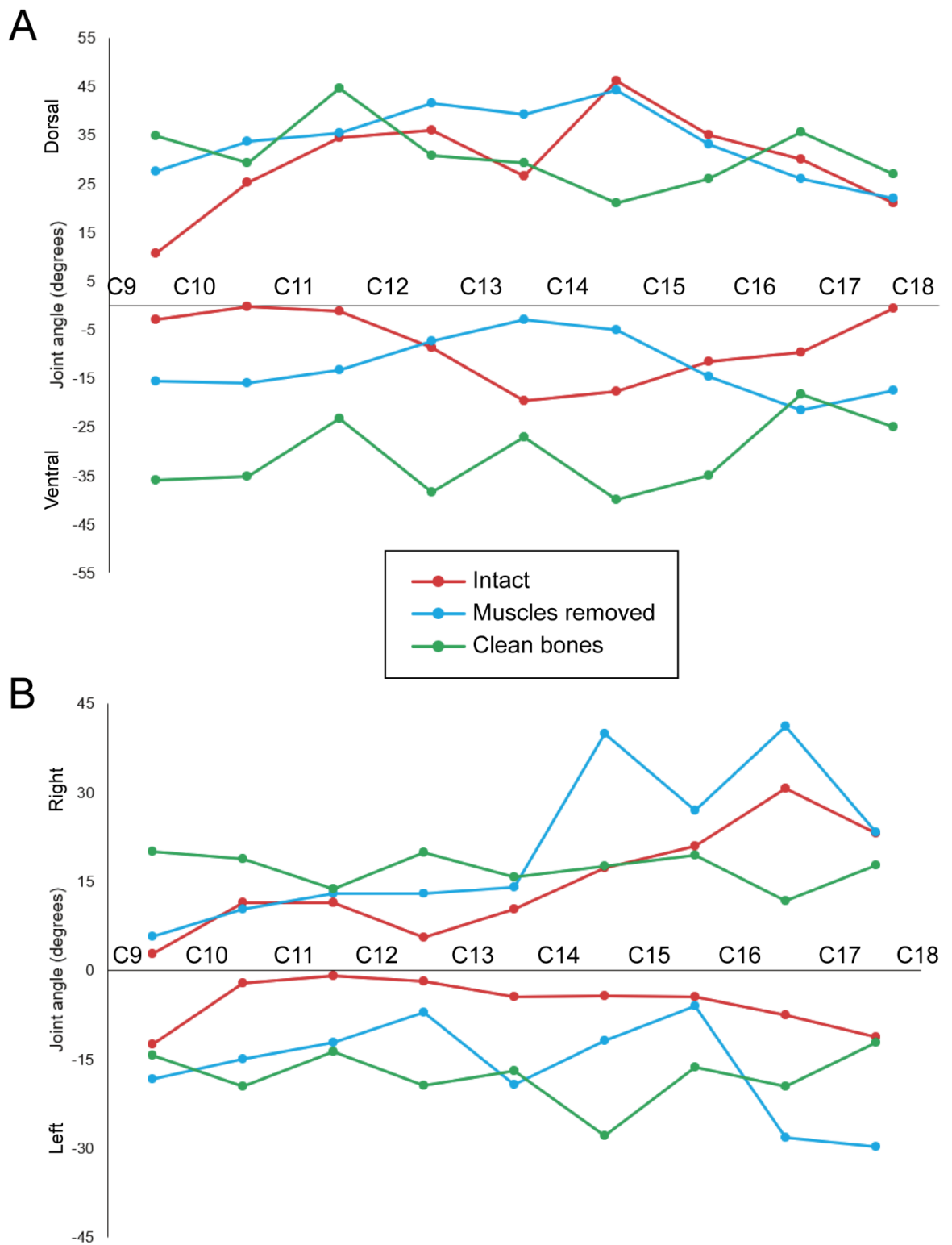


Figure 49: Dorsoventral (A) and lateral (B) rotation measurements from the physically manipulated intact ostrich neck (red), after all muscles had been removed from the neck (blue) and using only the clean bones (green) from cervical C9 to C18.

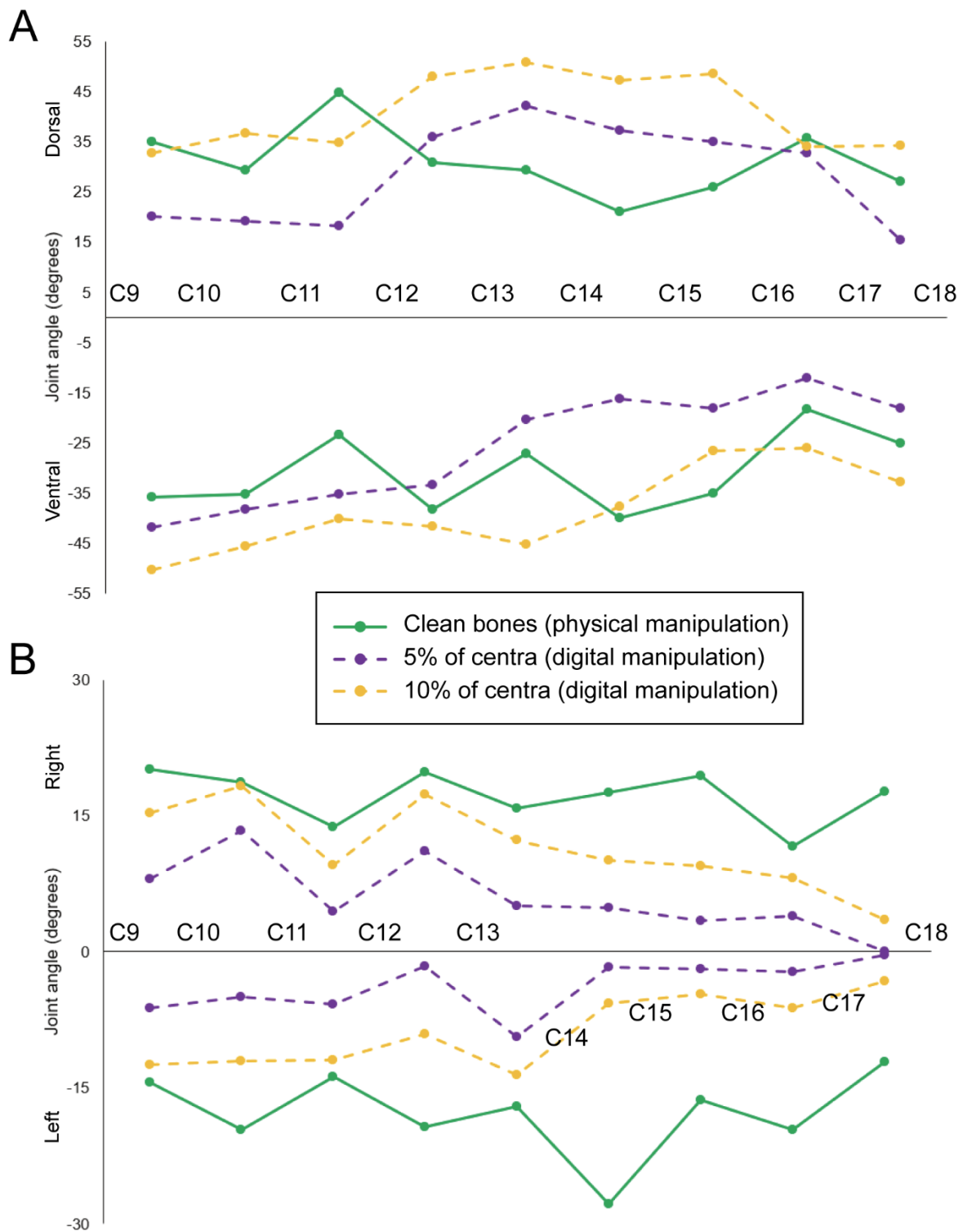


Figure 50: Dorsoventral (A) and lateral (B) rotation measurements from the digitally manipulated ostrich neck, using 5 % (purple dotted lines) and 10 % (yellow dotted lines) of the centra length as intervertebral distances between the adjacent cervical vertebrae (C9 to C18). The green lines illustrate the measurements of the clean bones from the physically manipulated neck for comparison to the results from the digitally manipulated neck.

After muscles had been removed (Figure 45A-B: blue lines), the maximum dorsoventral flexion for a single joint peaked at 49° for several joints (C10-C13, C14-C15). The range of motion increased in dorsal flexion and decreased in ventral flexion towards the middle part of the neck from both ends of the neck (anterior and posterior) (Figure 49A: blue lines). The lateral flexion for when muscles had been removed from the neck was greatest towards the posterior part of the neck, with a maximum of 69° in C16-C17 (Figure 49B: blue lines). Furthermore, lateral flexion increased to both sides (left and right) in the posterior end of the neck, with a maximum right lateral flexion in C16-C17 at 41° and in C17-C18 at 30° for maximum left lateral flexion (Figure 49B: blue lines).

Maximum range of motion recorded using the clean bones (Figure 49A-B: green lines) showed a maximum dorsal flexion of 45° in joint C11-C12, maximum ventral flexion of 40° in joint C14-C15 and maximum lateral flexion of 46° in joint C14-C15. For a single joint the maximum dorsoventral flexion was 71° in joint C9-C10 (Figure 49A: green lines), and in joint C14-C15 the lateral flexion peaked as 46° for a single joint (Figure 49B: green lines).

The results for the digitally manipulated neck showed joint angles for dorsoventral flexion (Figure 50A: purple and yellow dotted lines), and lateral flexion (Figure 50B: purple and yellow dotted lines) measured in the posterior part of an ostrich neck (C9-C18). For the trial using 5 % CID, the maximum dorsoventral flexion was measured as 62° in C13-C14, and the maximum lateral flexion as 18° in C10-C11. With 10 % CID trial, the maximum dorsoventral flexion occurred in C13-C14 as 96° , and the maximum lateral flexion was measured as 30° in C10-C11, which meant that the maximum flexions occurred in the same joint for both applied CID's. Overall, measuring range of motion using the digitally manipulated ostrich neck, lateral movement was the lowest among all measurements for the neck (Figure 50A-B: purple and yellow dotted lines).

Visualisation of the rotations for dorsal, ventral and lateral movements for all three dissection stages of the ostrich neck (C9-C18), as well as the two CID's using the digitally manipulated neck, are illustrated in Figure 51. The figure gives a clear indication of how the physically and digitally manipulated neck approaches differ in all rotations and demonstrates clearly the low amount of lateral flexion compared with dorsoventral flexion in all five manipulations.

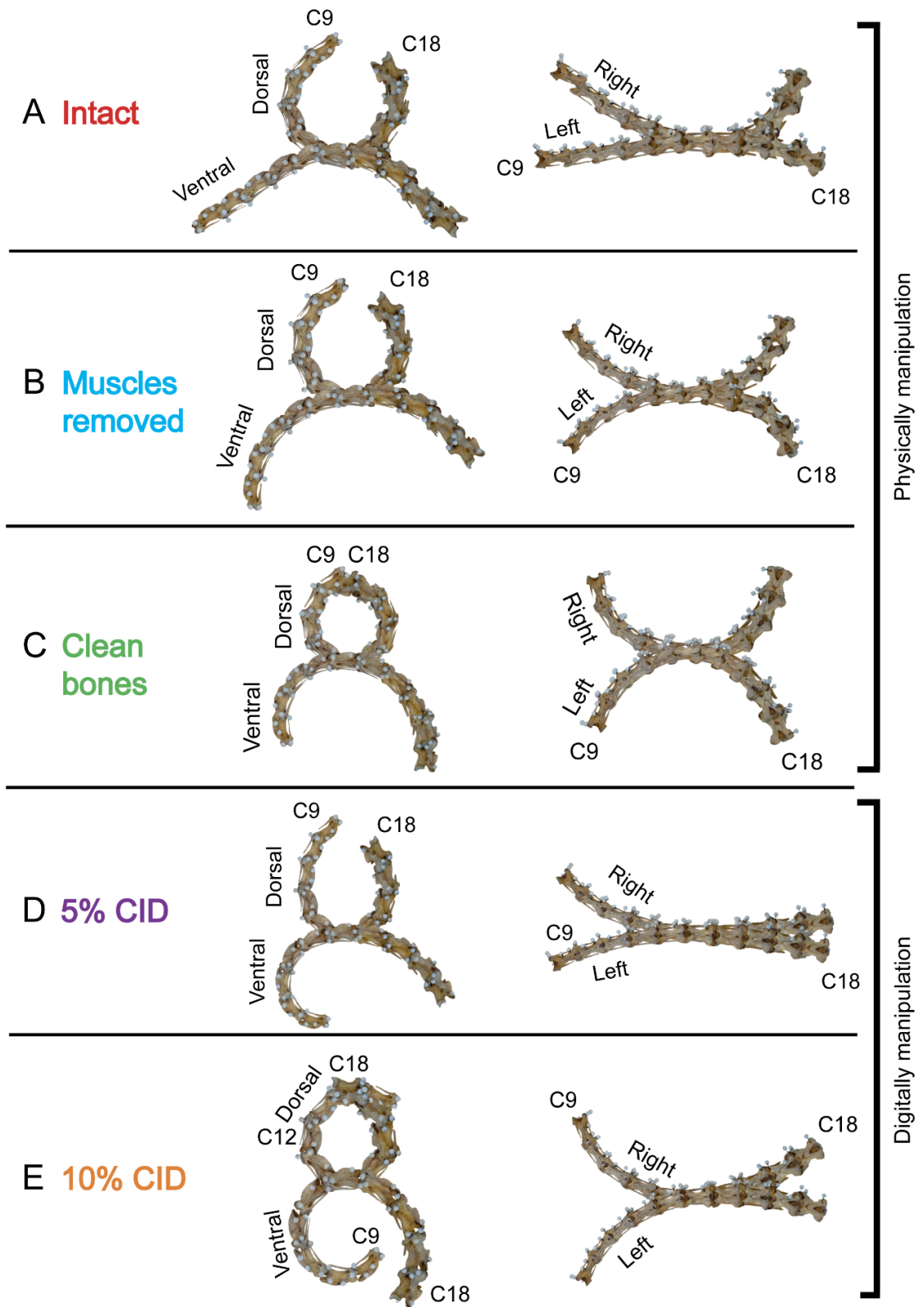


Figure 51: Dorsoventral and lateral rotation visualisations. A-C from the physically manipulated ostrich neck, and D-E from the digitally manipulated ostrich neck (C9-C18) used in the present study. (A) The intact neck, (B) after all muscles had been removed from the neck, (C) using only the clean bones, (D) using 5 % of the centra as intervertebral distance, and (E) using 10 % of the centra as intervertebral distance.

2.4 Discussion

2.4.1 Physically manipulated neck

The posterior-most part of the ostrich neck used in the present study was more flexible when muscles were removed, and again going from the dissection step “muscles removed” to “clean bones”. Dorsal and right lateral flexion was slightly reduced when going from “muscles removed” to “clean bones”. Thus, the results demonstrated what was expected prior to the study.

While intuitively removing soft tissue must increase flexibility, quantifying such an increase in flexibility requires an experimental rather than a simple intuitive approach. The experiments described in this chapter demonstrated that dorsal flexion was on average increased 14 % going from intact to muscles removed, and increased 8 % from muscles removed to clean bones. Ventral flexion was increased by more than half as much (61 %) going from intact to muscles removed, and more than doubled (145 %) from muscles removed to clean bones. Lateral flexion almost doubled (83 %) going from intact to muscles removed, and decreased 6 % on average from muscles removed to clean bones. Going from intact to clean bone the average ventral flexion almost tripled (292 %), dorsal flexion only had a 5 % increase, and lateral flexion increased $\frac{3}{4}$ (72 %).

For the joints C13-14 and C14-15, ventral flexion was lower when muscles were removed compared to when the neck was still intact, even though it would be expected to show the reversed scenario. The same case was shown for the difference between the dissection stage when muscles were removed to when only the clean bones were present, as five joints had a lower dorsal flexion and one joint had a lower ventral flexion, even though we would expect the opposite. A possible explanation for these results could be that each joint was not flexed to its maximum (or flexed below or above its maximum) when the neck was still intact, when muscles were removed or when going from muscles removed to clean bones. Therefore, the degrees of flexion would not have been equally controlled but would vary in flexion at the three dissection stages. Despite this, the overall ventral flexion showed a general increase in the movement going from an intact neck to muscles removed, as well as going from muscles removed to clean bones. Only the clean bones had a slightly lower dorsal and lateral flexion on average compared with the stage when the muscles removed.

For the intact neck, left and right lateral flexion measurements were noticeably different, with the most movement in the left direction in the middle part of the neck and towards the

right direction in the posterior part of the neck (Figure 49B and Figure 51A), which is not what would be expected as the ostrich should be able to move its head to both sides equally. By bending the neck physically, the soft tissue surrounding the neck restricts movement towards the left compared with bending the neck to the right. The restriction in the left direction could have been caused by how the neck was preserved prior to the present study, as the neck was bought frozen, curled up in dorsal flexion affecting the movement of the muscle when defrosted. From previous studies of lateral flexion in ostriches there is no clear indication of whether left and right lateral neck movements vary significantly (Dzemski and Christian, 2007; Böhmer, 2013; Cobley *et al.*, 2013), as the results for lateral flexion measurements in these studies have only been presented as “lateral” rather than a division of left and right such as in the present study. Thus, it cannot be excluded that lateral flexion in ostrich necks is significantly different in left and right rotations.

Cobley *et al.* (2013) found that the change from when all tissues were present, to when all muscles and ligaments were removed, resulted in a greater flexibility throughout the neck. This corresponds with the results from the present study for a few of the joints in the neck, as the increase in flexion with each dissection stage demonstrated how the dissection stages affect the rotation of the neck.

The range of motion data on dorsoventral flexion from the present study conflicts with existing data on range of motion in the posterior part of ostrich necks from Dzemski and Christian (2007), as their study showed most dorsoventral range of motion in the middle part of the neck while results presented here showed most dorsoventral and lateral flexion in the posterior part of the neck. Lateral flexion found by Dzemski and Christian (2007) increased towards the posterior end of the neck and was similar to the present study. It should be noted that this study only includes the posterior-most part of an ostrich neck, whereas Dzemski and Christian (2007) included a whole neck in their study. It is therefore not possible to state whether the present study and the study by Dzemski and Christian (2007) would have been similar if the present study included a complete neck rather than the posterior-most part. The dorsoventral flexion in the present study would have had to be greater in the anterior part of the neck before it would show similar results to that of Dzemski and Christian (2007). However, if the dorsoventral flexion in the present study was greater than what was in fact measured, the average dorsoventral flexion per cervical vertebrae would have exceeded the average of what has been found by Dzemski and Christian (2007). Therefore, the results produced from the present study differ from the results produced by Dzemski and Christian

(2007), most likely caused by variation in method and completeness of the neck used in the present study and the study by Dzemski and Christian (2007).

Furthermore, Cobley et al. (2013) found that both dorsoventral and lateral flexion was greatest in the anterior end of the neck, and we cannot be sure if that was the case in the present study, as the anterior part of the neck was missing. In contrast to Dzemski and Christian (2007) and Cobley et al. (2013), Böhmer (2013) found similar results to the present study, by means of range of motion increasing towards the posterior end of the neck in dorsal flexion, and ventral flexion being almost consistent throughout the neck. Lateral flexion did not change considerably in the neck according to Böhmer (2013), though in the present study the lateral flexion increased posteriorly, mostly towards the right direction showing dissimilarities to the results by Böhmer (2013).

The total dorsoventral and lateral flexion found in the present study most closely resembles the results from Cobley et al. (2013) and Böhmer (2013), and was the least similar to the study by Dzemski and Christian (2007). The difference in method used in the three previous studies (Dzemski and Christian, 2007; Böhmer, 2013; Cobley *et al.*, 2013) and the present study clearly shows how various approaches can lead to very different results, impacting how the results on overall range of motion are being interpreted in terms of biomechanics and ecology of the specific animal.

2.4.2 Digitally manipulated neck

The range of motion recorded using a digitally manipulated ostrich neck showed a limited lateral flexion in the whole neck decreasing posteriorly, whereas ventral flexion peaked around the middle part of the neck, and dorsal flexion peaked at the posterior end of the neck (Figure 50B: purple and yellow dotted lines). Using 5 % CID (Figure 50: purple dotted lines), dorsoventral and lateral flexion was lower than that of 10 % CID (Figure 50: yellow dotted lines). Dorsal and ventral flexion both almost increased 50 % going from 5 % to 10 % CID, and lateral flexion more than doubled going from 5 % to 10 % CID. Results from the present study using a digitally manipulated neck, demonstrated that an increase in intervertebral distance affected range of motion evenly throughout the posterior-most part of the neck.

2.4.3 Comparing the two methods

Prior to the study it was expected that the results from using the clean bones only by physically manipulating, an ostrich neck would have similar results to the method using a digitally manipulated ostrich neck. It is clear from this study that the two methods for

measuring range of motion in an ostrich neck using only clean bones showed almost similar results. The results from the digitally manipulated neck were consistent in both dorsoventral and lateral flexion (Figure 50A-B: purple and yellow dotted lines) compared with the method using physical manipulation (Figure 50A-B: green lines). Also, the amount of dorsoventral flexion in each joint was almost equal when using the physically manipulated bones compared with the digitally manipulated bones. The range of motion results using the clean bones in the physical manipulation most closely resembled the results of the 10 % CID range of motion using digital manipulation, though more than 10 % CID would be resembling lateral flexion better. However, the restriction of movement when the clean bones were physically versus digitally manipulated were slightly different for the one reason that the bones were not held in identical positions for each rotation, whereas it was easier to control the position of the bones digitally. The two methods can tell us that the intervertebral distance between the cervical vertebrae has a significant impact on the results when we only use digitally manipulated bones. The results from the digitally manipulated bones were not completely accurate compared with the physically manipulated bones, though the results showed that the method using digital manipulation can be used to indicate a closely resembling range of motion in long-necked animals, such as plesiosaurs, from using the cervical vertebrae only.

The results in the present study have allowed to interpret the importance of soft tissue when we want to know the flexibility of a neck. The average range of motion in the anterior and posterior most joints of the neck increased with each step of dissection, and especially for ventral flexion the amount of extra range of motion going from an intact neck to when only having the bones increased significantly. Clearly, the more intact the neck was, the closer to *in vivo* capabilities the flexibility of the neck would be. If we want to find out what the range of motion would be in the neck of a plesiosaur while it was still alive, we can at least say that it would typically be lower than the osteological maximum range of motion, even if intervertebral spacing was limited. The present study has helped to gain more knowledge on the meaning of soft tissue and the importance of intervertebral spacing in long-necked extant animals. The approach used in the present study can ultimately help to improve the current knowledge of soft tissue and the importance of intervertebral distance in extinct animals, such as plesiosaurs.

Generally, heterocoelous shaped centra (as in the case of the ostrich neck studied here) allow more range of motion in comparison with other centra shapes, partly due to the zygapophyses

being the restricting factor in this centra shape. The range of motion in a particular vertebrate neck will always depend on the type of vertebrae mostly. Also, the number of cervical vertebrae contributing to the shape of the neck has an impact and meaning for how much range of motion is possible, e.g. birds have a lot of cervical vertebrae in comparison to mammals and reptiles. Therefore, as the shape of the cervical vertebrae in birds differ from plesiosaur neck vertebrae, we will also have to consider the shape of the cervical vertebra before finding the flexibility in plesiosaur necks.

For the setup for the dissected neck, the results also showed limitations of the camera module hardware that meant high resolutions and short exposure times were difficult, making the current hardware unsuitable for moderate to fast motion. However, already more advanced camera modules are available at low cost, and this system (or similar systems) should become much more effective in the immediate future. With this system, it was possible to reconstruct 3D bone motions with promising levels of accuracy and precision compared to previous studies on neck movement in ostriches, and at a very low cost, and the method may be of use to researchers with limited resources.

2.5 Conclusions

This study has provided data on range of motion in the posterior-most part of an ostrich neck by means of progressive stages of dissection (PiROMM) using physical manipulation as well as digital manipulation, using only the bones of the cervical vertebrae. The maximum flexibility of an ostrich neck has been shown to mostly be restricted by muscles, tendons, and ligaments, as it has been observed that the overall flexibility of the neck in the present study increased with dissection stages, as would be expected. Results from using digitally manipulated cervical vertebrae to find range of motion in an ostrich neck has demonstrated through this study that results are somewhat similar to the range of motion found using an intact ostrich neck. Thus, a reliable measurement of the osteological maximum range of motion in the necks of extinct animals (including plesiosaurs) can be obtained by inserting an intervertebral distance which is comparable to modern long-necked tetrapods in the adjacent cervical vertebrae. We are able to interpret the results from studies like the present, to suggest biomechanical and ecological restrictions of the neck in extinct animals using the digitally manipulated approach as will be shown in the following chapter, using cervical vertebrae from plesiosaurs.

Chapter 3 – Range of motion in plesiosaur necks

3.1 Introduction

Range of motion (RoM), as seen in the previous chapter, can help explore ecology of a given species. RoM in the neck of plesiosaurs has previously been studied using various techniques, e.g. by physically manipulating cervical vertebrae (Zarnik, 1925; Welles, 1943), by mathematically calculating intervertebral distance using specific morphological characters of the cervical vertebrae and thereby calculating the RoM between each set of cervical vertebrae (Evans, 1993), or using 2D cardboard cut-outs (Zammit *et al.*, 2008). Recently, 3D models made from CT scans of plesiosaur cervical vertebrae have been used to measure RoM in a fully articulated specimen with cervical vertebrae arranged both as *in situ* and with minimal intervertebral spacing (Nagesan *et al.*, 2018).

In this chapter, the morphology of the plesiosaur neck is reviewed, with additional listing of previous RoM studies in plesiosaurs. Furthermore, the importance of intervertebral distance between adjacent cervical vertebrae is considered. The main part of this chapter focuses on new analyses assessing RoM in the neck region of four different plesiosaur specimens. 3D models were made using photogrammetry, and digital manipulation was applied to the 3D models to determine intervertebral flexibility. The results are discussed in the light of the results from the previous chapter, in connection with previous studies on the RoM in plesiosaurs, as well as what the results mean for plesiosaur ecology and other aspect of its biology.

3.1.1 Plesiosaur neck morphology

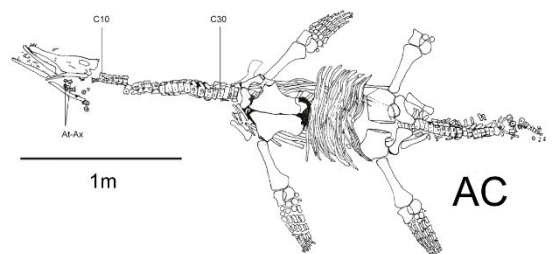
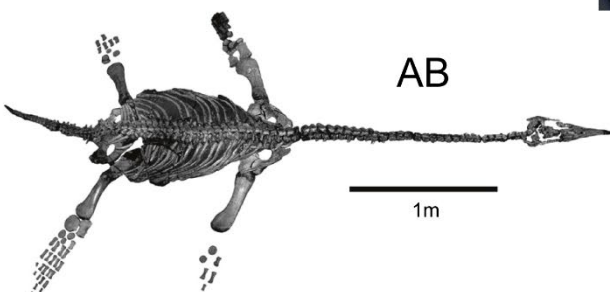
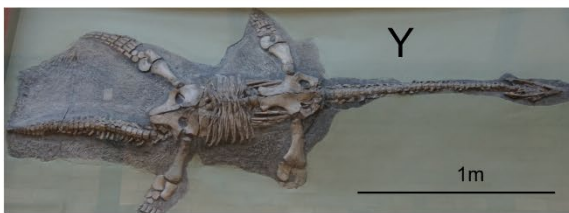
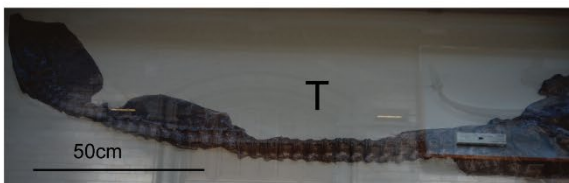
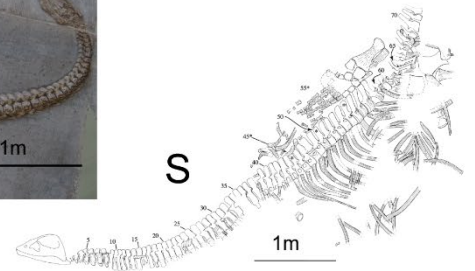
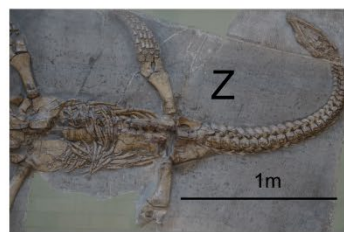
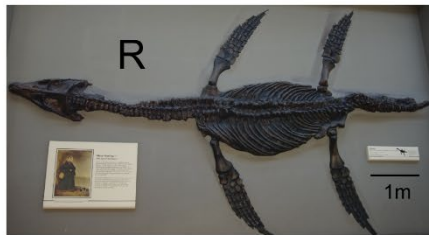
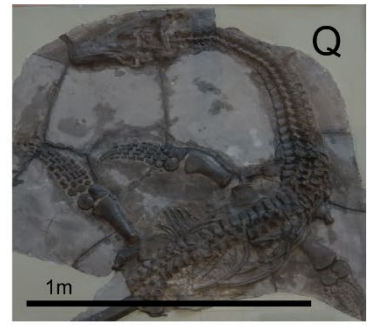
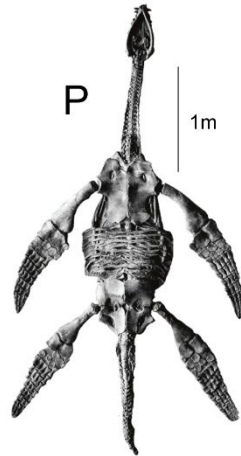
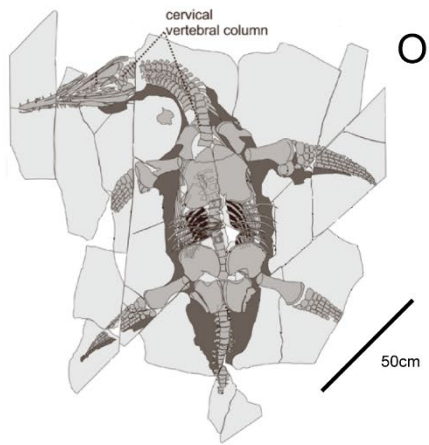
Plesiosaurs are extinct marine reptiles (cf. Chapter 1), and if we want to study the neck flexibility in these animals we are therefore limited to use only the morphology of the vertebrae. This is due to the restricted knowledge about neck myology of plesiosaurs as a result of the rare preservation of soft tissue with only two known examples (Frey *et al.*, 2017; Vincent *et al.*, 2017a), unlike what we see in ichthyosaurs (e.g. Martin *et al.*, 1986). By looking at the dimensions and number of vertebrae it is possible to spot evolutionary trends in plesiosaur necks. Preservation of articulated plesiosaur necks indicate various neck poses occurring post-mortem and allow us to study intervertebral distances *in situ* specimens as well as range of motion.

3.1.1.1 Preserved posture of plesiosaur necks

Many plesiosaurs have been preserved with necks articulated (Figure 52), and in numerous specimens the necks are curved. Several of the curved necks are only slightly bent in either the anterior or posterior part of the neck, though some are nearly straight. Extreme cases of neck bending may be related to opisthotonos, at least for dorsal flexion as the definition of opisthotonos is a dorsally hyperextended posture, opisthotonus (greek: *opistho* = behind, *tonos* = tightening (Reisdorf and Wuttke, 2012) which is characterized by the skull and neck being curved over backwards (Faux and Padian, 2007). Opisthotonic posture seems mostly to be a result of a post-mortem process (Reisdorf and Wuttke, 2012), and this posture must be seen as a normal phenomenon occurring after death. However, the posture does not represent a life posture or even range of motion during life. Indeed, the high amount of plesiosaur necks with opisthotonic posture shows that opisthotonus is not an automatic consequence of having a long neck as the posture occurs for both short- and long-necked plesiosaurs. Also, the opisthotonic posture in e.g. *Plesiosaurus microcephalus* (Figure 52Q) seem to have been caused by the neck broken off at the base, allowing higher movement in the preserved neck in the posterior region.

Figure 52 (following 2 pages): Examples of photos and illustrations of well-preserved articulated plesiosaur necks.

A) *Hydrotherosaurus alexandrae* (Welles, 1943), B) *Rhaeticosaurus mertensi* (Wintrich *et al.*, 2017a), C) *Nakonanectes bradti* (Serratos *et al.*, 2017), D) *Nichollssaura borealis* (Druckenmiller and Russell, 2008b), E) *Raptocleidus blakei* (Evans, 2012), F) *Albertonectes vanderveldei* (Kubo *et al.*, 2012), G) SMNS 51945 (Vincent *et al.*, 2017a), H) *Avalonnectes arturi* (NHMUK R14550) (Benson *et al.*, 2012a), I) *Eoplesiosaurus antiquior* (Benson *et al.*, 2012a), J) *Microcleidus tournemirensis* (Bardet *et al.*, 1999), K) *Plesiosaurus dolichodeirus* (Conybeare, 1824), L) *Futabasaurus suzukii* (Sato *et al.*, 2006), M) *Microcleidus melusinae* (Vincent *et al.*, 2017b), N) *Thililua longicollis* (Bardet *et al.*, 2003), O) *Mauriciosaurus fernandesi* (Frey *et al.*, 2017), P) *Meyerasaurus victor* (Smith and Vincent, 2010), Q) *Plesiosaurus microcephalus* (Owen, 1840), R) *Rhomaleosaurus cramptoni* (displayed at NHMUK), S) *Kaiwhekea katiki* (Cruikshank and Fordyce, 2002), T), *Plesiosaurus dolichodeirus* (displayed at NHMUK), U) *Archaeonectrus rostratus* (displayed at NHMUK), V) *Plesiosaurus dolichodeirus* (displayed at NHMUK), W) *Archaeonectrus rostratus* (displayed at NHMUK), X) *Microcleidus homalospondylus* (displayed at NHMUK), Y) *Thalassiodracon hawkinsii* (displayed at NHMUK), Z) *Thalassiodracon hawkinsii* (displayed at NHMUK), AA) *Microcleidus homalospondylus* (displayed at MMUM), AB) *Hauffiosaurus tomistomimus* (Benson *et al.*, 2011), AC) *Hauffiosaurus zanoni* (O'Keefe, 2001a; Vincent, 2011).



The level of completeness in the preservation in articulated plesiosaur necks allows us to study the movement of the neck. Bending of the neck mostly occurs in the anterior end (Figure 52A; C; D; O; S; U; Z; AA), but is also observed at the base of the neck (Figure 52E; Q; X) or broken into two pieces from the base of the neck (Figure 52B; F). Articulated plesiosaur necks also appear as bended evenly throughout the neck (Figure 52G; H; J). Generally, from the articulated necks the amount of movement seems to be restricted to around 10 degrees per cervical vertebra on average. Owen (1838) stated that *Plesiosaurus microcephalus* would have been capable of extensive mobility in lateral flexion due to the neck being preserved in a nearly semicircle position (Figure 52Q). Given that we know from modern animals, such as birds, that they are capable of achieving opisthotonic posture post-mortem, the preservation itself cannot tell us about how the animal used its neck while it was alive as muscles would have restricted motion of the neck (cf. Chapter 2).

3.1.1.2 Intervertebral distances in plesiosaur necks

Between two adjacent vertebrae, the intervertebral distance can be measured by examining an animal *in vivo* (e.g. by X-ray or CT) or post-mortem by dissection. Unfortunately, we are not capable of doing an examining *in vivo* or dissect extinct animals (such as plesiosaurs) because we are left only with the bones. By looking at articulated plesiosaur necks, we can measure the intervertebral distance *in situ*. The intervertebral distance varies depending on which side of the neck (dorsal, ventral or lateral) the specimen is measured, and how the neck was positioned at the time of death. The distance can also vary within the neck, e.g. as seen in the anterior part of the neck in the polycotyloid *Thalilua longicollis* (Fischer *et al.*, 2018) showing up to 10 mm between two cervical vertebrae and less in the middle and posterior regions, and up to 5 mm in the anterior part of the neck in the pliosaurid *Gallardosaurus iturraldei* (Gasparini, 2009) with less intervertebral distance in the middle and posterior regions. By studying the intervertebral distance in plesiosaurs, we are able to investigate and interpret how the animals moved while they were alive. For example, if the plesiosaur had a limited amount of intervertebral distance it could indicate that movement in the neck would be restricted, whereas with a larger amount of intervertebral distance would allow greater flexibility of the neck. Recently, Sassoon (2019) described the fusion of cervical centra found in four relatively long-necked plesiosaur specimens which would have caused neck stiffness in these specimens as the flexibility of the neck within the fused centra would have been near impossible. However, as this is the first reported case the extend of neck stiffness in plesiosaurs caused by fused cervical centra is unknown.

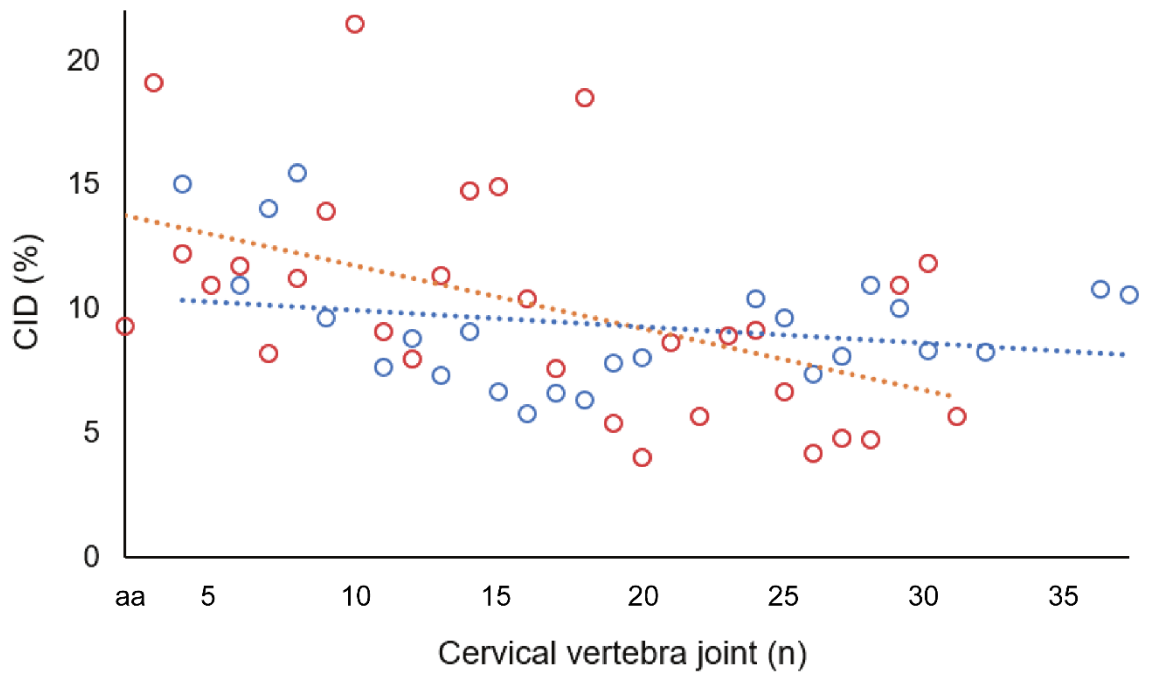


Figure 53: Intervertebral distance as % of centrum length (CID) vs. cervical vertebra joint (n), found in the cryptoclidid PMO 224.248 (blue) measured on the specimen in lateral view, and in the pliosaurid *Thalassiodracon hawkinsii* (cast of NHMUK 2020) (red) measured on the specimen in ventral view. Each point represents a joint between two adjacent cervical vertebrae (e.g. for joint 5 the intervertebral distance is measured between C5 and C6 and the % of centra length is then calculated for C5). Dotted lines indicate trend lines matching in colour with intervertebral distance. Abbreviation; aa: atlas-axis complex.

Registration of intervertebral distances measured from articulated plesiosaur necks have not been performed previously. So, for the present study, intervertebral distances were documented for two plesiosaurs to demonstrate how intervertebral distances vary with neck lengths and plesiosaur family, and what this could mean for the flexibility of the neck. Using photographs of the cryptoclidid specimen PMO 224.248 *in situ*, centra lengths and intervertebral distances were measured where possible (Figure 53 – blue circles). The intervertebral distances in PMO 224.248 varied from 2.7 mm to 5.8 mm (average: 3.9 mm) and the intervertebral distance measured as percentage of the centra length (CID) decreased slightly posteriorly (see trend line in Figure 53) with a maximum of 15.5 %, a minimum of 5.5 %, and an average of 9.3 %. This finding could indicate a relatively more flexible neck at the anterior end as the greater intervertebral distances here would allow higher movement. For the fully articulated neck in the pliosaurid *Thalassiodracon hawkinsii* (NHMUK 2020) (Figure 53 – red circles) intervertebral distances were measured directly on a cast of the specimen. Here, the spacing between the cervical vertebrae ranged from 0.8 mm to 3.4 mm (average: 1.8mm) and decreased towards the base of the neck (see trend line in Figure 53), with a maximum of 19 %, a minimum of 4 %, and an average of 10.1 %. The measurements

from *T. hawkinsii* demonstrated a more equal intervertebral distance throughout the neck compared with PMO 224.248. The average intervertebral distance was 100 % more in PMO 224.248 than what was found in NHMUK 2020, which was caused by the cervical vertebrae being twice as long. Preservation, number of cervical vertebrae, and the specific plesiosaur family thus seems to influence the range of spacing and how it is distributed throughout the neck. Other examples of intervertebral distances found in articulated plesiosaur necks are shown in Figure 54. The amount of intervertebral distance varies depending on the preservation of the neck (straight or curved) and the morphology of the cervical vertebrae. For a straight neck there is not a particular point where the intervertebral distances seem to vary more (Figure 54A), whereas at the highest point of curvature in Figure 54B gives a higher intervertebral distance measured on the right side (ventral side of the plesiosaur) compared with the left side (dorsal side of the plesiosaur) because the centra connect at this point. The highest point of curvature can also be found on the dorsal side if the neck is curved in ventral direction (Figure 52L; S).

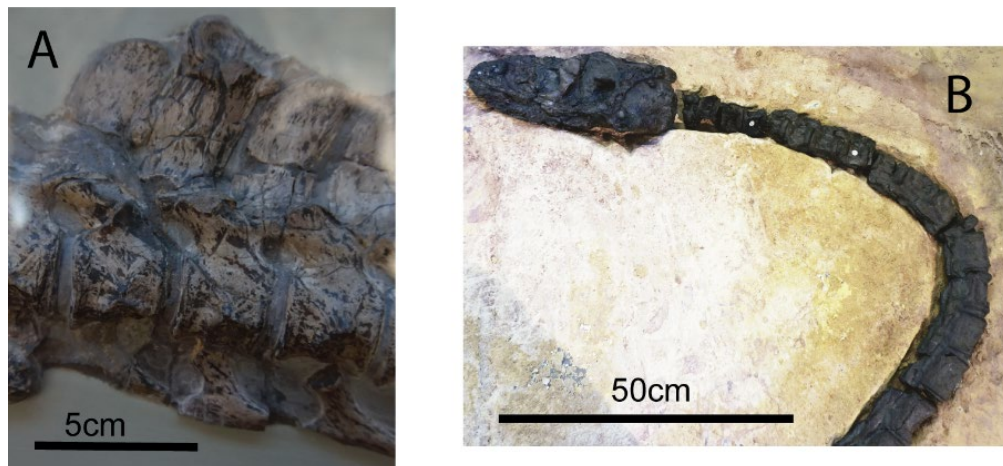


Figure 54: Intervertebral distances found in articulated plesiosaur necks. A) Close-up of four posterior cervical vertebrae in left lateral view of the straight neck in *Thalassiodracon hawkinsii* (NHMUK R14550) with ~0.5mm intervertebral distance between each vertebra. B) Anterior part of the curved neck of *Microcleidus homalospondylus* (MMUM LL. 7007) showing a variety of intervertebral distances (up to 15mm measured in ventral view) created by the dorsoflexed neck.

Elasmosaurids and microcleidids would probably have had less neck flexibility compared with cryptocleidids based on the smaller amount of intervertebral distance found in preserved articulated elasmosaurid necks and the spine of each cervical vertebrae allowing very little flexibility. Based on intervertebral distance, neck flexibility seems to have been different for the various plesiosaur families. Some studies indicate that intervertebral distances decrease during decay by shrinking (dehydration of cartilage) or increase by

displacement of neck vertebrae post-mortem (Faux and Padian, 2007; Reisdorf and Wuttke, 2012; Lingham-Soliar, 2013). This has to be taken into consideration when measuring intervertebral distances in articulated plesiosaur necks by allowing additional space between the adjacent vertebrae, as the cartilage between each cervical could possibly have been different while the animal was still alive.

3.1.2 Previous studies on neck flexibility in plesiosaurs

Range of motion (RoM) can help us understand what plesiosaurs were capable of in terms of neck movement. There are a number of factors that may affect the flexibility of the neck in plesiosaurs such as: geometry of centra faces; length and compliance of the intervertebral distances; angles and dimensions of the zygapophyses; width of the posterior neck vertebrae when the cervical ribs are articulated; and height of the neural spines on the posterior cervical vertebrae (Evans, 1993).

Previous studies on RoM in plesiosaurs give us an indication of the flexibility of necks within the clade (Table 8). In the first documented study on range of motion in plesiosaur necks, Zarnik (1925) found that the necks of several plesiosaur species were limited in dorsoventral flexion and more mobile in lateral flexion, both in the anterior and posterior parts of the neck (Table 8). The high spines in some plesiosaur cervical vertebrae would according to Zarnik (1925) limit the dorsoventral flexion, and zygapophyses would affect lateral flexion to a less degree than dorsoventral flexion. Welles (1943) later used the morphology of the cervical vertebrae to investigate dorsal neck flexibility in the elasmosaurid *Hydrotherosaurus* by placing contiguous vertebrae together, flexing them until the neural spines touched, and then measuring the angle of flexion. The results from Welles' study (1943) (Table 8) showed the posterior ten cervical vertebrae to be relatively inflexible, indicating elasmosaurs had a flexible neck close to the head, and stiffer closer to the trunk. However, as this study only included dorsal flexion it is unclear how lateral and ventral movements would have affected the neck performance in elasmosaurids. Evans (1993) calculated the intervertebral distance and applied the results to calculate neck flexibility in the cryptoclidids *Muraenosaurus leedsii* (NHMUK R2863) and *Cryptoclidus eurymerus* (NHMUK R2860), the former having on average 14 % of the centrum length as intervertebral distance and the latter 20 % on average. Evans (1993) showed that *M. leedsii* had less flexibility than *C. eurymerus* (Table 8) which corresponded with the intervertebral distance as the higher intervertebral distance creates more flexibility, as well the longer cervical vertebrae in *M. leedsii* which create less movement. Measurements of potential flexion in both vertical and horizontal planes in the

necks of elasmosaurids have been made by Zammit and colleagues (2008) based on life-sized two-dimensional models of individual vertebrae constructed out of cardboard. Lateral flexion was generally measured as higher than dorsoventral flexion for the elasmosaurids used in this study (Table 8). Most recently, Nagesan et al. (2018) studied the flexibility in the neck of the leptocleidid *Nichollssaura borealis* using two approaches: paired cervical vertebral mobility using the original intervertebral distance and by using a minimum intervertebral spacing. From the former approach dorsoventral and lateral flexion was more than the double of the latter approach (Table 8) indicating that the intervertebral distance has a great impact on the overall RoM.

Plesiosaur necks comprise many cervical vertebrae (Figure 12) compared with modern animals (cf. Chapter 1), so even a small amount of movement between each bone would sum to provide significant flexibility over the whole neck because of intervertebral space allowing a certain degree of bending between each pair of adjacent cervical vertebrae. A study by Cruickshank and Fordyce (2002) found that the elasmosaurid *Kaiwhekea katiki* provide no evidence of a serpentine mobility of the neck in this species due to its high neural spines. According to two recent studies by Noè et al. (2017) and Wintrich et al. (2017a) ventral flexion would be predominant in plesiosaurs, with dorsal and lateral movements restricted to a minimum. The major flexibility in ventral rotation would have been facilitated by the anatomy of the cervical vertebrae (Noè *et al.*, 2017; Wintrich *et al.*, 2017a). More recently, Otero et al. (2018) found that at least for the elasmosaurid *Aristonectes quiriquinensis*, the anterior-most cervical vertebrae along with the anterior portion of the skull and atlas-axis complex indicate restricted ventral and lateral movement of the skull. The restricted movement would be due to a blockage made by a frontally projected anteroventral boundary in the atlas-axis complex, which is unseen in elasmosaurids (Otero *et al.*, 2018).

Table 8: Overview of range of motion data from previous studies on plesiosaur necks, including specimen, maximum dorsal, ventral and lateral flexion (average per cervical vertebrae), position of the cervical vertebrae in the neck region, intervertebral distance used in each study, and respective references. For the study by Nagesan et al. (2018) two approaches were used (PCVM = paired cervical vertebral mobility, and MIS = minimum intervertebral spacing).

Specimen	Max. dorsal	Max. ventral	Max. lateral	Position	Intervertebral distance	Reference
<i>Muraenosaurus durobricensis</i>	-	-	(14°)	Anterior	~1 cm	Zarnik, 1925
			(12°)	Posterior		
<i>Plesiosaurus bavaricus</i>	(6°)	(5.30°)	(11°)	Anterior		
<i>Plesiosaurus guilelmi imperatoris</i>	(5°)	(6°)	(11°)	C12-C13		
	(5°)	(6°)	(15°)	C22-C23		
<i>Hydrotherosaurus</i>	(10°)	-	-	C1-C40		
	(5°)	-	-	C40-C50		
	(3°)	-	-	Posterior 10		
<i>Cryptoclidus eurymerus</i> (NHMUK R2860)	656° (22°)	656° (22°)	561° (19°)	Atlas-axis-C3	15-26 % (average 20 %) of centra length	Evans, 1993
<i>Muraenosaurus leedsii</i> (NHMUK R2863)	540° (13°)	540° (13°)	454° (11°)	C3-C4	4-19 % (average 14 %) of centra length	
<i>Aphrosaurus furlongi</i> (CIT 2832)	87° (1°)	75° (1°)	94° (1°)	The whole neck	1 mm	Zammit et al., 2008
	130° (2°)	135° (2°)	147° (2°)		2 mm	
	155° (3°)	177° (3°)	176° (3°)		3 mm	
SAM P6181 (elasmosaurid)	-	-	17° (1°)		1 mm	
			43° (4°)		2 mm	
			55° (4°)		3 mm	
AM F87826 (elasmosaurid)	-	-	43° (1°)		1 mm	
			77° (3°)		2 mm	
			177° (4°)		3 mm	
QMF 2567 (elasmosaurid)	-	-	23° (1°)		1 mm	
			39° (2°)	2 mm		
			60° (3°)	3 mm		
	-	-	11° (1°)		1 mm	

<i>Woolungasaurus glendowerensis</i> (RMF R271)			23° (2°)		2 mm	
			35° (3°)		3 mm	
<i>Nichollssaura borealis</i> (TMP 1994.122.0001)	PCVM: 216° (11°)	PCV M: 226° (11°)	PCVM: 258° (13°)	The whole neck	Original from <i>in situ</i>	Nagesan et al., 2018
	MIS: 81° (5°)	MIS: 102° (5°)	MIS: 106° (5°)		Vertebrae touch (only cavities between the articulated faces as spacing)	

3.1.3 Rationale of the present study

In this chapter the osteological range of motion (RoM) in four plesiosaur specimens is measured (cf. digital manipulation method from Chapter 2), and the general mobility of the neck throughout the clade is investigated via three questions: 1) What is the RoM in the four specimens, 2) how does RoM vary with increased or decreased intervertebral distance, and 3) can RoM be estimated without neural spines and cervical ribs (i.e. using just the centrum)? From the data we are able to see if RoM is the same or varies among the four specimens, as well as identify where in the neck RoM increases/decreases the most. The data will also allow us to explore ecological niches within the plesiosaur clade looking at RoM in various neck lengths and species. Furthermore, if RoM can be measured from using only the centra, it will be possible for future studies to measure RoM for incomplete cervical vertebrae where only the centra are preserved, which is very common among plesiosaur specimens, as spines and ribs break off easily. Establishing the flexibility of a vertebrate neck allows estimation of the ‘feeding envelope’ of a given species, giving the maximum range over which an individual could feed while motionless (Cobley *et al.*, 2013), eventually determining ecological possibilities and adaptations for the given species. In the case of extinct vertebrates (such as plesiosaurs), the range of motion of the neck can also tell us about palaeobiology for the given species. Cervical vertebrae from four plesiosaur specimens (all of which were disarticulated) were digitised and manipulated dorsoventrally and laterally to find the maximum osteological RoM using intervertebral distances of 5, 10, and 20 % of the cervical centra length. The present study is different to other studies because here the RoM is explored in 3D for several plesiosaur species which means that this study includes a more complete and quantitative dataset compared with previous studies (Zarnik, 1925; Welles, 1943; Evans, 1993; Zammit *et al.*, 2008; Nagesan *et al.*, 2018). From the data obtained in

the present study it will be possible to interpret what hunting style plesiosaurs would have practiced.

3.2 Materials and methods

3.2.1 Specimens

Disarticulated cervical vertebrae series from four cryptoclidid specimens were used:

- 19 cervical vertebrae from *Cryptoclidus eurymerus* (GLAHM V1610) which included the atlas-axis to C19 (~60 % of the complete neck).
- 25 cervical vertebrae from *Muraenosaurus sp.* (OUNHM J.95000) which included the atlas-axis to C26 (~63 % of the complete neck).
- 46 cervical vertebrae from an undescribed cryptoclidid (PMO 224.248) which included the atlas-axis to C47 (~94 % of the complete neck).
- 41 cervical vertebrae from *Muraenosaurus leedsii* (NHMUK R2863) which included the atlas-axis to C42 (100 % complete neck).

The specimens were chosen based on availability at the time of the study, as well as enabling complete 3D digitization of individual and nearly complete vertebrae. The 19 cervical vertebrae of *C. eurymerus* comprised slightly more than half of the anterior part of the neck which was the only part recovered from the field of this specimen. The posterior part of the neck of *Muraenosaurus sp.* (OUNHM J.95000) was not completely prepared out of the matrix at the time of data collection, and therefore only about half of the anterior part of the neck was included. A 3D model of the atlas-axis from OUNHM J. 95000 was made from CT-scanning the specimen. The number of cervical vertebrae used from PMO 224.248 comprised nearly the whole neck. The remaining 6 % (C48, C49 and C50) from PMO 224.248 were broken and incomplete, and therefore not included. Overall, a significant portion of the plesiosaur necks used in the present study were available, and provided an opportunity to examine range of motion over those necks portions.

3.2.2 Photogrammetry

Digitisation of the cervical vertebrae from the four plesiosaur specimens was achieved using photogrammetry (Falkingham, 2011). In order to capture the full 3D morphology of each vertebra, two sets of ~80 digital photographs taken with a Sony Nex-6 DSLR camera of each cervical vertebra including scale bar were taken of OUNHM J.95000 supported on a table, with the specimen rotated 180° between sets so as to capture the side previously against the table. The three other specimens, GLAHM V1610, PMO 224.248, and NHMUK R2863,

were individually photographed against a solid white background or using the background of the surface that the cervical vertebrae were placed on. Because the white (or evenly coloured) backgrounds possess no features, it was possible to capture GLAHM V1610, PMO 224.248 and NHMUK R2863 using only one set of ~140 photographs taken with a Sony ILCE-5000 DSLR camera of each cervical vertebra for each specimen, making the process less time-consuming compared with the approach used for OUNHM J.95000. The 3D models of each individual cervical vertebra were scaled to true size from measurements taken with callipers (or via scale bars in the case of OUNHM J. 95000). COLMAP (www.colmap.github.io/) (Schönberger and Frahm, 2016; Schönberger *et al.*, 2016) was used to generate the digital models of OUNHM J.95000 as the merging of the two sets of photographs created modelling issues in Agisoft Photoscan. The digital models of GLAHM V1610, PMO 224.248 and NHMUK R2863 were generated using the standard version of Agisoft Photoscan (www.agisoft.com). Models were scaled (and if necessary merged) in either Cloudcompare (www.cloudcompare.org), Agisoft Photoscan or Autodesk Maya 2017 (www.autodesk.com) depending on the most ideal solution for the specific 3D model.

3.2.3 Attaining range of motion data

Individual 3D models of each vertebra were manually aligned in Autodesk Maya 2017. For estimating RoM, the centre of rotation (CoR) in the aligned cervical vertebrae was determined. CoR has been placed at the centre of the intervertebral disc in previous studies (Stevens and Parrish, 2005a; Taylor *et al.*, 2009; Molnar *et al.*, 2015), and this approach was applied in the present study. The centre point of the centra in anterior view was used as guideline to place the joint between each cervical. In lateral view the cervical vertebrae were aligned so that each joint was positioned with the coordinates (0,0,0). Because *in vivo* intervertebral distances in plesiosaur necks are still an unknown (Welles, 1943; Evans, 1993; Zammit *et al.*, 2008), three alignments were created for each specimen, with intervertebral distances of 5, 10, and 20 % of the centrum length of the anterior cervical. The intervertebral distances were based on the results from Evans (1993) of 14 % and 20 %, as well as percentages below Evans' percentages. Rotation points were moved to 50 % of the intervertebral distance posterior to the relevant cervical, i.e. half way between vertebrae. Each bone was then manually rotated until colliding with the previous bone in dorsal, ventral and lateral direction (Figure 55).

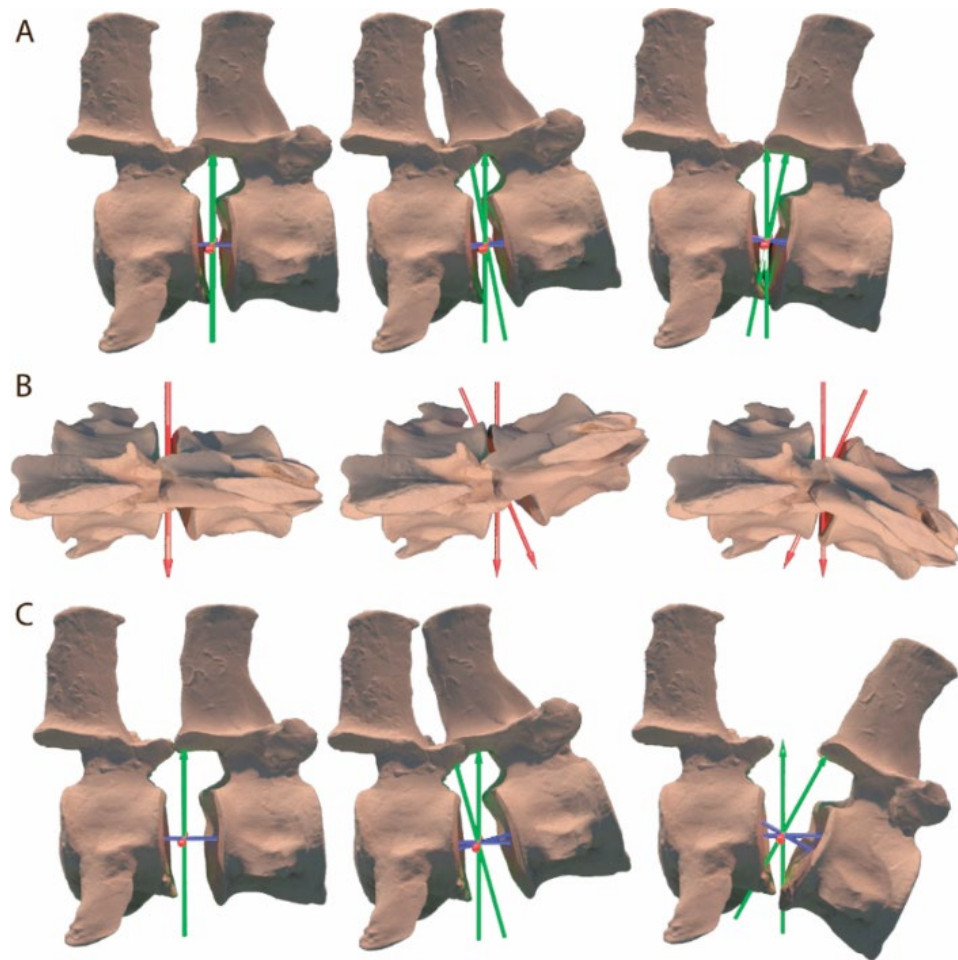


Figure 55: Visualisation of the method applied for measuring range of motion using two adjacent cervical vertebrae (C22-C23 in OUNHM J.95000) rotated until collision between the two. A) Lateral view of 10 % of centra as intervertebral distance in neutral position, dorsoflexion and ventroflexion. B) Dorsal view of 10% of centra as intervertebral distance in neutral position, left lateral flexion and right lateral flexion. C) Lateral view of 20 % of centra as intervertebral distance in neutral position, dorsoflexion, and ventroflexion. Green axes (A and C) illustrate dorsal and ventral flexion, and red axes illustrate lateral flexion (C).

3.2.3.1 Deformed vertebrae

In the cervical vertebrae from the four plesiosaur specimens used in the present study, some of the neural spines, cervical ribs and centra were somewhat deformed (twisted, wedged, eroded or crushed) during fossilisation. The deformations, particularly of the neural spines and pre- and post-zygapophyses, would alter the locations of contact, and hence would alter range of motion results. Various fossils have previously been retro-deformed, e.g. in sauropod tail vertebrae to improve the results on range of motion (Vidal and Díaz, 2017) and a gorilla skull to improve the bilateral symmetry (Schlager *et al.*, 2018). If deformed vertebrae are altered for retro-deformation the results are based on hypothetical models rather than the authentic fossils, making the results even further unreliable as they do not represent the true fossil. Therefore, in the present study an element of subjectivity was used

to determine if collision between bones was due to taphonomic distortion, rather than retro-deforming the cervical vertebrae to have the results based on the actual vertebrae.

3.3 Results

For the purpose of simplicity, results will be stated as 5 %, 10 % and 20 % CID (short for “percent of Centra as Intervertebral Distance”). Lateral flexion was stated as the average of left and right rotations.

The four cryptoclidid specimens used in the present study showed an increase in range of motion with increase in intervertebral distance (Table 9), as would be expected. The total maximum flexion and the average flexion per cervical vertebrae in the neck in the four specimens are shown for each CID in Table 9. Total maximum is mentioned in order to compare with previous RoM studies on plesiosaur necks. Dorsal, ventral and lateral flexion generally increased ~50 % for each step which was expected due to the 50 % increase in intervertebral distance between each CID.

Table 9: Total maximum flexion in degrees (°) of the neck in dorsal, ventral, and lateral rotations for the four cryptoclidid specimens used in the present study (GLAHM V1091, OUNHM J.95000, PMO 224.248, NHMUK R2863) with 5, 10, and 20 % CID. Average flexion per cervical vertebrae is specified in brackets.

Specimen	Dorsal flexion			Ventral			Lateral		
	5 %	10 %	20 %	5 %	10 %	20 %	5 %	10 %	20 %
GLAHM V1091	157° (9°)	269° (16°)	469° (28°)	143° (8°)	265° (16°)	476° (28°)	135° (8°)	239° (14°)	422° (25°)
OUNHM J.95000	397° (17°)	508° (21°)	757° (32°)	265° (11°)	436° (18°)	762° (32°)	351° (15°)	509° (21°)	817° (34°)
PMO 224.248	323° (7°)	595° (13°)	1068° (24°)	427° (9°)	838° (19°)	1551° (34°)	272° (6°)	536° (12°)	1023° (23°)
NHMUK R2863	364° (9°)	544° (14°)	790° (20°)	384° (10°)	670° (17°)	1163° (29°)	400° (10°)	682° (17°)	1158° (29°)

In the four specimens total neck rotation varied from 135° - 1551° depending on CID (Table 9). Among the four specimens, with a CID of 5 %, OUNHM J.95000 had the greatest range of motion on average for dorsal (17°), ventral (11°) and lateral flexion (15°) (Figure 56). Dorsal and lateral flexion were, on average, lowest in PMO 224.248 at 5 % CID (7° in dorsal flexion and 6° in lateral flexion), and ventral was lowest in GLAHM V1091 (8°). From the results at 5 % CID there was an increase (up to twice the amount of the average) in dorsal flexion in OUNHM J.95000 in the anterior part of neck investigated in this study (Figure

56B: C5-C13). The increase in flexion in the anterior part of the neck was caused by the lack of neural spines. A greater rotation compared with averages was observed at the joint between the atlas-axis complex and C3 (all except OUNHM J.95000 due to the great portion of the spine being present in this specimen compared with the three other specimens). Here the intervertebral distance would be larger in the joint following the longer atlas-axis bone compared with the subsequent vertebrae. At 5 % CID, all specimens but PMO 224.248 had even spacing on average between the three rotations, and PMO 224.248 had more space on average from ventral to dorsal and lateral.

With 10 % CID dorsal and lateral flexion was on average highest in OUNHM J.95000 (Figure 57), at 21° in both rotations. Ventral flexion was on average highest (19°) in PMO 224.248 with 10 % CID. On average both PMO 224.248 had the lowest dorsal flexion (13°) at 10 % CID. Ventral flexion was lowest in GLAHM V1091 (16°) and lateral flexion was lowest in PMO 224.248 (12°) at 10 % CID. Again, as seen in 5 % CID, there was an extreme increase in dorsal flexion in the anterior part of neck of OUNHM J.95000 due to the lack of missing neural spines in this part of the neck (Figure 57B). At 10 % CID, all four specimens had uneven spacing on average between the three rotations with the highest spacing seen in PMO 224.248 from ventral to dorsal and lateral.

For 20 % CID dorsal and lateral flexion was on average highest in OUNHM J.95000 (Figure 58), 32° and 34°, respectively. Ventral flexion was on average highest in PMO 224.248 (34°) with 20 % CID. NHMUK R2863 had the lowest dorsal flexion (29°), ventral was lowest in GLAHM V1091 (28°), and lateral flexion was lowest in PMO 224.248 (22°) at 20 % CID. Again, as seen in 5 % and 10 % CID, there was a high increase in dorsal flexion in the anterior part of neck of OUNHM J.95000 due to the absence of neural spines in this part of the neck (Figure 58B). At 20 % CID, all four specimens but OUNHM J.95000 had uneven spacing on average between the three rotations, with the highest spacing seen in PMO 224.248 from ventral to dorsal and lateral.

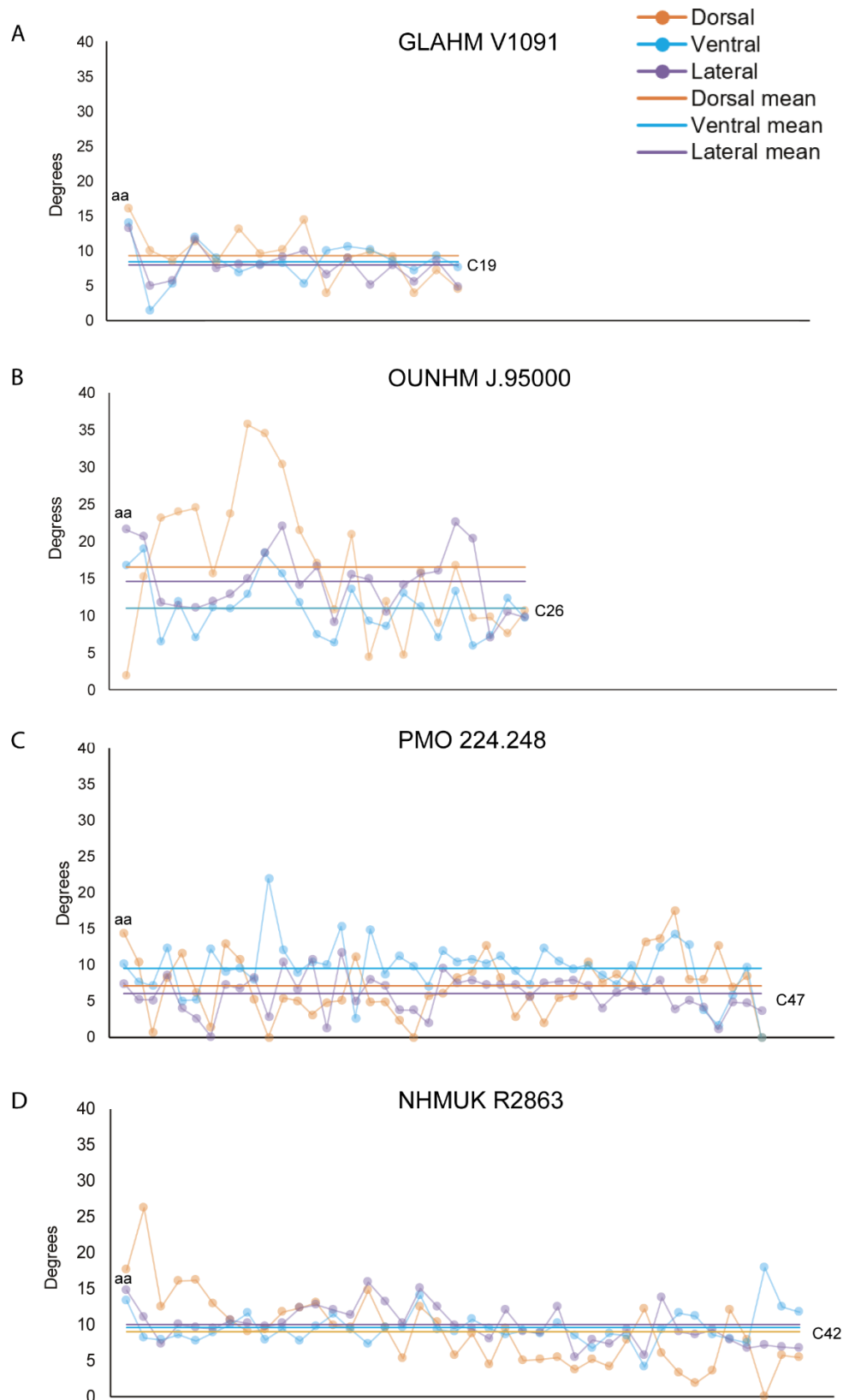


Figure 56: Maximum osteological range of motion (degrees) with 5 % CID vs. cervical vertebrae in the neck of A) GLAHM V1091, B) OUNHM J.95000, C) PMO 224.248, and D) NHMUK R2863. Dorsal flexion: orange; ventral flexion: blue; lateral flexion: purple. Means of dorsal, ventral and lateral flexion with identical colouration.

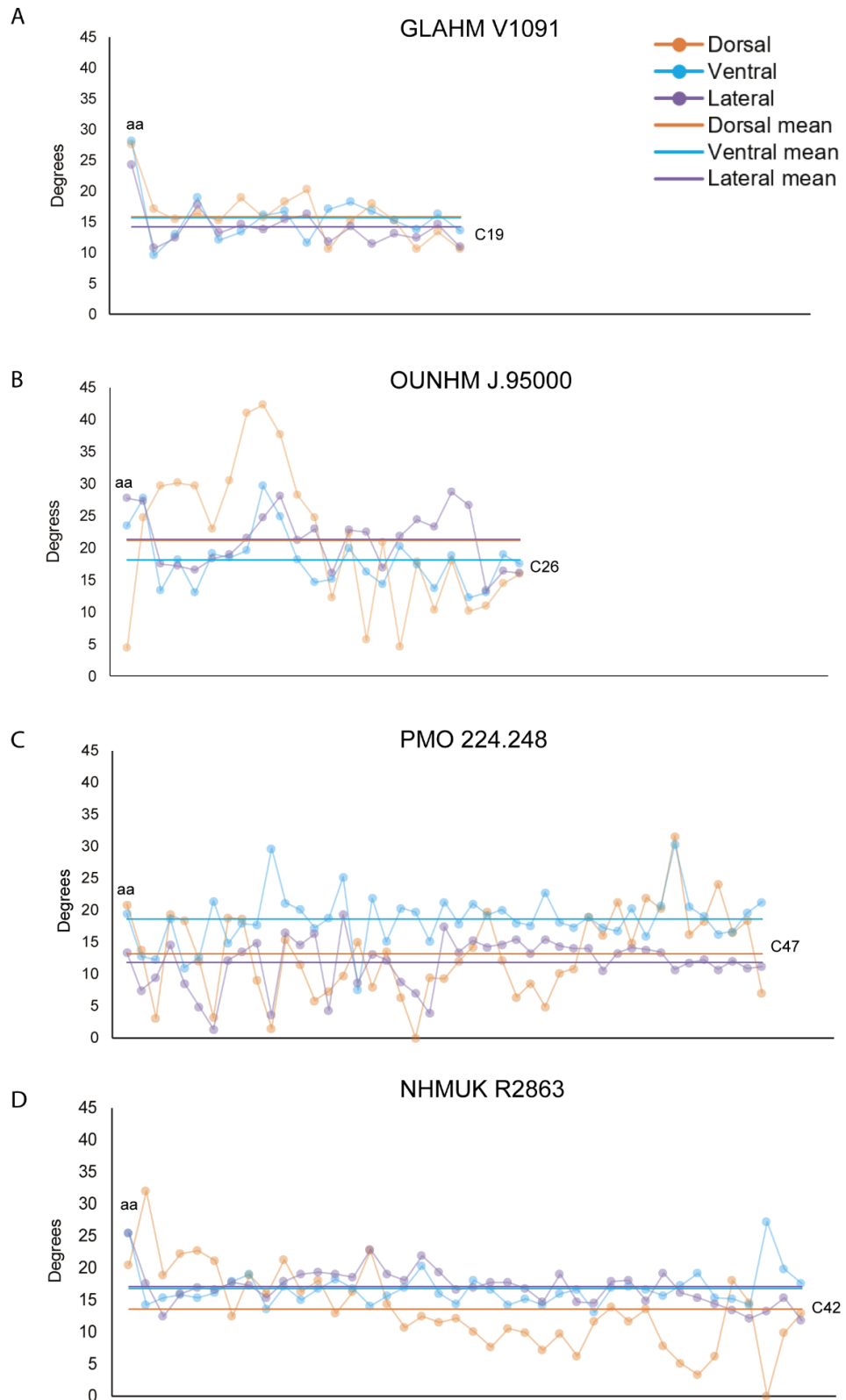


Figure 57: Maximum osteological range of motion (degrees) with 10 % CID vs. cervical vertebrae in the neck of A) GLAHM V1091, B) OUNHM J.95000, C) PMO 224.248, and D) NHMUK R2863. Dorsal flexion: orange; ventral flexion: blue; lateral flexion: purple. Means of dorsal, ventral and lateral flexion with identical colouration.

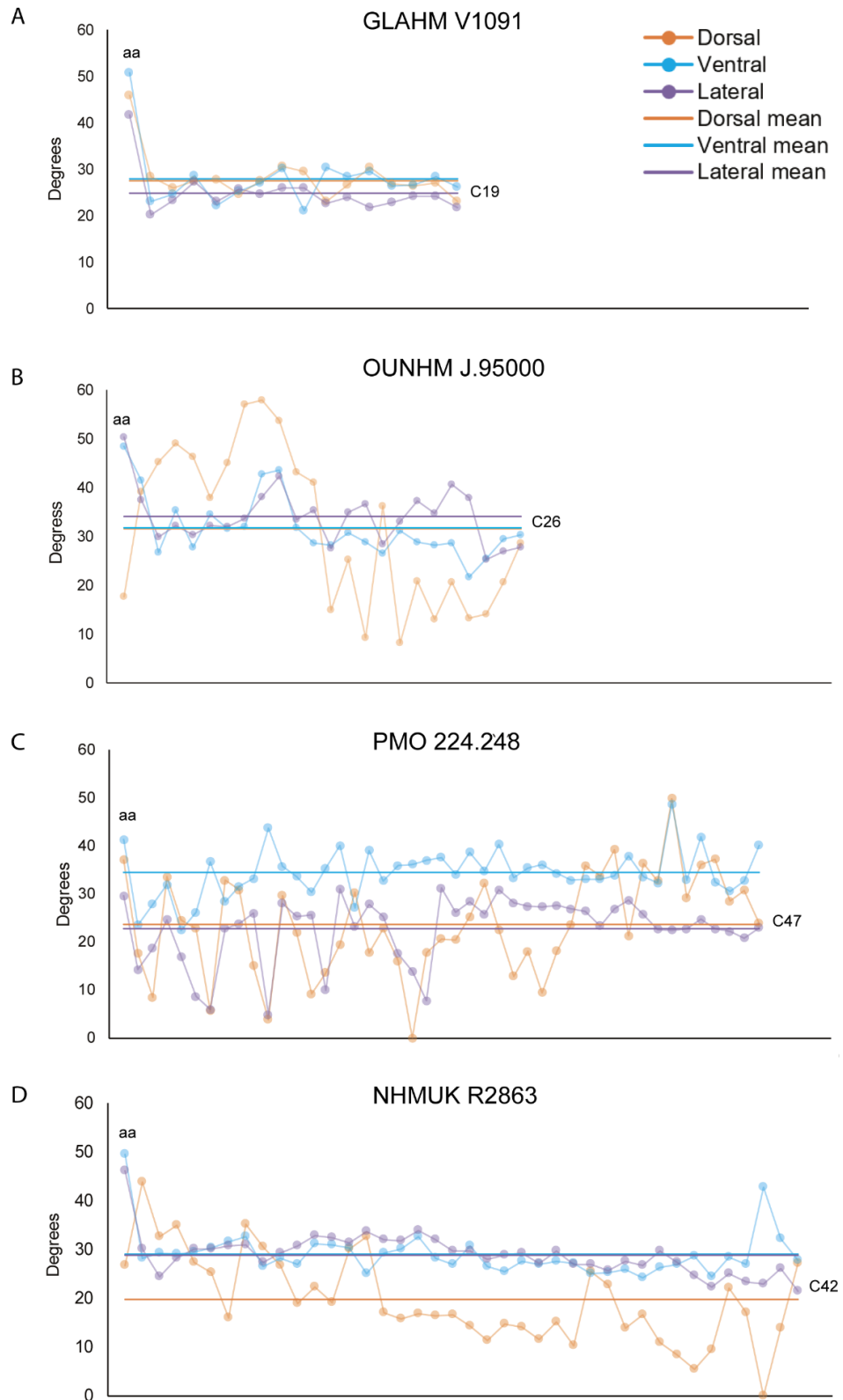


Figure 58: Maximum osteological range of motion (degrees) with 20 % CID vs. cervical vertebrae in the neck of A) GLAHM V1091, B) OUNHM J.95000, C) PMO 224.248, and D) NHMUK R2863. Dorsal flexion: orange; ventral flexion: blue; lateral flexion: purple. Means of dorsal, ventral and lateral flexion with identical colouration.

In addition to the results on range of motion, the colliding point of the cervical vertebrae between each joint were documented simultaneously. An increase of dorsal flexion was generally observed in joints where neural spines were missing in the cervical vertebrae pre- and/or postpositional to the joint.

In dorsal flexion, it was noticeable that for all pairs of adjacent cervical vertebrae that included neural spines the collision point was the neural spine, and if the vertebrae did not include neural spines the collision point was the anterior dorsal part of the centra. Although, in a very few cases (C17-C18 in OUNHM J.95000 at all CID's, and C31-C32 in NHMUK R2863 at all CID's) the two neural spines did not collide due to deformation of the cervical vertebrae. The deformation led to neural spines pointing in opposite directions (anterior and posterior) instead of aligning vertically with the adjacent spines. Deformation of the vertebrae also affected where the colliding part would be on the cervical if one of the neural spines were not complete, even with pairs of adjacent cervical vertebrae both possessing neural spines, as the case for C24-C25 in OUNHM J.95000. If one cervical vertebra included a neural spine and the cervical vertebrae posterior to it did not, for a few incidents the neural spine was colliding with the centrum in the posterior vertebra, which happened mainly at 20 % CID (C8-C9 in GLAHM V1091, and C8-C9; C15-C16 in NHMUK R2863). Furthermore, in dorsal flexion for all CID's, complete zygapophyses collided with adjacent cervical vertebrae if the zygapophyses were present and complete, like in the case of PMO 224.248. Of the 31 cervical vertebrae in PMO 224.248 possessing either pre-, post- or both the zygapophyses, 23 of the joints (5 % CID), 25 of the joints (10 % CID) and 27 of the joints (20 % CID) collided with the zygapophyses. This result demonstrated how the collision point was affected by the intervertebral distance increasing in the number of cases with increase of intervertebral distance.

Unlike dorsal flexion, ventral flexion in all four specimens showed the centrum to be the colliding part of the cervical vertebrae, and did not change in colliding part with increase in intervertebral distance. If the cervical vertebrae had complete zygapophyses and only a few had neural spines, the colliding point would be positioned on the zygapophyses in lateral flexion, which was the case for 9, 12, and 13 joints at 5, 10, and 20 % CID, respectively in PMO 224.248. Lastly, if the cervical vertebrae included ribs the colliding point in dorsal, ventral or lateral flexion with the adjacent vertebra was not connected with the rib(s) in any of the four specimens, but rather colliding with the centrum or the neural spine.

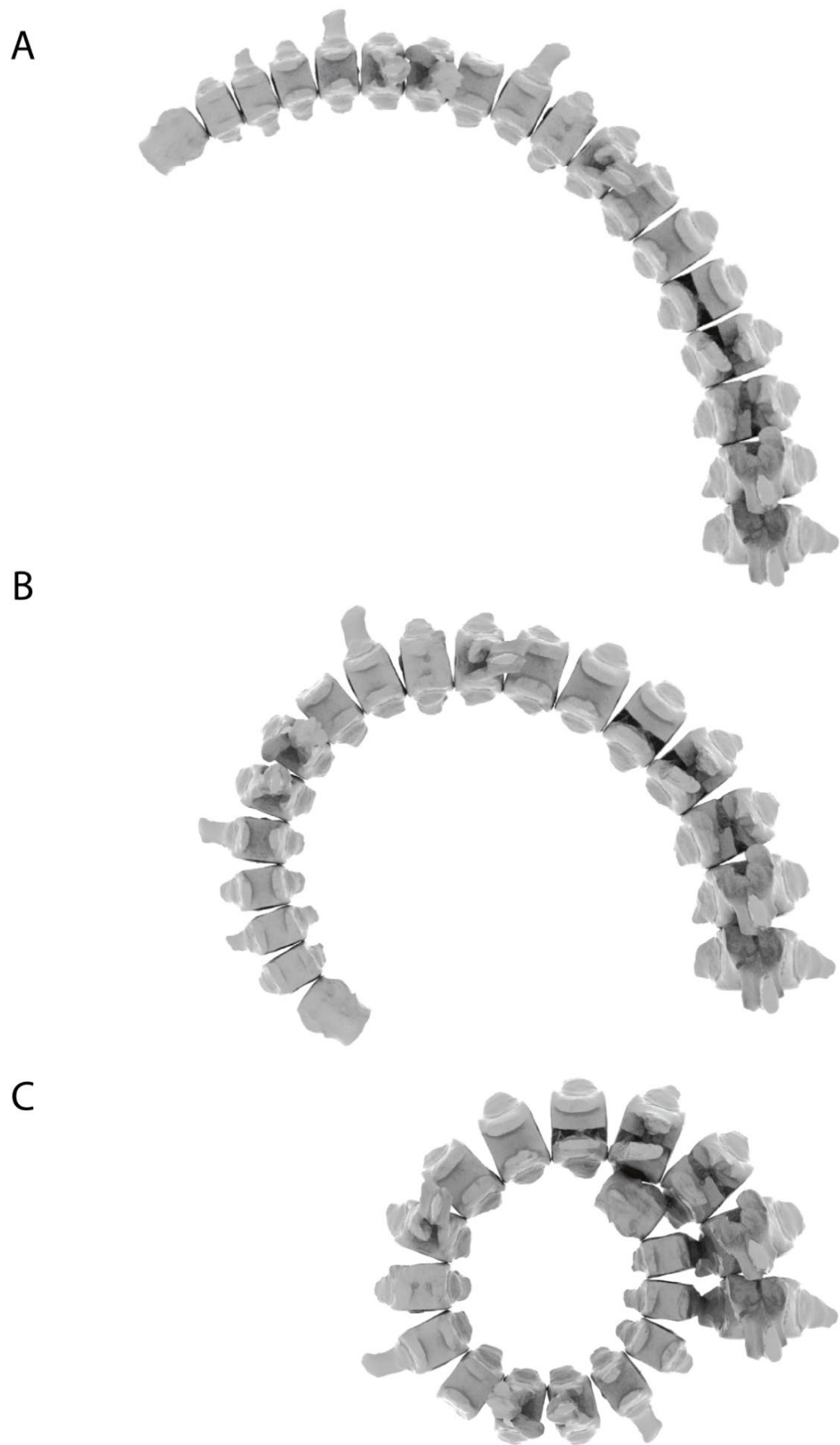


Figure 59: Digital models in dorsal view of maximum osteological lateral flexion towards the left in the partial neck of GLAHM V1091 with (A) 5 % CID, (B) 10 % CID, and (C) 20 % CID.

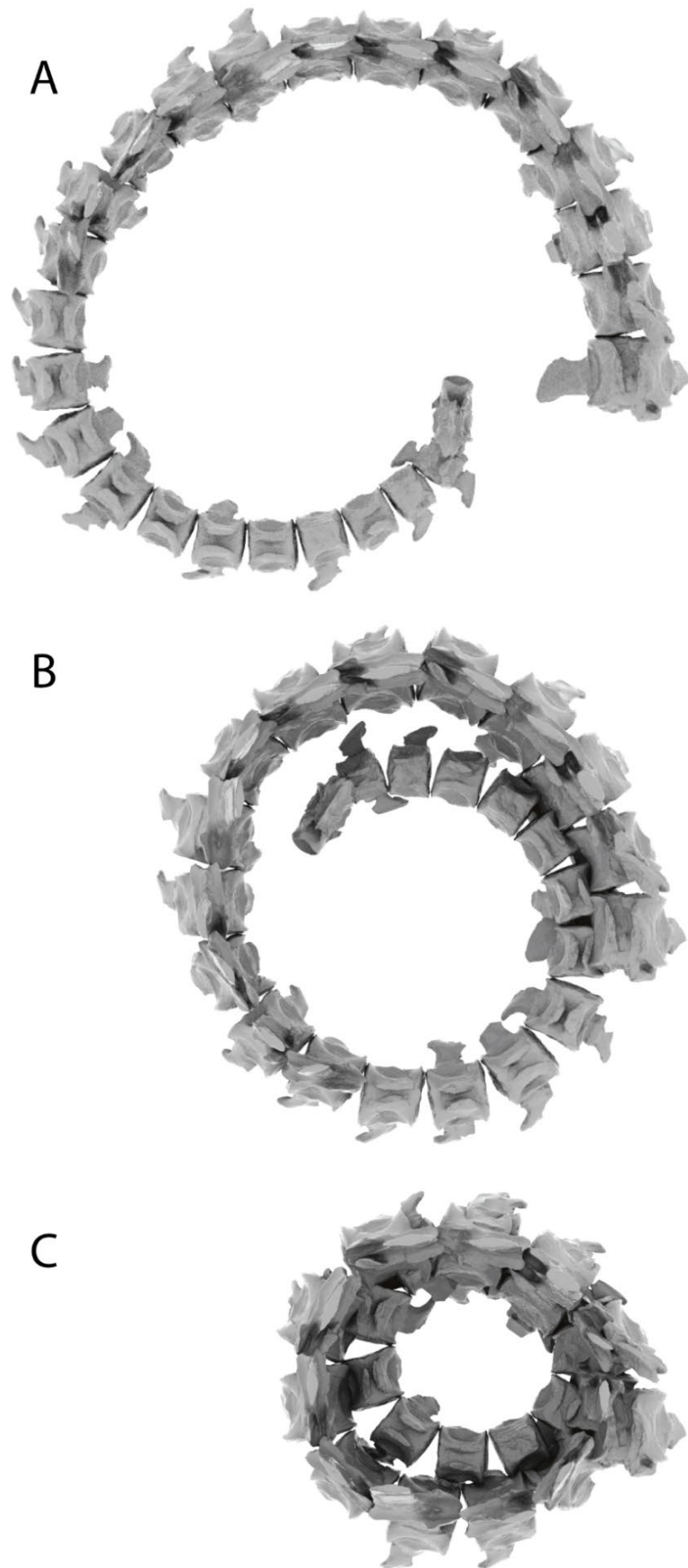


Figure 60: Digital models in dorsal view of maximum osteological lateral flexion towards the left in the partial neck of OUNHM J.95000 with (A) 5 % CID, (B) 10 % CID, and (C) 20 % CID.

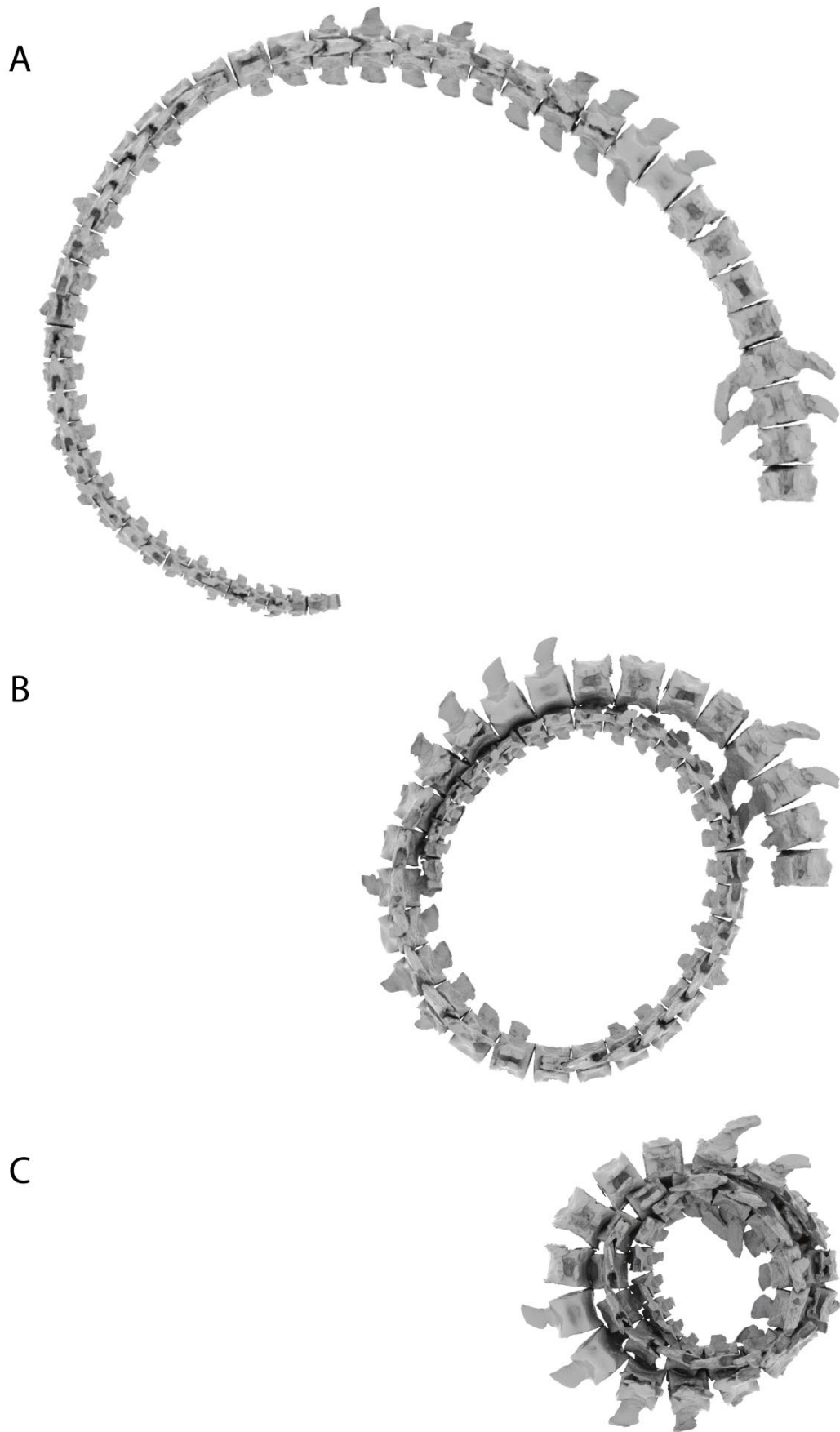


Figure 61: Digital models in dorsal view of maximum osteological lateral flexion towards the left in the nearly complete neck of PMO 224.248 with (A) 5 % CID, (B) 10 % CID, and (C) 20 % CID.

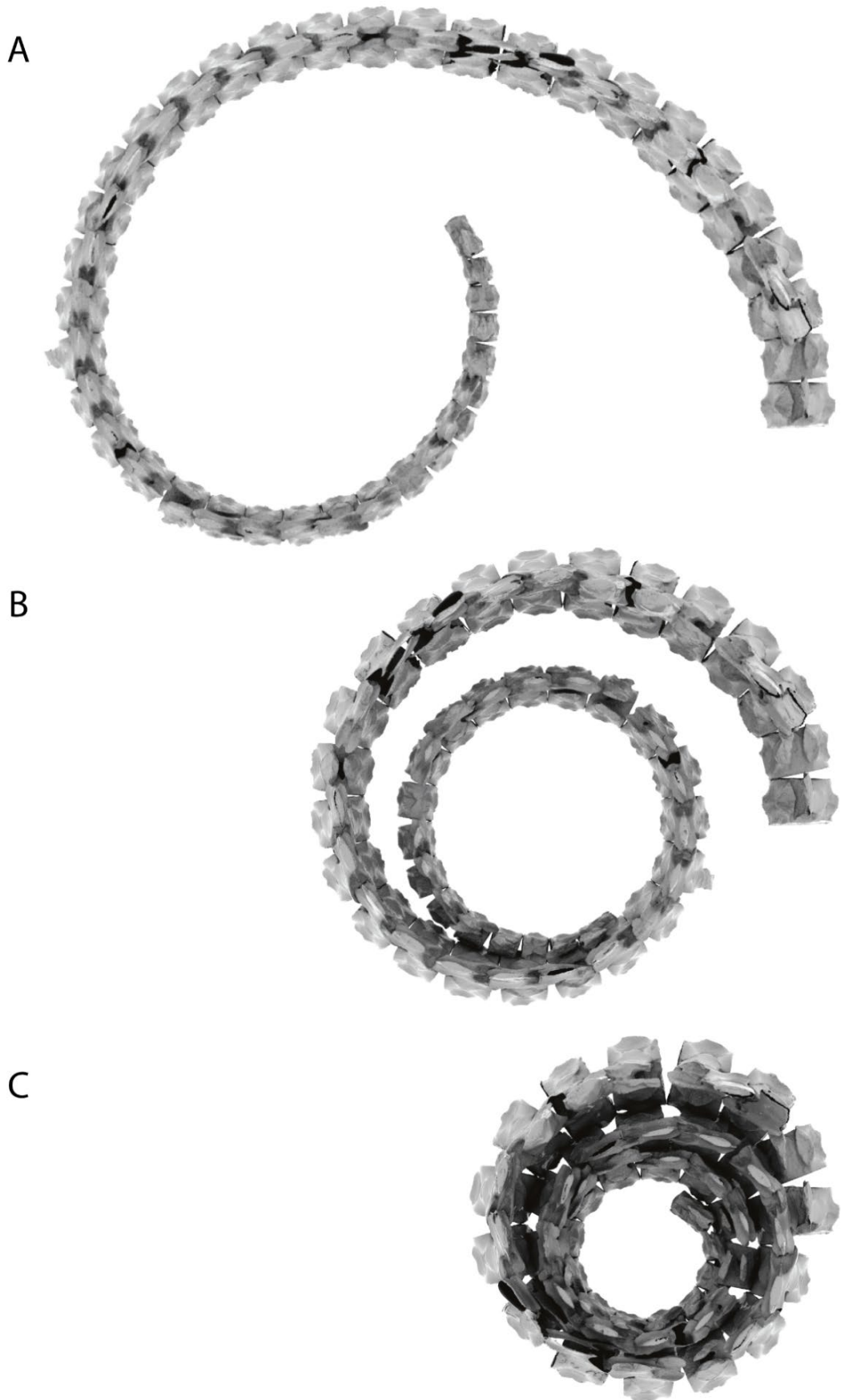


Figure 62: Digital models in dorsal view of maximum osteological lateral flexion towards the left in the full neck of NHMUK R2863 with (A) 5 % CID, (B) 10 % CID, and (C) 20 % CID.

Visualised in dorsal view, all four specimens showed the same pattern of the neck curling up around itself with increase of the intervertebral distance (Figure 59-Figure 62). The more cervical vertebrae included in the neck, the more extreme the neck curvature was. Furthermore, the increase in intervertebral distance created greater curvature of the neck. For example, the noticeable difference between the total curvature of the 19 cervical vertebrae in GLAHM V1091 in Figure 59 vs. the total curvature of the 46 cervical vertebrae in PMO 224.248 in Figure 61.

3.4 Discussion

3.4.1 Neck movement in plesiosaurs

The relatively high degrees of bending in plesiosaur necks found in the present study represent maximum osteological range of motion (RoM), thus the effect of the cartilage is not taken into account. Soft tissue restricts range of motion in comparison to having bones only (cf. Chapter 2). Neck muscles often restrict movement differently throughout the neck, though this information cannot be obtained if studying only the bones. The present study only involves maximum osteological RoM, and as such RoM *in vivo* would be less than this by an unknown amount (cf. Chapter 2: range of motion in the ostrich neck was decreased by a third of the ventral flexion and $\frac{3}{4}$ of the lateral flexion going from clean bone to intact neck). If we were to include intervertebral cartilage in a plesiosaur neck, the RoM would thus have been considerably less than what was observed with the 20 % CID. If we compare with how much cartilage affects modern long-necked animals, like ostriches (cf. Chapter 2), as well as look at the results presented here (Figure 56 - Figure 62), the 10 % CID used in the present study showing $\sim 15^\circ$ per cervical would most closely resemble the intervertebral distance found in plesiosaurs *in vivo*. Hence, a maximum osteological dorsal, ventral, and lateral flexion of $\sim 15^\circ$ per cervical vertebrae would be realistic for cryptoclidids. Comparing with the study by Evans (1993), the 10-20 % CID used in the present study resembles the intervertebral distance found by Evans (1993) the most. At 10 % CID would allow enough spacing between adjacent cervical vertebrae when bending the neck as bone-to-bone would not be realistic in life. The results presented in this study reject the swan-like posture, previously illustrated for plesiosaurs, as this would only have been possible for plesiosaurs to perform if the cervical vertebrae would pass through each other (e.g. Shuler, 1950).

One of the specimens Evans (1993) used in the study of range of motion was NHMUK R2863 (*Muraenosaurus leedsii*) which was also used in the present study. By comparing the results from Evans (1993) using 14 % CID on average with the present study using 10 %

CID (mentioned as Troelsen here for simplicity), the total maximum dorsal flexion was almost equal (Evans 540° vs. Troelsen 544°) whereas total maximum ventral flexion (Evans 540° vs. Troelsen 670°) and total maximum lateral flexion (Evans 454° vs. Troelsen 682°) were a lot higher in the present study. The results from the present study are therefore higher in all rotations even though the CID is lower in comparison to Evans (1993). The reason for the difference in the results between the two studies could for instance be the method applied in each study. Intervertebral distances were individual percentages for each joint in the study by Evans (1993) and were calculated by taking the zygapophyseal length and subtracting with the post-zygapophyseal facet length and the centra length. In the present study the intervertebral distances were calculated by measuring the centra length and taking 5, 10 or 20 % of the length as intervertebral distance. The difference in method and intervertebral distance clearly affects the total flexion of the neck, and from this observation the studies can tell us dissimilar interpretations of biomechanics and ecology in this specimen. Though, by acknowledging the variety of results on RoM in plesiosaurs we have a broader understanding of the behaviour of this specific specimen, because we can tell how intervertebral distance will lead to great variations in neck flexibility depending on how much intervertebral distances was inserted and how the method of measuring range of motion was applied.

In the present study lateral flexion was taken as the average of left and right rotations. The reason for this is that it would be expected that plesiosaurs, being nearly symmetrical animals were capable of almost equal amounts of flexion to left and right directions, as observed from osteological range of motion measurements found in an ostrich (cf. Chapter 2). The reason why there is a slight difference between left and right flexion is due to asymmetrical deformation of the vertebrae during fossilisation. To counteract for this factor the average was therefore chosen to represent the lateral flexion. It should be noted however, that the left and right flexions were just about the same amount of degrees, and where mainly observed being different in the most severe cases of vertebra deformation.

From the documentation on collision points, both the centra, spines and zygapophyses tend to restrict neck movement in plesiosaurs depending on CID. It was observed that the plesiosaur specimens used in the present study were mainly restricted in dorsal neck movement by the neural spines and zygapophyses. Limitation of neck movement caused by the zygapophyses is also observed from studying RoM in an ostrich (cf. Chapter 2). With increasing CID, the collision point would in many incidents change from centrum to either

zygapophyses or neural spine, depending on the completeness and degree of deformation of the cervical vertebrae. If the neural spines are missing the RoM is higher in dorsal flexion. Therefore, the higher completeness of cervical vertebrae, the more accurate the results will be. However, we can get a good idea of how much RoM is changing with the increase of the intervertebral distance from the centra alone, especially for ventral flexion, observed in the present study, as the centra were the colliding point in all ventral flexion measurements.

The cervical ribs were not present in many of the cervical vertebrae used in the present study. In the documentation on collision point, the effect on restricting RoM was none-existent by the ribs, as there were no observed collisions with ribs in lateral flexion in any of the four plesiosaur specimens. The cervical ribs would therefore not be a limiting factor on plesiosaur neck movement but rather serve along with muscles and ligaments as support for the neck while the plesiosaur was moving around in the water column.

In the present study, the length of cervical vertebrae increased towards the base of the neck, and the intervertebral distance also increased posteriorly because the intervertebral distance at each joint was based on the length of the cervical vertebra anterior to the joint, thus increasing posteriorly. Therefore, the size of the cervical vertebrae in any parts of the neck did not affect the RoM by itself, but rather the morphology of the whole vertebra. In contrast, the total maximum RoM was affected by the number of cervical vertebrae, which was observed in the results as the total flexion in dorsal, ventral and lateral directions was higher in the specimens with higher number of cervical vertebrae (OUNHM J.95000, PMO 224.248 and NHMUK R2863) compared with a lower number (GLAHM V1091) investigated for the present study.

The size of the centra in cervical vertebrae in a specific part of the neck will affect the range of motion. As an example, the elasmosaurid *Hydralmosaurus serpentinus* has anterior and posterior cervical vertebrae that are broader than long, but with the middle part of the neck the cervical vertebrae are longer than broad (Welles, 1952). The morphology of the cervical vertebrae in *H. serpentinus* would allow more flexibility in the anterior and posterior parts of the neck, and less flexibility in the middle region based on knowledge about how the centra shapes affect range of motion (Buchholtz and Schur, 2004). As only two (PMO 224.248 and NHMUK R2863) of the plesiosaur specimens used in the present study were complete or almost (94 %) complete, at least for these two specimens the centra length pattern was not like the one seen in *H. serpentinus* but rather an increase in relative length

all the way from the anterior-most to the posterior-most cervical vertebrae. The centra shape was therefore not a limiting factor in the range of motion results found in at least PMO 224.248 and NHMUK R2863. Centra shape does not seem to be a limiting factor for GLAHM V1091 and OUNHM J.95000 either, as the ~60 % complete necks in the two specimens also have increasing centra length from the anterior part of the neck up to the last cervical investigated in the present study.

Previous studies on neck flexibility in plesiosaurs have demonstrated results with both relatively high (Evans, 1993; Nagesan *et al.*, 2018) and low (Zarnik, 1925; Welles, 1943; Zammit *et al.*, 2008) degrees of flexion in dorsoventral and lateral rotations. In the present study we see an almost equal amount of flexion dorsoventrally and laterally with 5 % CID, even bearing in mind that some of the cervical vertebrae were deformed and/or incomplete. Unlike the present study, Noè *et al.* (2017) and Wintrich *et al.* (2017a) stated that all plesiosaurs would likely have had predominant flexibility in ventral rotation and be relatively restricted in dorsal and lateral flexion. Summing up the results from the present study, previous studies on RoM in plesiosaurs (Zarnik, 1925; Welles, 1943; Evans, 1993; Zammit *et al.*, 2008; Nagesan *et al.*, 2018), and the statements by Noè *et al.* (2017) and Wintrich *et al.* (2017a), plesiosaurs were probably more likely to have predominant ventral and lateral flexion suggested from the present study, rather than lateral flexion (Zarnik, 1925; Welles, 1943; Zammit *et al.*, 2008; Nagesan *et al.*, 2018), ventral flexion (Noè *et al.*, 2017; Wintrich *et al.*, 2017a) or dorsoventral flexion (Evans, 1993) as predominant neck movement.

The fossils of plesiosaurs are the only evidence we have for their existence, and our knowledge of them depends entirely on how they have been preserved (Lautenschlager, 2017). From plesiosaur fossils preserved with articulated complete necks we are able to interpret neck movement post-mortem. The articulated necks give a clear indication to whether plesiosaurs were capable of high flexibility in their necks during life. If plesiosaurs had stiff necks, we would most likely not see the high amount of flexibility found in the present study as well as previous RoM studies on plesiosaurs (Zarnik, 1925; Welles, 1943; Evans, 1993; Zammit *et al.*, 2008; Nagesan *et al.*, 2018).

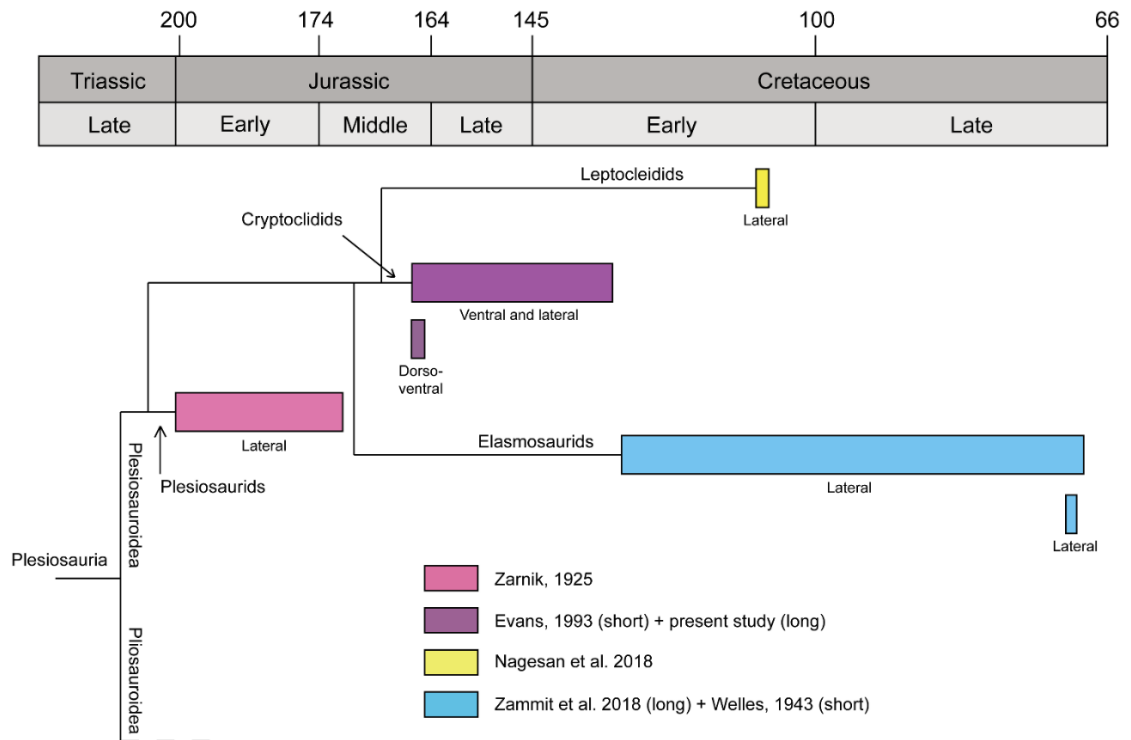


Figure 63: Geological age (millions of years ago) illustrating time of existence of the plesiosaur specimens used in the present and previous RoM studies (Late Triassic to Late Cretaceous) and their predominant flexion (dorsal, ventral, lateral). Bars colour-coded according to families similar to Figure 50 and Figure 51. Pink: Plesiosaurids from Zarnik (1925). Purple: Cryptocleidids from Evans (1993) as the short bar and the present study as the long bar. Yellow: Leptocleidid from Nagesan et al. (2018). Light blue: Elasmosaurids from Welles (1943) as the short bar and Zammit et al. (2008) as the long bar.

Throughout the clade of Plesiosauria, range of motion seem to have been predominantly lateral flexion (Figure 63), regardless of family, neck length, number and/or morphology of the cervical vertebrae. Though, the results from the present study indicate that cryptocleidids were mostly capable of lateral and ventral movement of the neck, and were more restricted in dorsal flexion, regardless of neck length and/or completeness of the neck. This is in agreement with some RoM studies (Zarnik, 1925; Zammit *et al.*, 2008; Nagesan *et al.*, 2018) and unlike the study by Evans (1993). The main part of the flexion would occur in the anterior part of the neck and decrease towards the base of the neck, although flexion for each joint would not deviate much from the average amount of rotation for the whole neck.

3.4.2 Plesiosaur ecology and other aspects of biology

Plesiosaurs have been thought to rely on neck flexibility to capture prey, because their heads and jaws were short, though shorter-necked forms like *Rhomaleosaurus* would be capable of pincer feeding because of its bigger jaws and longer snout (Taylor, 1987). Long-necked plesiosaurs were therefore previously thought of feeding by lunging and ambush their prey

in a similar way to modern snakes that employ “spear fishing” to capture their prey, and feed on a wide range of prey size, similar to that of modern toothed whales (Taylor, 1987). However, the present study as well as previous studies (Zarnik, 1925; Welles, 1943; Zammit *et al.*, 2008; Nagesan *et al.*, 2018), have indicated that plesiosaurs had relatively high neck flexibility ($\sim 15^\circ$ per cervical with 10 % of the centra length used as intervertebral distance) due to the number of successive cervical vertebrae. From the more rigid necks seen in at least some elasmosaurids (Welles, 1943; Zammit *et al.*, 2008), it seems that long-necked plesiosaurs were more likely to have approached their prey by surprise (like we see in cetaceans due to their compressed neck, cf. Chapter 2). For example, by approaching a group of fish where the fish would not be able to detect the long neck and large body of the plesiosaur before being swallowed by the plesiosaur. The opposite is seen in relatively short-necked plesiosaurs (similar to some plesiosaurs used in the present study), where hunting strategies would be similar to some modern aquatic mammals like sea lions (Cheneval *et al.*, 2007; Zammit *et al.*, 2008) due to the high neck flexibility.

3.5 Conclusions

In the present study, maximum osteological range of motion was measured, and the results showed that the most realistic rotation in the necks of the cryptoclidid plesiosaurians was at a maximum 15° per cervical vertebra (10 % CID) in dorsal, ventral, and lateral flexion. Dorsal flexion was primarily restricted by neural spines, ventral flexion by the centra, and lateral flexion by the zygapophyses or centra depending on completeness of the cervical vertebrae in the specimen studied and inserted CID. The high amount of flexibility found in the cryptoclidid necks from the present study tells us about their possible behaviour, having foraging strategies similar to that of e.g. modern pinnipeds (Cheneval *et al.*, 2007; Zammit *et al.*, 2008). Plesiosaurs with longer necks (e.g. elasmosaurids) would probably have been incapable of tighter neck turns (like e.g. sea lions, cf. Chapter 2) compared with shorter necked forms due to the high number of rigid vertebrae found in long-necked forms. Long-necked plesiosaurs would most likely have relied on surprising their prey due to their long and stiffer necks. The present study improves our current understanding of the biomechanical implications in long-necked plesiosaurs, such as cryptoclidids, by providing range of motion data from digitised cervical vertebrae.

Chapter 4 – Fluid dynamics

4.1 Introduction

4.1.1 Fluid dynamics

A fluid is defined as a substance that deforms when acted on by a shearing stress of any size, and this shearing stress is created when a tangential force acts on a surface as seen in Figure 64 (Munson *et al.*, 2009). The fluid of interest in this thesis is water.

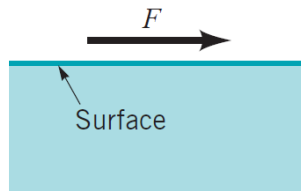


Figure 64: Force acting on a surface. From Munson *et al.* (2009).

Fluid mechanics is the study of fluids either in motion (fluid dynamics) or at rest (fluid statics) (White, 2010). The main part of fluid dynamics is flow, which depends on different parameters, such as physical size of the flow (length), velocity of the flow (v), viscosity (μ) and pressure (ρ) (Hoerner, 1965; Munson *et al.*, 2009; White, 2010). For this thesis, only fluid dynamics is of importance.

The viscous force is defined as the force that holds fluid particles together. When this force is dominant, the fluid flow is laminar, and particles move in parallel lines (Figure 65) (Fletcher *et al.*, 2014). Laminar flow indicates a state of flow where different fluid “sheets” do not mix with each other, and all stream tubes (path of the flow) keep parallel to each other and velocities are steady (Hoerner, 1965). When the velocity of the fluid increases, the inertial forces dominate and the flow becomes turbulent, showing irregular movements, though simultaneously with the average motion in the mean direction of the flow (Figure 65) (Fletcher *et al.*, 2014).

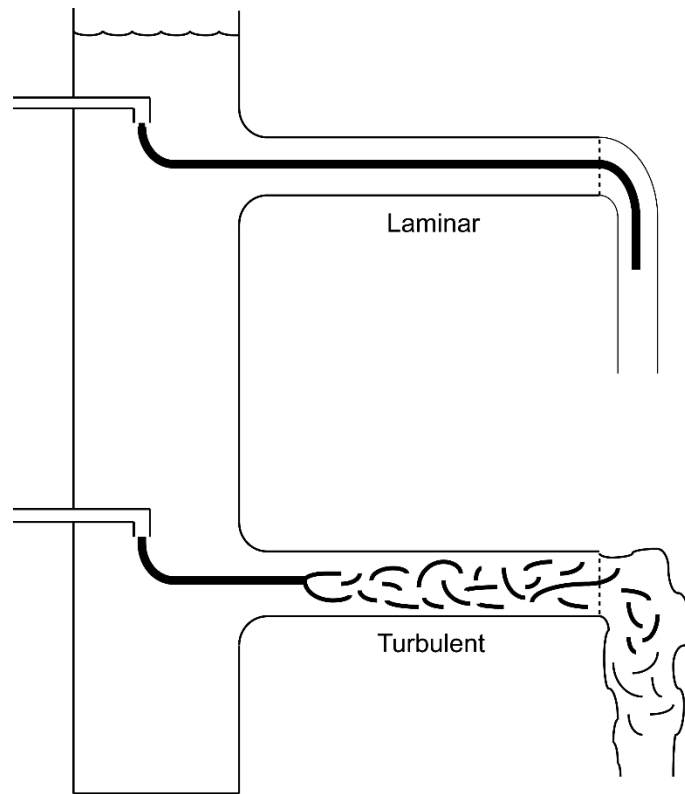


Figure 65: Laminar and turbulent flow. Redrawn from Vogel (1989).

According to Newton's 2nd Law, force is equal to mass multiplied by acceleration ($F = m \times a$), and momentum is equal to mass times velocity ($p = m \times v$) (Alexander, 2003). Thus, force is proportional to the rate of change in momentum. Kinetic energy is energy in the form of motion (Alexander, 2003), and is determined by mass and velocity. In most cases fluid-dynamic forces are proportional to the dynamic pressure (density), which relies on the velocity (Hoerner, 1965). Thus, momentum is an indication for the impact that the dynamic pressure can produce when stopped, as the pressure is transferred from a moving object upon the surrounding fluid (Hoerner, 1965).

4.1.1.1 Steady vs unsteady flow

Having introduced laminar and turbulent flow, another important factor in fluid dynamics is whether the flow is steady or not. When the properties of the fluid do not change with time the flow is said to be steady (also called stationary flow) whereas the opposite is the case for unsteady flow (also called transient flow) (Rahman, 2017). Usually laminar flows are stationary, and turbulent flows are transient, although if the mean flow properties do not change with time a turbulent flow can also be stationary (Rahman, 2017).

4.1.1.2 Reynolds numbers

The Reynolds number (Re) is a dimensionless quantity used to predict flow patterns. Re is greatly influenced by the size of the object (Fletcher *et al.*, 2014). The equation to determine the Re (Equation 5) includes the density of the fluid (ρ), the velocity of the fluid with respect to the object (u), the characteristic length of the object (L) in the direction of the flow (McHenry *et al.*, 2016), and the dynamic viscosity of the fluid (μ) (Vogel, 1989).

Equation 5: The Reynolds number equation and definition.

$$Re = \frac{\text{inertial forces}}{\text{viscous forces}} = \frac{(kg/m^3) * (m/s) * (m)}{kg/m * s} = \frac{\rho u L}{\mu}$$

Laminar flow occurs at low Re (Figure 66a) where the viscous forces are dominant, and turbulent flow occurs at high Re where inertial forces are dominant (Figure 66d) (Munson *et al.*, 2009; White, 2010; Rahman, 2017). Vortices start to evolve at $Re = 10 - 40$ (Figure 66b) where the steady laminar flow stops existing (Rodríguez *et al.*, 2014). Critical Re occurs at the transition between the laminar and turbulent flow at $Re = 10^5 - 10^6$ (Hoerner, 1965; Vogel, 1989; Rodríguez *et al.*, 2013a), and the transition varies with flow geometry, surface roughness and the level of fluctuations in the inlet stream (White, 2010). During the transition, the separation point moves towards the rear end of the object until it reaches a static point (Rodríguez *et al.*, 2013a). It is also within the critical Re that the flow produces vortices in its wake, also known as Karman vortex street/trail (Figure 66c) (Vogel, 1989; Lamura *et al.*, 2001; Li *et al.*, 2017). At Reynolds number $>200,000$ a fully turbulent wake can be observed (Figure 66d).

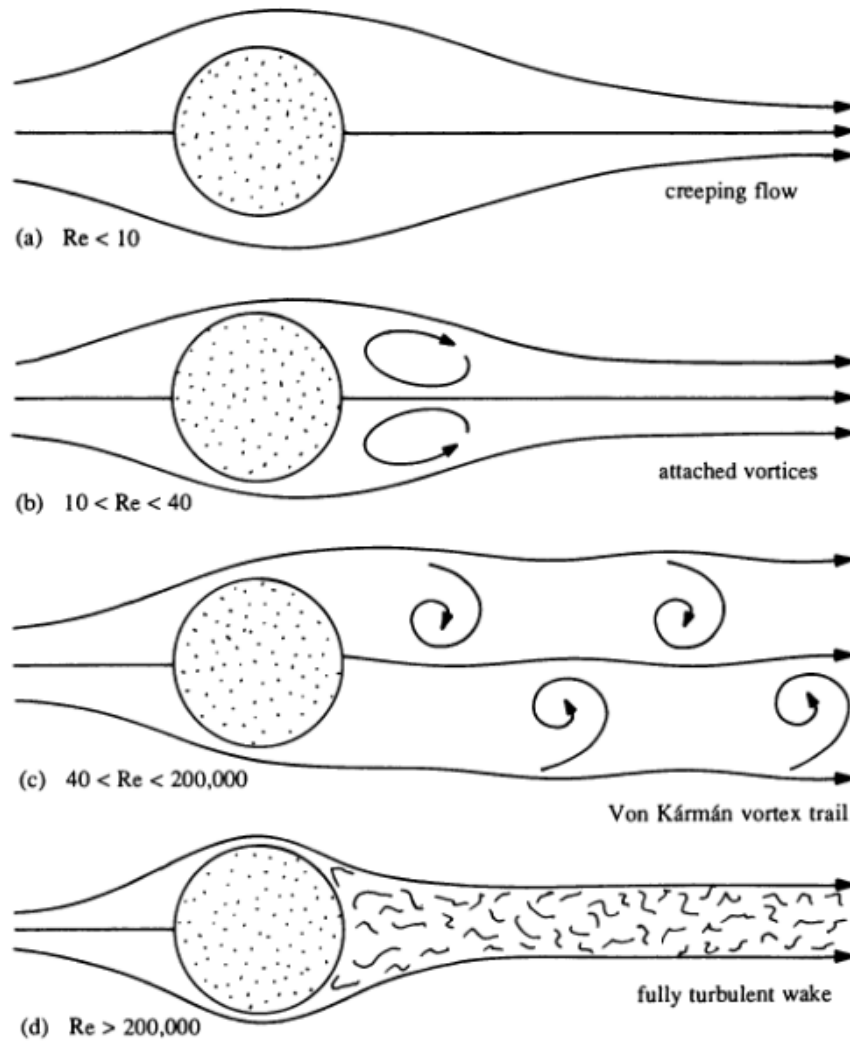


Figure 66: Simplified flow patterns around a sphere at different Reynolds numbers (Re). Note how vortices are being created at higher Reynolds numbers. From Vogel (1989).

4.1.1.3 Governing equations for fluid flow

When working with fluid dynamics there are a number of governing equations that need to be solved in order to find out how the flow, pressure, drag etc. is moving around an object (Versteeg and Malalasekera, 1995), and these are the so-called Navier-Stokes equations (Vogel, 1989). In order to solve the Navier-Stokes equations we can only use Newtonian fluids (air, water, alcohol, glycerol etc.) for which the shearing stress is linearly related to the shear rate (Munson *et al.*, 2009).

The Navier-Stokes equations represent the conservation of momentum (three momentum equations), and the continuity equation which represents the conservation of mass (Versteeg and Malalasekera, 1995). The Navier-Stokes equations are effectively following Newton's 2nd Law; acceleration of fluid is equal to forces acting on an object. The Navier-Stokes

equation involve three velocities from the three directions included in a 3D space (X, Y and Z), the four equations included in the Navier-Stokes equations therefore have three unknowns; u (velocity in X-direction), v (velocity in Y-direction), w (velocity in Z-direction). The fourth unknown is pressure and all four unknowns are solved simultaneously. The continuity equation is the following for unsteady, compressible fluid:

Equation 6: The Continuity equation. From Versteeg and Malalasekera (1995).

$$\frac{\partial p}{\partial t} + \frac{\partial(pu)}{\partial x} + \frac{\partial(pv)}{\partial y} + \frac{\partial(pw)}{\partial z} = 0$$

Here (Equation 6), p is pressure, t is time, v/u/w are velocities, and x/y/z are the three forces in each direction. The equation for conservation of mass (Equation 6) concerns pressure gradients whereas the three equations for conservation of momentum (Equation 7) concerns the three velocity gradients. The momentum equations are the following:

Equation 7: The Conservation of Momentum equations. Top equation is the u-momentum (x-component), middle is the v-momentum (y-component), and bottom is the w-momentum (z-component). From Versteeg and Malalasekera (1995)

$$\begin{aligned} \frac{\partial(pu)}{\partial t} + \frac{\partial(pu^2)}{\partial x} + \frac{\partial(puv)}{\partial y} + \frac{\partial(puw)}{\partial z} &= -\frac{\partial p}{\partial x} + \frac{\partial}{\partial x} \left(\lambda \nabla \cdot \vec{v} + 2\mu \frac{\partial u}{\partial x} \right) + \frac{\partial}{\partial y} \left[\mu \left(\frac{\partial v}{\partial x} + \frac{\partial u}{\partial y} \right) \right] + \frac{\partial}{\partial z} \left[\mu \left(\frac{\partial u}{\partial z} + \frac{\partial w}{\partial x} \right) \right] + pf_x \\ \frac{\partial(pv)}{\partial t} + \frac{\partial(puv)}{\partial x} + \frac{\partial(pv^2)}{\partial y} + \frac{\partial(pvw)}{\partial z} &= -\frac{\partial p}{\partial y} + \frac{\partial}{\partial x} \left[\mu \left(\frac{\partial v}{\partial x} + \frac{\partial u}{\partial y} \right) \right] + \frac{\partial}{\partial y} \left(\lambda \nabla \cdot \vec{v} + 2\mu \frac{\partial v}{\partial y} \right) + \frac{\partial}{\partial z} \left[\mu \left(\frac{\partial w}{\partial y} + \frac{\partial v}{\partial z} \right) \right] + pf_y \\ \frac{\partial(pw)}{\partial t} + \frac{\partial(puw)}{\partial x} + \frac{\partial(pvw)}{\partial y} + \frac{\partial(pw^2)}{\partial z} &= -\frac{\partial p}{\partial z} + \frac{\partial}{\partial x} \left[\mu \left(\frac{\partial u}{\partial z} + \frac{\partial w}{\partial x} \right) \right] + \frac{\partial}{\partial y} \left[\mu \left(\frac{\partial w}{\partial y} + \frac{\partial v}{\partial z} \right) \right] + \frac{\partial}{\partial z} \left(\lambda \nabla \cdot \vec{v} + 2\mu \frac{\partial w}{\partial z} \right) + pf_z \end{aligned}$$

The equations for conservation of momentum (Equation 7) contain density, an unsteady term (temporal/time-based acceleration), an advective term (spatial acceleration due to change of position in flow field), a pressure gradient (because we go from low to high pressure), viscous forces, and body forces (e.g. magnetic forces, gravity) (Seddighi and Allanson, 2017a). Only the x, y, and z directions change, and therefore one equation applies to each direction.

Flows in the laminar regime are completely described by Equation 6 and Equation 7 (Versteeg and Malalasekera, 1995). However, many flows are turbulent, but the Navier-Stokes equations are too simple to describe the turbulent flow and require expanding/additional terms. Therefore, more equations are needed to solve and describe the transport of the diffusion or convection of particles, energy or other physical quantities of the flow or energy involved in the specific turbulence model.

However, the derivation of these more complex equations is beyond the scope of this thesis, and it is enough to say that such equations are the underpinnings of computational fluid dynamics, introduced below.

4.1.1.4 Flow separation

A solid object that moves through a fluid obtains a boundary layer of fluid around it where the viscous forces occur (Hoerner, 1965; Munson *et al.*, 2009). The boundary layer, or so-called shear layer, around a solid has either a laminar or turbulent flow pattern, and the presence of this layer can cause flow separation (Hoerner, 1965), also called boundary layer separation (Munson *et al.*, 2009). Whether the flow in the boundary layer is laminar or turbulent can be determined by looking at the frictional drag on the object, as this will be higher for turbulent flows than laminar flows due to pressure drag (See section ‘Drag and angle of attack’) and unsteadiness in the flow caused in turbulent boundary layers (Stelle *et al.*, 2000). The separation of flow in the boundary layer happens where the part of the boundary layer closest to the wall is reversed in the flow direction because of a decrease in velocity, and the particles in this region are rotated (Figure 67). Particles above the separation are not rotated as they are positioned in the outer flow regime (Seddighi and Allanson, 2017a). The vertical lines in Figure 67 must always be positioned at right angles to the solid, or there will be a mixing of viscosity making it difficult to interpret results. The separation eventually leads to the many vortices created in the wake, and this increases in complexity with the increase of Reynolds number (Figure 66), and the amount of drag experienced by the object.

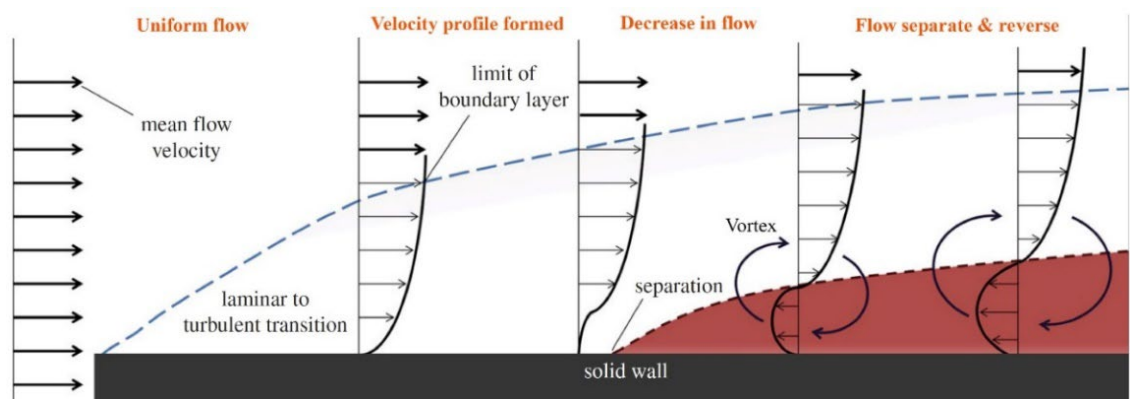


Figure 67: Velocity distribution (arrows) and flow pattern of the stages of boundary layer (blue dotted lines) development in a positive pressure gradient including separation on a flat plate causing vortex formation/wake (red area). Modified from Fletcher *et al.* (2014).

4.1.1.5 Drag and angle of attack

There are three categories of drag: pressure drag, induced drag, and friction drag (Fletcher *et al.*, 2014). Pressure drag is the energy used to move fluid away from the frontal area of an object and then push it behind it again (also called form drag) (Fletcher *et al.*, 2014). Induced drag is the energy that is lost to the lift force that acts against the direction of motion at an angle of attack against the flow (Hoerner, 1965; Fletcher *et al.*, 2014). Finally, friction drag (sometimes also called skin friction drag) is the finer interaction of flow acting over a surface (Fletcher *et al.*, 2014). The three types of drag are combined for a total drag force on the object moving in the fluid (Kogan *et al.*, 2015). The forces acting on a moving sphere can be seen in Figure 68.

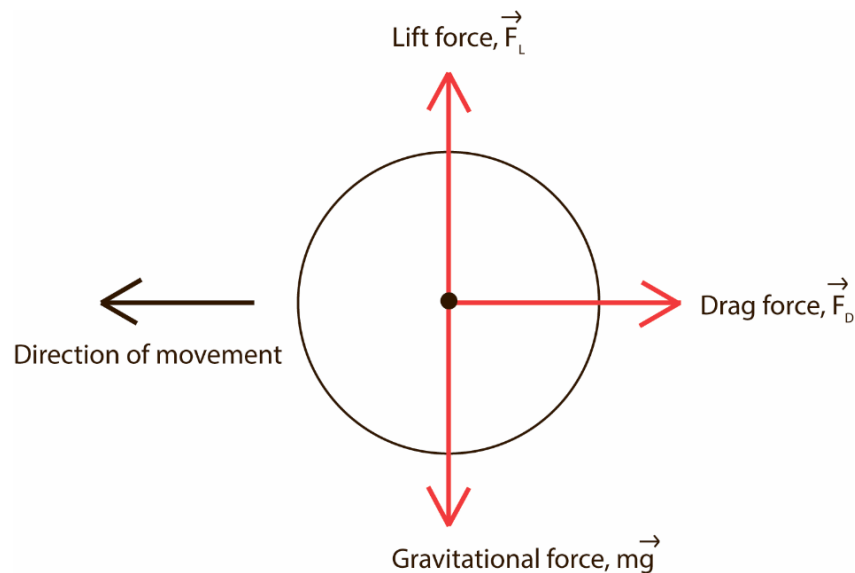


Figure 68: Moving sphere and the three forces acting on it (red arrows); lift force (F_L), gravitational force (mg) and drag force (F_D). Lift and gravitational force counteract each other while drag force counteract the velocity of the object in the direction of movement.

The total drag force F_d (N) is defined by the force component in the direction of the flow velocity (Equation 8).

Equation 8: The drag force (N) equation include the drag coefficient, density of the fluid (kg/m^3), cross-sectional area of the object, and the velocity of the object (m/s). From Hoerner (1965) and Vogel (1989).

$$F_d = \frac{1}{2}(C_d * \rho * A * V^2)$$

In Equation 8 and Equation 9, C_d (dimensionless) is the coefficient of drag, ρ (kg/m^3) is the mass density of the fluid, V (m/s) is the velocity of the object relative to the fluid, and A (m^2) is the area of the object. The latter parameter can be one of three types: Frontal area (object area seen from the stream, suitable for e.g. spheres, cylinders, and stubby objects),

planform area (object area seen from above, suitable for wide, flat objects like wings and hydrofoils) or wetted area (object area in contact with the fluid; suitable for surface ships and barges) (White, 2010).

As C_d is affected by the shape and the size of the object, and the density, viscosity, and relative speed of the fluid (Hoerner, 1965), the total drag force increases when velocity is increased and with the intensity of turbulence (Kogan *et al.*, 2015). We can isolate C_d from Equation 8 that gives us Equation 9.

Equation 9: The drag coefficient equation includes drag force (N), density of the fluid (kg/m^3), velocity of the object (m/s), and cross-sectional area of the object. From Vogel (1989).

$$C_d = \frac{2 * F_d}{\rho * V^2 * A}$$

The justification that C_d varies with cross-sectional/frontal area for a sphere/cylinder has previously been shown by Vogel (1989) with the use of three different objects, their respective C_d and Reynolds numbers (Figure 69). These experiments are significant when comparing to validation experiments made in this chapter. A sphere within a flow regime of $\text{Re} = 10^4 - 10^5$ has a drag coefficient of 0.47, and a cylinder within a flow regime of $\text{Re} = 10^4 - 10^5$ has a drag coefficient between 0.82 and 1.17 depending on the length of the cylinder (Figure 69).

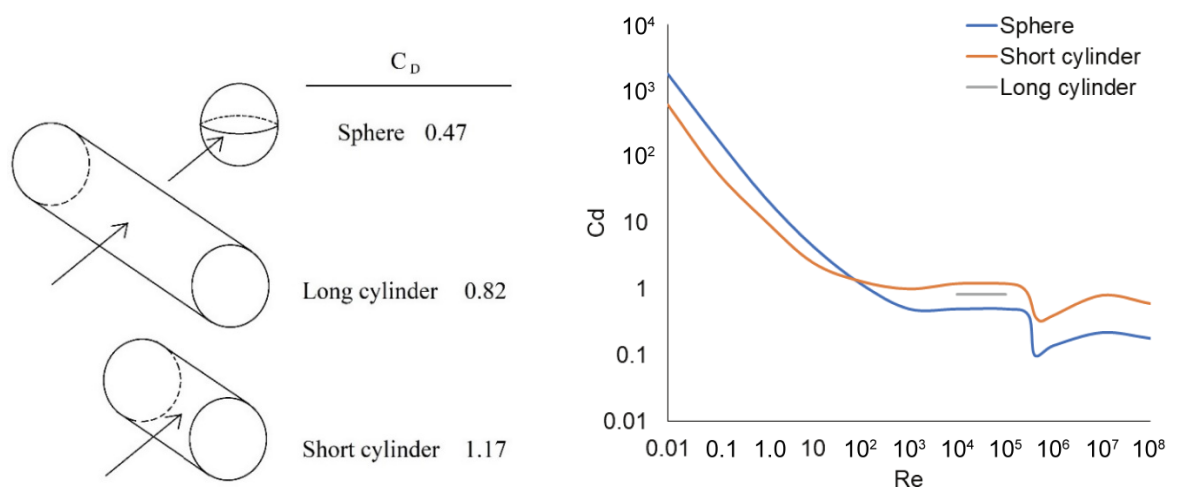


Figure 69: Drag coefficients (C_d) (left) and corresponding Reynolds numbers (Re) (right) based on frontal area for three shapes with the same diameter and Reynolds number (10^4 - 10^5): Sphere, long cylinder and short cylinder. Modified from Vogel (1989).

Drag is mainly influenced by friction drag at low Re (McGowan, 1999; Fletcher *et al.*, 2014). This friction has less influence on drag at higher Re as pressure drag and induced drag increases and dominates at higher velocities (McGowan, 1999; Kogan *et al.*, 2015). The origin and characteristics of pressure drag have frequently been investigated using a sphere

or circular cylinder as examples (Hoerner, 1965; Vogel, 1989). These “simple” bodies have basic characteristics of pressure drag, such as the triggering effect of the boundary layer, the phenomenon of flow separation, and the critical Reynolds number of round bodies (Hoerner, 1965). A sphere has a constant drag coefficient between $Re = 10^4$ and 10^5 that decreases rapidly by almost an order of magnitude in the critical Re range ($\sim 10^{5.5}$, see Figure 70). This phenomenon can be explained by the boundary layer separation causing an area of minimum pressure in the flow pattern (Hoerner, 1965). In addition, a cylinder has a similar pattern as a sphere when it comes to its constant drag coefficient, with the only difference being that the drag coefficient is slightly higher at $Re < 10^2$ which is caused by the difference in shape to the sphere (Vogel, 1989). However, depending on the surface of the round body, e.g. a sphere or cylinder, the drag coefficient will drop at various Re depending on the roughness of the surface, and this is also caused by the boundary layer separation (Hoerner, 1965).

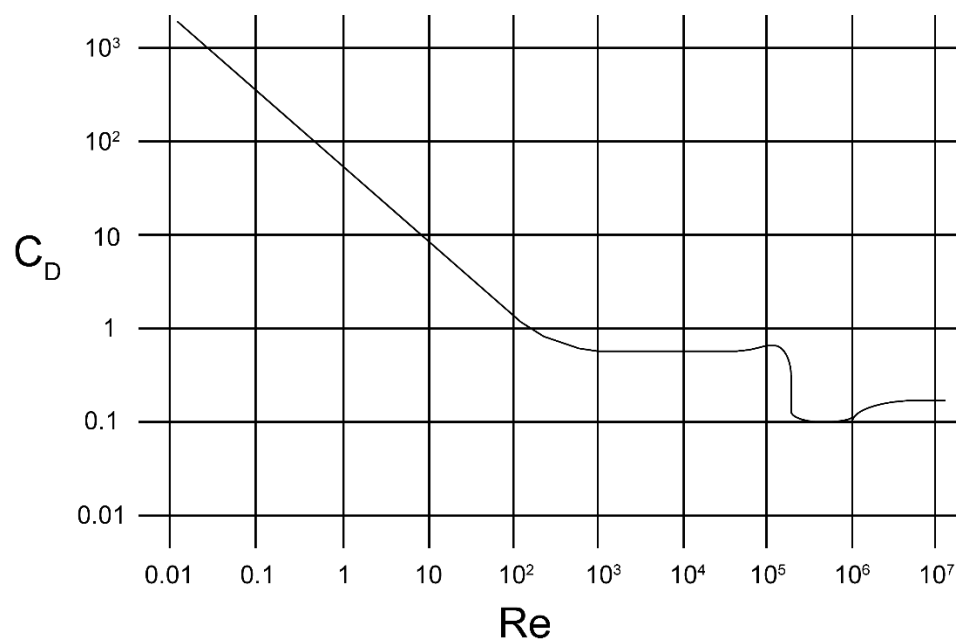


Figure 70: Reynolds number (Re) vs. drag coefficients (Cd). Experimental data on drag coefficients of a sphere in different scenarios as a function of Reynolds numbers. Modified from Hoerner (1965).

Drag is different for objects such as hydrofoils where the angle between the axis and the horizontal plane, also known as the angle of attack (Figure 71) (Hoerner, 1965; Alexander, 1967) plays an important role for the drag. The higher the angle of attack, the more force is added against the foil, and the more the foil needs to add propulsive force in order to keep moving (Alexander, 1967; Vogel, 1989). When the foil is moving in a fluid (air or water) the more asymmetric the foil is, the more it can save energy and vice versa for a more

symmetric foil (Hoerner, 1965). Summing up, the greater the angle of attack is the higher coefficient of drag is as the frontal area increases (Hoerner, 1965; Alexander, 1967).

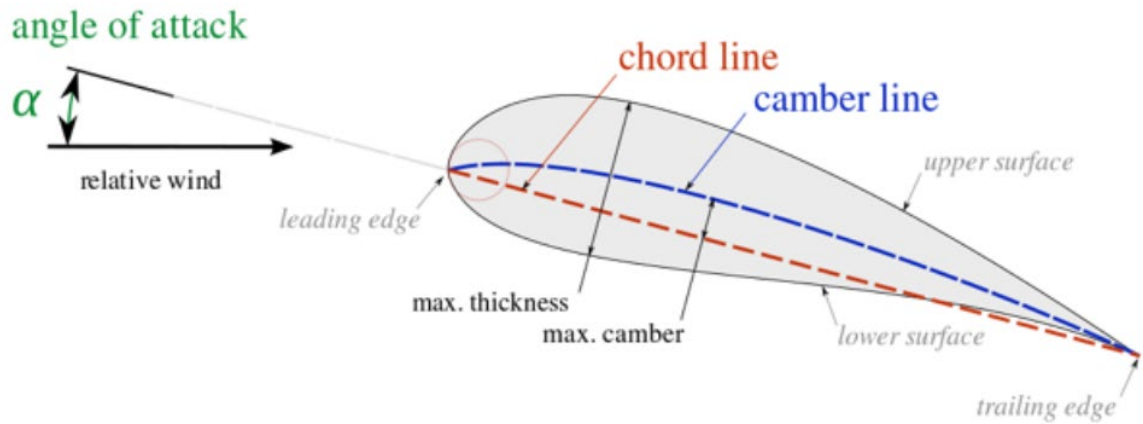


Figure 71: Diagram of air-/hydrofoil cross-section and where the angle of attack affects the air-/hydrofoil. From DeBlois (2013).

4.1.2 Computational Fluid Dynamics

A sub-discipline to the study of fluid dynamics is Computational fluid dynamics (CFD), which is a numerical approach to solve the flow governing equations using computers (Munson *et al.*, 2009; Dynowski *et al.*, 2016; Li *et al.*, 2017; Rahman, 2017). CFD is essentially an *in silico* version of testing a physical model in a wind tunnel or flow tank. This method has been used widely in engineering for several decades (e.g. Evans and Harlow, 1957; Harlow and Welch, 1965), and it uses Navier-Stokes equations to describe how the velocity field and pressure of a moving fluid are related (Munson *et al.*, 2009). CFD involves replacing the partial differential equations with discretized algebraic equations that solve the partial differential equations (Munson *et al.*, 2009). This tool requires information about the size, content and layout of a 3D model, and uses the information to create a grid/mesh of the 3D model which can help identify how the flow of a fluid surrounds the 3D model (Rahman, 2017). As the 3D models are approximations of reality it is important to understand the modelling parameters (Anderson *et al.*, 2012). In CFD we simplify reality with the use of 3D models, and all the unforeseen parameters of nature is therefore unrealistic to include in the simulation.

A simplified version of what CFD does can be seen in Figure 72. First, the solver starts with an initial “guess” derived from the setup (parameters chosen) for the specific simulation/problem we want to solve. Then the solver uses the initial guess to solve the simultaneous equations of Navier-Stokes iteratively as a steady-state or transient flow to get

a result. The equations are solved for the velocity in X, Y, and Z direction, the pressure, TKE (Turbulent Kinetic Energy) and TED (Turbulent Energy Dissipation). The two turbulence equations describe the transport of these two types of energy (Autodesk, 2018a). A new result is created, and the solver checks if the equations have converged or diverged. If the new result has converged but is still without the resolution to the problem, CFD returns to the solver-step and tries to solve it again with a corrected guess, and when the result has stabilised (after a certain amount of iterations) the iterations stop, the simulation has finished, and we have our answer for that specific scenario/problem. The numbers of trials in CFD (meaning if there is yet not a converged result) is equal to the number of iterations run when solving. The iterations take longer to solve the finer the mesh becomes due to the more complex grid and increase in grid cells that CFD must solve to find the result to the problem.

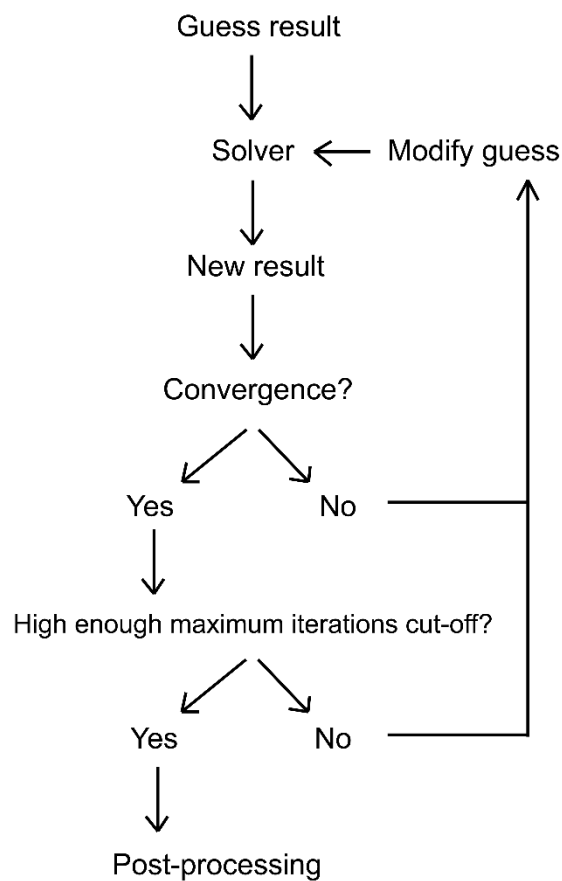


Figure 72: A simplified flow diagram of a generalised iterative solver similar to the process of CFD.

4.1.2.1 Validation/verification

Sources of error in CFD include modelling errors (validation) to determine the degree to which a model is an accurate representation of the real world, and numerical errors (verification) to determine that a model implementation accurately represents description of the model and the solution to the model (Seddighi and Allanson, 2017c). Results are

validated with a set of test models with known results. Some models are compared against experimental results whereas others against empirical hand calculations (Autodesk, 2018a). To demonstrate the minimum amount of numerical error Autodesk Simulation CFD produces, a cylinder model (length: 50.8 cm, diameter: 2.54 cm) closely resembling the one used in this chapter showed an error of only 0.993 % at $Re = 10^5$ when calculating drag force (according to the 2016 version of the software) (Autodesk, 2018a). However, the numerical error is always dependent on object and analysis characteristics used in the software.

4.1.2.2 Setup

First a 3D model is imported to Autodesk Simulation CFD. The model can be created in any computer-aided design (CAD) software (Rahman, 2017). Throughout this thesis Autodesk Maya 2017/2018 was used to generate input models in the form of NURBs-based objects.

Materials, domain, boundary conditions, and mesh size are all parameters included in the setup, each with their own characters and set of rules in order to perform the simulation further on. As almost every CFD problem is defined by the boundary conditions these conditions are crucial in order to get a correct outcome from the simulation, e.g. force of drag, pressure etc. The importance of this is to be discussed later in this chapter.

4.1.2.2.1 Geometry Tools

In order to allow a fluid (e.g. air or water) to flow around a model an external volume must be created, also called the computational fluid domain (Bradney *et al.*, 2016; Rahman, 2017) (Figure 73). This domain will have boundary conditions and a mesh dedicated to it, and the surfaces and edges of the domain cannot contact or intersect any part of the model. It is recommended to have a minimum of 5 % (Autodesk, 2018a) from edge of domain to the edge of the model in all three directions (X, Y, and Z-axis). Experience indicates it is recommended (pers. comm. Peter Falkingham, David Allanson, and Mehdi Seddighi) that a domain should be at least five times the object/model size to avoid edge effects. However, it is convenient to keep the domain as small as possible to reduce computation time. Thus, it is always important to test for the right domain size before collecting results from CFD.

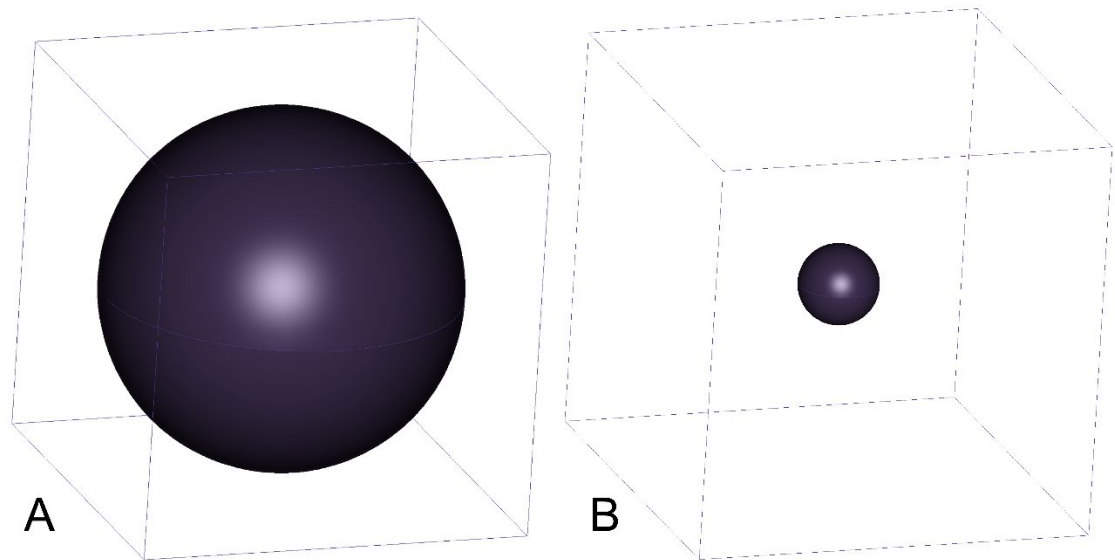


Figure 73: After applying domain to a 1m sphere with no specific domain size (A), and after applying an appropriately large domain to the same 1m sphere (B) in Autodesk Simulation CFD.

4.1.2.2.2 Materials

Material properties must be assigned to both the object and the domain. Autodesk Simulation CFD includes a library of material properties from aluminium to rubber, and from sea water to air. It is also possible to customise a material in the material editor.

4.1.2.2.3 Boundary conditions

The surface of the object is the most common boundary encountered in fluid flow problems (Versteeg and Malalasekera 1995). The boundary conditions are what allow the governing equations to differentiate between different flow fields (for example, flow past a car or flow past a person running) and produce a solution unique to the given flow geometry (Versteeg and Malalasekera, 1995; Munson *et al.*, 2009). The boundary conditions must be appropriately specified for the inlets, outlets, and wall gradients (Munson *et al.*, 2009).

If we simulate a flume rather than moving the object through static water, we can link the boundary conditions to the fixed domain size specified prior to the boundary conditions. A common configuration for incompressible flow has the velocity specified at the inlet and the pressure fixed at zero at the outlet (Rahman, 2017). The inlet velocity depends on the preferred velocity for the specific object.

No-slip/symmetry boundary conditions are sometimes needed to constrain the fluid velocity at zero relative to the object (Versteeg and Malalasekera, 1995; Rahman, 2017). This is because the slip/symmetry function in the boundary conditions causes the fluid to flow along a wall instead of stopping at the wall allowing frictionless walls (Rahman, 2017). Fluid is prevented from flowing through the wall, however.

4.1.2.2.4 Mesh sizing

CFD simulations solve for the relevant flow variables only at the discrete points which make up the grid or mesh of the solution (Munson *et al.*, 2009). CFD breaks the model into manageable chunks called elements/grid cells made in either 2D or 3D. Generally, there are two types of grids: structured and unstructured, depending on whether or not there exists a systematic pattern of connectivity of the grid points with their neighbours (Munson *et al.*, 2009). A structured grid (Figure 74) has some type of regular, coherent structure to the mesh layout that can be defined mathematically, with the simplest kind being a uniform rectangular grid (Figure 74; left) (Munson *et al.*, 2009). If the grid is structured, the grid cells are made of rectangular faced elements, and unstructured grids are made of triangular (2D), quadrilateral (2D), tetrahedral (3D), hexahedral (3D) or five sided elements (Autodesk, 2018b). In each corner of one element is a node, and the more nodes/elements the model has, the longer it takes for CFD to solve, but the finer the resolution of the solution.

The type of grid developed for a given problem can have a significant impact on the numerical simulation, including accuracy of the solution (Munson *et al.*, 2009). The grid must represent the geometry correctly and accurately, since an error in this representation can have a significant effect on the solution (Munson *et al.*, 2009). The geometry of the grid has a substantial impact on the rate of convergence and solution accuracy. Therefore, it is necessary to increase the number of grid points (finer mesh) where large gradients are to be expected, such as in the boundary layer near a solid surface (Munson *et al.*, 2009).

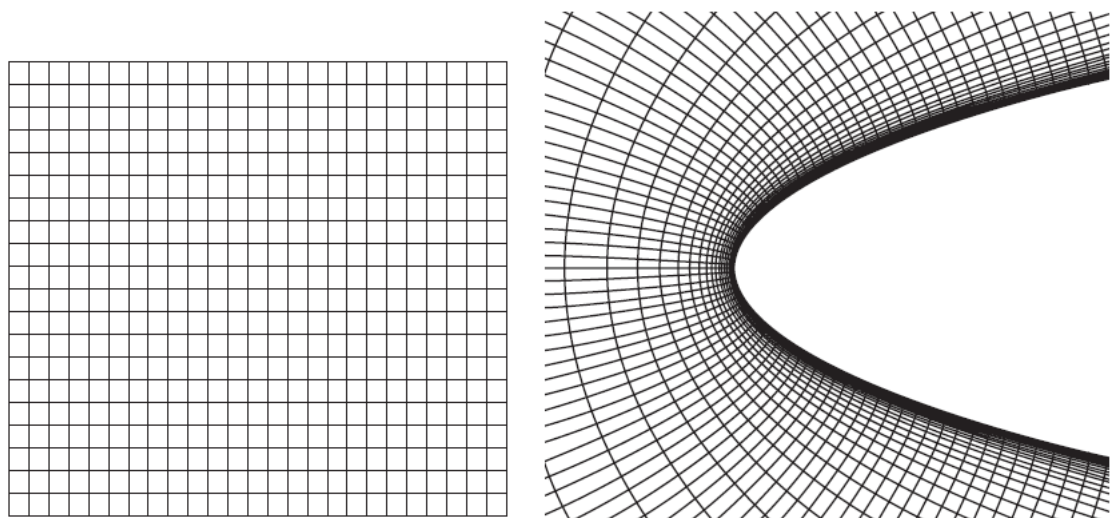


Figure 74: Structured grids. Left = Rectangular grid. Right = Structured grid around a parabolic surface. From Munson *et al.* (2009).

The more complex the mesh is, the more grid cells are included, and it is normal for today's CFD problems to involve several million grid cells (Munson *et al.*, 2009). In an unstructured grid (Figure 75), the grid cell arrangement is irregular and has no systematic pattern (Munson *et al.*, 2009). The grid cell geometry usually consists of various-sized triangles for two-dimensional problems and tetrahedral or hexahedral elements for three-dimensional grids (Munson *et al.*, 2009; Rahman, 2017). Unlike structured grids, in an unstructured grid each grid cell is defined separately because the neighbouring cells are different in size (Munson *et al.*, 2009), so that there is a gradual transition from coarse to fine in the mesh. This produces an increase in the computer code complexity as well as a significant computer storage requirement (Munson *et al.*, 2009). However, the advantage to an unstructured grid is that it can be applied to complex geometries, whereas structured grids would have severe difficulty doing this from a computational point of view (Munson *et al.*, 2009).

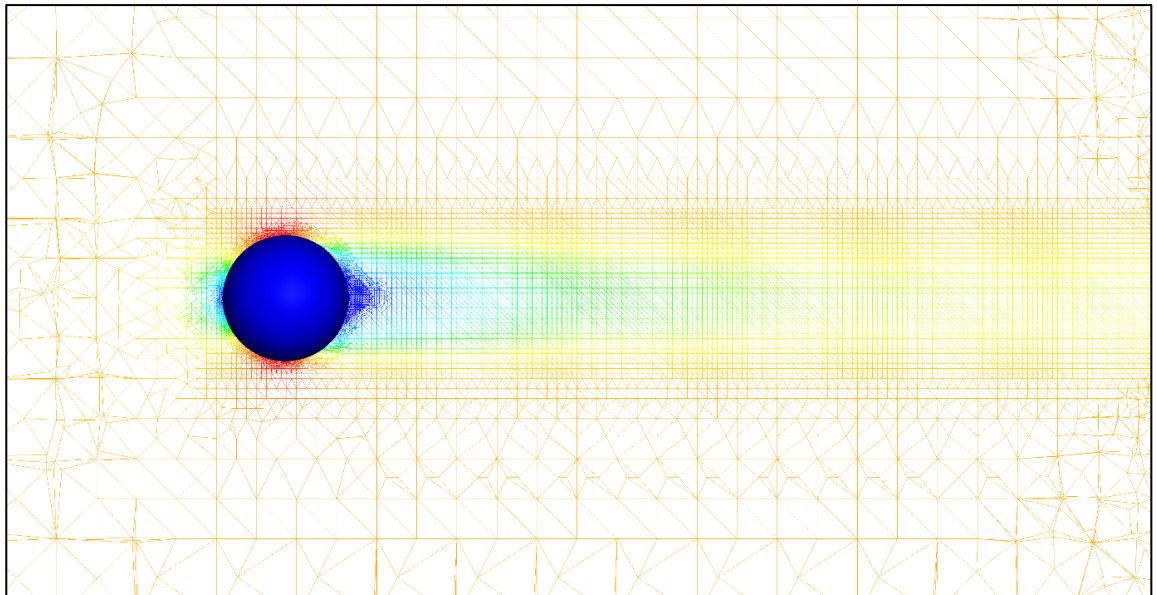


Figure 75: Example of an unstructured grid around a sphere and in its wake. Made in Autodesk Simulation CFD. Colours indicate flow velocities with blue being the lowest and red the highest velocity.

The separation of flow around an object is an important part of the general dynamics of the fluid. It also occurs at relatively small spatial scales, which means that the mesh needs to be finest in this area. As seen in Figure 75 the grid is very complex in the areas of flow separation, where more grid cells are created. Outside this area the mesh is much coarser, and generally the mesh of the domain will be a lot coarser than the 3D model. This is because there is no need to spend a lot of computational power on the domain outside the flow separation, as it will not affect the result for total drag if this area is finer in mesh size.

In Autodesk Simulation CFD, mesh generation can be automated, but manual refinement might be necessary for complicated objects, and can be adjusted for all volumes and surfaces of the 3D model imported. As the mesh defines the model for the analysis, we want to make sure the mesh is adequate so that we see a smooth curvature of the solid in the critical area. If the mesh is too coarse the number of nodes will be less than six across the thinnest direction/circumference, eventually resulting in divergence leaving the simulation unsolved. In addition to manual refinement, it is also possible to use region refinement, which creates a region around a specifically chosen area of the model to be refined individually to allow a higher resolution within the area (Figure 76).

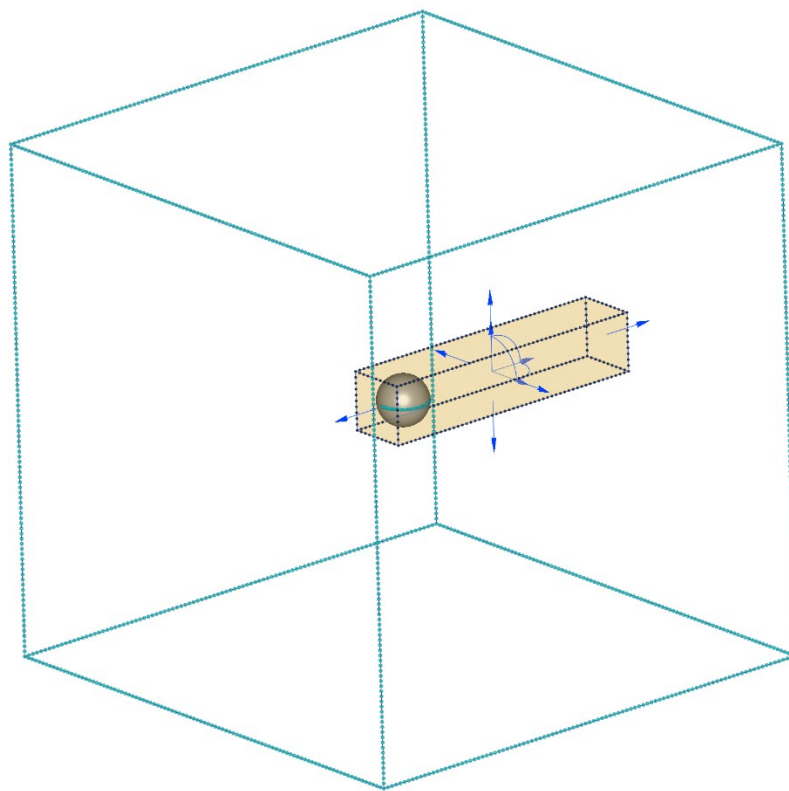


Figure 76: Region refinement in domain in the wake of the sphere in Autodesk Simulation CFD.

As previously mentioned in the ‘Flow separation’ section, the flow separation in the boundary layer occurs when there is a change in flow around a moving object due to rotated particles (Figure 67). In CFD we can adjust the number of wall layers to avoid layers of diffusion so that the results will not be affected by this factor. The wall layers are additionally applied to the domain. As seen in Figure 77 the wall layers are parallel and perpendicular to the surface of the object to avoid mix of flow in the area of flow separation, and this feature is automatically applied with a default setting of three layers when using Autodesk Simulation CFD.

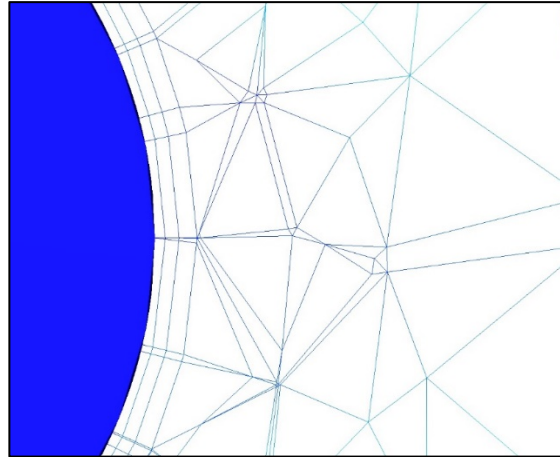


Figure 77: Wall layers (here shown with a total of three) and the mesh around a cylinder (marked in blue) using Autodesk Simulation CFD.

The thickness of each wall layer can also be adjusted. For example, if we need to reduce the thickness of the boundary layer we can do this by reducing the layer factor. As this factor will be applied for all wall layers, we will observe a reducing in total thickness.

4.1.2.3 Solve and Iterations

Before solving, it is important to assign an appropriate flow model, depending on the Reynolds number for the model. In Autodesk Simulation CFD there are a total of 10 turbulence models to choose from in the solve settings, and each of them have specifically recommended uses (Table 10).

Some simulations in CFD do not use turbulence models, e.g. Direct Numerical Solution (DNS) and LES (Large Eddy Simulations). This is because the Navier-Stokes equations are numerically solved when using these types of simulations. The whole range of spatial and temporal scales of the turbulence must be resolved. Computational requirements of numerically solving the Navier-Stokes equations mean DNS and LES are only suitable for very simple flows (Seddighi and Allanson, 2017a).

Reynolds Averaged Navier-Stokes (RANS) equations are the oldest and largest field in turbulence modelling (Seddighi and Allanson, 2017a). Different from the numerically solved models RANS only resolve a small part of the range of spatial and temporal scales of the turbulence, allowing more complex flows (e.g. including turbulence) with less computational requirements in comparison to the numerically solved models. RANS models can be divided into two broad approaches: Eddy viscosity models (EVM) and Reynolds stress model (RSM) (Seddighi and Allanson, 2017b). EVM include e.g. the standard k-

epsilon and k-omega turbulence models which have two transport equations; one equation for kinetic energy or the property of the flow, and one for a specific dissipation rate (epsilon, omega etc.) (Seddighi and Allanson, 2017b). RSM include the Reynolds stress model which solve a total of seven transport equations for the turbulence, including terms of inertia (rate of change), advection, production, turbulent transport rate, viscous diffusion, pressure velocity-gradient of strain and diffusion, and turbulence dissipation (Seddighi and Allanson, 2017b). As we are not interested in the specific details of the transport equations for the individual turbulence models, only the definition and recommended use is stated to clarify when to use the different models (Table 10). Autodesk Simulation CFD uses EVM, and mainly the two equation turbulence models.

Table 10: The 10 available turbulence models in Autodesk Simulation CFD, what defines them, and their recommended use. From Autodesk (2018a, 2018b).

Turbulence model	Definition	Recommended use
<i>k-epsilon</i>	Default turbulence model. Typically, more accurate than the constant eddy viscosity model, but more intensive computationally and slightly less robust.	General purpose model. Can be used for many applications.
<i>SST k-omega</i>	Robust across a wide range of flow types. Does not use wall functions but simulates turbulence all the way to the wall. To use efficiently, make mesh fine in the boundary layer region (10 layers max).	External aerodynamics, separated or detached flows, and flow with adverse pressure gradients.
<i>SST k-omega SAS</i>	SAS (Scale Adaptive Simulation) can use steady state simulations. Turbulence structures cannot be animated but predicts formation and shape better than steady-state k-epsilon. To use efficiently, make mesh fine in the boundary layer region (10 layers max).	Flows with turbulence structures like vortex shedding and variable wake structures.
<i>SST k-omega RC (Smirnov-Menter)</i>	Menter two-equation model with Rotation and Curvature (RC) correction. Requires a fine mesh and may require several thousand iterations for convergence.	High curvature flows like those commonly found in cyclone separators.
<i>SST k-omega (Hellsten)</i>	Menter SST two-equation models with Hellsten's Simplified Rotation/Curvature correction. Show good flow prediction over convex surfaces where detachment point is difficult to predict with other turbulence models.	Certain airfoils. Small, high speed rotating devices. Highly curved flows and over convex surfaces.

<i>SST k-omega DES</i>	It is a hybrid between SST k-omega and large eddy simulation (LES). Is sensitive to the mesh distribution and computationally intensive. Works best with uniform mesh distribution.	Separated and high Re external aerodynamics flows.
<i>RNG</i>	Slightly more accurate than k-epsilon, particularly for separate flows. It is often recommended to start with k-epsilon and after fairly well converged enable the RNG model.	Reattachment point for separate flows, particularly for flow over a backward-facing step.
<i>Low Re k-epsilon</i>	Does not use wall functions, so always enable mesh enhancement and increase its layers to 5. High Re flows run with low Re turbulence model will generally produce the same solution as would the k-epsilon model.	Low speed and turbulent flow with Re of typically 1500 to 5000. Flows with both low and high-speed regions. Pipe flows and external aerodynamic flow transitioning between laminar and turbulent. High-speed jets entering a large room of with slow-moving flow. Buoyancy-drive flows that are barely turbulent.
<i>Mixing length</i>	In some cases, reduces run times and improves accuracy for internal buoyancy-driven flows. Designed for gas flows (such as air) and will not produce good results for liquid.	For internal natural convection analyses.
<i>Eddy Viscosity</i>	Less rigorous than the k-epsilon model, and more numerically stable. Useful if divergence occurs with one of the other models.	Lower speed turbulent flows and some buoyancy flows.

In Autodesk Simulation CFD we can also enable adaptation of the mesh. By doing so, we can adjust the number of cycles run, if we want to save those cycles and/or if we want to “Allow Coarsening”. For each cycle CFD runs the software automatically refines the mesh in the area of separation around the object as it adapts to the results from the previous cycle. In “Additional Adaptation” we can also apply free shear layers if we suspect strong velocity gradients will occur. Under “Advanced Adaptation” we can change the refinement limit to prevent over-refinement if the adaptation of the mesh is enabled.

If testing different variables for one object, it is possible to save time by running a batch process, meaning a series of jobs being run without interaction. The way to do this in Autodesk Simulation CFD is to make several scenarios, all with different variables changed

according to the preferred conditions for the tests. When the first scenario has been solved, the next will start, and so on - this way simulations can be run over night, eventually saving a lot of working hours.

4.1.2.4 Results

After setting all parameters specific for the problem needs solving, the discretized equations can be solved, and the fluid flow can be simulated (Rahman, 2017). The more complex the geometry, usually the more time and iterations it takes to solve. An iteration is a numerical sweep through the entire model (Autodesk, 2018a).

4.1.2.4.1 Output Bar

Output from the simulation includes a “Convergence Plot” (Figure 78). The convergence of each degree of freedom is monitored here. Early in the analysis, results will change a lot from one iteration to the next, and the convergence lines may oscillate up and down (Figure 78). Horizontal convergence lines indicate when the results stop changing and that the solution is converged/stabilized, and several iterations are required to attain full convergence (Autodesk, 2018a). The number of iterations varies based on the application and physics settings (Autodesk, 2018a), e.g. a higher velocity creates more iterations. Therefore, it is important to have set a high enough maximum iterations cut-off in order to undertake quantitative analysis, as only qualitative trends can be obtained before a complete convergence is reached (Autodesk, 2018a). When convergence is reached, the plot will fill out the whole graph and another simulation can be set up to solve.

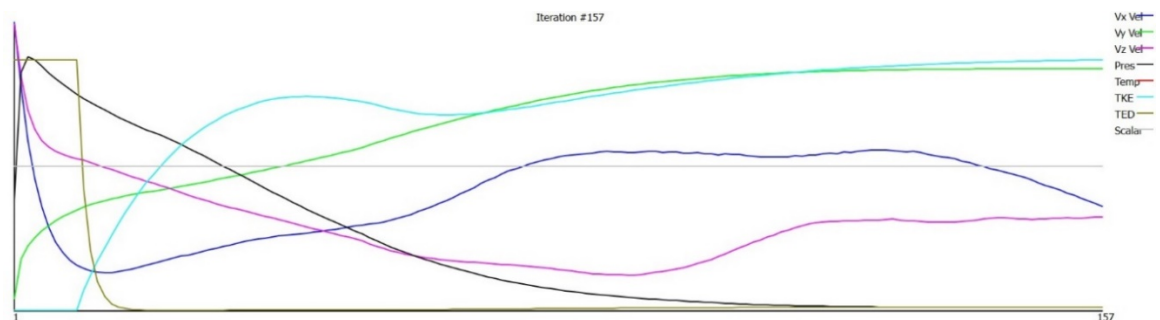


Figure 78: Example of Convergence Monitor result in Autodesk Simulation CFD. Here the analysis converged after 157 iterations.

4.1.2.4.2 Analysing/Visualizing CFD results

The results of the CFD simulation can be visualised in various informative ways, with the most commonly used being plots of flow velocity, pressure or vorticity (Rahman, 2017).

4.1.2.4.2.1 Planes

One way of illustrating the results from simulations is to add *Planes* to the domain (Figure 79). This application visualises results on cutting planes, which means variables (pressure, velocity, heat etc.) around the object can be visualised. However, this way of illustrating the flow is only in a 2D-slice of the model.

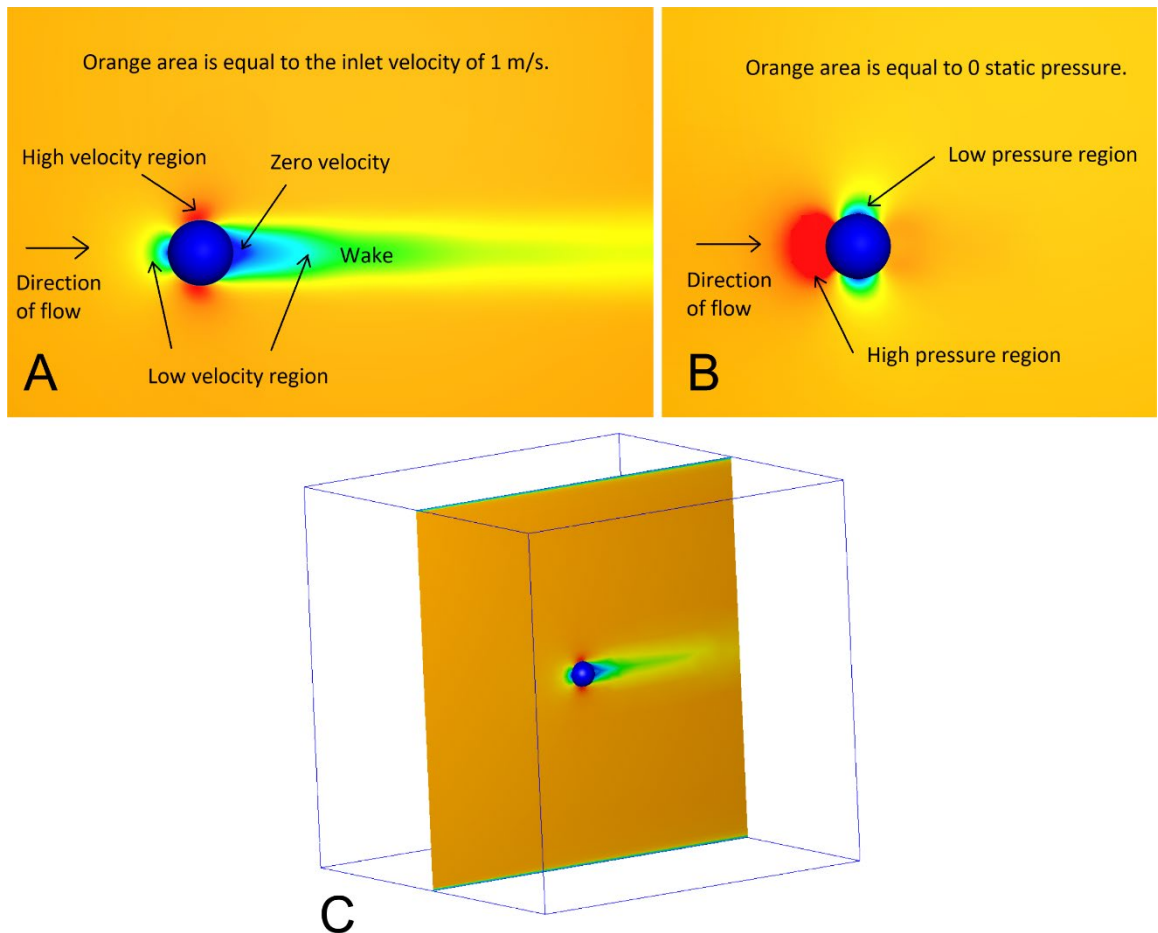


Figure 79: Plane visualisation in Autodesk Simulation CFD. A) The velocity distribution visualized using a plane parallel to the direction of flow, showing a low velocity region at the front and back of the sphere. The blue regions in front and behind of the sphere are areas of zero velocity. Flow speeds up along the sides of the sphere. Note the long wake region that is many times longer than the diameter of the sphere. B) The unequal pressure distribution visualized using a plane. Red region is the high-pressure region occurring at the front of the sphere, and blue is the low-pressure region occurring at the sides and back of the sphere. Maximum pressure occurs in the front of the sphere (red region), also called the stagnation pressure. C) Oblique view of domain with plane visualising how plane is included and cut in the middle of the domain.

4.1.2.4.2.2 Traces

Another way to visualise the flow is by adding particle *Traces* along/around the object. Particle traces can add 3D information to the flow. Pattern type of the particle traces can be adjusted by seed type, seed pattern, and seed density, and the colours of the traces can be

adjusted to a preferred choice. Seed types applicable are point, line, ring, circular, rectangular, region or as Key-in with exact X, Y, and Z coordinates. Seed patterns applicable are as a diamond, grid, or hexagon. Depending on what type of 3D model used in the simulation some seed types, patterns and densities are more suitable for visualisation than others. As an example, the sphere in Figure 80 has its traces visualised with seed type “lines”, seed pattern “grid” and a density of 0.5.

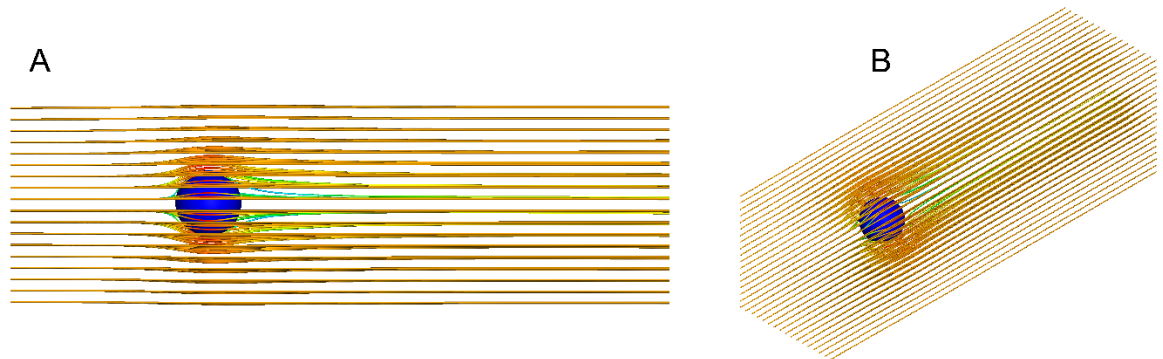


Figure 80: Particle traces visualized in Autodesk Simulation CFD showing a recirculation/vortex region on the back-side of a sphere caused by boundary layer separation at a high Reynolds number. The recirculation is in 3D and wraps around the side of the sphere. Here the traces are visualised as a line of seeds. A) Side view. B) Isometric view.

4.1.2.4.2.3 Iso Surfaces and Volumes

For objects inside the domain *Iso Surfaces* and *Iso Volumes* can be used to visualise results on surfaces with a constant value and for the volumes between two values, respectively. The application also includes static pressure that can be applied to the volume inside the domain, visualising how pressure is distributed (Figure 81).

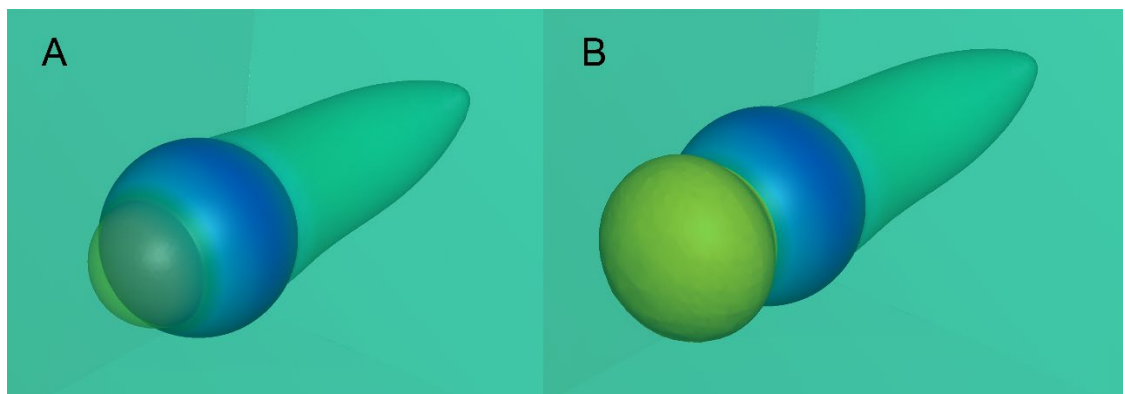


Figure 81: Isometric view of the static pressure added to a sphere in Autodesk Simulation CFD shown as iso volume (A) and iso volume with iso surface (B). Yellow area indicates the part of the sphere with the most pressure whereas the blue areas indicate the least pressure.

4.1.2.4.2.4 Wall calculator

The wall calculator can calculate flow-induced forces on solid and wall surfaces (Figure 82). Additionally, the wall calculator can determine drag and lift on aero/hydrodynamics bodies, wall temperatures, pressures, heat flux, film coefficients, torque about an axis and the centre of force (Figure 82), making it sufficient for many types of designs and systems.

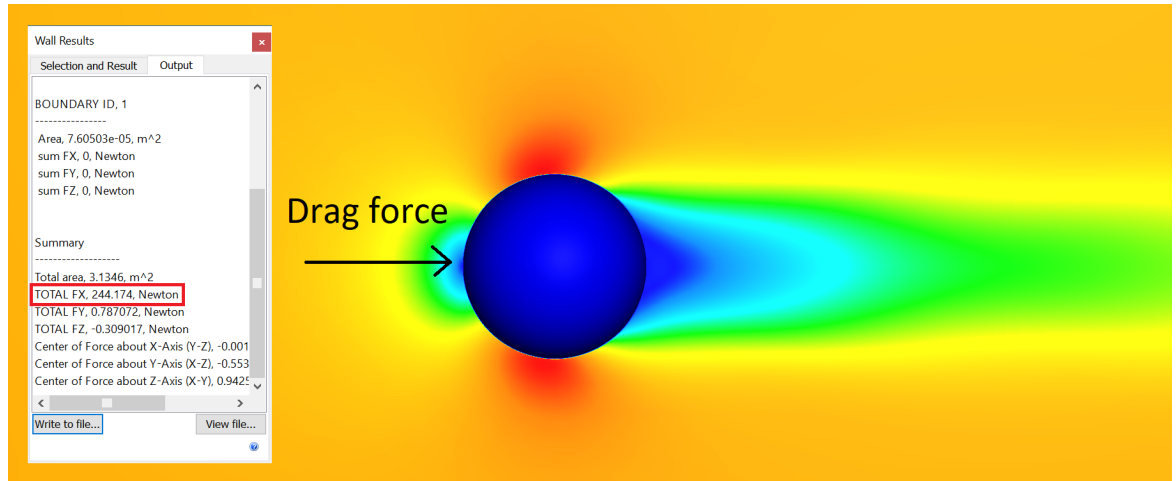


Figure 82: Example of Wall Calculator. The computed force in the direction of the flow (here X-axis) is 244.174 Newton for this specific analysis made in Autodesk Simulation CFD. This means the total drag force on the sphere is 244.174 Newton in this example.

4.2 Validation experiments

Subsequent chapters will apply CFD to explore aspects of plesiosaur palaeobiology. Obviously, we cannot validate flow around a plesiosaur, so instead we must validate the method using simple objects. To validate the workflow of Vogel (1989), simple objects (a sphere and a cylinder) with known responses to flow were simulated using Autodesk Simulation CFD. The software allowed calculating drag forces and those forces were then used to obtain drag coefficients manually by applying Equation 9. The coefficients of drag were illustrated against Reynolds numbers (equivalent to velocity) to compare and discuss results from CFD with the work of Vogel. Additionally, parameters that might influence the results were tested and discussed according to the theoretical coefficient of drag numbers for a sphere and cylinder and the usage of parameters tested.

4.2.1 Methods

3D models of unstructured meshes of spheres and cylinders with diameters of 0.1m and 1m (cylinders with lengths 0.3m and 3m, respectively) were made in Autodesk Maya and exported to Autodesk Simulation CFD (www.autodesk.com). Settings applied in CFD were the following:

Fluid type (for the domain) was set as seawater, as it matches the material of the domain for the plesiosaur. The density of seawater is 1021.2kg/m^3 and the viscosity is $0.0011404\text{ Pa}\cdot\text{s}$. Solid type (for the sphere and cylinder) was set as glass as it closely matches the theoretical scenarios (smooth sphere/cylinder), and its density is 2700 kg/m^3 .

The following parameters were systematically changed to explore their effects on the drag coefficient on the sphere and cylinder: rate of flow, boundary condition settings, mesh size settings, and solve settings. If not otherwise stated, the parameters of the setup in each test were as default. Reynolds numbers were calculated manually using Equation 5, with the length of the object being the diameter of the sphere and cylinder, and coefficient of drag was calculated manually using Equation 9.

In frontal view, the sphere and cylinder models were placed centrally in the domain (Figure 83A). In side view, the sphere and cylinder models were placed $\frac{1}{4}$ of the domain length from the inlet and approximately $\frac{3}{4}$ from the outlet (Figure 83B). The space between model and domain allowed fluid to flow on each side of the sphere and cylinder models. The size of the domain is defined as its total length, with all sides of the domain of equal length.

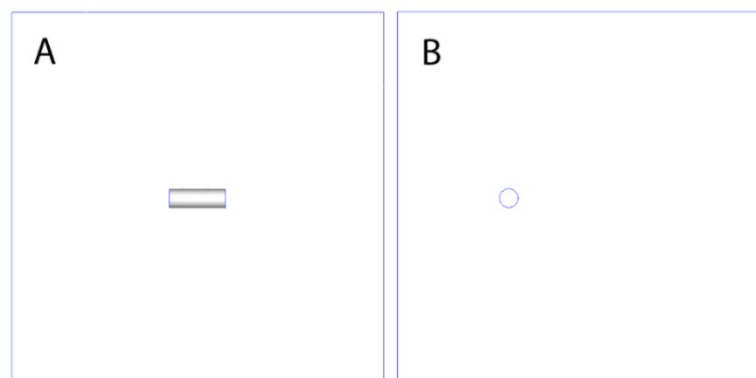


Figure 83: Frontal view (A) and side view (B) of the cylinder model in domain.

4.2.2 Results with respective approaches

4.2.2.1 Change of flow

First, it was important to find out whether the size of the sphere and cylinder would change the flow velocity pattern, by using the two distinctively sized spheres and cylinders mentioned above. The mesh size was set to auto-sizing for both spheres and cylinders for this test. As would be expected the flow velocity pattern was similar for both spheres (Figure 84A-B) and cylinders (Figure 84C-D), as they had the same Reynolds number ($Re \approx 900,000$). The sphere and cylinder with a diameter of 0.1m (velocity = 1m/s) were solved at

one order of magnitude lower than the sphere with a diameter of 1m (velocity = 0.1m/s). In addition, as no changes were observed when comparing the flow velocity pattern for a 0.1m and 1m sphere and cylinder, this test was the only one including a sphere and cylinder of 0.1m. All other tests were carried out using spheres and cylinder of 1m in diameter.

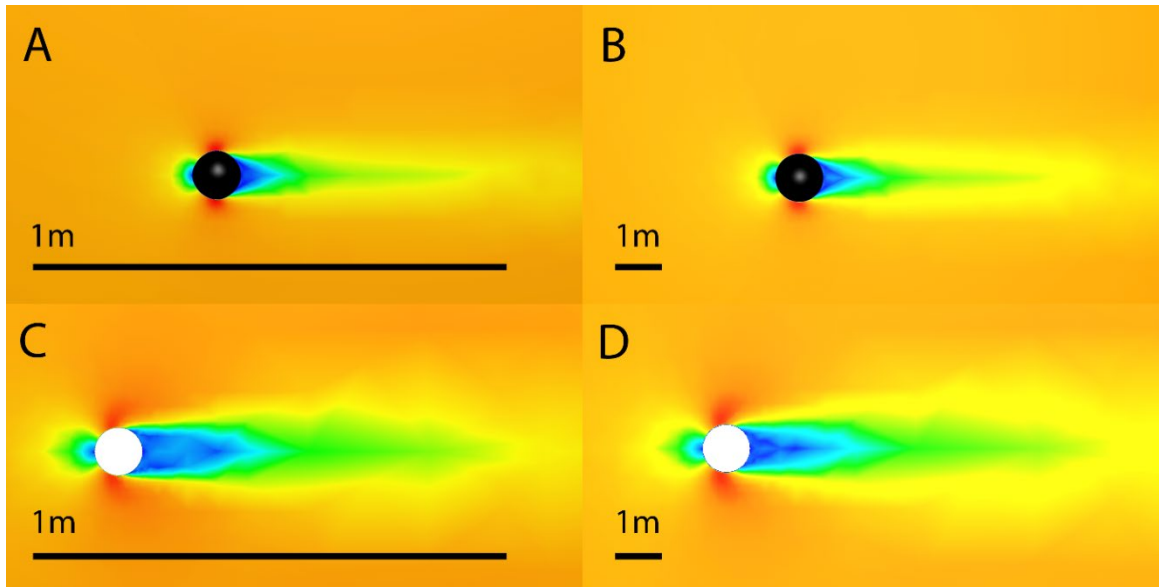


Figure 84: Flow velocity around a sphere (black) with (A) a diameter of 0.1m and (B) a diameter of 1.0m, and around a cylinder in side view (white) with (C) a diameter of 0.1m and (D) a diameter of 1.0m. Reynolds numbers for A-D were $\sim 900,000$. Flow is visualised using a plane through the middle of the domain. Colour gradients relate to flow velocity; blue colours are the lowest and red are the highest velocities.

The effect on object size to the flow velocity pattern was important for demonstrating the simulation retained accuracy over a range of sizes. The reason for the similarity in flow velocity pattern for the objects can be found in the Reynolds number equation (Equation 5); by adjusting the velocity so that the sphere and cylinder with a diameter of 0.1m was solved at a magnitude lower than the sphere and cylinder with a diameter of 1.0m the Reynolds numbers would remain the same.

4.2.2.2 Boundary Condition settings

The first test with boundary conditions was to add slip/symmetry to the walls and compare to results without this boundary condition added. This test was performed at Reynolds numbers similar to the test of Vogel (within the Re range of $0.01 - 10^6$) for a total of 22 simulations (11 for with added slip and 11 without added slip) to compare the coefficient of drag with theory. Without added slip/symmetry means the walls are frictionless though solid walls, and when the slip/symmetry is added it causes the fluid to flow along the wall instead of stopping at the wall. However, fluid is still prevented from flowing through the wall. The

sphere and cylinder showed disparate results compared with theory (Vogel, 1989) as the coefficient of drag was higher than expected at $Re = 0.1$ to 10 and at $Re = 1,000$ for both with and without added slip/symmetry for the sphere (Figure 85) and cylinder (Figure 86). Furthermore, coefficient of drag was lower than expected at $Re = 90$ and $Re < 10,000$ for both with and without slip/symmetry for the sphere (Figure 85) and at $Re = 100$ and $Re < 10,000$ for both with and without slip/symmetry for the cylinder (Figure 86). The close resemblance to theory was observed when testing without added slip/symmetry, with only $Re = 100$ and 1000 as outliers. In that case the slip/symmetry boundary condition was not something to consider of great importance when performing CFD if working with external fluid flows around an object.

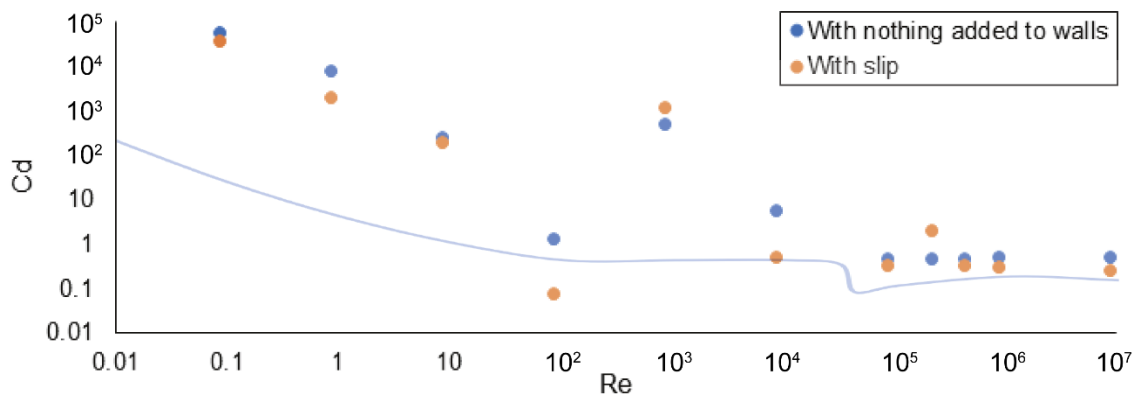


Figure 85: Reynolds number (Re) vs. coefficient of drag (Cd) with and without slip/symmetry boundary conditions for a sphere. Theoretical curve indicated by blue line.

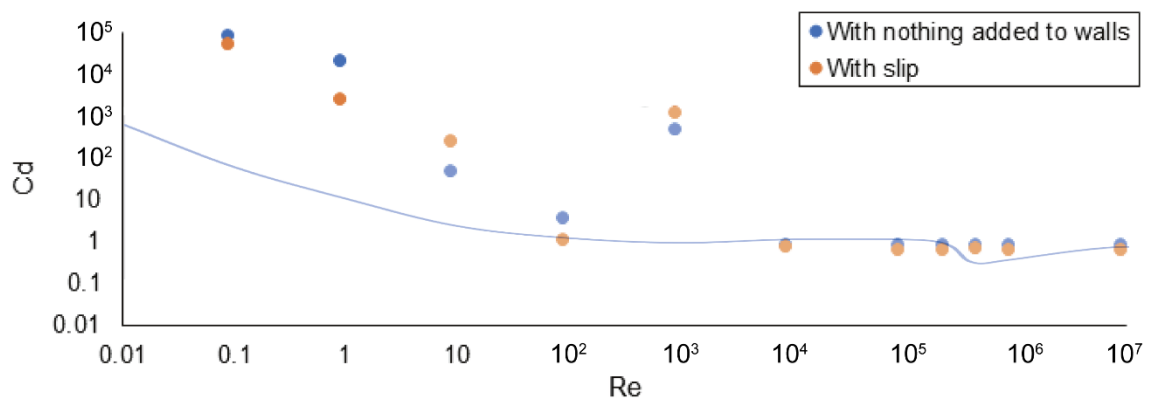


Figure 86: Reynolds number (Re) vs. coefficient of drag (Cd) with and without slip/symmetry boundary conditions for a cylinder. Theoretical curve indicated by blue line.

Another test for the slip/symmetry boundary condition was performed, which included domain size instead of Reynolds numbers. The domain sizes used for the test included cubes of 3.3m, 5m, 7m, 10m and 20m at $Re = 900,000$ (equal to 1m/s). The test was performed to

compare if change in domain size affected the coefficient of drag for a sphere and cylinder with and without added slip/symmetry. The test showed a lower coefficient of drag for all domain size compared to theory when slip/symmetry was added for both the sphere and cylinder (Figure 87 and Figure 88). Coefficient of drag remained fairly stable for both with (around 0.3 for the sphere, 0.65 for the cylinder) and without (around 0.47 for the sphere, and 0.82 for the cylinder) slip/symmetry boundary conditions, and thus without slip/symmetry was consistent with theory (Vogel, 1989), allowing no need to add such setting to the walls. However, an increase in drag coefficient was observed for the cylinder at a very low domain size (3.3-5m) in both cases (with and without slip/symmetry), which was probably caused the domain size creating less space for the flow to act in the domain. As mentioned earlier the recommended domain size is at least five times the object length in order to avoid edge effects. This is also what is observed in this test, and it is therefore concluded that domain size is a highly important parameter to include when doing CFD.

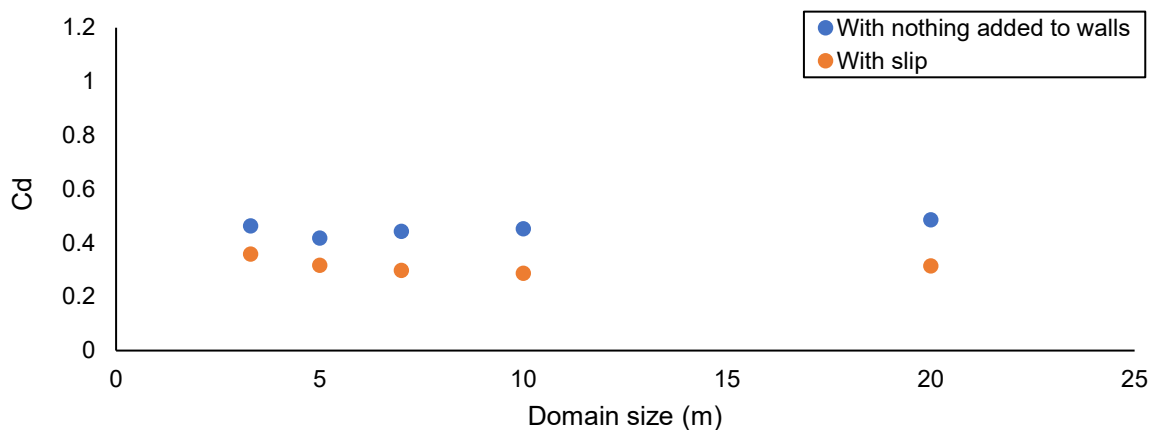


Figure 87: Domain size (m) vs. coefficient of drag (Cd) with/without slip/symmetry boundary conditions for a sphere.

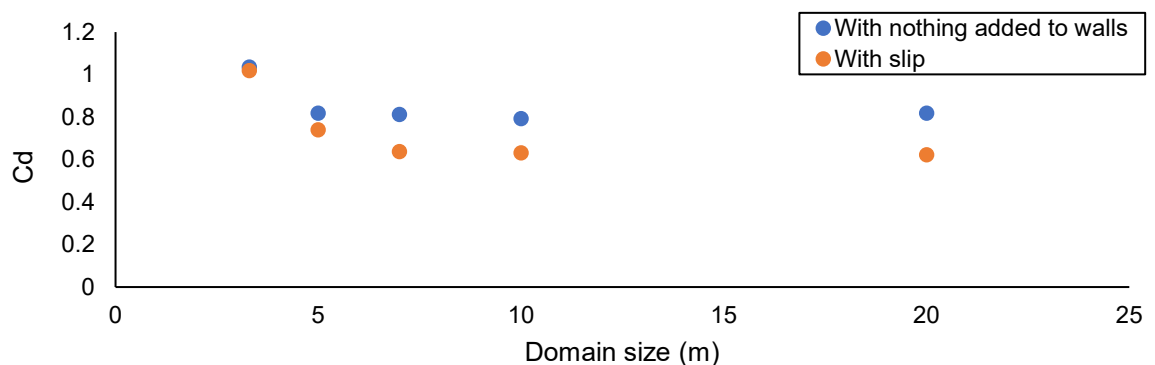


Figure 88: Domain size (m) vs. coefficient of drag (Cd) with and without slip/symmetry boundary conditions for a cylinder.

Likewise, with testing the slip/symmetry boundary condition, the walls were also tested at different velocities (0.0000001 – 10m/s) with a domain size of 10m to find out whether the coefficient of drag would remain stable for all Reynolds numbers or if there would be a notable difference in coefficient of drag here as well. This test showed that coefficient of drag was a lot more stable (Figure 89 and Figure 90) compared to when slip/symmetry was added (Figure 85 and Figure 86). However, coefficient of drag still was not consistent with theory as it was both above ($Re < 10$) and below ($Re > 10$) the theory for the sphere and cylinder. Coefficient of drag was stable with only $Re = 1,000$ deviating when nothing was added to the walls, and thus both the sphere and cylinder had values above theory.

The two outlier points in Reynolds numbers in Figure 85, 86, 89, 90 could be caused by the domain size being too small, as there is an observed change in coefficient of drag (Figure 87 and Figure 88) with change in domain size.

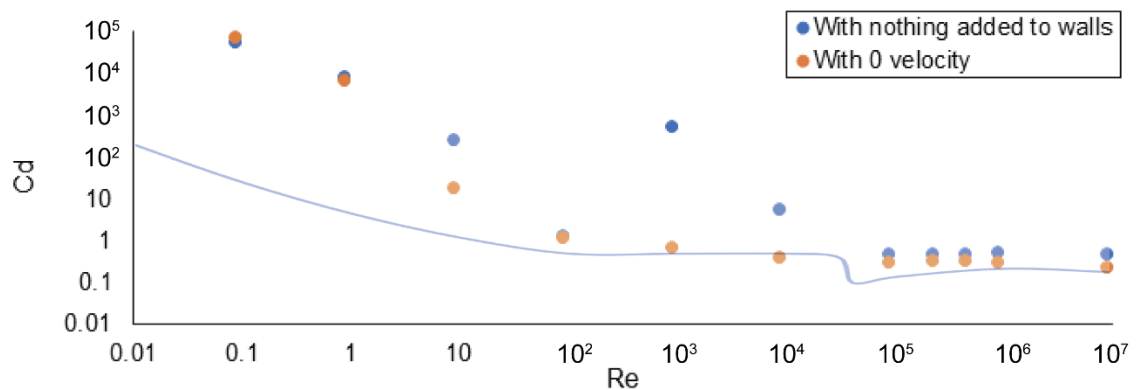


Figure 89: Reynolds numbers (Re) vs. coefficient of drag (Cd) with and without walls set to velocity at 0m/s for a sphere. Theoretical curve indicated by blue line.

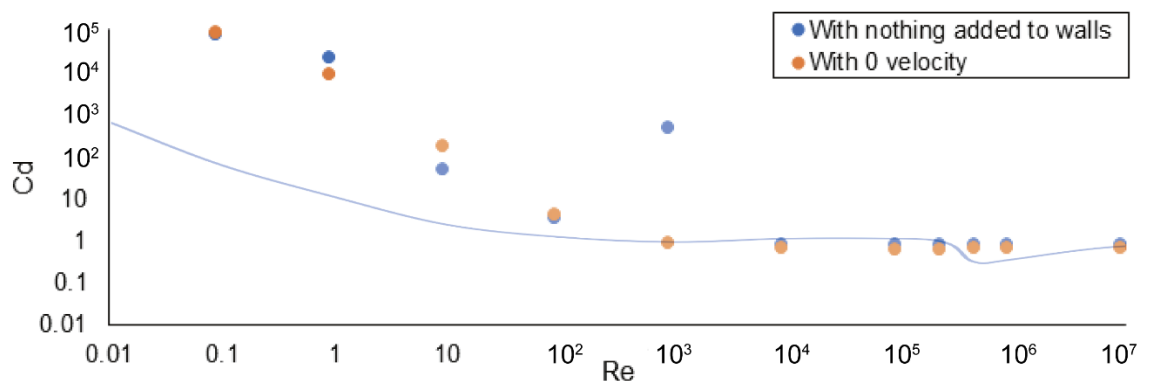


Figure 90: Reynolds numbers (Re) vs. coefficient of drag (Cd) with and without walls set to velocity at 0m/s for a cylinder. Theoretical curve indicated by blue line.

Testing domain sizes with and without 0m/s in velocity for the wall showed the same trend as slip/symmetry for the sphere (Figure 87), with a generally lower coefficient of drag for

all domain sizes tested when added zero velocity to the walls (Figure 91) compared to when adding slip/symmetry (Figure 87). Coefficient of drag was consistent with theory when nothing was added to the walls for the sphere (Figure 91).

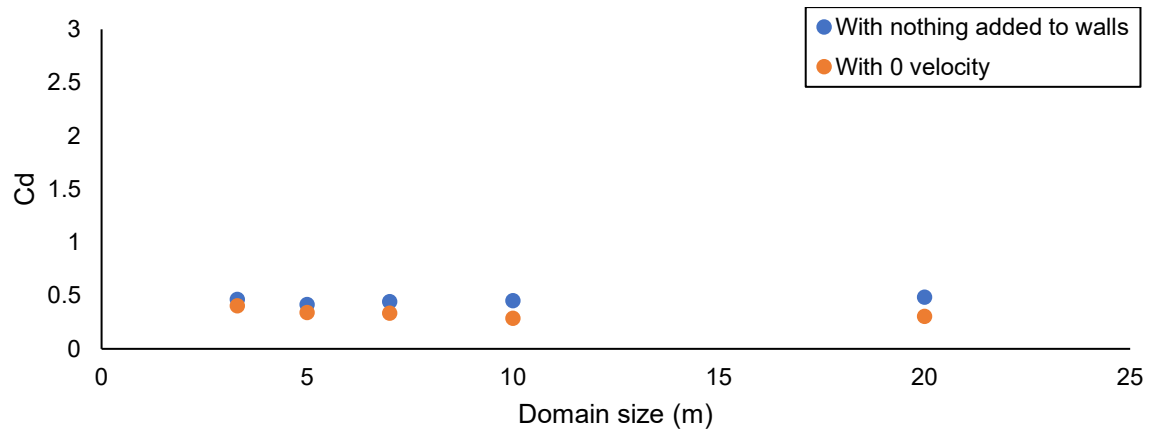


Figure 91: Domain size (m) vs. coefficient of drag (Cd) with and without walls set to velocity 0m/s for a sphere.

For the cylinder the test showed a lower coefficient of drag when 0 m/s in velocity was added to the domain sizes, and generally a stable coefficient of drag for all domain sizes (Figure 92). However, there was an instability observed at the smallest domain size (3.3m) showing an extremely high coefficient of drag of 2.39 when added 0 m/s in velocity to the walls of the domain (Figure 92), probably caused by the less space for the flow to act in the domain as seen in Figure 88. As the tests performed for parameters changed for the boundary conditions, it can be concluded there is no need for change/add boundary conditions of the walls.

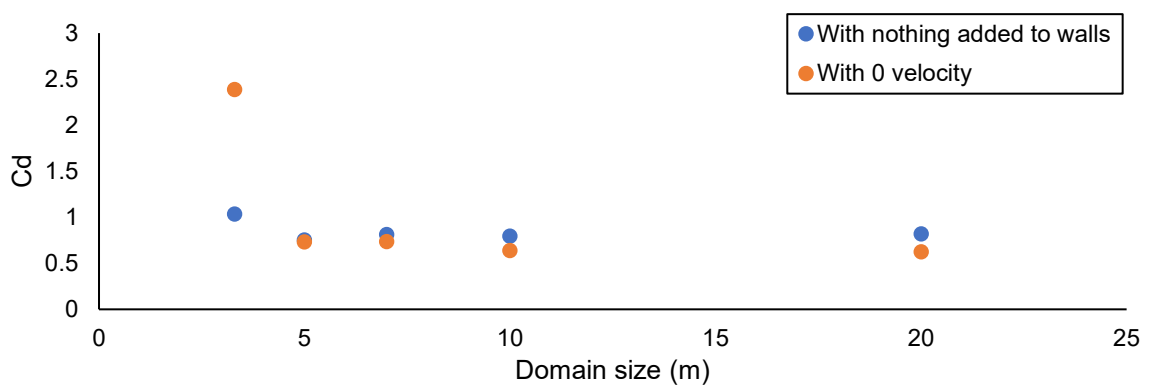


Figure 92: Domain size (m) vs. coefficient of drag (Cd) with and without walls set to velocity 0m/s for a cylinder.

4.2.2.3 Mesh size settings

4.2.2.3.1 Object mesh size

Mesh size of the sphere and cylinder was altered (mesh size ranging from 0.01m to 0.5m) to test if it influenced the coefficient of drag, computation time and flow velocity pattern. The shape of the flow velocity pattern was also observed to change with different mesh sizes (Figure 93 and Figure 95). Coefficient of drag and computation time also changed dramatically depending on mesh size (Figure 94 and Figure 96). The increase in computation time with mesh refinement was expected as the more refined the mesh the more elements to analyse, and the more time it takes for CFD to solve. Noticeably, the cylinder (Figure 96) took a lot longer to be solved at mesh size 0.01m compared to the sphere (Figure 94) probably caused by it being a larger object than the sphere having more elements to solve. At the finest option the coefficient of drag was about 0.47 for the sphere which is in accordance with theory (Vogel, 1989) and 0.75 for the cylinder which was lower than according to the theory being 0.82. Mesh sizes from 0.01 to 0.1m showed a linear increase in coefficient of drag for the sphere (Figure 94) and cylinder (Figure 96). This seems reasonable as the coarser a mesh gets the greater the roughness of the model is and thus it creates an increase in the drag coefficient. The closer the mesh size was to zero the closer the drag coefficient was to the theoretical value of the specific shapes (0.47 for a sphere and 0.82 for a cylinder). The mesh size tests therefore show how important it is to test mesh size every time a new model gets solved in CFD.

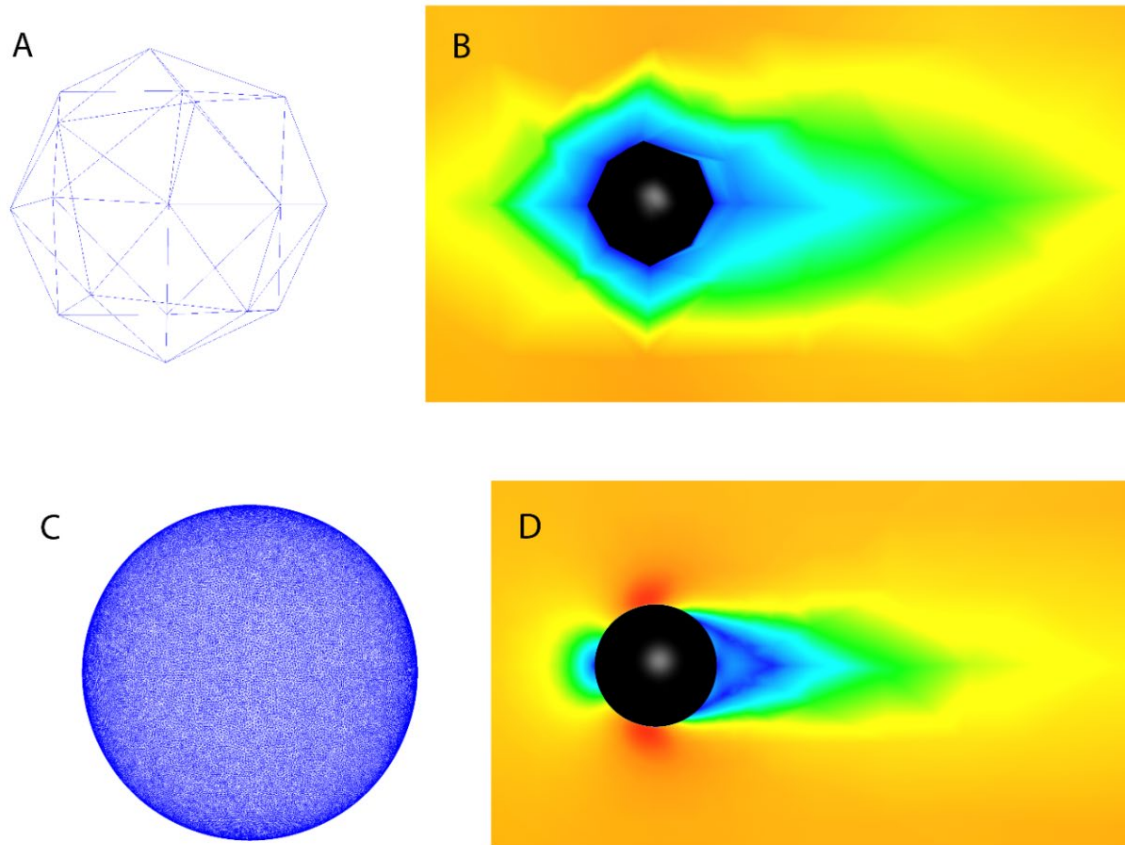


Figure 93: Change in mesh size of a sphere (A, C) causing differences in flow velocity patterns (B, D) (orange = 1m/s). A: sphere with mesh size of 0.5m. B: Flow velocity pattern using plane vertically cut through sphere with mesh size at 0.5m. C: Sphere in with mesh size of 0.01m. D: Flow velocity pattern using plane vertically cut through sphere with mesh size at 0.01m.

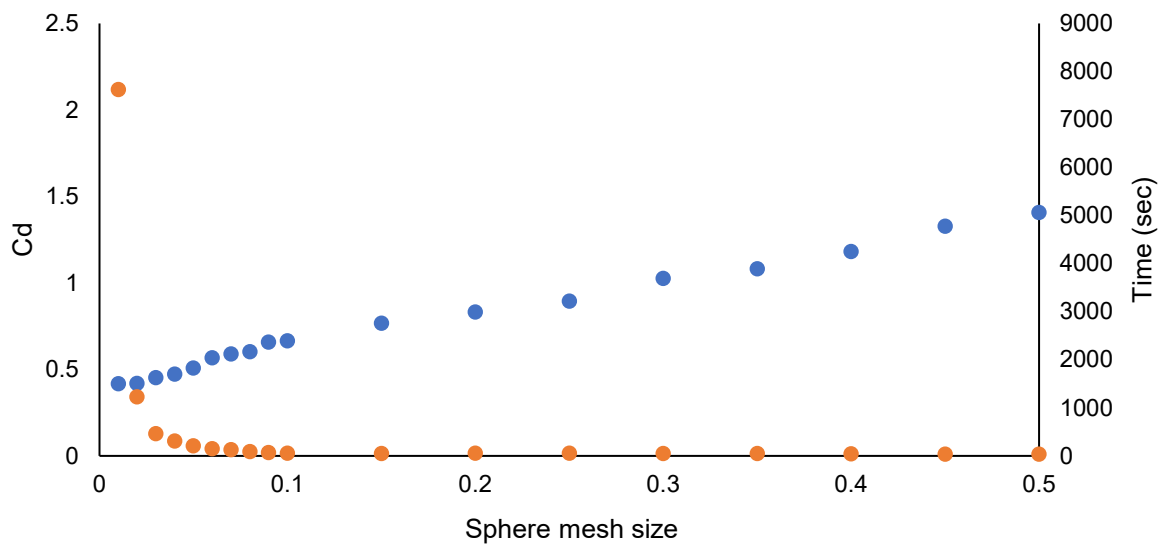


Figure 94: Mesh size (m) of the sphere vs. coefficient of drag (Cd) (blue) and computation time (sec) (orange).

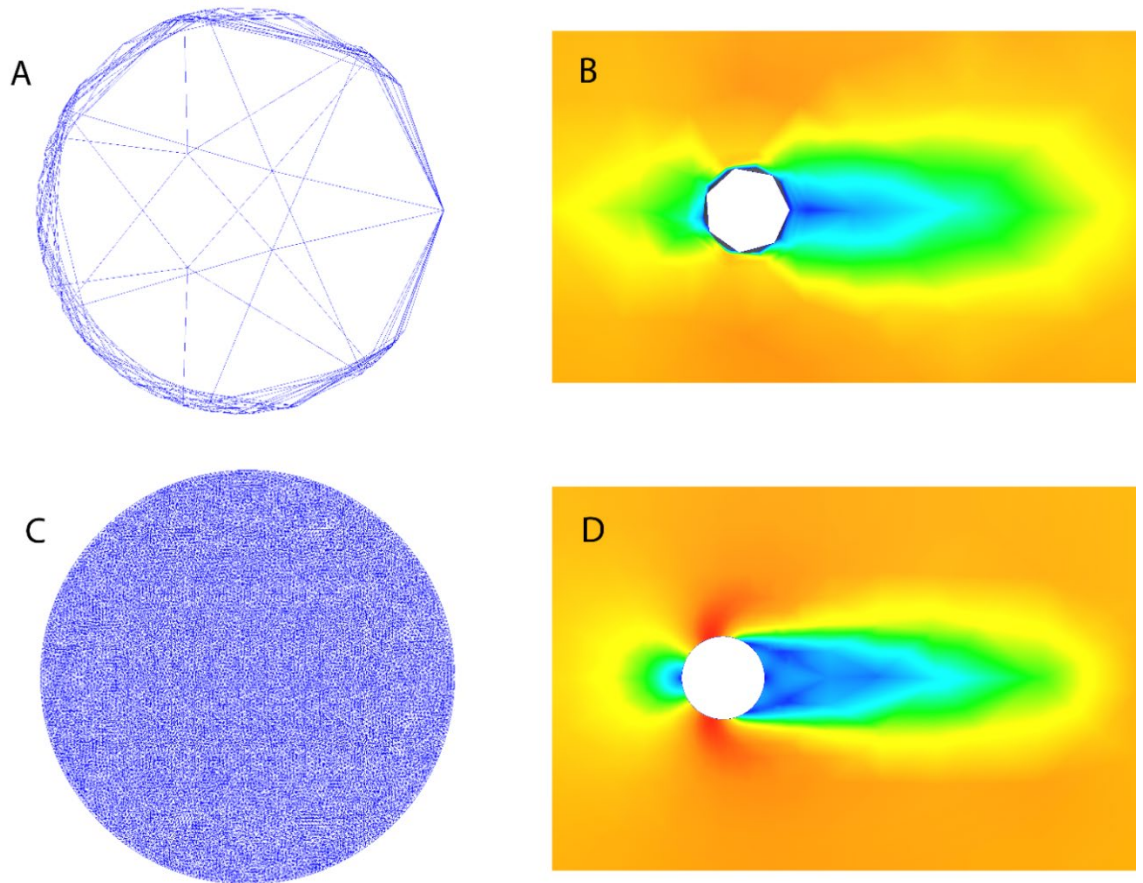


Figure 95: Change in mesh size of a cylinder (A, C) causing differences in flow velocity patterns (B, D) (orange = 1m/s). A: Cylinder in side view with mesh size of 0.5m. B: Flow velocity pattern using plane vertically cut through cylinder with mesh size at 0.5m. C: Cylinder in side view with mesh size of 0.01m. D: Flow velocity pattern using plane vertically cut through cylinder with mesh size at 0.01m.

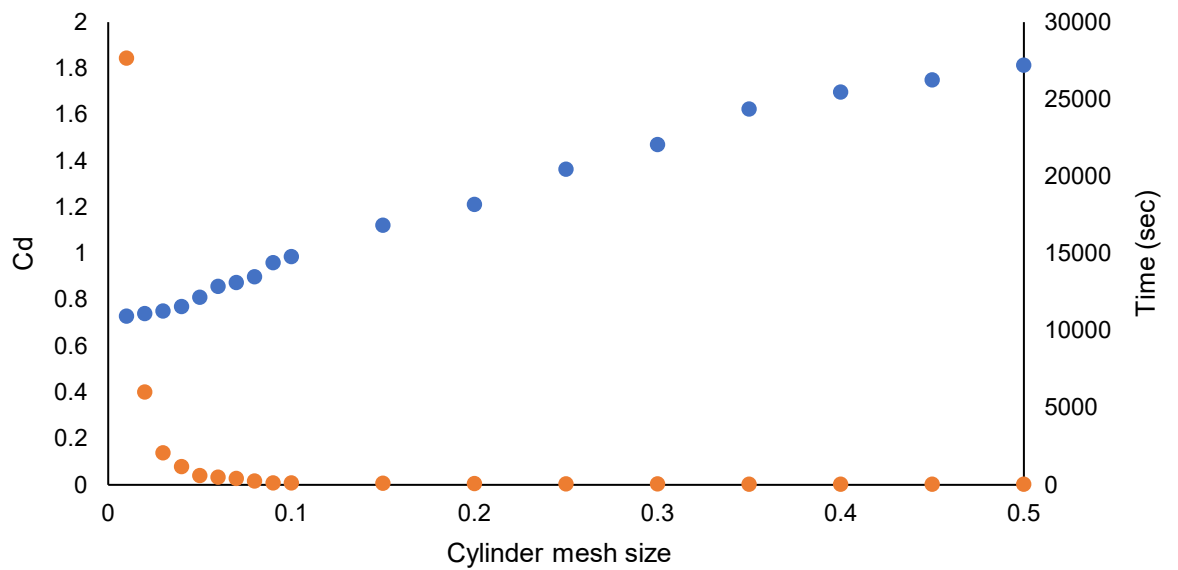


Figure 96: Mesh size (m) of the cylinder vs. coefficient of drag (Cd) (blue) and computation time (sec) (orange).

As an example, for mesh generating, the sphere (mesh size 0.05m) contained 32,239 nodes (20,109 fluid nodes and 12,130 solid nodes) and 146,977 elements in total. The cylinder (mesh size 0.05m) contained 105,462 nodes (47,031 fluid nodes and 58,431 solid nodes) and 494,105 elements in total. This indicated a clear difference in the mesh structure for the two objects just by looking at node and element counts, caused by the total volume of the cylinder being larger than the sphere's.

4.2.2.3.1 Domain mesh size

Testing the mesh size of the domain including a sphere showed stability from mesh size around 0.3-1.4m and around 0.2-2.0m for a cylinder (Figure 97). For the sphere a mesh size of less than 0.3m and above 1.4m was below and above the theoretical drag coefficient value of 0.47 for a sphere (Figure 97), and the stable mesh size was reached around a drag coefficient of 0.47 which was consistent with theory (Vogel, 1989). For the cylinder, only a slight decrease in drag was observed at a mesh size for the domain at 0.1m (Figure 97). The stable mesh size interval was around 0.82m which was consistent with theory (Vogel, 1989). This means that a domain mesh size of 1.0m is equally as good to use as a mesh size of 0.3m for a sphere, and 0.1m for a cylinder, eventually saving computational power and time.

The fact that the sphere was a smaller object in total compared to the cylinder, as the sphere had a volume of 10.99m^3 and the cylinder a volume of 3.14 m^3 could help explain the observed difference between domain mesh size and drag coefficient between the sphere and cylinder. Thus, the total volume would also be much bigger in the case of the cylinder, and thus a greater volume to add meshes to. If the objects were larger the domain mesh size and drag coefficient would increase proportionally. However, in terms of testing method and accuracy the approaches are according to the theory from Vogel (1989). Testing the domain mesh size showed the importance of exactly this issue when working with really small objects in CFD. However, the bigger the object the more even and stable the coefficient of drag becomes at most mesh sizes. We therefore need to take the mesh size of the domain into account when working in CFD. Recommended domain size would be at a minimum of five times and a maximum of ten times the length of the object.

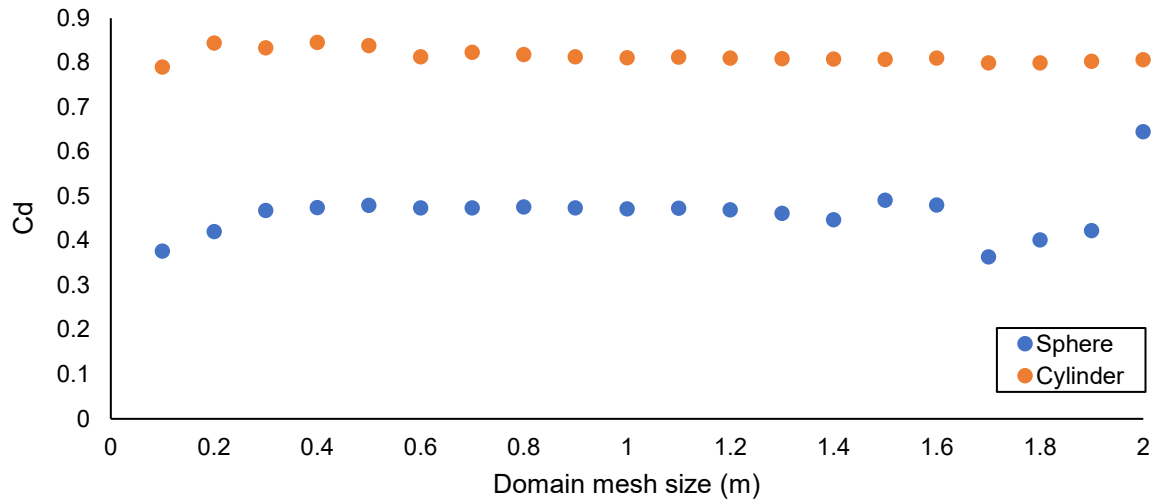


Figure 97: Mesh size (m) of the sphere and cylinder domain vs. coefficient of drag (Cd).

4.2.2.3.1 Region refinement mesh size

Region refinement was also tested against the drag coefficient, to know how the mesh refinement of the region would affect drag on a sphere and cylinder. The drag coefficient remained stable for all mesh sizes tested for both the sphere and the cylinder (Figure 98). Additionally, the mesh size was consistent with theory (Vogel, 1989) for both the sphere and cylinder. Therefore, a region refinement is recommended to include when working in CFD with objects that require high resolution of the flow velocity pattern, as it affects the final results if not included in the domain.

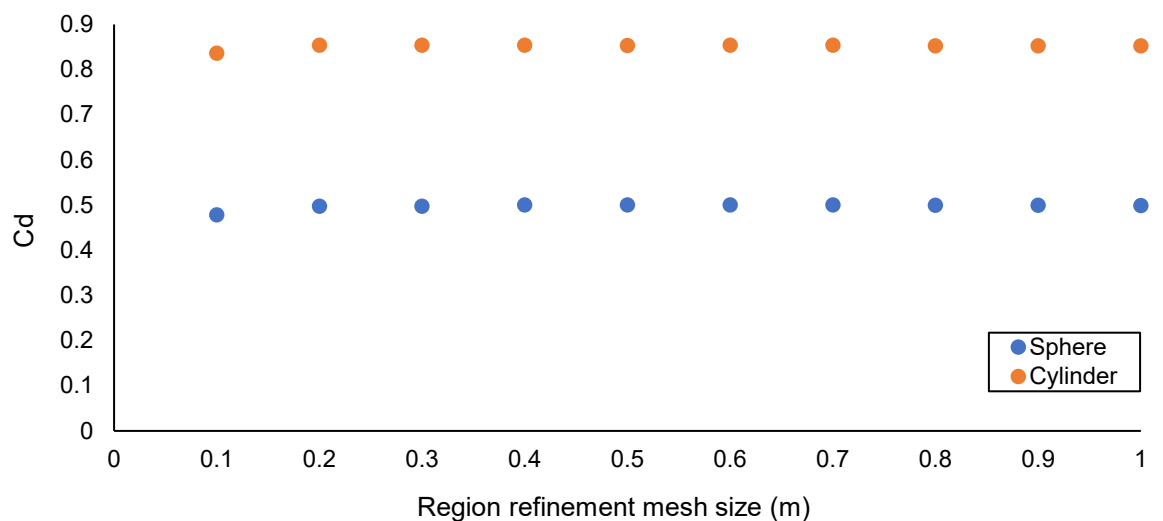


Figure 98: Region refinement mesh size (m) with sphere and cylinder inside vs. coefficient of drag (Cd).

4.2.2.3.1 Wall layers

The number of wall layers (see section ‘Mesh sizing’ in introduction) were also changed around the mesh of the sphere and cylinder to see if this parameter would change the drag coefficient. For both the sphere and the cylinder there was an increase in drag coefficient at 10 layers and above, and the drag coefficient was stable and consistent with theory (Vogel, 1989) at wall layers from 1-9 (Figure 99). Thus, it seems there is no reason to add to or reduce the default setting of three layers applied by the software, as it does not show an effect on the drag coefficient around the number of wall layers in the default setting.

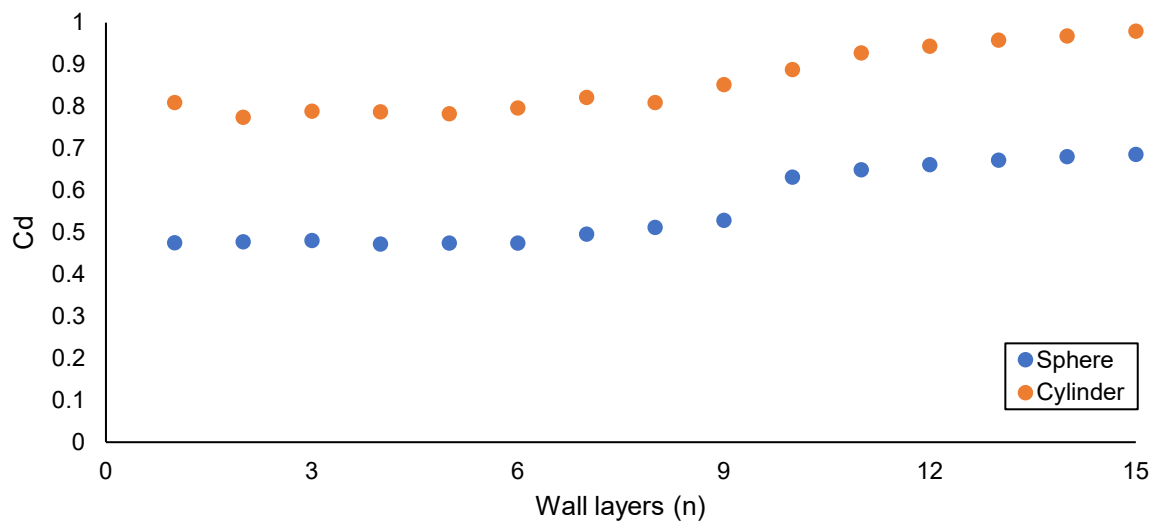


Figure 99: The number of wall layers (n) added to the mesh of the sphere and cylinder vs. coefficient of drag (Cd).

4.2.2.3.1 Layer factor

The layer factor for the wall layers was also tested against the drag coefficient. The coefficient of drag remained stable for both the sphere and cylinder, with the only exception at a layer factor of less than 0.1 for both the sphere and cylinder (Figure 100). Here the drag coefficient increased from 0.458 to 0.523 for the sphere and from 0.755 to 0.825 for the cylinder (Figure 100). Furthermore, the default setting applied by the software at layer factor 0.45 showed a drag coefficient consistent with theory for both the sphere and the cylinder. As the coefficient of drag only changed very little below a layer factor of 0.1 it was not enough to be taken into consideration for parameters needed adjusting for when doing CFD.

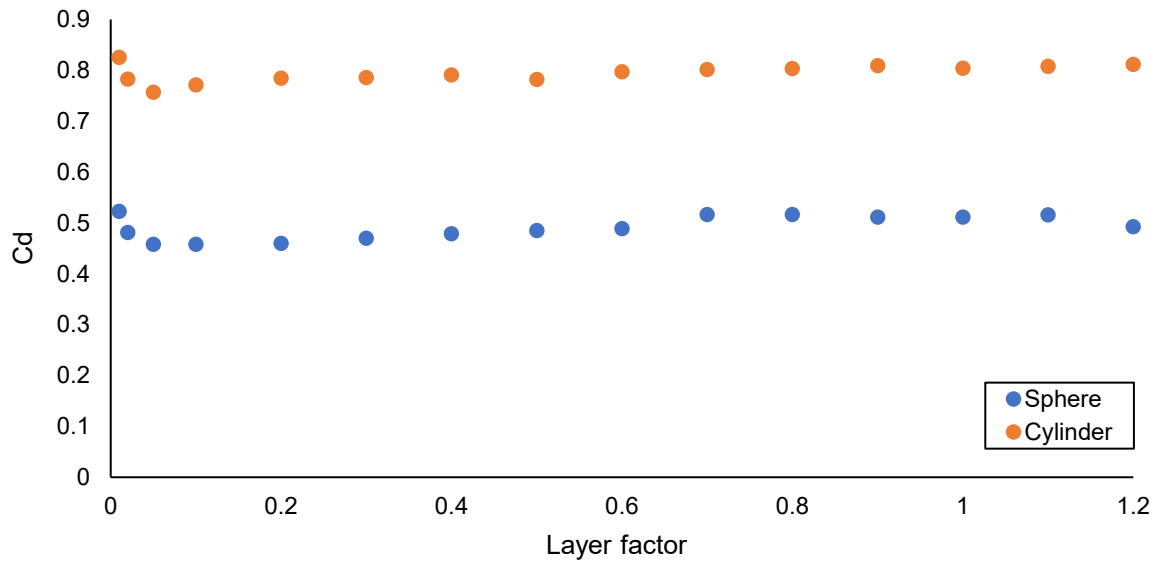


Figure 100: Layer factor for wall layers of a sphere and cylinder vs. coefficient of drag (Cd).

4.2.2.3.1 Layer gradation

As the default settings for the layer gradation for the wall layers is set to “auto” it was also important to look at how, and if, this parameter would change the drag coefficient accordingly. The layer gradation showed an insignificant effect on drag coefficient for the sphere and cylinder as the drag coefficient remained stable for all layer gradations tested (Figure 101). Thus, this parameter is not something which will be considered significant to the overall results using CFD, and there is therefore no reason to change the “auto” setting already applied in the software.

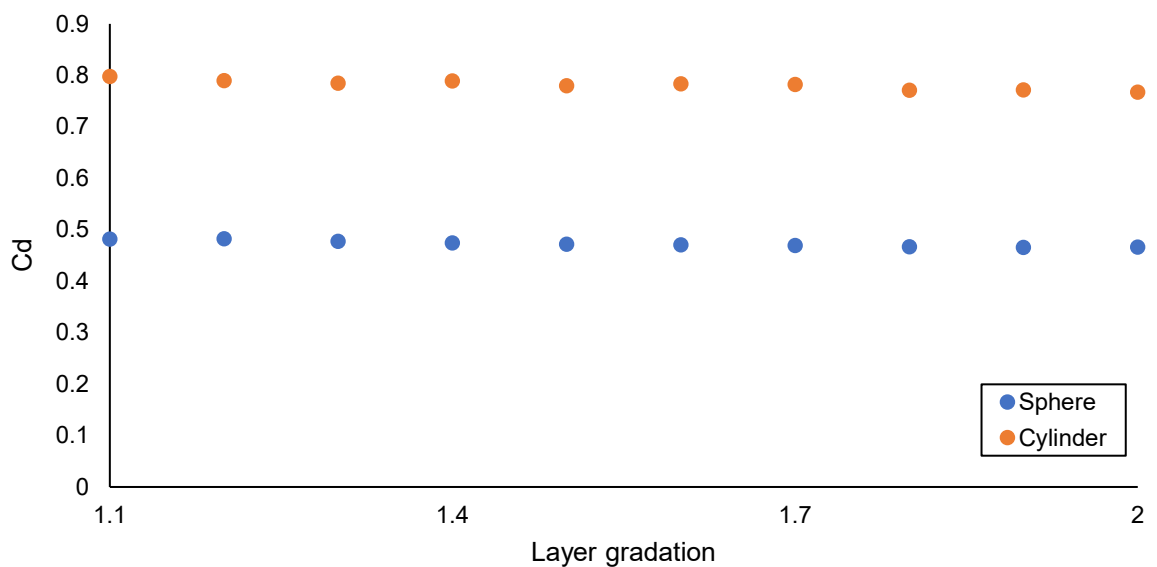


Figure 101: Layer gradation for wall layers of a sphere and cylinder vs. coefficient of drag (Cd).

4.2.2.4 Solve settings

A few solve settings were also tested on how they would affect the drag coefficient. Enabling adaptation with and without Free Shear Layers (FSL) was the first solve setting tested. Shear layers (see section 'Flow separation' in introduction) are the boundary layer around the solid object, in this case the sphere and cylinder. If we suspect strong velocity gradients will occur around the object (separation region) or in the wake of the object, it is good to test with FSL as we do not know beforehand if this is the case for our model.

The sphere and cylinder showed a stable drag coefficient with each cycle run when FSL were added to the sphere and cylinder compared to when FSL were not added (Figure 102). However, the drag coefficient increased at cycles 1 for both when FSL were added and not added to the cylinder compared to the rest of the cycles (Figure 102). Both with and without FSL showed the same drag coefficient at cycle one, as they started with the same conditions/settings for the first cycle. The results therefore indicate that there is no need to adjust the number of cycles solves, or even to enable adaptations, or add FSL. Although, this could be different for other objects, and thus important to test for when doing CFD in general.

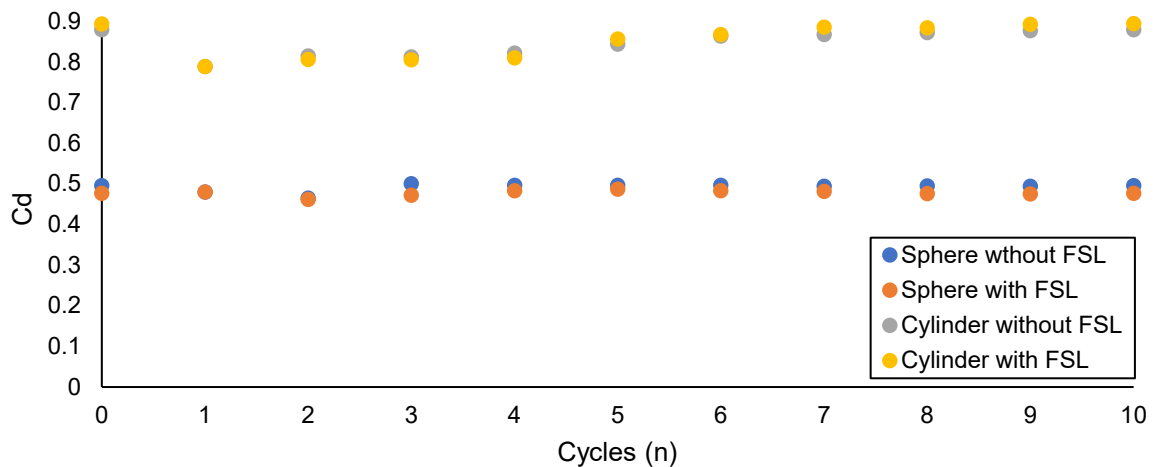


Figure 102: Number of cycles when enabling adaption, with and without free shear layers (FSL) for sphere and cylinder vs. coefficient of drag (Cd).

Testing the refinement limit with three and 10 cycles enabled, the sphere did not show a difference between the drag coefficient and cycles run, even when tested for a refinement limit of 0.00001 to the maximum possible in Autodesk Simulation CFD which is 1.0 (Figure 103). The cylinder did not show difference between the drag coefficient at all refinement limits, but did show a slightly lower coefficient of drag between the three and ten numbers of cycles, as the coefficient of drag was slightly lower with three cycles run compared with ten cycles run (Figure 103). With only three cycles run, the cylinder had a coefficient of drag

consistent with theory (Vogel, 1989) compared with ten cycles run. Therefore, this parameter is not important to adjust for when doing CFD as the default setting is 0.001 in refinement limit.

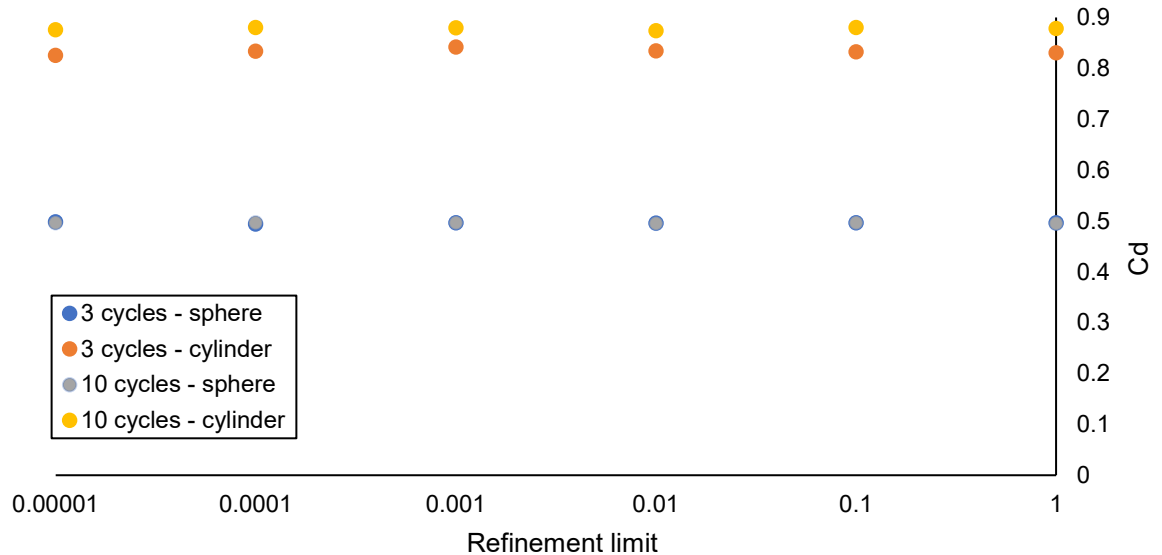


Figure 103: Refinement limit for sphere and cylinder vs. coefficient of drag (Cd).

To find the best turbulence model, the ten turbulence models proposed in Autodesk Simulation CFD were tested for a sphere and cylinder with two different mesh sizes (lowest mesh size possible for 0.03m for the cylinder, due to computer capacity) plotted against the drag coefficient. This test showed a great diversity in drag coefficients when using the different turbulence models (Figure 104 and Figure 105), as would be expected as they solve differently. The model closest to the theoretical drag coefficient value for a sphere was SST (Shear Stress Transport) k-omega for mesh size 0.05m, and RNG and Mixing length for mesh size 0.01m (Figure 104). For the cylinder the lowest mesh size possible was 0.03m, whereas this 0.01m for the sphere, all due to computational power. The model closest to the theoretical drag coefficient value of a cylinder was RNG for both mesh size 0.05m and 0.03m (Figure 105).

The best fitting models for the sphere were RNG and Mixing length for the mesh size of 0.01m as these two turbulence models are not for external flows, but rather for flow over a backward-facing step (RNG) and internal flow (mixing length). As would be expected the results for the mesh size of 0.05m had SST k-omega (for external flow) as best fit for the sphere. For the cylinder the results were different, as both mesh sizes had RNG as best turbulence model fit. Nevertheless, the k-epsilon (general purpose model) turbulence model was the subsequent best fit for the cylinder, so the results are not too far off of what would

be expected. Thus, it is of great importance to choose the right turbulence model from the recommended use (Table 10) as the results will change according to the object and environment used for the specific simulation.

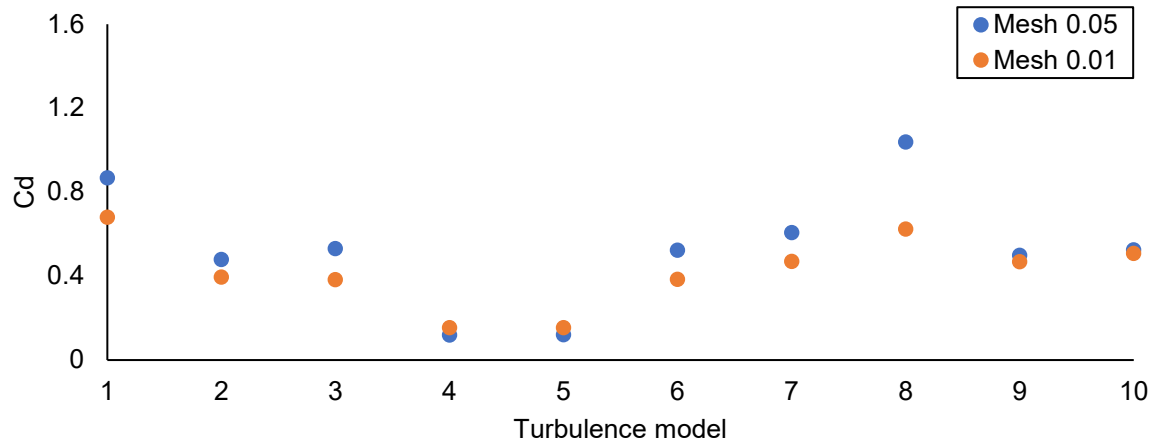


Figure 104: Sphere with a mesh size (m) of 0.01 and 0.05 applied to different turbulence models vs. coefficient of drag (Cd). 1 = k-epsilon, 2 = SST k-omega, 3 = SST k-omega SAS, 4 = SST k-omega RC (Smirnov-Menter), 5 = SST k-omega RC (Hellsten), 6 = SST k-omega DES, 7 = RNG, 8 = Low Re k-epsilon, 9 = Mixing length, 10 = Eddy Viscosity.

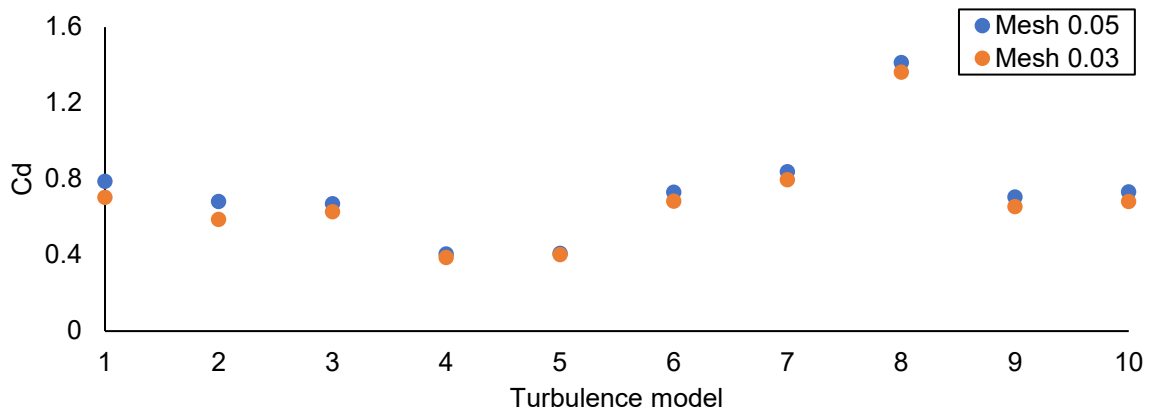


Figure 105: Cylinder with a mesh size (m) of 0.03 and 0.05 applied to different turbulence models vs. coefficient of drag (Cd). 1 = k-epsilon, 2 = SST k-omega, 3 = SST k-omega SAS, 4 = SST k-omega RC (Smirnov-Menter), 5 = SST k-omega RC (Hellsten), 6 = SST k-omega DES, 7 = RNG, 8 = Low Re k-epsilon, 9 = Mixing length, 10 = Eddy Viscosity.

To find the turbulence model that gave the closest fit to the theoretical drag coefficients over a range of Reynolds numbers a comparison the different turbulence models was performed for a sphere and cylinder. This test showed that none of the models were completely consistent with the theory for either the sphere nor the cylinder (Vogel, 1989). However, the models closest resembling the theory proposed by Vogel for the sphere were Low Re k-epsilon at $Re = 1 - 50,000$, and SST k-omega, SST k-omega DES and Mixing length at Re

= 100 – 50,000 (Figure 106). For the cylinder the models closest were SST k-omega, SST k-omega DES, Low k-epsilon, and Mixing length at Re = 50 – 5,000, and Low k-epsilon at Re = 5,000 – 500,000 (Figure 107). As the testing of a sphere and cylinder showed no turbulence model consistent with theory tells us that CFD will never be completely according to the theory, as theory does not take all the different variables into account that is applied by CFD. Depending on the Reynolds number of the object and type of object and domain (internal or external flows) specific turbulence models will be more suitable to use than others. For instance, high Reynolds numbers that use external aerodynamic flows the SST k-omega DES is recommended to use because aerodynamics are used for high speeds, whereas with pipe flows Low Re k-epsilon is recommended to use for Reynolds number between 1500 and 5000 because it looks at the transition between laminar and turbulent flow (see Table 10). Therefore, it is always important to determine the most suitable turbulence model for the specific problem before solving by looking at specifics and recommendations for the individual turbulence models.

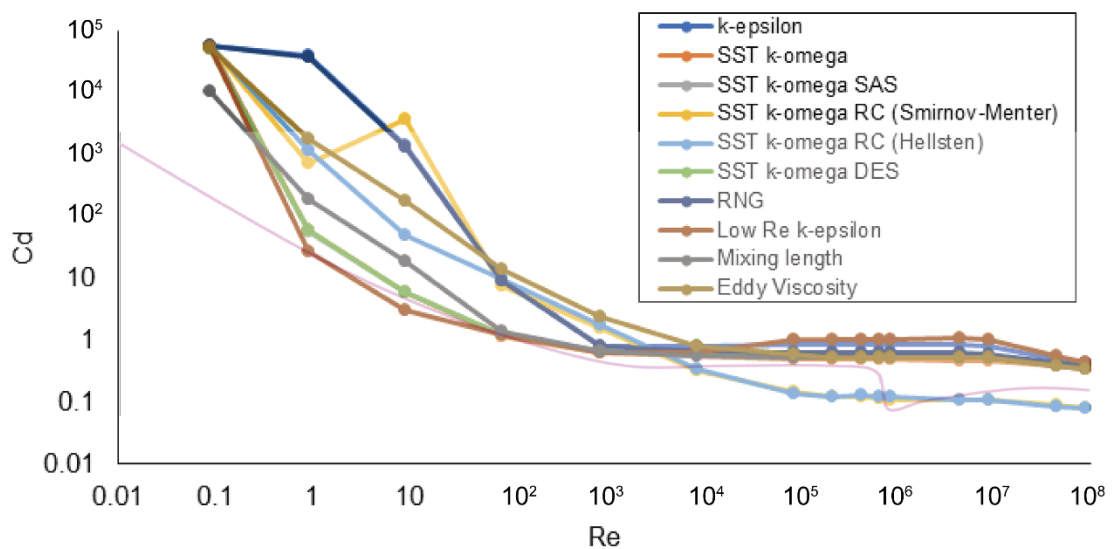
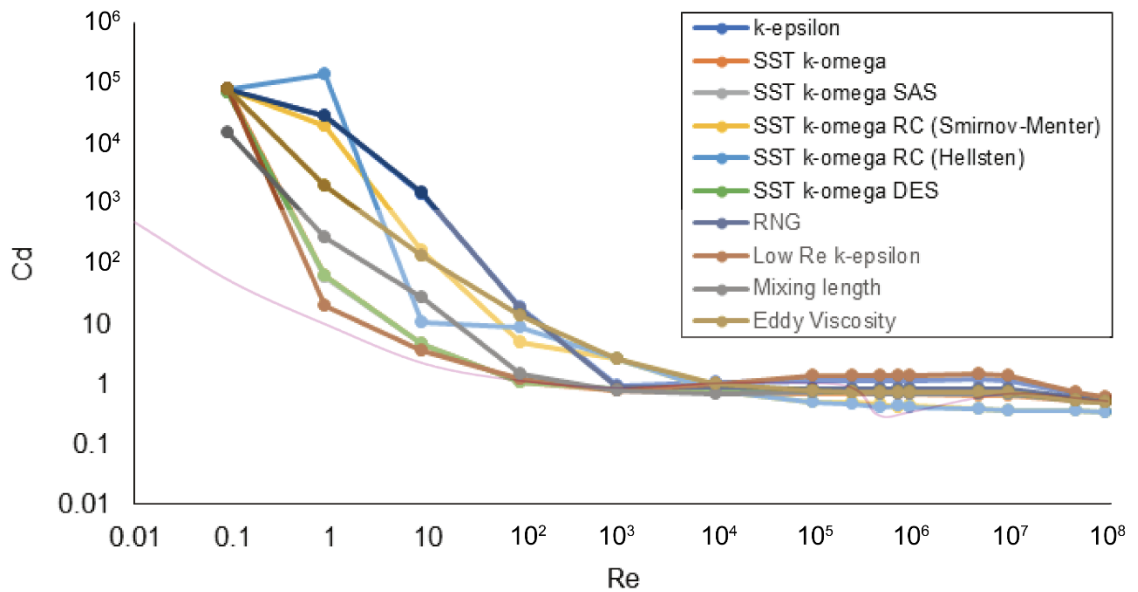


Figure 106: Turbulence models for a sphere applied at different Reynolds numbers vs. coefficient of drag (Cd). Theoretical curve indicated by pink line.



**Figure 107: Turbulence models for a cylinder at different Reynolds numbers vs. coefficient of drag (Cd).
Theoretical curve indicated by pink line.**

4.2.2.5 Cd vs. Re

As a final test, a sphere and cylinder were analysed at different Reynolds numbers to see how the drag coefficient would be affected, and to test whether the model of the sphere and cylinder would show coefficient of drag consistent to theory, if all previously tested parameters and their results of best fit were applied. The specific parameters for this test were as follows:

Assigned velocity as inlet

Zero pressure as outlet

Domain mesh size of 1m

Domain size of 15m

Object mesh size of 0.04m for the sphere and 0.05m for the cylinder

This test showed a fairly close correlation with theory for the sphere and the cylinder (Figure 108) at $Re > 1$. However, the lowering in drag coefficient which was expected to occur at critical Re (500,000) were absent for the sphere and cylinder and could be a case of calculation error in this software. However, the missing drop in drag coefficient is not important for the overall understanding of CFD and testing its settings in this chapter. The reason being the plesiosaur models used in later chapters have Reynolds numbers higher than the critical Re range and we therefore do not rely on the data in the critical Re range. For a plesiosaur model to be in the critical Re range it would have to be below 0.55m in total

length, which is the size of a juvenile plesiosaur and far smaller than any adult plesiosaur species known. The plesiosaur models used in later chapters are thus in the good-fit range.

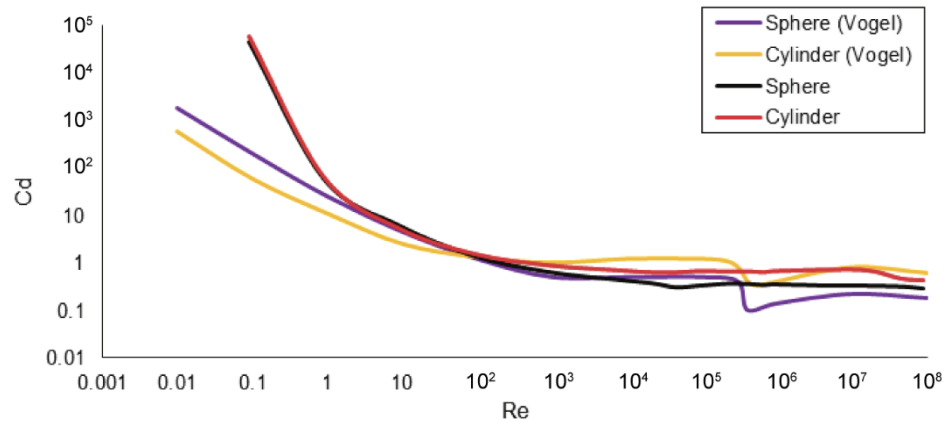


Figure 108: Reynolds numbers (Re) vs. coefficient of drag (Cd) for a sphere and cylinder, with theoretical values from Vogel (1989).

From the literature we already know that flow past a circular cylinder is associated with flow separation, turbulence transition, reattachment of flow and further turbulent separation of the boundary layer at critical Reynolds numbers (e.g. Rodríguez *et al.*, 2013a; Rodríguez *et al.*, 2013b; Lehmkuhl *et al.*, 2014). However, this instability is generally not observed in the results from this chapter as all tests comparing coefficient of drag with Reynolds numbers are missing the drop in Cd at the Re range $10^5 - 10^6$, which is the range of critical Reynolds numbers. However, as this is not crucial for this chapter it is not something worth going into further detail with. For upcoming chapters on plesiosaurs analysed in CFD the models are at a Reynolds number in the turbulence range ($Re < 10^6$). This is due to the size of the plesiosaur models as they will be modelled as life-sized giving a longer characteristic length creating a higher Re compared with the sphere and cylinder used in the current chapter. Thus, for later chapters we therefore do not need to test the coefficient of drag at Reynolds numbers in the laminar or critical Reynolds number region.

4.3 Conclusions

Turbulent flow around bodies such as a sphere or cylinder has long been of great interest for understanding fundamental fluid mechanics problems (Hoerner, 1965). In the use of computational fluid dynamics (CFD) simulations the setup and various parameters (e.g. mesh size and domain size) needs to be adjusted for every 3D model as CFD is used for various purposes depending on what problem needs solving.

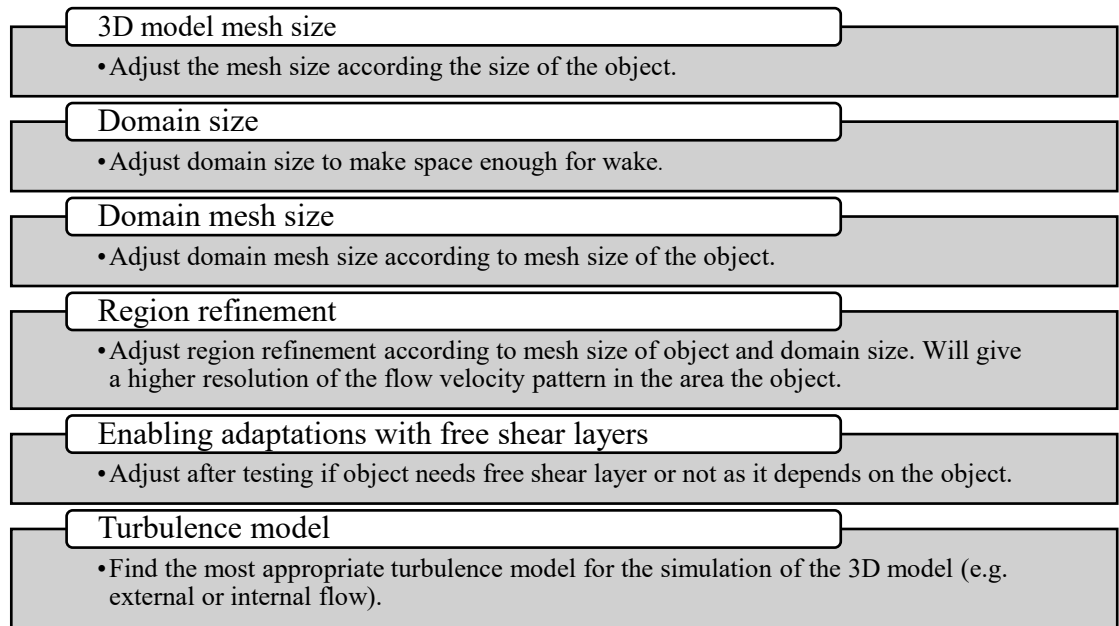


Figure 109: Variables to test in CFD.

Figure 109 shows the variables found by validation experiments for this chapter that have to be tested in order to find the best solution giving a better estimate of drag and resolution of the flow velocity pattern, and is a good way to start when doing a simulation in CFD using an unfamiliar object.

Mesh size will need to be altered per model as plesiosaurs all are far more complex, and thus will have a completely different mesh in comparison to the sphere and cylinder tested in this chapter. This can be tested by using a wide range of mesh sizes and observe where the drag force converges. The domain size also needs adjusting as the rule of thumb is to have a domain size of at least five times the object/model size to avoid edge effects. Furthermore, the mesh size of the domain will additionally have to change with domain size. Slip/symmetry boundary condition is not needed, but a region refinement around the object is. Finally, from testing differences in turbulence models in this chapter we now know to use either k-epsilon or SST k-omega in the CFD work on plesiosaurs models in proceeding chapters as these models are useful for doing simulations with external flows.

Chapter 5 – The hydrodynamic implications of neck elongation and thickness in plesiosaur necks

5.1 Introduction

For nearly 200 years (Conybeare, 1824), illustrations and restorations of plesiosaur necks have been subject of imaginative reconstructions of what these animals might have looked like during life, and how their necks would have functioned (Rudwick, 2008). The reason for the long neck in plesiosaurs is not well understood. What are the implications for such a long neck during forward swimming? Previous studies have mainly focused on swimming speeds or flipper locomotion. The selective pressures driving the evolution of ever longer necks are unclear, with several hypotheses regarding functional adaptations for feeding strategies being proposed (Taylor, 1981; Callaway and Nicholls, 1997; McHenry *et al.*, 2005; Zammit *et al.*, 2008; Wilkinson and Ruxton, 2012; Noè *et al.*, 2017).

5.1.1 Soft tissue in plesiosaurs

Soft tissue reconstruction of fossil organisms is clearly of importance when making palaeobiological inferences, particularly concerning the ecology and lifestyle of extinct animals (Witmer, 1995). This is difficult as three-dimensional soft tissue preservation is extremely rare in the vertebrate fossil record. While there have been many ichthyosaurs preserved with carbonaceous skin outlines (Martin *et al.*, 1986), the same is not the case for plesiosaurs. This may be due to the minimal number of plesiosaurs found compared to ichthyosaurs, or maybe ichthyosaurs had a much higher chance of ending up in an anoxic sediment.

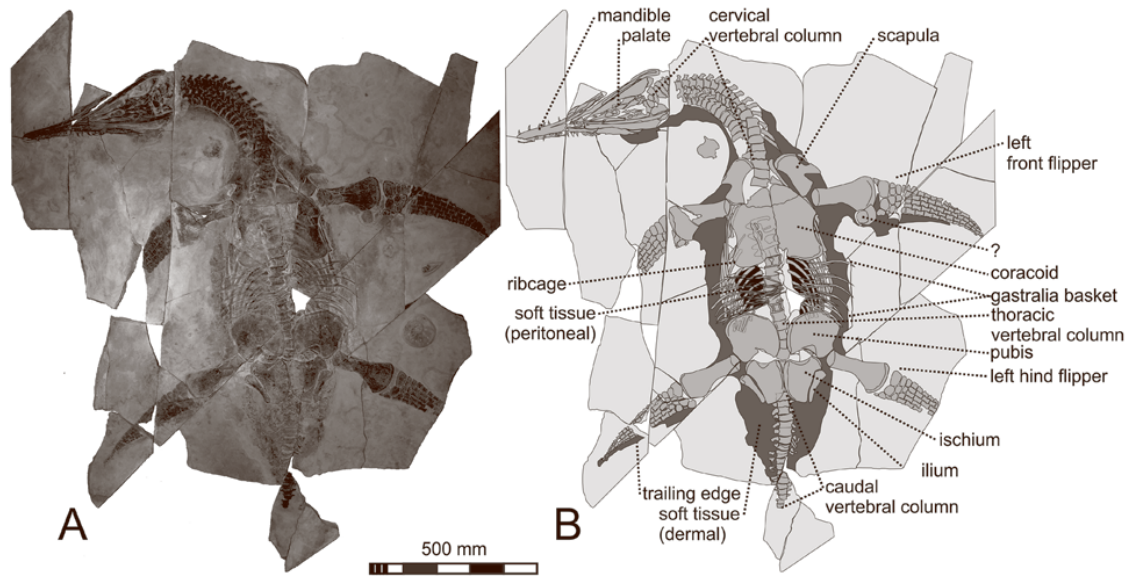


Figure 110: Soft tissue preservation of the short-necked plesiosaur *Mauriciosaurus fernandezi* preserved in ventral view. A) Photograph of the specimen after preservation, and B) interpretation line drawing. From Frey et al. (2017).

Nevertheless, two plesiosaur specimens possessing diverse neck lengths have been discovered with what has been interpreted as preserved soft tissue (Frey *et al.*, 2017; Vincent *et al.*, 2017a). The short-necked plesiosaur described by Frey et al. (2017) is preserved in ventral view and shows subdermal dorsal skin tissue, especially in the caudal region and between the ribs (Figure 110). Additionally, the long-necked plesiosaur described by Vincent et al. (2017a) is preserved in lateral view and includes dark-coloured structures of different material around the neck (Figure 111), hind flippers and tail. The structures identified as soft tissue around the neck extend ca. 2-3cm from the cervical vertebrae, indicating a thicker neck of about 4 cm longer in diameter compared with the specimen described by Frey et al. (2017).

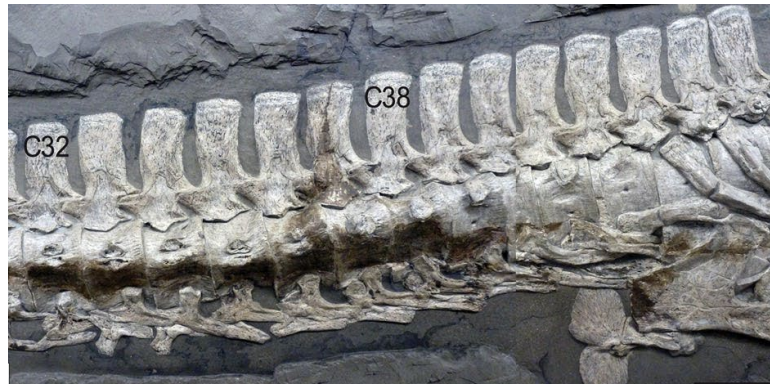


Figure 111: Soft tissue preservation surrounding the posterior neck vertebrae in the long-necked plesiosaur specimen SMNS 51945, preserved in lateral view. Here the soft tissue is indicated by the dark structures at the top and bottom of the neck vertebrae. Scale bar = 5 cm. Abbreviations: C32 = cervical vertebra 32; C38 = cervical vertebra 38. Modified from Vincent *et al.* (2017a).

5.1.2 Hydrodynamics

Hydrodynamics is the study of moving fluids that are practically incompressible, and in the context of swimming performance has been explored for various aquatic taxa including extant marine mammals (Fish and Rohr, 1999; Fish *et al.*, 2008; Segre *et al.*, 2016), extant and extinct fish (Lauder and Madden, 2006; Borazjani and Sotiropoulos, 2010; Fletcher *et al.*, 2014; Van Wassenbergh *et al.*, 2014; Kogan *et al.*, 2015; Van Wassenbergh *et al.*, 2015; Fish and Lauder, 2017), ichthyosaurs (Gutarra *et al.*, 2019), and leatherback turtles (Dudley *et al.*, 2014).

Hence, streamlined aquatic animals, such as fish, sea lions and cetaceans experience low pressure drag, making them well adapted for moving through water (Feldkamp, 1987; Fish and Rohr, 1999; Fletcher *et al.*, 2014). As extant fully aquatic animals do not exhibit long necks, we are lacking a good living model for plesiosaur hydrodynamics. Several studies have explored and discussed the possible swimming ability and speed of plesiosaurs (Conybeare, 1824; Hutchinson, 1893; Andrews, 1910; Watson, 1924; Shuler, 1950; Taylor, 1981; Massare, 1988, 1994; Halstead, 1989; Bakker, 1993; O'Keefe, 2001b; Motani, 2002; Henderson, 2006; Long *et al.*, 2006; Carpenter *et al.*, 2010; DeBlois, 2013; Liu *et al.*, 2015; Muscutt *et al.*, 2017). However, none of the previous studies have focused specifically on the locomotory implications of the neck, instead tending to focus on flippers and manoeuvrability thereof.

5.1.3 Computational Fluid Dynamics

The governing equations, namely continuity and Navier-Stokes, relate velocity components and pressure of fluid flow. The system of equations is highly coupled and nonlinear, making

analytical (exact) solutions of the governing equations difficult. In fact, the exact solutions are available only for a very few laminar flows in simple geometries. The rise of fast computers has allowed these equations to be extensively used in simulations in an engineering context. CFD requires information on size, speed, and shape of an object to create a simulation that can help identify how the flow of a fluid responds to said object (Versteeg and Malalasekera, 1995).

This chapter aims to explore hydrodynamic changes associated with variations in neck length and thickness in plesiosaurs. First, it was asked if longer necks affected overall drag of plesiosaurs during forward motion relative to shorter necks. Secondly, the idea that drag might be altered by a thicker neck compared to a thinner neck was addressed. Finally, an evaluation was made of how the answers to the above questions affect existing hypotheses of what the neck was used for.

5.2 Materials and methods

Two overall experimental scenarios were simulated by changing 1) plesiosaur neck lengths, and 2) plesiosaur neck thicknesses using idealized plesiosaur models. Both experiments were performed with the same overall approach; creating a 3D model in Autodesk Maya and then using that model as part of a simulation in Autodesk Simulation CFD (www.autodesk.com).

5.2.1 Selected plesiosaur species

The CFD simulations involved creating idealised plesiosaur models around which to simulate flow. By idealised it means a model taking the general form of a real-life plesiosaur model concerning body outline and volume. In order to simulate the three neck lengths, three plesiosaur species were chosen as a basis for neck proportions. Total body length for the species chosen included the distance from the tip of skull to the end of tail. For the long-necked model, *Albertonectes vanderveldei* (73.5 Ma) was chosen as it is the plesiosaur with the longest neck found to date (7 m neck and 11 m in total: Kubo *et al.*, 2012), *Muraenosaurus leedsii* (162 Ma) was used for the intermediate-necked model (2.5 m neck and 6 m in total: Andrews, 1910), and *Meyerasaurus victor* (182 Ma) for the short-necked model (0.7 m neck and 3.35 m in total: Smith and Vincent, 2010). As these three species have very different neck lengths, and are from three different plesiosaur families (elasmosaurids, cryptoclidids, and rhomaleosaurids, respectively), they provide a range of plesiosaur morphologies to model.

5.2.2 Modelling the plesiosaur

The first 3D model was created based on *Me. victor* (see Figure 112A-B) and then the neck was scaled in length to match the neck:body ratios of *Mu. leedsii* and *A. vanderveldei*. All models had identical frontal area (the area when cutting through the neck at the base). The percentage of neck length of the total body length was 21 % for the short-necked, 42 % for the intermediate-necked, and 64 % for the long-necked plesiosaur model. The intermediate-necked plesiosaur model was used as a template for the thick- and thin-necked plesiosaur simulations.

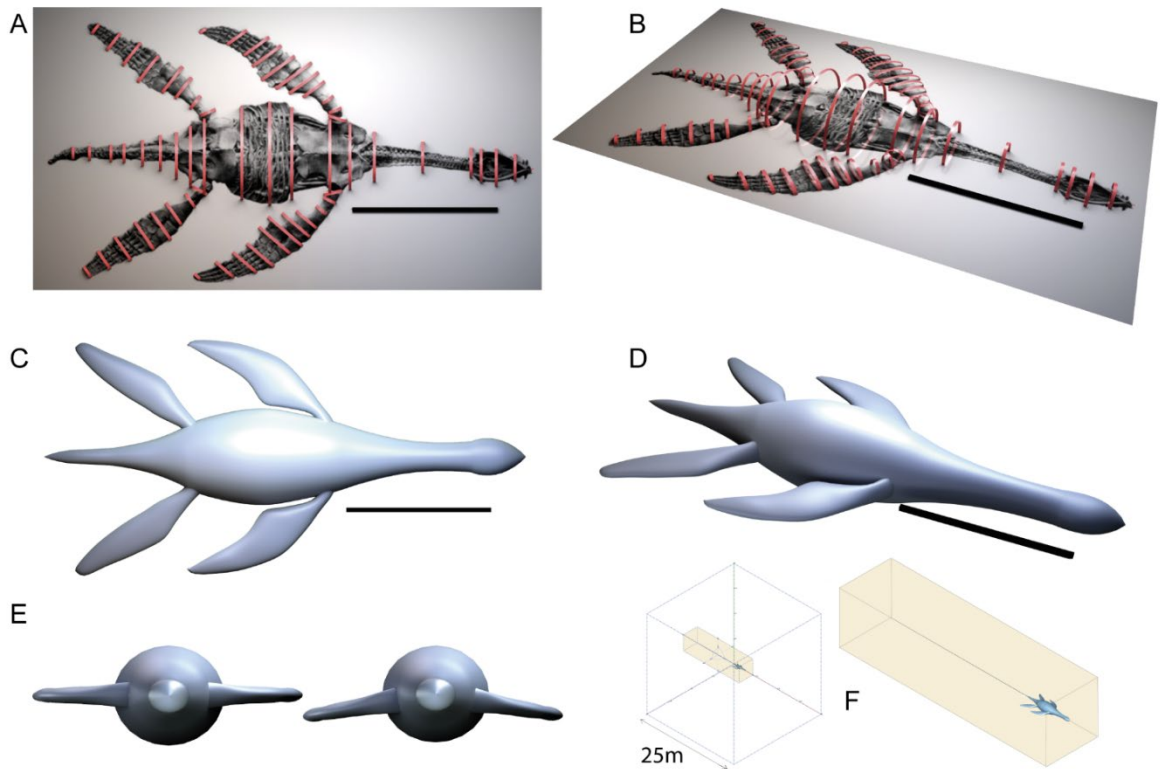


Figure 112: Dorsal (A) and isometric oblique (B) view of the plesiosaur model constructed using NURBs circles around photograph from Smith and Vincent (2010). Dorsal (C) and isometric (D) view of closed body cavities surfaces were then generated by ‘lofting’ a continuous surface through consecutive NURBs circles to produce discrete body volumes for each segment. Frontal view lofted plesiosaur model showing even flippers and at 10° angle from centre of body (E). Full computational domain including refined region (yellow) (F). Scale bar representing 1 meter.

To create the plesiosaur base model a ventral view (Figure 112A-B) of the short-necked plesiosaur species (Smith and Vincent, 2010) was imported into Autodesk Maya. The image was scaled accordingly and used as a basis for modelling the 3D plesiosaur. First, the body was formed using Non-Uniform Rational Basis Spline (NURBs) circles created along the length of the plesiosaur and scaled accordingly in the parts of the plesiosaur body changing in size (Figure 112A-B). All circles were selected and lofted to form a solid volume (Figure

112C-D), a method previously employed by Bates et al. (2009a; 2009b; 2012) and Hutchinson et al. (2011) on dinosaurs. NURBs are used when working with highly flexible shape modelling formats and can be used to produce anything from simple 2D geometry shapes (e.g. parabolic curves, circles, and ellipses) to complex 3D free-form curves (Bates et al., 2009b). In Autodesk Maya, cubic interpolation was used to loft between the circles to ensure smoothness to the transition of each circle resulting surface. To make the model watertight, the anterior- and posterior-most parts were ‘capped’ with two tiny (i.e. not visible) planar end surfaces. The flippers were formed using the same approach but with ellipsoids instead of circles, with additional rotation to the ellipsoids to place them correctly relative to the body of the plesiosaur. Flippers were built on one side of the plesiosaur then duplicated and mirrored for the opposite side. The model was then straightened by aligning the NURBs circles forming the neck, body, and tail to the Y-axis. The flippers were rotated 10° down from the horizontal plane (Figure 112E).

For the intermediate- and long-necked plesiosaur models the neck part of the short-necked model was extended according to the neck/body ratio above. For the thick-necked plesiosaur model, the NURBs circle at the base of the neck was increased in size until it equalled the most anterior body circle, creating a smooth transition. This increase in circle size, 343 % cervical radius, was then applied to the NURBs circles making up the rest of the neck. Conversely, the thin neck was produced by shrinking the NURBs circles making up the neck until they touched the outlines of the cervical vertebrae (i.e. each NURBs circle diameter was equal to 100 % cervical radius). All models were exported as IGES surface files.

5.2.3 Computational fluid dynamics simulations

The 3D models were individually imported to Autodesk Simulation CFD (version 2017) where the simulations of water flow around the plesiosaur models were undertaken. Simulations were based on the RANS approach using the turbulence model k-epsilon (cf. Chapter 4). The external boundaries of the computational domain over which the governing equations are solved consisted of a 25m cube with one face in front of the plesiosaur model defined as an inlet, where water velocity was specified in m/s. The opposite face of the cubic domain, located posterior to the plesiosaur, was defined as an outlet boundary condition (zero pressure gradient across the boundary). Mesh and domain independence studies have been undertaken to determine the appropriate mesh size and computational domain of the models (cf. Chapter 4). As a result, the mesh size and domain were set to 0.01m and 1.0m, respectively. A cuboid region of refinement with mesh size of 0.5m was applied to the

computational domain surrounding the plesiosaur model in order to capture the wake, resulting from the relative motions of fluid and plesiosaur (Figure 112F).

In all cases, 3D incompressible water flow was simulated with the plesiosaur models held stationary. Fluid type (for the domain) was set as seawater, as it matches the material of the domain for the plesiosaur. The density of seawater is 1021.2kg/m^3 and the viscosity is $0.0011404\text{ Pa}\cdot\text{s}$. Solid type was set as glass as it closely matched a smooth surface to exclude the surface variable from the scenario, and its density was 2700 kg/m^3 . This is computationally simpler than moving the animal through a stationary fluid; however, the physics is effectively identical. Flow-stream velocities of 1, 3, 5, 7 and 10 m/s were simulated for all five plesiosaur models. The velocities were chosen because the swimming speeds of long-necked plesiosaurs have been proposed to be within this range depending on when the plesiosaur would use its sustained swimming speed (2.17-2.51 m/s in Massare, 1988, and 3.8-4.0 m/s in Massare, 1994). Note that Massare (1988) suggested these calculated speeds were likely too high – hence the use of speeds lower than 4.0 m/s. Furthermore, velocities up to 10 m/s were chosen as to see how/if flow velocity patterns and the drag coefficient would change dramatically at this point. In addition, data for modern cetaceans also suggest speeds towards the lower end of the range. For example, speeds of 2.2 – 2.8 m/s are typical for small dolphins like the common dolphin *Delphinus delphis* although Killer whales *Orcinus orca* (that in terms of body size could be comparable to plesiosaurs) have sprint speeds in excess of 8.3 m/s (Wilson and Mittermeier, 2014). The results were visualised as two-dimensional cross sections of flow velocity magnitude, and in isometric view with flow streamlines (cylinders). The drag force was calculated by Autodesk Simulation CFD to quantify flow around the digital reconstructions of plesiosaurs, and drag coefficients were manually calculated using the frontal area of the plesiosaur models.

The Reynolds numbers used in this study were in the turbulent flow range (see introduction from Chapter 4). Consequently, based on pre-studies (see validation experiments from Chapter 4) the turbulence model k-epsilon was used on reference shapes of a sphere and cylinder model to allow comparison with data from Vogel (1989).

5.3 Results

Visually the simulations showed the flow velocity following the hydrodynamic body of the plesiosaur models (Figure 113A-E: left) with areas of low velocity in the parts behind the flippers and tail regions (Figure 113A-E: right). Additionally, areas of low velocity were observed around the neck for especially the long-necked model (Figure 113E: middle). In the rest of the models the low velocity area in the neck region was only detectable on the lateral sides of the neck. The thin-necked model showed a strong difference in water pressure towards the frontal part of the flippers (up to 200 pa) and less pressure around the head (down to 100 pa) compared with the thick-necked model (Figure 113F) caused by the hydrodynamic body of the thick-necked model.

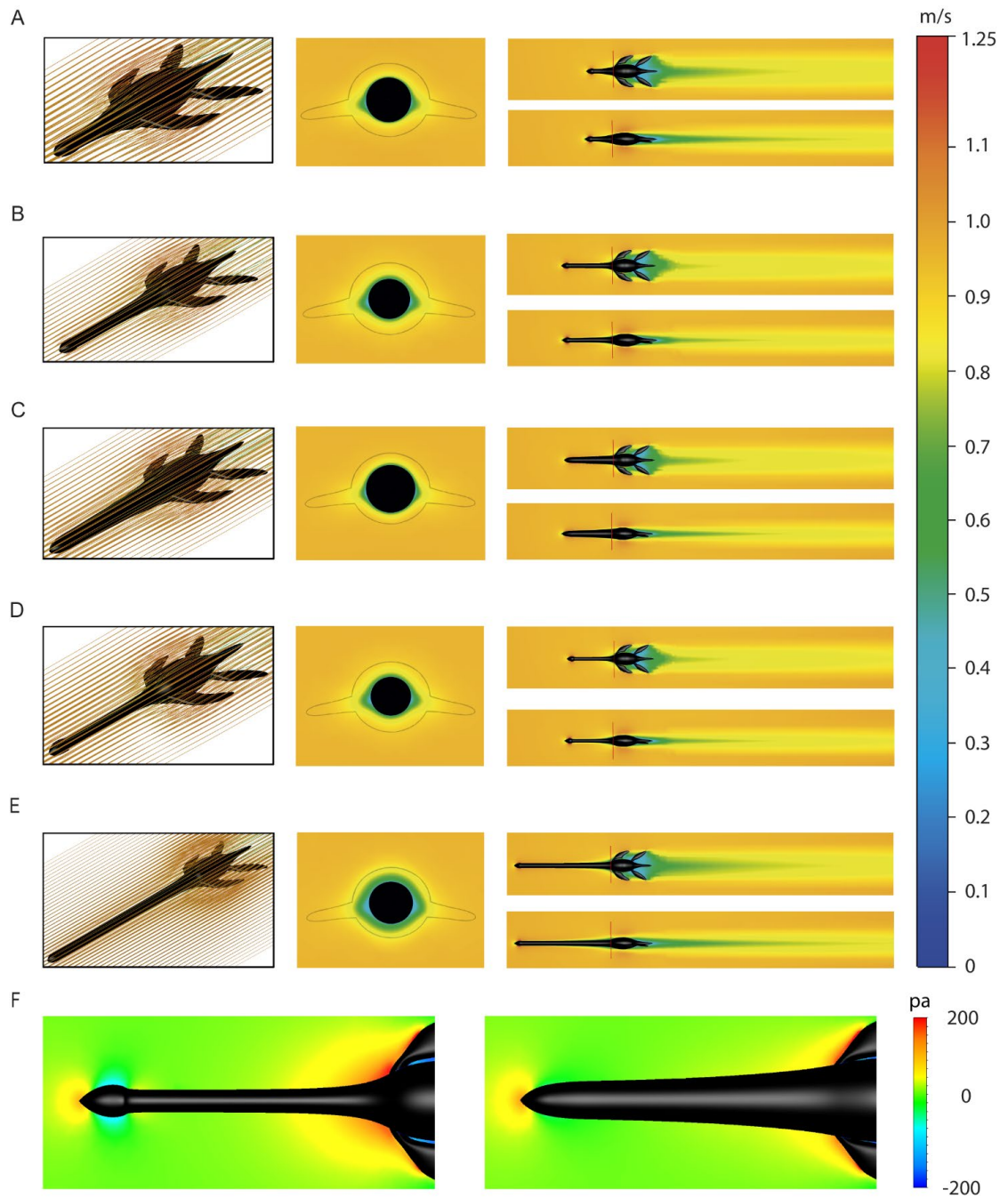


Figure 113: Three-dimensional (3D) flow velocity pattern surrounding plesiosaur models at 1m/s creating flows of different velocities in the wake shown with flow traces (left images) and flow velocity magnitudes in frontal view (middle images) and dorsal/side view (right images). (A) Short neck, (B) intermediate neck, (C) thick neck, (D) thin neck, and (E) long neck. (F) close-up of pressure around head and neck region in dorsal view of the thin neck (left image) and thick neck (right image). The direction of flow (left and right images) is from left to right. Red line (right images) indicated plane position on the models for frontal view. Abbreviations: m/s = meter/second; pa = pascal.

Consistent with theoretical expectations, the simulations showed that with increasing velocity, higher drag coefficients were experienced by the plesiosaur models of all three different neck lengths. The thin-necked plesiosaur model showed little difference in velocity and drag force patterns from the intermediate neck (Figure 114). However, the thick-necked plesiosaur model was observed exhibiting a generally lower drag coefficient noticeably above speeds of 5-10 m/s (Figure 114). The relative difference in percent in drag coefficient between the thick and thin-necked models was 17 % at 5m/s, 16 % at 7m/s and 18 % at 10m/s, so the thicker neck saw a drag reduction of 15-20 % compared with the thin-necked model.

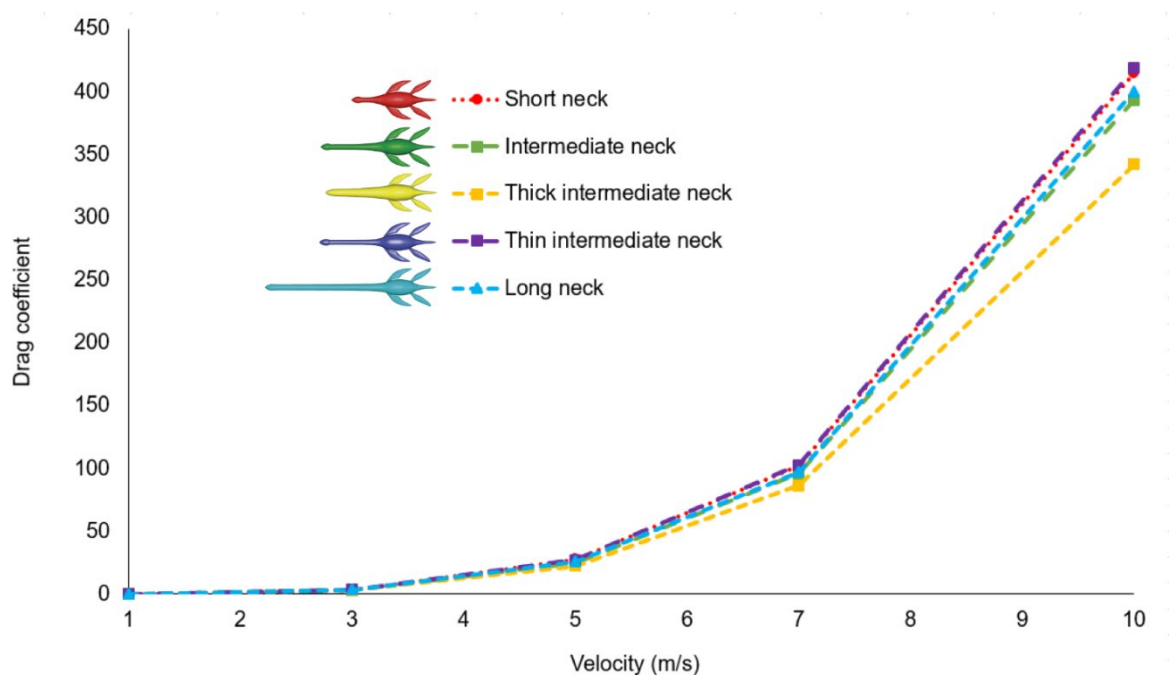


Figure 114: Simulation results using the five plesiosaur models with different neck lengths and thicknesses shown as velocity (m/s) against drag coefficient. Short neck (red), intermediate neck (green), thick neck using intermediate neck (yellow), thin neck using intermediate neck (purple), and long neck (blue).

5.4 Discussion

5.4.1 Neck elongation and thickness

From the results it was found that elongation of the neck had little effect on the hydrodynamics when held completely straight (Figure 114). It is qualitatively understandable that the longer the neck is the more drag it will experience if not held completely straight (cf. Chapter 6). Also, the density of the body would affect the movement of the animal as more lift would be needed for the animal to move (e.g. upwards) and it follows that more drag would be created. Making manoeuvres in the water, such as flexing the neck, would almost certainly have required more muscular strength than would be

available to the animal (Noè *et al.*, 2017), so plesiosaurs swimming with straight necks is likely in cases where the animals would have to approach prey fast over a short distance. Here, the plesiosaurs would benefit from reduced energy costs to a minimum in order to keep the speed steady, and therefore having nearly straight necks when swimming. In addition, an animal swimming any distance would use less energy overcoming drag if the neck was straight – as suggested by the simulations. To ensure prey capture, plesiosaurs might have spent extra energy by moving the neck to match the escaping maneuverers of the prey.

The CFD simulations also indicate that neck thickness had a noticeable effect on the amount of drag force and water pressure generated by the plesiosaur, with the greatest water pressure occurring when the plesiosaur model was reconstructed with thinnest neck length, and the largest wake size and highest drag force occurring with the shortest and thinnest neck length (Figure 114). As the surface area did not change significantly in the plesiosaurs, friction drag would remain the same, and pressure drag would dominate, although being low in the thick-necked model due to the more streamlined body shape. The change in wake size and drag force was only apparent for water velocities above 5.0 m/s. This would be a speed substantially faster than typical for a small dolphin (see section 5.2). Drag forces experienced by the plesiosaur models were similar across different neck lengths, though longer necks experienced slightly less overall drag force. The largest reduction in drag at any given speed was observed in the thick-necked model (Figure 114).

The thickness of plesiosaur necks has been a longstanding difficulty in reconstructing the life appearance of these animals, with both thin- and thick-necked plesiosaurs being illustrated in the past (Cope, 1869; Zarnik, 1925; Welles, 1943; Welles and Bump, 1949; Shuler, 1950; Rudwick, 2008). A thin neck would, according to these results, have been a disadvantage for the plesiosaur during locomotion as it would have created more drag force and water pressure in comparison to a thicker-necked plesiosaur, especially if the animal was moving quickly (>5m/s).

Bite marks have been found in various plesiosaur bones. With only one known exception (Sato *et al.*, 2006), the bite marks observed in plesiosaur bones occur on humeri and flippers (Forrest and Oliver, 2003; Everhart, 2005; Sato *et al.*, 2006), which might suggest that plesiosaurs had thick necks. Having a thicker neck makes it harder for predators to leave bite marks on the actual vertebrae, especially the neck vertebrae. Thicker necks would therefore

reduce the likelihood of finding cervical vertebrae with healed bite marks, as any bite deep enough to reach the vertebrae would likely be fatal. However, again we need more plesiosaur specimens observed with bite marks in vertebrae to clarify that plesiosaurs had thin necks.

The soft tissue preservation found in fossils can help us understand how extinct animals would appear and move, as the muscles form an integral part of the anatomy and play a fundamental role in feeding, locomotion and other physiological activities (Witmer, 1995; Lautenschlager, 2017). If the soft tissue is taken into account it allows us to justify a certain ecology and phylogeny for a given animal (Witmer, 1995). Although many plesiosaurs are found complete and fully articulated preserved soft tissue is rare throughout the Plesiosauria clade (O'Keefe, 2001b; Frey *et al.*, 2017), making it difficult to interpret their ecology and paleobiology. The specimen described by Vincent *et al.* (2017a) is covered with more soft tissue around the neck compared with the specimen reported by Frey *et al.* (2017). The two specimens discussed by Frey *et al.* (2017) and Vincent *et al.* (2017a) have two different neck lengths. Combining the difference in neck thickness among the two plesiosaur specimens with the results from the present study suggests that short-necked plesiosaurs would have benefited more from slender necks (if that was the case in reality) than the long-necked species because the long-necked plesiosaur described by Vincent *et al.* (2017a) is covered by more soft tissue in comparison with the short-necked plesiosaur described by Frey *et al.* (2017). However, more plesiosaur specimens including soft tissue are required to clarify whether plesiosaurs had thick or thin necks.

5.4.2 Ecology and behaviour of plesiosaurs

Wilkinson and Ruxton (2012) suggested long necks in most cases could be explained in terms of foraging requirements. An aquatic animal with a long neck by itself does not necessarily benefit in terms of foraging as the animal needs flexibility to move around in the water in search of prey, which might be impaired by the presence of a long neck. Indeed, in extant aquatic animals like sea lions we see a great flexion in the neck region as the animals turn in the water (Fish *et al.*, 2003; Cheneval *et al.*, 2007). Previous studies and Chapter 3 have suggested that plesiosaurs had some extent of neck flexibility (Zarnik, 1925; Evans, 1993; Zammit *et al.*, 2008; Noè *et al.*, 2017; Nagesan *et al.*, 2018). Furthermore, the fused atlas-axis complex in plesiosaurs could provide additional cranial movement because of the cup-shaped occipital bone (VanBuren and Evans, 2016) allowing the plesiosaur to scan for possible prey more efficiently. Plesiosaurs would presumably have benefited in terms of foraging by using a combination of the long necks, manoeuvrability of the head, and thrust

from the flippers to pursue and capture prey. A study on the hydrodynamic implications of bent plesiosaur necks during forward motion is explored in the following chapter.

The long neck in plesiosaurs was clearly a successful adaptation as shown by their long evolutionary history (Smith, 2007). The results from the CFD simulations show that having a long neck would be hydrodynamically neutral up to 5 m/s and could mean that plesiosaurs increased in diversity as a response to the development of diverse neck lengths, as the neck length did not affect the drag force added on to the plesiosaur model (Figure 114).

For the present study the characteristic length of the plesiosaur models could be determined as either total body length or trunk length. If Reynolds numbers are a crucial part of the study, it is important to consider whether to use the total body length or the trunk length of the animal. This is because the Reynolds number will be the same for all five models in case of using trunk length as characteristic length. In addition, the total body length will change the Reynolds number depending on which model is the case of study, which can also be observed in the validation experiments from Chapter 4. The Reynolds number was not used for further analysis in this study, but rather drag force which is only affected by the velocity.

Plesiosaurs have been considered both as relatively slow (Conybeare, 1824; Andrews, 1910; Watson, 1924; Shuler, 1950; Taylor, 1981; Massare, 1988, 1994) and fast swimmers (Hutchinson, 1893; Halstead, 1989; Bakker, 1993). To avoid the energetic cost of high amounts of drag, plesiosaurs might have evolved thicker necks to allow effective hunting strategies like ambushing prey – fast acceleration of the body over a short distance. Therefore, it is more reasonable that plesiosaurs had a variety of swimming speeds in accordance with neck length, as suggested by Massare (1994), instead of being labelled as either fast or slow swimmers. The results indicate that thicker necks reduced drag, which lends support for a more expanded neck than is traditionally incorporated into reconstructions.

5.5 Conclusions

A thick-necked plesiosaur would have a hydrodynamic advantage compared with a thinner-necked plesiosaur, however, these effects are only seen at velocities which may be faster than what was typical, or even possible, for most plesiosaur species. Broader necks reduce the surface area normal or near normal to flow direction, and thus reduce pressure drag. This suggests that any plesiosaurs using a pursuit hunting strategy may have been under selective pressure to evolve a thicker neck. The consistent drag force experienced by the three neck lengths used in this study indicated that, at least for straight forward motion, hydrodynamic implications were not a limiting selective pressure on the evolution of long necks in plesiosaurs. Massare (1994) found that the long necks in plesiosaurs did experience increased drag, and therefore suggested slower swimming speeds and different foraging models for the long-necked plesiosaurs compared with short-necked plesiosaurs. In contrast, the present study suggests that short- and long-necked plesiosaurs did not vary greatly in drag experienced during forward locomotion. Given the long survival of the plesiosaurian body plan in the geological record, it is not surprising that the quantitative results from the present study support the notion that the long neck was not particularly disadvantageous hydrodynamically. In conjunction with soft-tissue preservation reported in plesiosaur necks, the simulations provide support for reconstructing plesiosaurs with more sea lion-like neck morphology than they have traditionally been reconstructed with.

Despite the “modelling” approximation based on RANS CFD simulations used for the present study, the CFD tool can help to explore the hydrodynamic effects on a plesiosaur neck when simulated with different lengths and thicknesses as found in this study. This study and the following chapter on the hydrodynamic implications of bent plesiosaur necks during forward motion will help to shed light on the biomechanical implications of the long neck in plesiosaurs, and more broadly inform hypotheses concerning the lifestyles and evolutionary history of plesiosaurs.

Chapter 6 – Hydrodynamic effect of plesiosaurs bending the neck during forward motion

6.1 Introduction

The understanding of the relationship between morphology and locomotor performance continues to be a dominant theme in biomechanics (Vogel, 2013). In aquatic locomotion, the two key components involved are hydrodynamic stability and turning ability (Stevens *et al.*, 2018). Energetic costs of swimming can be reduced by increasing stability, whereas avoiding and capturing prey is facilitated by turning performance (Stevens *et al.*, 2018). As animals rarely move continuously in straight lines (Fish and Rohr, 1999), it is obvious that turning performance holds a central part in the fundamental understanding of locomotor performance of animals. Turning performance has been investigated in great detail in many extant aquatic vertebrates (Walker, 2000; Drucker and Lauder, 2001; Alexander, 2003; Fish, 2002; Weihs, 2002; Fish *et al.*, 2003; Maresh *et al.*, 2004; Cheneval, 2005; Rivera *et al.*, 2006; Cheneval *et al.*, 2007; Fish *et al.*, 2008; Pierce *et al.*, 2011; Segre *et al.*, 2016; Clifton and Biewener, 2018; Stevens *et al.*, 2018), and is typically evaluated by two metrics: manoeuvrability and agility (Stevens *et al.*, 2018). Manoeuvrability is normally measured as the space required to execute a turn, whereas agility is the rate of turning. Most marine animals have a morphology that is a compromise between high stability and high turning performance (Van Wassenbergh *et al.*, 2014; Stevens *et al.*, 2018), and animals living in complex environments often tend to have high turning performance but low stability (Walker, 2000). In contrast, migratory animals are often highly stable but possess poor turning performances (Fish, 2002). Based on mechanical principles, animals with compact bodies are expected to be able to turn in tight spaces, whereas elongate bodies would be expected to enhance stability by helping to resist turning moments (Walker, 2000).

The role of plesiosaur necks in turning performance has not yet been explored. Previous studies on plesiosaur hydrodynamics have mainly focused on flipper locomotion (Watson, 1924; Welles and Bump, 1949; Robinson, 1975, 1977; Taylor, 1981; Halstead, 1989; DeBlois, 2013; Liu *et al.*, 2015; Muscutt *et al.*, 2017) and forward swimming speeds (Massare, 1988, 1994; O'Keefe, 2001b; Motani, 2002; Carpenter *et al.*, 2010). While Chapter 5 showed no negative side of plesiosaurs possessing long necks during forward locomotion, bending the long neck would possibly make swimming more challenging. Determining the bending effects of such long necks could help explore the ecology of plesiosaurs, and by

combining such knowledge with hydrodynamics of plesiosaur flippers and neck flexibility will allow us to understand the possible feeding strategies in long-necked plesiosaurs. Combined with the literature, methods and data from the previous chapters, the present study explored and evaluated the hydrodynamic implications and turning effects of three different plesiosaur models flexed laterally during forward swimming.

The present study used CFD to investigate the individual effect of drag on three neck lengths to answer five questions:

- 1) What are the drag coefficients for the frontal forces for plesiosaurs swimming forward with bent necks?
- 2) What are the lateral forces for plesiosaur swimming forward with bent necks?
- 3) Is there a clear difference between short-, intermediate-, and long-necked plesiosaurs when the neck is curved?
- 4) What do the results from the former question indicate that plesiosaur were capable of in terms of turning performance?
- 5) Would moving a bent neck through the water be potentially problematic for a plesiosaur?

Using two approaches, bending effects in plesiosaur necks were here explored using computational fluid dynamics (CFD). Firstly, a simplified plesiosaur model constructed from primitive shapes was used to study the effect of bending location and distribution (at head-region, mid position, and evenly over the neck) on the plesiosaur neck from 0-90° with 10° intervals was explored. This first approach was performed in order to test possible scenarios for plesiosaurs turning their necks; would it be most likely that plesiosaurs turned their necks evenly or at specific locations on the neck based on drag generated by the bent neck? Combining the results found here with the neck flexibility results from Chapter 3 it will be possible to come up with an assessment of what turning performance will be the most realistic for plesiosaurs.

The second approach included short-, intermediate, and long-necked plesiosaur models (identical to the models used in Chapter 5) with bent necks. In this case, the bend was distributed evenly over the length of the neck in lateral horizontal flexion at 22.5°, 45°, 67.5°, and 90°. The more realistic models in this approach were used to investigate the hydrodynamic implications for a plesiosaur swimming forward with a bent neck.

6.2 Methods

6.2.1 Building the plesiosaur models

6.2.1.1 Plesiosaur model made from primitives

To investigate the effects of bending position and distribution, a consistent and simple model which approximated plesiosaurian body proportions was constructed via simple primitive objects. Using the primitives, the aim was to test what the location of the bending would mean for hydrodynamic implications of the neck. The simplified plesiosaur model was made in Autodesk Maya (www.autodesk.com) and consisted of a body region (ellipsoid), a neck region (cylinder), and a head region (ellipsoid), excluding flippers and tail (Figure 115). The model was scaled to a total length of 4m, which is comparable to the average length of many known plesiosaur species (Massare, 1994). The model was symmetrical, meaning that there was no difference in lateral, dorsal or ventral bending. Using a “bend former” in Maya the neck was bent at three different locations by inserting the desired amount of curvature anteriorly in the neck, at a mid-point in the neck, and evenly throughout the neck.

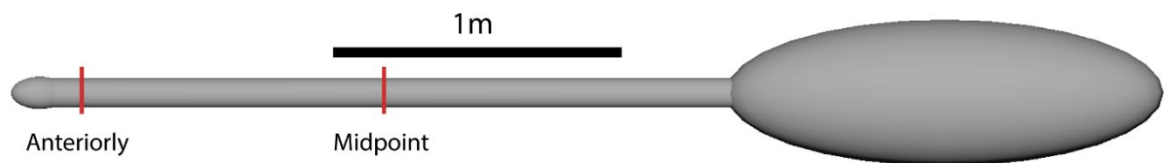


Figure 115: Lateral view of the plesiosaur model made using primitives (two ellipsoids and a cylinder). Red lines indicate locations for bending the neck anteriorly and at the midpoint.

Each location was bent from 0-90° at 10° increments, and the model was saved individually in IGES format with each rotation interval in Autodesk Maya.

6.2.1.2 Short-, intermediate-, and long-necked idealized plesiosaur models

The hydrodynamic implications for bending necks in idealized plesiosaur models were also tested using a short-, intermediate-, and a long-necked model. The models from Chapter 5 were used, modified by the addition of neck bends performed in Autodesk Maya (Figure 119). For each model, a number of connected ‘joints’ were added equal to the number of cervical vertebrae (CV) present in the representative plesiosaur species (short-necked model: *Meyerasaurus victor*, 28 CV; intermediate-necked model: *Muraenosaurus leedsii*, 42 CV; long-necked model: *Albertonectes vanderveldei*, 76 CV). These joints formed a ‘rig’ which was used to drive the motion of the neck. An example of the rigging for the plesiosaur model with intermediate neck length is shown in Figure 116.

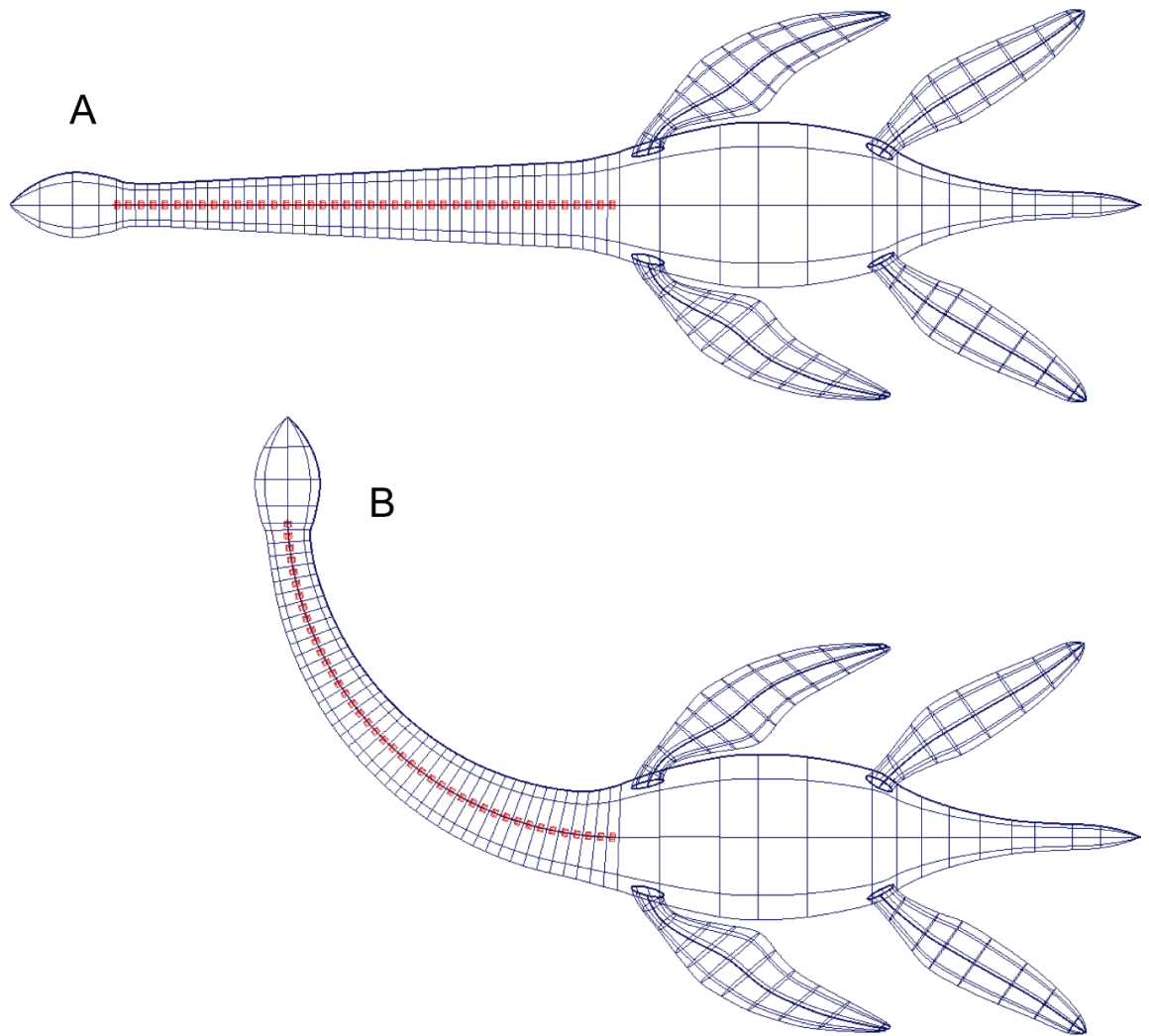


Figure 116: Example of the rigging for the idealized plesiosaur models. Dorsal view of the skeleton for the plesiosaur model with intermediate neck including joints and cylinders (coloured in red) inserted to illustrate each cervical vertebra. A) Model with straight neck. B) Model with the neck bent 90°.

Joints between each pair of cervical vertebrae were inserted midway between each NURBs circle. The models had one extra joint attached in the posterior end of the head in order to have a smooth bending transition from head to neck. Each joint was paired by parenting the joint to the respective cervical using “NURBs circles” along the neck. By parenting each joint to its respective NURBs circle the two objects will be associated with one another and this makes the number of all joints and NURBs circles more organised, this way the rotation and translation information for each pair (joint + NURBs circle) will follow the adjacent joint and circle (Figure 117).

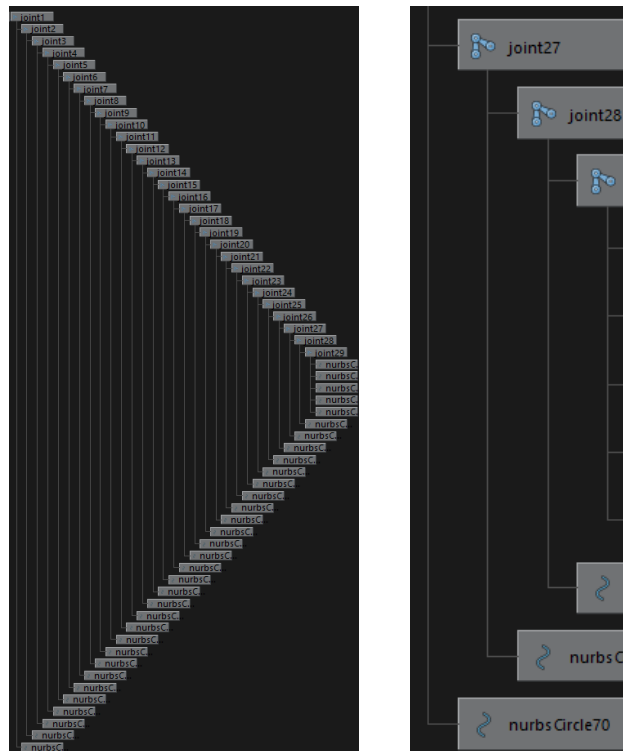


Figure 117: Organisation of joints and connections with their respective NURBs circles. Left: All joints and NURBs circles for the short-necked plesiosaur model. Right: Close-up of some of the joints and NURBs circles, with the link between each pair illustrated by a vertical line, and the connection with the adjacent joint by a horizontal line.

The total neck length of each model was measured from the posterior end of the head to the base of the neck. The neck lengths were measured in order to find out how much distance there should be in between each joint, by dividing the total neck length with the number of cervical vertebrae for the given species. The short-necked model was 0.8 m in neck length, and with a total number of 28 joints; a joint was positioned at every 0.03 m. For the intermediate model the neck length was 2.0 m and with a total of 42 joints inserted, at every 0.048 m a joint was inserted. For the long-necked model 76 joints were inserted in the neck making it a joint situated at every 0.058 m and a total neck length of 4.4 m. To calculate Reynolds numbers, the total length of each model with the neck straight was used as the characteristic length (but see below for the implications of this when the neck is curved).

Table 11: Average rotation between joints (degrees) calculated as total rotation of the neck divided by the number of joints/CVs, e.g. for the short-necked plesiosaur model $90^\circ/29$ joints = 3.10° .

Plesiosaur model	Degrees of bending			
	22.5°	45°	67.5°	90°
Short neck	0.77°	1.55°	2.33°	3.10°
Intermediate neck	0.52°	1.05°	1.57°	2.09°
Long neck	0.29°	0.58°	0.88°	1.17°

After insertion of joints in the neck region of the plesiosaur models the necks were bent laterally into four different poses (total neck curvature: 22.5°, 45°, 67.5°, and 90°). Lateral rotation was chosen because turning in the horizontal plane (rather than diving or rising through dorsal/ventral flexion) ignores effects of buoyancy, i.e. lateral flexion required no prior knowledge of whether plesiosaurs moved up- or downwards in the water column.

Each joint in the neck of the three idealized plesiosaur models was equally rotated, distributing the curvature over the entire length. The specific rotations required between each vertebra/joint to reach the four poses of neck bending are shown in Table 11, and calculated by dividing bend angle by the number of joints. The five poses for each model are shown in Figure 118. At very small rotations between each vertebra a large whole-neck rotation is achieved (cf. Chapter 2 and 3: digital manipulation of neck vertebrae). The plesiosaur models were saved individually in IGES format after each rotation was entered in Autodesk Maya.

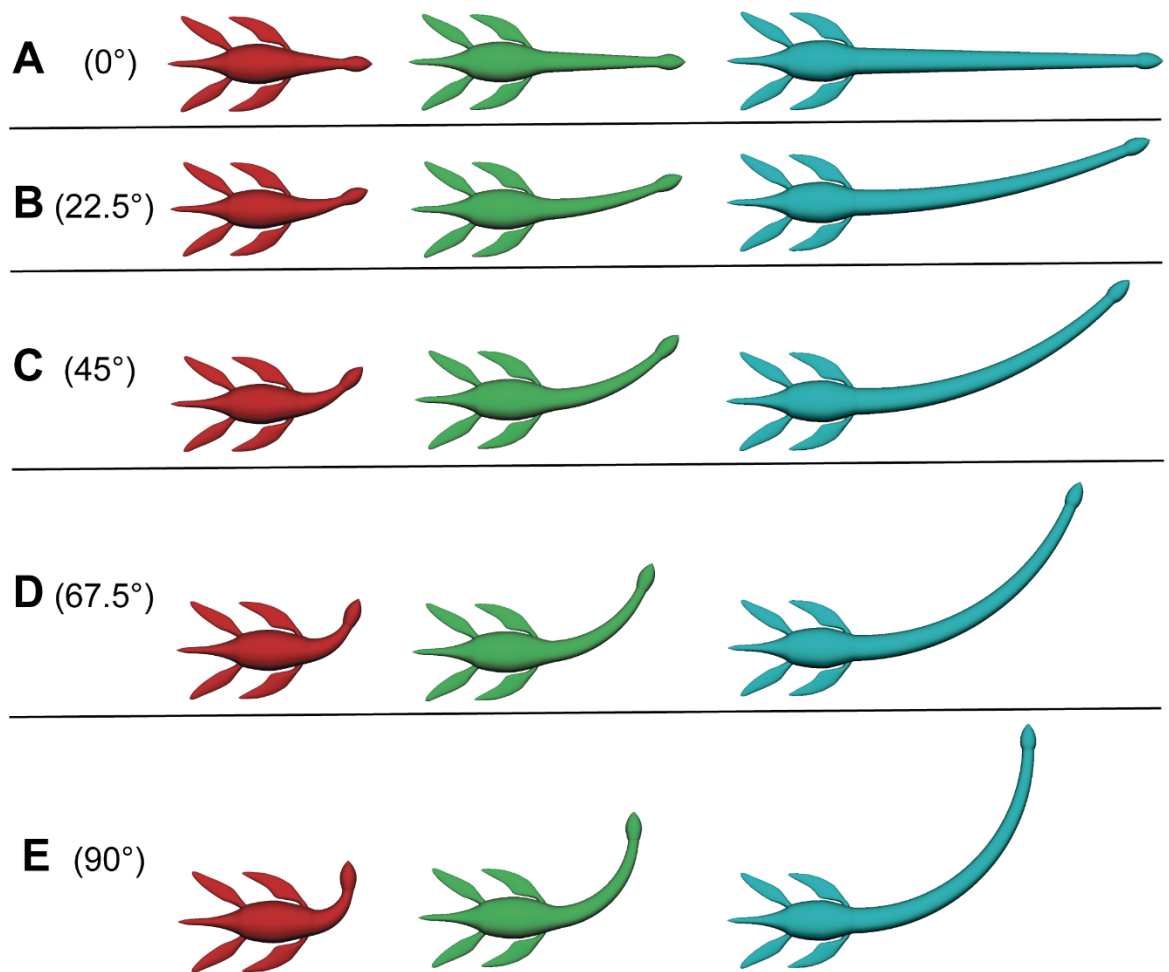


Figure 118: Illustration of the short-necked (red), intermediate (green), and long-necked (cyan) idealized plesiosaur models shown as straight (A) and with the four stages of total neck curvature of B) 22.5°, C) 45°, D) 67.5° and E) 90°.

In order to illustrate how cervical number and size can affect the amount of total rotation when intervertebral rotation is kept constant, three additional models (one for each neck length) were produced where each joint was rotated 2° (Figure 119). The value of 2° was based on that the long-necked model would exceed the 90° curvature of the neck if each vertebra were to be rotated more than 2° . The total rotation in the neck for the three models were 56° (short-neck), 84° (intermediate), and 152° (long-neck), showing that the longer the neck is the more rotation it will have even though all three models had the same amount of each joint inserted, eventually creating a larger intervertebral distance between adjacent cervical vertebrae.

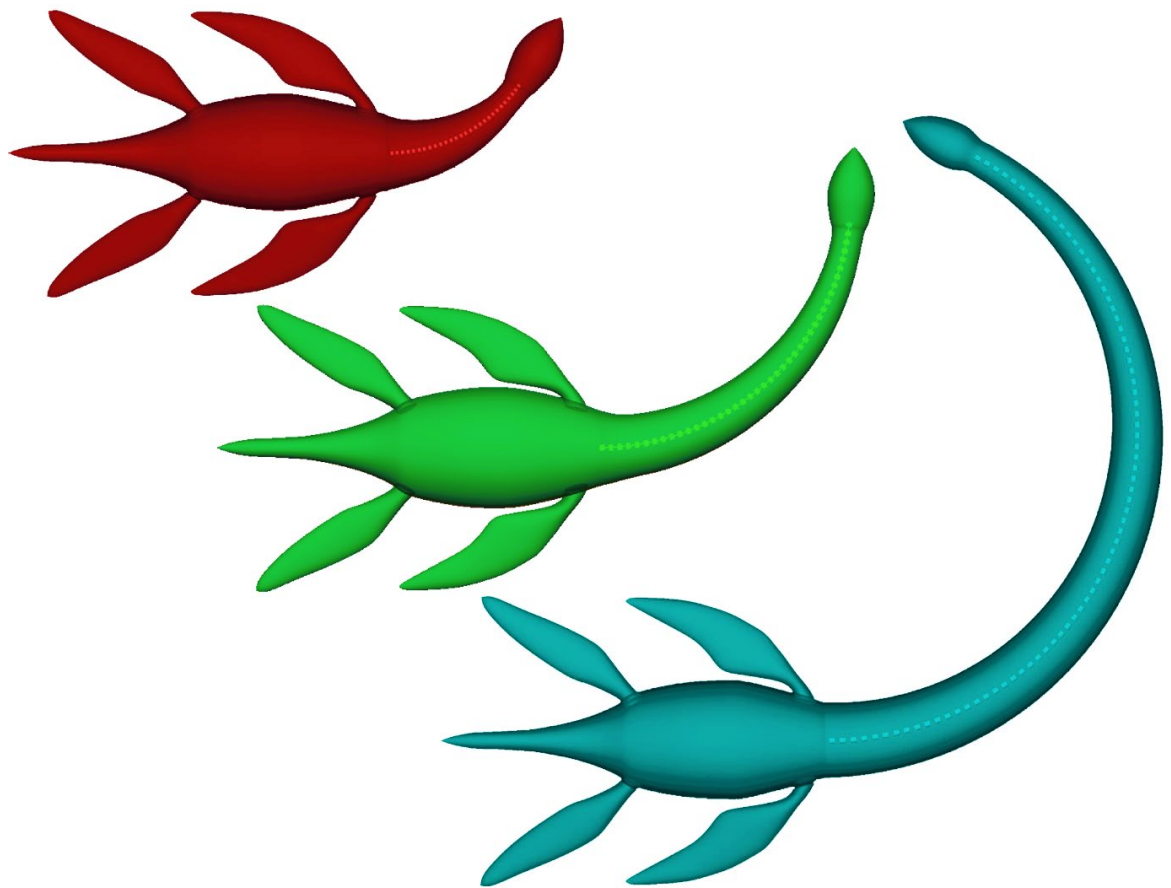


Figure 119: 3D models of the short-necked (red), intermediate neck (green), and long-necked (cyan) plesiosaur models with the neck bent laterally. The short-necked model had 28 joints, intermediate neck 42 joints, and the long-necked model had 76 joints, and each CV is visualised as a cylinder, with an additional joint at the posterior end of the head to allow smooth transition when adding rotation to the neck. Each joint was rotated 2° to the left.

Notice the diversity in the amount of bending in the three neck lengths using a consistent 2° per cervical.

6.2.2 Characteristic length for a plesiosaur model with bent neck

The ‘Characteristic length’ used to calculate Reynolds numbers (Re) is based on the overall length of the plesiosaur relative to the direction of flow. However, when the neck is bent, this length decreases (Figure 120), which means that Re is technically decreased as well. Therefore, to calculate the specific Re for the plesiosaur models, the characteristic length should be taken as shown in Figure 120B, rather than the actual length of the model when the neck is held straight (Figure 120A).

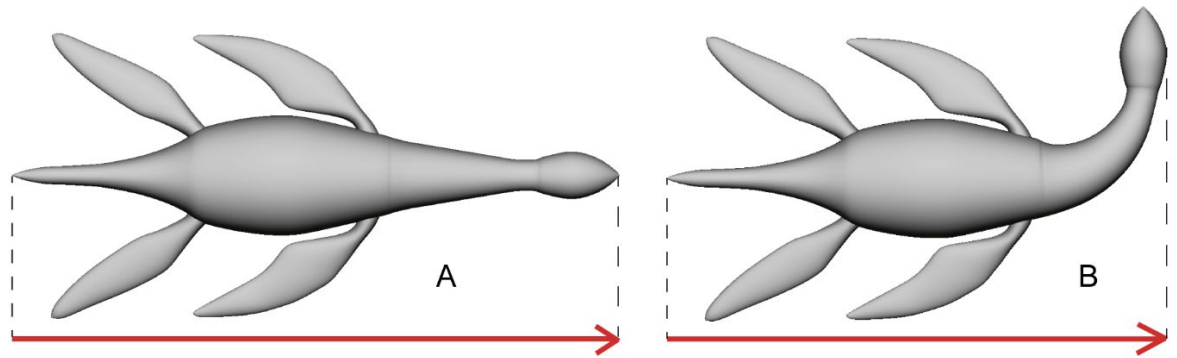


Figure 120: Determination of characteristic length of the short-necked idealized plesiosaur model with (A) straight neck and (B) bent 90°.

However, as the present study is within the turbulent flow regime (cf. Chapter 4: $Re < 10^6$), changing the characteristic length because the neck is bent will not create laminar flow nor change Re significantly even at low speeds (Table 12), and the results for the present study will not be affected by using the straight neck instead of the bent neck as characteristic length. Because this chapter is exploring the effects of bending the neck during forward motion, it makes sense to keep the flow rate consistent, rather than altering velocity each time in order to keep Re consistent between simulations. For consistency and clarity, reference to Re in the remainder of this chapter refers to the Re calculated from a characteristic length based on each model with the neck held straight.

Table 12: Reynolds numbers at 1 m/s for the three plesiosaur models with the neck held straight and bent 90°.

Plesiosaur model	Straight	Bent 90°
Short neck	2.9×10^6	2.5×10^6
Intermediate neck	4.0×10^6	3.1×10^6
Long neck	6.2×10^6	4.5×10^6

6.2.3 Computational fluid dynamics

The models created in Autodesk Maya (both the plesiosaur made of primitives and the idealized plesiosaur models) were imported into Autodesk Simulation CFD (version 2018) (www.autodesk.com) individually for each simulation performed.

6.2.3.1 Plesiosaur model made from primitives

For the part of the study investigating the effects of bending position and bending distribution the computational domain consisted of a 20m cube with one face in front the plesiosaur model defined as the inlet, with water velocity specified as m/s. The opposite face of the cube domain, located posterior to the plesiosaur model was defined as the outlet

boundary condition (zero pressure gradient across the boundary). Mesh size of the 3D model and domain was 0.01m and 0.5m, respectively. A region refinement was added with appropriate mesh size (according to stable mesh size of models and domain). The region refinement (mesh size 0.1m) was created to have a refined area surrounding the plesiosaur model and its wake for better resolution and more accurate results from the simulations. Fluid type (for the domain) was set as seawater, as it matches the material of the domain for the plesiosaur. The density of seawater is 1021.2kg/m^3 and the viscosity is $0.0011404\text{ Pa}\cdot\text{s}$. Solid type was set as glass as it closely matched a smooth surface to exclude the surface variable from the scenario, and its density was 2700 kg/m^3 . A flow velocity of 1 m/s was simulated to look at the difference in drag between the various bending locations in the neck at a relative low speed (higher speeds were performed for the idealized plesiosaur models). Drag force was calculated by Autodesk Simulation CFD, and flow patterns were visualised as planes in dorsal view to capture the flow around the model. Drag coefficients were manually calculated using the frontal area of the plesiosaur model.

6.2.3.2 Short-, intermediate, and long-necked idealized plesiosaur models

Similar to Chapter 5, the idealized plesiosaur model of a short- and long-necked plesiosaur had a computational domain which consisted of a 25m cube with one face in front of the plesiosaur model defined as the inlet, with water velocity specified as m/s. The opposite face of the cube domain, located posterior to the plesiosaur was defined as the outlet boundary condition (zero pressure gradient across the boundary). Mesh size of the 3D models and domain was the same as that used in Chapter 5 (plesiosaur: 0.01m; domain: 1.0m).

Similar to Chapter 5, a region refinement was additionally inserted with appropriate mesh size (according to stable mesh size of models and domain). The region refinement (mesh size 0.5m) was created to have a refined area surrounding the plesiosaur model and its wake for better resolution and more accurate results from the simulations. Additionally, a region refinement was created around the neck only (mesh size: 0.05m) to improve resolution even further round the neck region. Flow velocities of 1, 5 and 10 m/s were simulated to look at the difference in drag between the short and long-necked plesiosaur model when the neck was bent. The velocity of 5 m/s was chosen based on the maximum sustained swimming speed calculated for plesiosaurs from previous studies (Massare, 1988, 1994). The velocities of 1 m/s and 10 m/s were chosen because they were lower and higher than this putative maximum sustainable speed of plesiosaurs. Frontal and lateral drag forces of the plesiosaur models were calculated by Autodesk Simulation CFD. Flow velocity patterns surrounding

the plesiosaur models were taken in dorsal view to visualise changes in flow. Pressure around the models in dorsal and frontal view were visualised as planes to look at changes in pressure around the plesiosaur models. Drag coefficients for the frontal drag forces were manually calculated using the frontal area of the plesiosaur models.

6.3 Results

6.3.1 Effect of bending location and distribution using primitives

The results from the simulations using a plesiosaur model with a bent neck made of primitives showed greater drag coefficients as degree of bending was increased; up to an increase of almost one order of magnitude from when the neck was held straight to 90° of bending evenly (Figure 121). The least drag was experienced for the model with the anterior bending location and the most drag for the evenly bent.

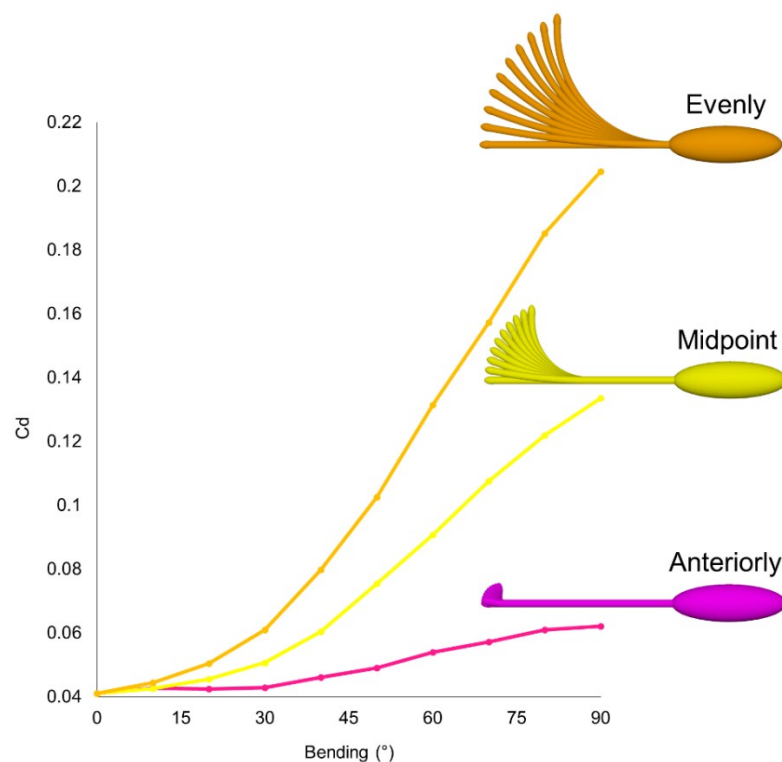


Figure 121: The plesiosaur model made of primitive shapes showing respective bending degrees (°) vs. drag coefficients at different locations (evenly throughout, at midpoint, and anteriorly) at 1 m/s. Drag coefficients increased with degrees of bending for all locations.

Furthermore, the evenly curved neck created a more complex flow velocity pattern including zones of low velocity behind the neck and to the side of the body. With the neck bent anteriorly the flow velocity pattern changed a lot in appearance in comparison with the evenly bended neck (Figure 122). For all three bending locations, the flow velocity pattern

at the base of the bent neck decreased with the least velocity closest to the neck, and the flow velocity in the wake behind the model also decreased compared with the area on the lateral sides of the model all three bending locations, indicating that the body of the plesiosaur model created an area of higher amounts of turbulence.

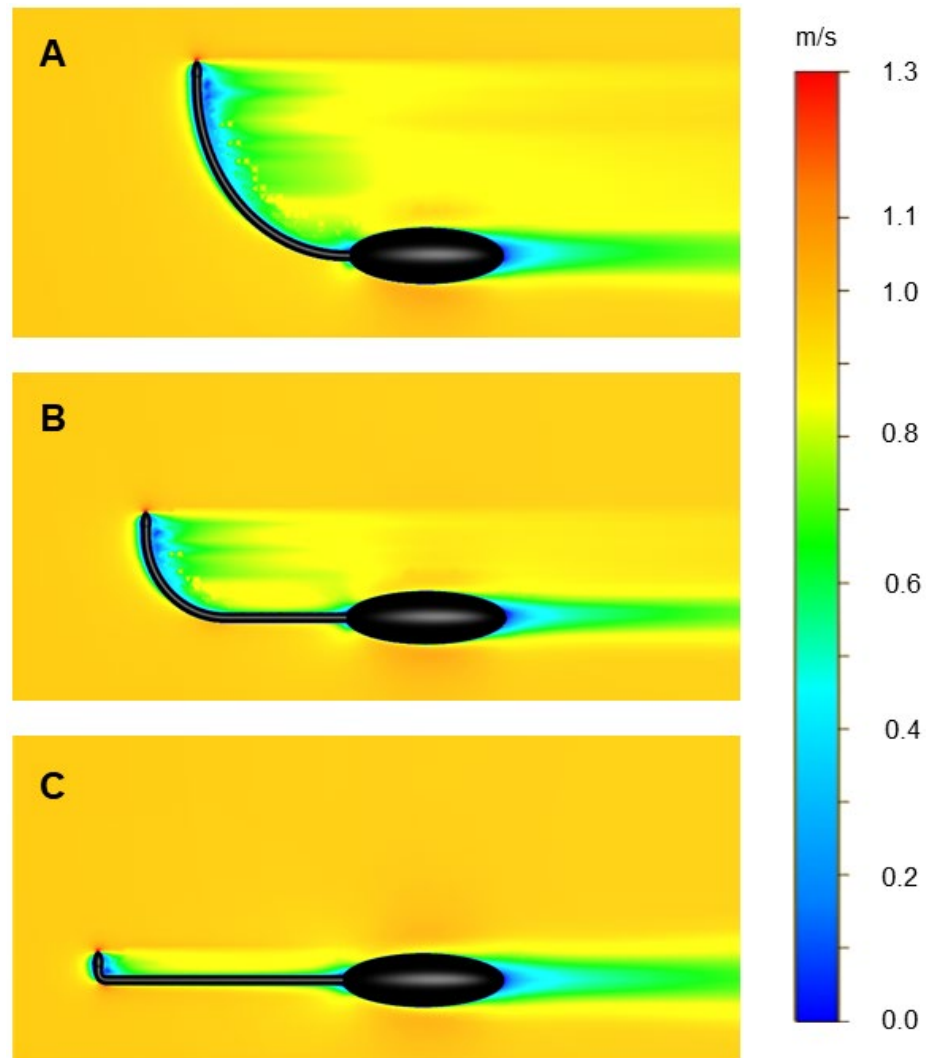


Figure 122: Flow velocities surrounding the forward swimming plesiosaur model made of primitives at 1 m/s at 90° when A) bent evenly throughout the “neck”, B) bent at midpoint, and C) bent anteriorly. Flow inlet from left to right.

6.3.2 Effects of bending the neck in idealized plesiosaur models

When comparing drag coefficients for the idealized plesiosaur models with bent necks, the short-necked model experienced the least drag, and the long-necked experienced the most drag at 0° or higher (Figure 123 and Figure 124). All three models demonstrated a nearly linear relationship in the increase of drag for bending of 45° – 90° at all three velocities (Figure 123). As was expected the drag was highest for the long-necked model, and the least for the short-necked model with the intermediate neck being between the two. The lateral

drag forces experienced to the left side all three models peaked in drag at 67.5° and decreased slightly from $67.5^\circ - 90^\circ$, with the highest drag force seen in the long-necked model and the least in the short-necked model with the intermediate neck being between the two (Figure 124). The drag was almost the same for all three models until around 22.5° and diverges thereafter for the long-necked model, with a higher increase compared with the short- and intermediate-necked model caused by the greater frontal area for the long-necked model when bent. At all three speeds, the intermediate-necked model experienced slightly more than double amount of drag compared with the short-necked model, and the long-necked model almost tripled compared with the intermediate-necked model. There was an increase of four orders of magnitude in drag from 1 m/s – 10 m/s for all three models, and three orders of magnitude from 1 m/s – 5 m/s.

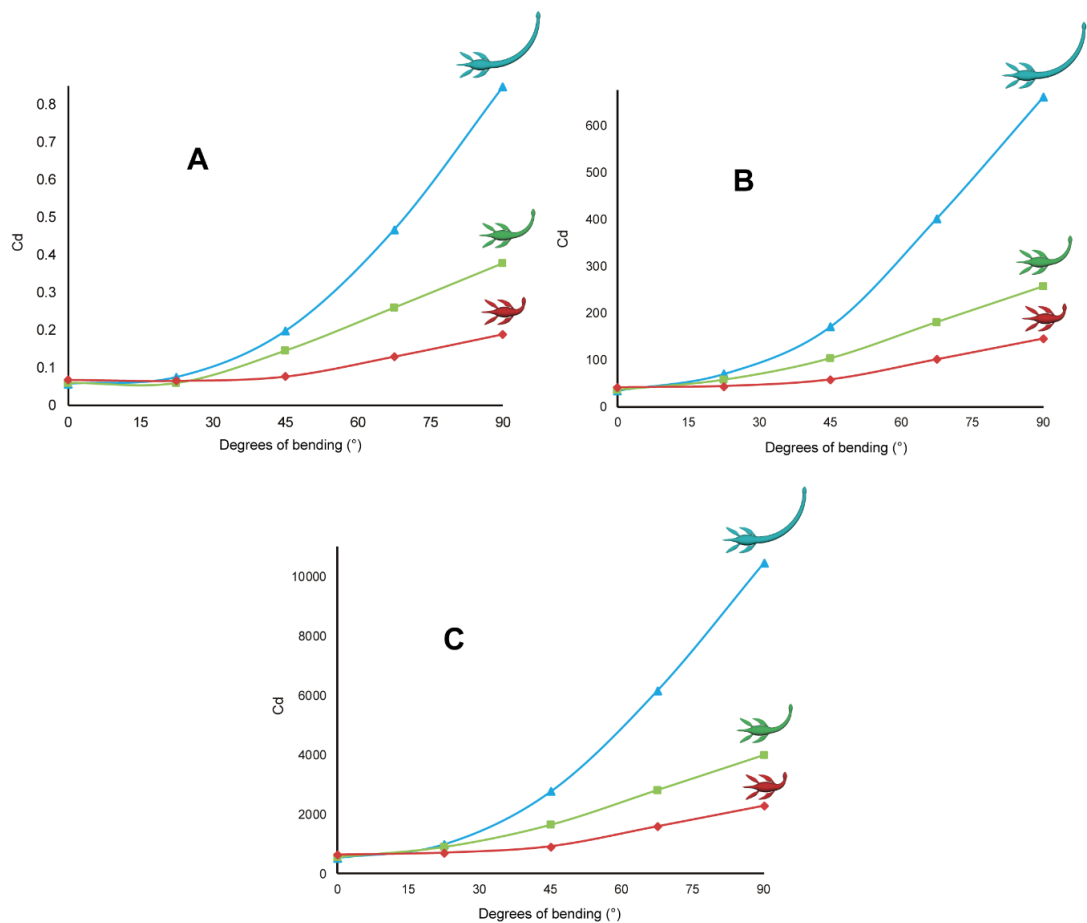


Figure 123: Frontal drag coefficients with increase in neck bending ($0 - 90^\circ$ with 22.5° interval) for the idealized plesiosaur models with short (red), intermediate (green), and long (blue) necks at (A) 1 m/s, (B) 5 m/s, and (C) 10 m/s. Drag force was calculated in X-direction of the 3D coordinate system, using frontal area of the plesiosaur models to calculated drag coefficients.

The flow velocity patterns at 1, 5 and 10 m/s were clearly different for the short-, intermediate and long-necked idealized plesiosaur models when the necks were bent 90° . At

5 m/s and 10 m/s the flow velocities were almost identical for all three neck lengths. The long-necked model experienced a relatively larger area of low flow velocity at all three flow velocities in the path behind the neck (Figure 125A-C). The flow velocity patterns in the wake behind the three plesiosaur models showed that the velocity here decreased, especially behind the flippers and in the tail region. In frontal view, the flow velocity patterns in the area surrounding the three plesiosaur models decreased, especially for the long-necked plesiosaur model (Figure 125E).

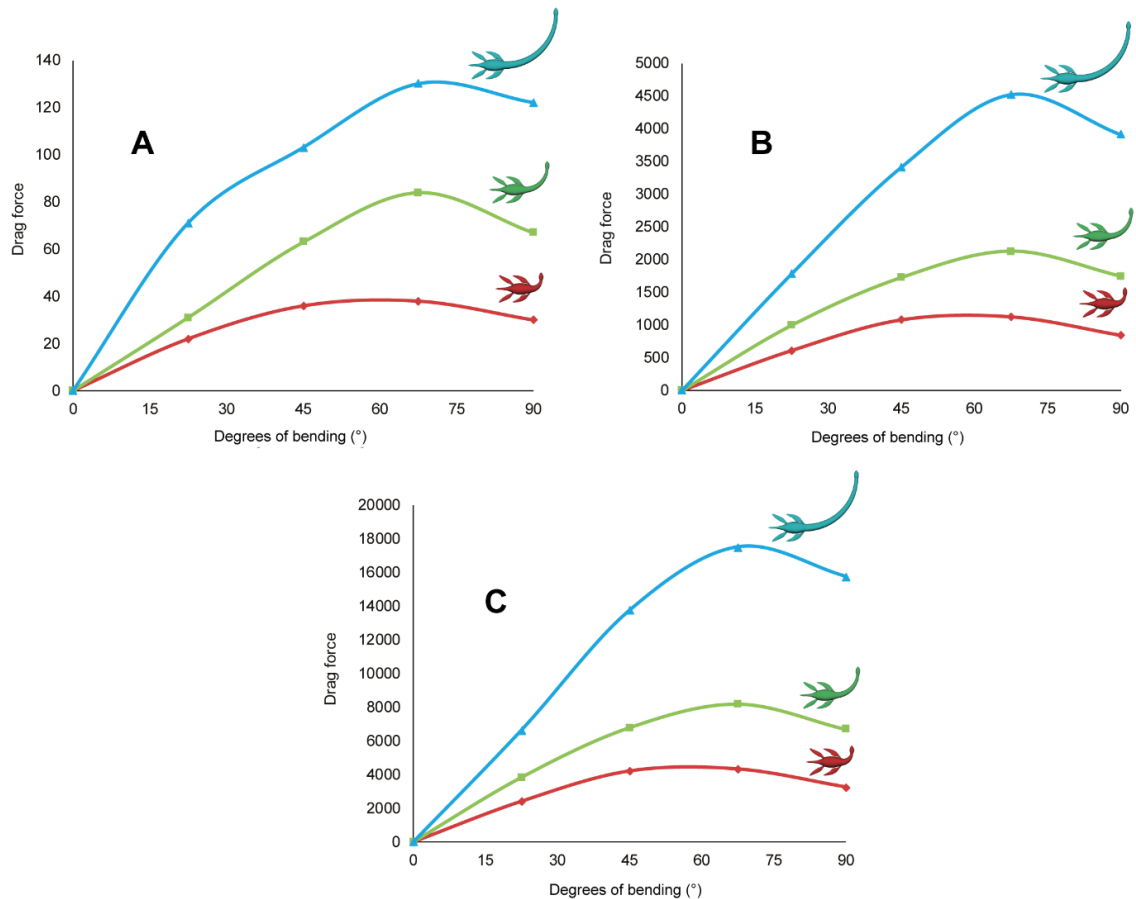


Figure 124: Lateral drag forces with increase in neck bending (0 – 90° with 22.5° interval) for the idealized plesiosaur models with short (red), intermediate (green), and long (blue) necks at (A) 1 m/s, (B) 5 m/s, and (C) 10 m/s. Drag force was calculated towards the left lateral side of the plesiosaur models.

The pressure experienced towards the bent neck in the direction of flow was visibly different for the three neck lengths. The area of increased pressure on the neck covered most of the neck length for the short-necked plesiosaur model and about 2/3 of the intermediate-necked plesiosaur model, whereas for the long-necked plesiosaur model only half of the neck length had an area with increased pressure (Figure 125D). The least pressure was seen around the flippers and the backside of the bended neck for all three plesiosaur models.

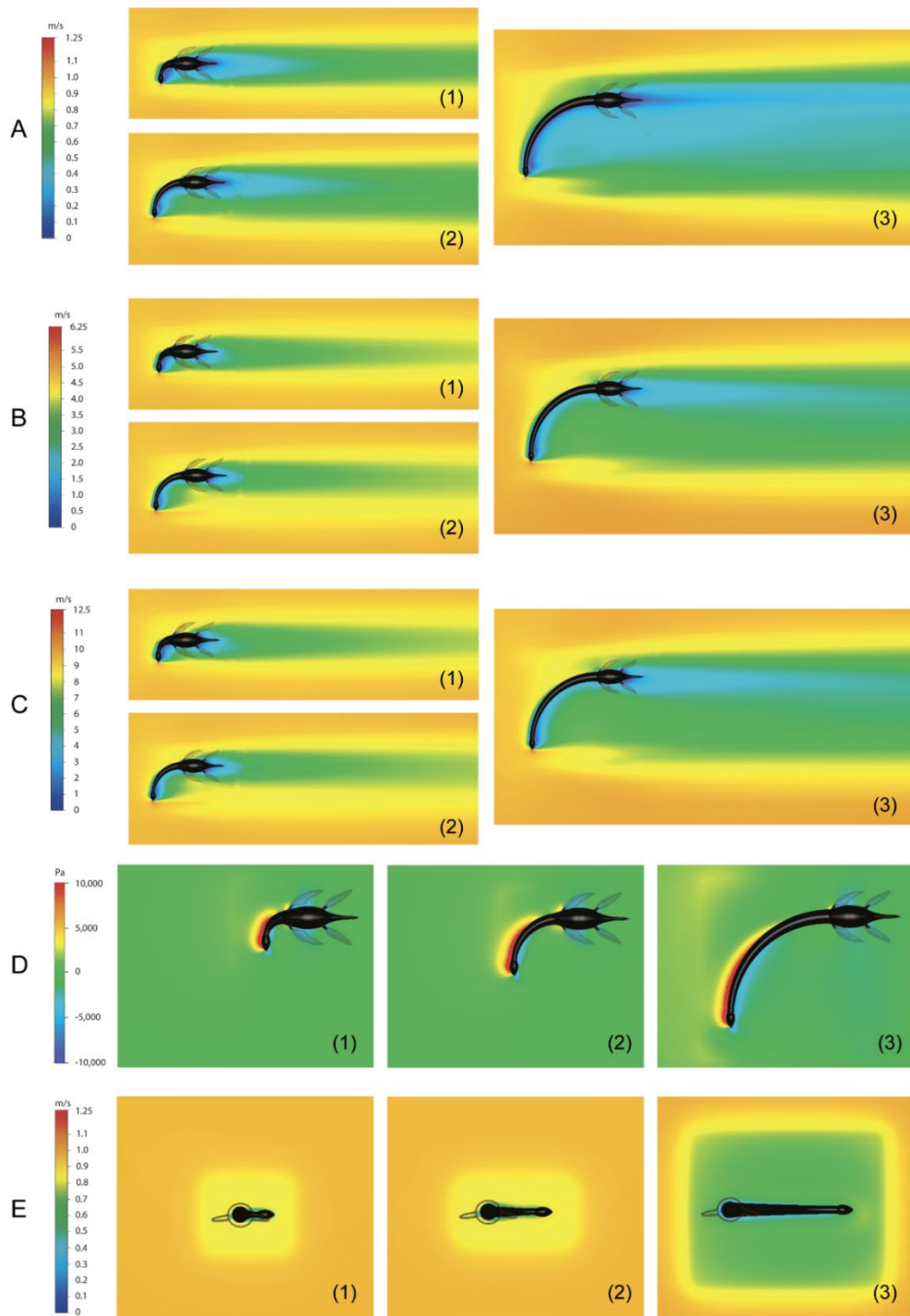


Figure 125: Flow velocity patterns (A-C and E) and pressure distributions created by the water flow for the (1) short-, (2) intermediate, and (3) long-necked idealized plesiosaur models bended at 90°. A) Top view of the flow velocity pattern at 1 m/s, B) top view of the flow velocity pattern at 5 m/s, and C) top view of the flow velocity pattern at 10 m/s. D) Top view of pressure distribution at 5 m/s. E) Frontal view of the flow velocity pattern at the base of the neck at 1m/s (square surrounding the plesiosaur model represent the region of refinement). Notice in A-D that the flippers were located below the planes cut midway through the body, as indicated by the transparent flippers, and in E) the bodies were located behind the planes as indicated by the body-outlines cut at the base of the neck. Flow inlet from left to right in A-D.

6.4 Discussion

6.4.1 Effect of bending location and distribution using primitives

Using a plesiosaur model with a bent neck made of primitives, bending the neck evenly resulted in a large cross-sectional area to the flow, and subsequently a high C_d that would greatly slow down the animal. Bending just the head had almost no effect on the hydrodynamics of the animal but failed to take advantage of the neck.

6.4.2 Effects of bending the neck in idealized plesiosaur models

For the idealized plesiosaur models, the long-necked model experienced higher forces of drag the more the neck was bent, compared with the short- and intermediate-necked models. Extreme bending of the neck would have had major consequences during forward motion at moderate to high velocities. At lower angles of neck bend plesiosaurs with various neck lengths would be able to turn their necks sideways without creating high amounts of drag, which could indicate that plesiosaurs could possibly have fed on prey using a strategy where the neck would move sideways in order to capture prey close to it.

The amount of pressure towards the part of the bent neck exposed by the water flow at 5 m/s was different for the three neck lengths as the area of the neck exposed to the flow was different in size. The short-necked model was exposed to high amounts of pressure towards most of its neck, the intermediate-necked model was exposed to the pressure for about 2/3 of its neck, and the long-necked model only had great amounts of pressure pushing towards the anterior-half of the neck.

6.4.3 Comparing the two studies

The models made of primitives did not include flippers and tail whereas the idealized models did. Therefore, the amount of drag experienced was slightly less in the study using primitives in comparison with the idealized plesiosaur models. Despite this, if we compare the two studies, long-necked plesiosaurs would have experienced higher amounts of drag when turning their necks evenly compared with short-necked forms.

6.4.4 Turning performance

The streamlined bodies of many aquatic vertebrates represent a balance between stability and manoeuvrability in locomotion. This balance has been extensively studied in extant aquatic vertebrates, such as pinnipeds (Fish *et al.*, 2003; Cheneval, 2005; Cheneval *et al.*, 2007; Pierce *et al.*, 2011), cetaceans (Fish, 2002; Maresh *et al.*, 2004; Fish *et al.*, 2008),

turtles (Rivera *et al.*, 2006; Stevens *et al.*, 2018), fish (Drucker and Lauder, 2001; Weihs, 2002), and diving birds (Clifton and Biewener, 2018).

The unique morphology of plesiosaurs makes it difficult to make inferences about stability and manoeuvrability based on extant taxa. Plesiosaurs, as far as we can tell from the fossil record, did not have a fluke to generate thrust or for steering their bodies in the water like cetaceans. If plesiosaurs possessed a fluke, they could have increased their swimming speed significantly by applying thrust through a combination of flippers and fluke. Nor did they seem to possess necks being tucked in, like penguins do in order to avoid creating more drag. Therefore, plesiosaurs might have used a combination of the flippers and head/neck movement to turn their bodies (and eventually necks) slowly to avoid high energy costs.

The influence of turning performance throughout ontogeny has been measured in turtles at three stages of life (hatchling, juvenile and adult) swimming in 90° turns (Stevens *et al.*, 2018), which is also similar to the bending degrees used in the present study. The turtles studied by Stevens *et al.* (2018) showed that turning performance changed relative to mass and length of the turtles, with adults being more stable than smaller turtles (hatchlings and juveniles), but hatchlings having higher agility than juvenile and adults. These seem to indicate that the difference in turning performance is more likely caused by morphology than behaviour of the individual. Thus, comparing results from the present study with the study by Stevens *et al.* (2018) could indicate that relatively small and short-necked plesiosaurs being able to turn faster to avoid predators, whereas relatively large and long-necked plesiosaurs may have needed to turn fast due to the anti-predator effect of large size.

The radius of the space used in turning the neck was greater for the long-necked plesiosaur model and least for the short-necked plesiosaur model, making relatively short-necked plesiosaurs more manoeuvrable compared with longer-necked forms due to the smaller turning path and higher neck flexibility (Walker, 2000). If plesiosaurs used their turning forces from the neck to turn, the long-necked plesiosaurs would have had an advantage over short-necked forms due to the elongated neck. When a plesiosaur turns its neck, it would go from travelling forward, bending its neck and then make the actual turn. As in sea lions (Cheneval *et al.*, 2007), the speed of travel when swimming forward would eventually have to be reduced in order to turn the neck and body due to the forces, torques and momentum involved. From Newton's 2nd Law, we know that force is equal to mass times acceleration. So, speed would ultimately have a great influence on movement and especially for turning

performance. If a plesiosaur wanted to maintain the same speed in a turn, it would have to use more energy (force), eventually increasing the energy costs used for turning its neck (Alexander, 2003). Following from classical mechanics (Newton's 2nd Law), torque is defined as the rotation vector times the force vector, which means that the torque applied to a turning plesiosaur neck is determined by the angle of rotation and the direction and length of the force. Therefore, long-necked plesiosaurs would have to use less force to bend the neck compared with short- and intermediate-necked forms due to the length of the torque (being the longest in the long-necked plesiosaur model), as the angle of rotation is the same for all three plesiosaurs used in the present study. Momentum is equal to mass times velocity (Alexander, 2003), and therefore it is dependent on the amount of water moved when a plesiosaur moves forward or turns (O'Keefe and Carrano, 2005). The necks of plesiosaurs are a relatively small proportion of overall mass, thus long-necked plesiosaurs would have to move only a slightly larger volume of water compared with shorter-necked forms. The energy-cost needed to combat momentum when changing direction would therefore be marginally higher in the long-necked plesiosaurs.

For lateral flexion the maximum osteological RoM found in Chapter 3 was consistent throughout the neck, only different for specific species and not for neck length or the number of cervical vertebrae. This could indicate that the scenario tested in this study with an evenly bended neck would be possible for all plesiosaurs. Thus, the only limiting factor for turning the neck at relatively high velocities laterally would be pressure drag and not the RoM for both short-, intermediate-, and long-necked plesiosaurs. Thus, on the other hand, at a low swimming velocity (close or similar to stationary) the limiting factor would then be RoM.

6.4.5 Plesiosaur ecology

If the neck is the main turning tool the flexibility in a plesiosaur neck it can help determine how fast the animal can manoeuvre when trying to escape predators or search for prey. The average of $\sim 15^\circ$ rotation between vertebrae (with 10 % of centra as intervertebral distance, cf. Chapter 3) would mean that the intervertebral lateral range of motion (RoM) would have to be at around a third (5°) due to restriction of movement caused by neck muscles and ligaments (cf. Chapter 2 – going from clean bones to intact neck) of that to resemble a realistic life-RoM for plesiosaurs. Based on the RoM data from plesiosaur necks (cf. Chapter 3), the neck appears to have been relatively flexible, at least for short-necked forms. Given the drag coefficients calculated here, this seems to have been particularly important when swimming at higher speeds ($>5\text{m/s}$). The higher number of neck vertebrae would logically

create more flexibility in long-necked forms (e.g. elasmosaurids and microcleidids), even if individual intervertebral rotations were small. However, if we compare the centra length in short- and long-necked plesiosaurs (cf. Chapter 3), the relatively long-necked forms would eventually have stiffer necks due to the morphology of the neck vertebrae being longer than high and wide centra (Buchholtz and Schur, 2004; O'Keefe and Hiller, 2006) as well as vertebrae fitting closely together (Kubo *et al.*, 2012). Relatively short-necked forms have more space between each neural spine (Sachs *et al.*, 2016), as well as relatively shorter centra (Smith and Araújo, 2017) creating space for higher flexibility (Evans, 1993). It is highly likely therefore, that plesiosaurs exhibited a range of feeding strategies that varied with neck length and stiffness, and swimming performance (Massare, 1988, 1994; O'Keefe, 2001b; Motani, 2002; Carpenter *et al.*, 2010).

The potential feeding envelope of an animal is affected by its ability to manoeuvre its head via the neck. The feeding envelopes of the three plesiosaur models with respective arc lengths are visualised in Figure 126, showing a clear difference between the three models in both area and arc length. The arc lengths of the three feeding envelopes would be around 2.22 m for the short-necked model, 3.83 m for the intermediate-necked model, and 7.93 m for the long-necked model. Having a relatively long neck would mean that long-necked plesiosaurs would have a larger foraging area compared to shorter-necked forms (Figure 126). Comparing plesiosaurs with extant long-necked vertebrates, such as ostriches, camels and giraffes, the lateral feeding envelope is stretched over a large area, due to the high amount of lateral flexibility at the base of the neck found in ostriches (cf. Chapter 2) and camels and giraffes (Dzemoski and Christian, 2007). This increased feeding envelope would be equally applicable if plesiosaurs acted as floating feeding stations, extending the neck beneath the body (Noè *et al.*, 2017).

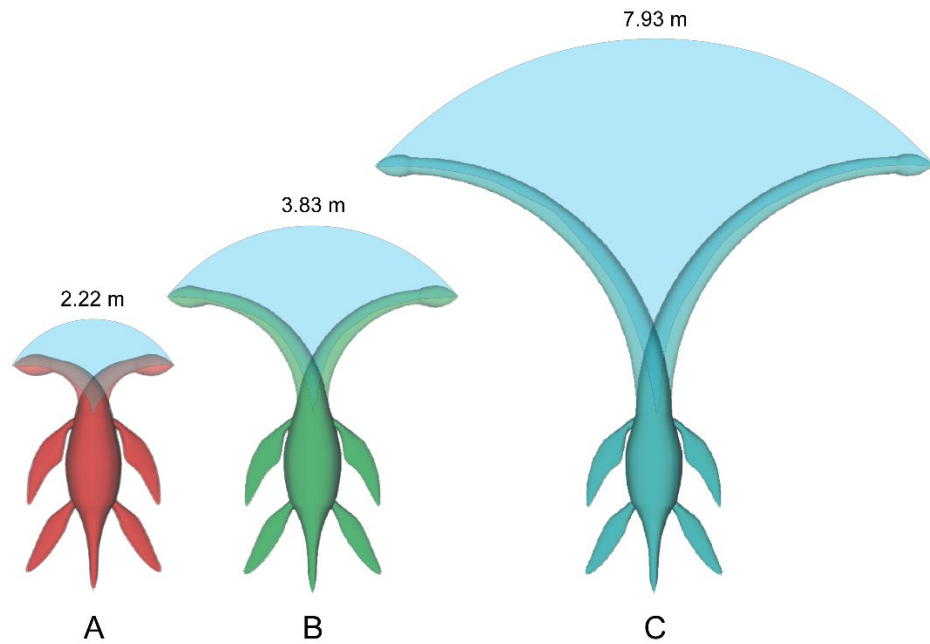


Figure 126: Potential feeding envelopes (blue circle slices) in lateral movements for the short-necked (A), intermediate-necked (B), and long-necked (C) plesiosaur models, including arc length (on top of circles slices) for each plesiosaur model.

Noè et al. (2017) recently stated that manoeuvrability in plesiosaur necks would be affected by drag generated by the length of the neck, which would be greater than the muscular strength in the neck. The high drag forces on the long-necked plesiosaur model with bent neck support this. Due to the physical restrictions in turning the neck, shorter-necked plesiosaurs would likely have turned their necks while moving at relatively higher speeds than long-necked forms. Short-necked plesiosaurs would therefore have been more efficient at grabbing their prey quickly than long-necked plesiosaurs.

6.5 Conclusions

The present study looked at the individual biomechanical implications for plesiosaurs with short, intermediate and long necks having their necks laterally flexed. Using computational fluid dynamics, the study showed an increase of four orders of magnitude in drag from 1 m/s – 10 m/s and three orders of magnitude from 1 m/s – 5 m/s for all three neck lengths. The difference between hunting styles of short-, intermediate-, and long-necked plesiosaurs would potentially have been quite diverse, especially at high speeds, due to the variation in drag experienced by the various plesiosaurs with diverse neck lengths. If plesiosaurs fed at high velocities with bent necks (though not simultaneously turning the body), the physical restrictions (drag forces and torques) of manoeuvrability and large turning radius caused by having a long neck would mean that the degree of bending the neck laterally would not have been as high for long-necked plesiosaurs as it would for short- and intermediate-necked plesiosaurs. Relatively short-necked plesiosaurs would be capable of turning the neck faster compared with long-necked forms due to the difference in neck length. Therefore, the three groups of neck length would most likely have adopted various foraging styles as an adaptation to spend less energy.

Chapter 7 – Discussion

7.1 Summary of preceding chapters

Knowledge about plesiosaurs, long-necked extant taxa (cf. Chapter 1) and fluid dynamics (cf. Chapter 4) were incorporated to introduce the literature for the thesis. The combination of the two chapters formed the base of the studies on range of motion (RoM) in an ostrich neck (cf. Chapter 2) and four plesiosaur necks (cf. Chapter 3). The RoM studies were used to constrain experiments on hydrodynamic implications of forward swimming to study neck elongation and thickness (cf. Chapter 5) and lateral bending performance (cf. Chapter 6) in plesiosaurs. The discussions and conclusions of each study (cf. Chapters 2, 3, 4, 5 and 6) are summarised in the following sections.

7.1.1 Range of motion in ostrich necks

In Chapter 2, cervical vertebrae from the posterior-most half of an ostrich neck were physically and digitally manipulated. Both approaches demonstrated that an intact ostrich neck is three-times less flexible compared to if only the bones of the cervical vertebrae were rotated in pairs of two. The osteological maximum RoM using the cervical vertebrae from the ostrich was measured using 5 % and 10 % of the centra as intervertebral distance between adjacent vertebrae. The study showed that an increase in intervertebral distance from 5 % to 10 % would increase flexibility evenly throughout the posterior-most part of the neck. The study verified a reliable measurement of the osteological maximum RoM in the necks of extinct animals (including plesiosaurs) obtained by inserting a realistic intervertebral distance in the adjacent cervical vertebrae.

7.1.2 Range of motion in plesiosaur necks

Using 5 %, 10 % and 20 % of the cervical centra as intervertebral distance, Chapter 3 showed that the osteological maximum RoM in the neck of four cryptoclidid plesiosaur specimens had almost equal RoM in dorsal, ventral and lateral rotation ($\sim 15^\circ$ per joint between adjacent cervical vertebrae). Neck movement in the four specimens were highest in lateral flexion, similar to what has been found in other studies (Zarnik, 1925; Welles, 1943; Zammit *et al.*, 2008; Nagesan *et al.*, 2018). Measuring RoM using only the cervical vertebrae, in plesiosaurs at least, it seems that if the neural spine is missing, dorsal flexion will increase greatly and not be according to reality. However, if we only want to look at lateral or ventral flexion in the neck, RoM can be obtained using only the centra of the cervical vertebrae. The centra do not affect flexibility no matter the intervertebral distance inserted between the adjacent

vertebrae. The study demonstrated maximum osteological RoM, and soft tissue would have reduced the RoM even more in live plesiosaurs.

7.1.3 Fluid dynamics

Simple objects such as a sphere and cylinder were used in Chapter 4 to explore, through validation experiments using a virtual flume, the relative influence of parameters to change for each simulation setup and to test if the simulation experiments would work. The variables that were found as being of most importance were the mesh size, domain size, domain mesh size, region refinement, and turbulence model. The validation experiments were performed in order to find the best solution giving a more accurate estimate of drag compared with physical flume experiments, and were pre-studies for further use of CFD in later chapters.

7.1.4 The hydrodynamic implications of neck elongation and thickness in plesiosaur necks

In Chapter 5, five 3D models of idealized plesiosaurs having three various neck lengths and two different neck thicknesses demonstrated that it is not disadvantageous in the hydrodynamic performance swimming forward at 1 m/s – 10 m/s for plesiosaurs to possess long necks when held straight. Furthermore, the plesiosaur model possessing a thick neck experienced lower drag forces compared with the thin-necked model at swimming speeds from >5 m/s, suggesting that a thick-necked plesiosaur would spend less energy on swimming forward compared with a thin-necked plesiosaur at high swimming speeds (>5 m/s).

7.1.5 Hydrodynamic effects of plesiosaurs bending the neck during forward motion

Knowledge and results from preceding chapters were combined in Chapter 6. Using two approaches (plesiosaur model made from primitive shapes and idealised plesiosaur models from Chapter 5), rotating the neck evenly in lateral flexion showed that turning radii and drag forces would have been greatest in relatively long-necked plesiosaurs and the least in relatively short-necked plesiosaurs. The study also showed an increase of four orders of magnitude in drag from 1 m/s – 10 m/s and three orders of magnitude from 1 m/s – 5 m/s for all three neck lengths. Relatively short-necked plesiosaurs were more likely to make faster neck turns compared with relatively long-necked forms due to the difference in neck length.

7.2 *Wider implications of this work*

Following the summary of the preceding chapters, further aspects of plesiosaur ecology, evolution and selective pressures of the long neck in plesiosaurs are here discussed.

7.2.1 **Digitisation of specimens**

There are several advantages of digitising the bones from extinct vertebrates. Digitisation of specimens can help museums to display the specimen to the public in 3D on a screen or via 3D prints, which allows 360° view of the bone(s) without displaying the fossils physically. This way the public can interact with the fossils without them breaking, or worst being stolen. The space required for the screens will also save the space that fossils would have required for an exhibition, allowing more room for other activities at the museum. Another good reason to digitise the specimens is the possibility to study the morphology of the bones if they get lost or broken in the future after e.g. a fire or natural disaster. Particularly for neck vertebrae, scientists would also benefit from the digitisation as they would be able to find the right order of the neck by aligning it digitally to get a better overview of all the bones. This could be the case if e.g. the bones have been misplaced during storage in the museum, and would then help sort out what pieces goes with what in broken specimens that need restoration after excavated from the field. An example of this could be C40 in *Muraenosaurus leedsii* (NHMUK R2863) which was studied for Chapter 3. The inaccurate restoration in some pieces of a specimen, like in the case of some of the neck vertebrae used in Chapter 3, will affect measuring the accurate range of motion because of the deformation of the vertebrae. Lastly, digitised models can be used in functional morphology studies such as the once presented within this thesis.

7.2.2 **Plesiosaur palaeobiology**

Throughout the clade of Plesiosauria, range of motion (RoM) seems to have been predominantly lateral flexion, regardless of family, neck length, number and/or morphology of the cervical vertebrae (cf. previous RoM studies and results from Chapter 3), in contrast with what has been stated by Noè et al. (2017). The predominantly lateral flexion would mean that a plesiosaur would probably have accessed a resource on either side of its body, rather than from above or below it (Evans, 1993). Previous studies on RoM in plesiosaurs (Zarnik, 1925; Welles, 1943; Zammit *et al.*, 2008; Nagesan *et al.*, 2018) as well as Chapter 3 have indicated that plesiosaurs had relative high neck flexibility with predominately lateral rotation (maximum osteological RoM of ~15° per cervical with 10 % of the centra length

used as intervertebral distance), unlike what has been suggested by Noè et al. (2017). The high flexibility seems to be due to the number of cervical vertebrae.

The intervertebral distance in plesiosaur necks was investigated in Chapter 3. The 5 % of centra length used was equal to 1.5 mm – 3 mm in the four cryptoclids investigated, with the lowest intervertebral distance being anteriorly and highest posteriorly. The intervertebral distance in articulated plesiosaur specimens have shown to be somewhere between 1 mm – 6 mm (cf. Chapter 3) depending on the species, with an average of 10 % of centra length as the intervertebral distance. As suggested by Sato (2003) the intervertebral distance would be 5 mm in elasmosaurids, which fits within the range found in Chapter 3. However, as elasmosaurids have more rigid and relatively longer cervical vertebrae than other plesiosaur families, the flexibility in the neck would probably be less than what has been found in cryptoclids. The results from Chapter 3 combined with the literature ultimately suggests that plesiosaurs had a wide range of neck flexibility (and intervertebral distances) across the clade, and shows how important range of motion studies are for interpreting ecology of plesiosaurs.

7.2.2.1 Regionalisation of the vertebral column

The vertebral column and the number of cervical vertebrae is derived and determined from two embryonic tissues, the somites and the notochord, where the somites are the first visible sign of segmentation in the embryo (Galis *et al.*, 2006; Böhmer, 2013; Ward *et al.*, 2018). In tetrapods, changes in size and number of vertebrae is especially noticeable in extant lepidosaurs which include scaled reptiles (Soul and Benson, 2017). This change has allowed great variation in function and adaptation of the vertebral column in tetrapods as a whole (Burke *et al.*, 1995; Böhmer *et al.*, 2015). Three underlying mechanisms allow this change: 1) somitogenesis, determining the number of presacral vertebrae formed while the animal is still an embryo, 2) changes in Hox gene expression domains/homeotic effects, shifting between axial regions resulting in various proportions of the cervical or dorsal vertebrae, and 3) variance in growth patterns of somites in the axial region that determines the length of vertebrae (Soul and Benson, 2017).

Vertebral regionalisation has been associated to specific Hox genes (Böhmer, 2013, 2017; Böhmer *et al.*, 2015; Böhmer and Werneburg 2017), and is the division of the vertebral column into separate regions. Using quantitative morphological analyses, like geometric morphometrics (GMM) and character coding, regionalisation of the vertebral column has

been studied in great detail in recent years for various animal groups (Dzemeski and Christian, 2007; Böhmer, 2013, 2017; Ward and Mehta, 2014; Böhmer *et al.*, 2015; O'Gorman and Fernandez 2016; Arnold *et al.*, 2017; Böhmer and Werneburg, 2017; Randau *et al.*, 2017; Soul and Benson, 2017; Jones *et al.*, 2018). The regionalisation of the axial skeleton into cervical, dorsal/thoracic, sacral and caudal parts is a key attribute of amniotes, which reflect an improved specialisation of the vertebral column to perform different functions (Böhmer, 2013). Recent studies have suggested that the cervical region can be divided further into components (Böhmer, 2013, 2017; Böhmer *et al.*, 2015), showing crocodiles possessing four regions (axis, anterior, middle, and posterior), birds five regions (axis, anterior, middle, mid-posterior, and posterior) and mammals three regions (axis, anterior, and posterior) (Böhmer, 2013, 2017; Böhmer *et al.*, 2015, 2018; Arnold *et al.*, 2017). Turtles possess four or five regions depending on the species, although the longstanding debate about the transition from cervical vertebrae to dorsal vertebrae in turtles is still going (Böhmer and Werneburg, 2017). Using geometric morphometrics, the plesiosaur *Muraenosaurus leedsii* have recently been suggested by Glasgow *et al.* (2019) to possess four cervical regions, which is one more region than the basal cervical format. As plesiosaurs show a disparate cervical count between species (O'Keefe, 2002) plesiosaurs might have had different numbers of cervical vertebrae within the regions of the neck.

7.2.2.2 Muscles

In order to reconstruct muscle tissue in an extinct vertebrate, we need general characters of the muscles from extant taxa. Anatomical frameworks for extinct vertebrates have been proposed by several authors, and modern crocodylians and birds provide an extant phylogenetic bracket for soft-tissue reconstructions for the case of archosaurs and pterosaurs (e.g. Gauthier *et al.*, 1988; Witmer, 1995; Snively and Russell, 2007). However, as the morphology of archosaurs and pterosaurs are quite diverse, is it even appropriate to compare extinct vertebrates with modern birds and crocodylians? As we do not have modern analogues to archosaurs, pterosaurs or plesiosaurs, we have to compare with animals that resemble long-necked or aquatic modern animals, and thus birds, aquatic mammals and crocodylians are the only possible candidates we can compare with.

The difficulty to reconstruct muscles surrounding the bones of plesiosaurs, is especially due to the rare soft tissue preservation, unlike what we see in the case of ichthyosaurs (e.g. Martin *et al.*, 1986). There are only two known plesiosaurs specimens which have what has been suggested as preserved soft tissue impressions (cf. Chapter 5). The short-necked plesiosaur

described by Frey et al. (2017) is preserved in ventral view and shows subdermal dorsal skin tissue, especially in the caudal region and between the ribs. Additionally, the long-necked plesiosaur described by Vincent et al. (2017a) is preserved in lateral view and includes dark-coloured structures of different material around the neck, hind flippers and tail. The structures identified as soft tissue around the neck extend ca. 2-3cm from the cervical vertebrae, indicating a thicker neck in the specimen described by Vincent et al. (2017a) compared with the specimen described by Frey et al. (2017). The two specimens discussed by Frey et al. (2017) and Vincent et al. (2017a) have two different neck lengths. Combining the difference in neck thickness among the two plesiosaur specimens with the results from Chapter 5 suggests that short-necked plesiosaurs would have benefited more from slender necks than the long-necked species. The benefit would be due to a hydrodynamic body in the short-necked plesiosaurs, as thin- and long-necked plesiosaurs would have experienced higher amount of drag. Reconstruction of various body parts of plesiosaurs have previously been done, such as for the head (Taylor, 1992) and the shoulder girdle (Araújo and Correia, 2015). However, more plesiosaur specimens including soft tissue around the neck region are required to clarify whether plesiosaurs had thick or thin necks, and how the thickness of the neck would vary among the clade of Plesiosauria.

7.2.2.3 Nutritive foramina and metabolism

On the cervical centra in plesiosaurs, paired foramina (openings) appear all across the clade (Wintrich *et al.*, 2017b), and are positioned on the ventral side of the centrum. This character is noticeable in all four specimens studied for Chapter 3 (Figure 127). The paired foramina have been suggested to be for nutritive purposes allowing blood supply to the interior of the centra through blood vessels (Rothschild and Storrs, 2003). The paired foramina are also observed in modern whales in posterior caudal and fluke vertebrae (Slijper, 1939). The paired foramina would have supplied all the cervical vertebrae in the neck of plesiosaurs with blood, suggesting the possibility of diving in plesiosaurs as seen in modern whales as well as thermoregulation.

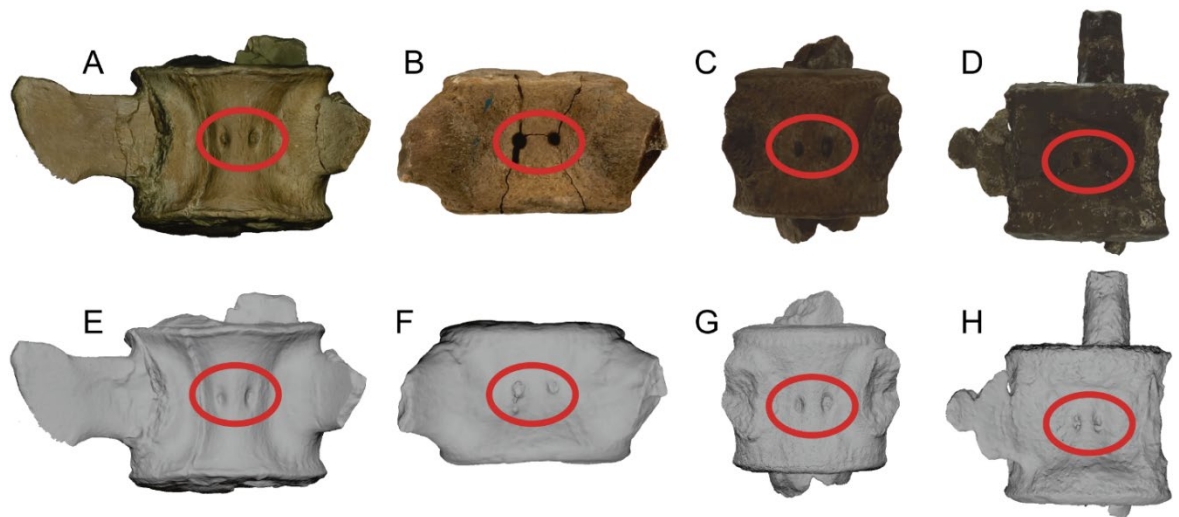


Figure 127: Paired foramina found in the four cryptoclidid specimens used in the study from Chapter 3. Ventral view of the centra in A+E) C26 from OUNHM J. 95000, B+F) C17 from GLAHM V1091, C+G) C21 from NHMUK R2863, and D+H) C21 from PMO 224.248. A-D with texture included, and E-H with texture excluded.

Having relatively large body masses, plesiosaurs would have had high energy costs as active predators (Ferrón *et al.*, 2017). It has been suggested, based on body mass (Ferrón *et al.*, 2017), bone growth rates (Fleischle *et al.*, 2018) and oxygen isotopes (Bernard *et al.*, 2010), that plesiosaurs may have been endothermic. If plesiosaurs were endothermic it would mean they could have generated heat in order to keep a constant body temperature, at about 33°C to 37°C (Bernard *et al.*, 2010). Based on intersegmental arteries interpreted to exist in the neck vertebrae of plesiosaurs and the evidence of decompression syndrome, it has also been suggested that plesiosaurs were deep divers as well as being endothermic as a consequence of the adaptation to a pelagic habitat, foraging across the water column (Rothschild and Storrs, 2003; Wintrich *et al.*, 2017b). Deep diving plesiosaurs would have decreased their travel speed compared to when swimming in shallow waters, as their body temperature would most likely have been extensively affected by the cold water at great depth (Wilson *et al.*, 2017). Having a long neck (increased surface area compared with shorter-necked forms) when foraging at deep waters would therefore only have been possible for short durations of time to avoid high energy costs due to heat loss, which is unlike what is seen in modern aquatic vertebrates that swim at high speeds and possess shorter necks (cetaceans and sea lions) or neck being tucked in (penguins) (Wilson *et al.*, 2017).

7.2.2.4 Hunting and swimming styles

Mobility for migrating animals is essential in e.g. foraging, in order to find a partner, or escaping predators (Herrel *et al.*, 2007). Modern aquatic and aerial animals use a variety of movements in the water or air depending on their morphology. Sea lions are capable of high manoeuvrability (expressed as minimum turning radius) as shown by the turning of their bodies rapidly in order to capture their prey (Fish *et al.*, 2003). Sea lions propel themselves using their forelimbs (English, 1976; Friedman and Leftwich, 2014) and turn by flexing the vertebral column and steer with their pectoral flippers and pelvic limbs (Godfrey, 1985). Cetaceans are generally considered relatively inflexible animals compared with sea lions and fish (Maresh *et al.*, 2004), and generate thrust and turn their bodies using their flukes (acting like a rudder) and flippers (acting as oars), as the flexibility of the body is constrained (Fish, 1993; Long *et al.*, 1997; Segre *et al.*, 2016). Stability factors of dolphins consist of e.g. anterior position of the centre of gravity, similar to an arrow, creating reduced flexibility of the body (Fish and Rohr, 1999; Fish, 2002). To keep at constant speed in a turn, dolphins use their fluke for propulsion and thereby generate momentum (Fish, 2002). Turtles use their paired hydrofoils for propulsion and manoeuvrability (Alexander, 2003), and capture their elusive prey using their relatively long necks, though tucked in while swimming (Herrel *et al.*, 2007). Fish produce thrust using their caudal fin, and their relatively flexible vertebral column as well as paired pectoral fins help them turn (Drucker and Lauder, 2001; Park and Sung, 2018). Birds produce thrust by propelling their wings, but when diving and performing underwater swimming birds use foot propulsion (Lovvorn, 2001; Lovvorn *et al.*, 2001; Lovvorn and Liggins, 2002). However, in semi-aquatic birds, such as penguins, thrust is made by usage of the wings (DeBlois, 2013) and the neck is tucked in to improve hydrodynamic and reduce energy costs (Guinard *et al.*, 2010). Loons are capable of executing tight but slow turns, while diving, compared to other aquatic swimmers, using only their feet (Clifton and Biewener, 2018). Plunge-diving seabirds are generally capable of preventing the neck from bending under compressive loads by contracting the muscles that help to keep the neck straight, stabilising the neck at relatively high speeds (Chang *et al.*, 2016).

The hunting strategies of plesiosaurs have been a matter of debate for almost 200 years (Conybeare, 1824). It seems most likely that plesiosaurs would have propelled themselves through the water by use of their four flippers, as well as providing stability and manoeuvrability (Robinson, 1975; O'Keefe, 2001b; Carpenter *et al.*, 2010; Muscutt *et al.*,

2017). Thus, plesiosaurs might have had a swimming style somewhat similar to a combination of modern sea lions, turtles and penguins (Fish and Lauder, 2017), and the head and long neck of plesiosaurs could have acted as a rudder helping them to perform turning manoeuvres, similar to sea lions. Due to the creation of a high amount of drag in turning the neck, to avoid high forces long-necked plesiosaurs would probably only have turned their necks at low swimming speeds, and shorter-necked forms at a variety of speeds (cf. Chapter 6), which has also been suggested by Noè *et al.* (2017). The relatively high flexibility in the neck could indicate an anterior- or lateral- snapping-ambush hunting style, similar to modern sea lions and river dolphins (Hocking *et al.*, 2017), rather than surprise (cf. Chapter 3), and a thick neck could help save energy while hunting (cf. Chapter 5). Following the predominantly lateral flexion found in plesiosaurs (cf. Chapter 3), short-necked plesiosaurs would likely have been snapping their prey quicker than long-necked plesiosaurs because of the higher flexibility in relatively short-necked forms (cf. Chapter 3). The inner ear of plesiosaurs also seems to justify this. The inner ear helps stabilise the head when moving, and Neenan *et al.* (2017) found that short-necked plesiosaurs had a reduced labyrinth compared to longer-necked forms. The long-necked plesiosaurs would have benefited from larger labyrinths to help stabilise their heads due to the more elongated neck compared with short-necked forms. So, combining the results in the thesis (variation in skull and teeth morphology in plesiosaurs cf. Chapter 1, neck flexibility with and without muscles in ostriches cf. Chapter 2 and without muscles in plesiosaurs cf. Chapter 3, neck elongation and thickness in plesiosaurs cf. Chapter 5, and turning performance cf. Chapter 6), hunting strategies of plesiosaurs would have been different depending on the neck lengths and plesiosaur family.

Buoyancy would also have had an impact on the possible hunting style of plesiosaurs (Henderson, 2006; Henderson and Naish, 2010; Richards, 2011). A study by Henderson (2006) investigated the floating point of plesiosaurs, and found that plesiosaurs would not have been able to maintain straight necks above the water surface due to the unbalanced buoyancy torques acting on the body and the long neck. Especially elasmosaurids, having the longest necks found in plesiosaurs (Carpenter, 1999; O'Keefe and Hiller, 2006; Sachs *et al.*, 2013; O'Gorman and Fernandez, 2016; Otero, 2016; Serratos *et al.*, 2017), would additionally have had the heaviest necks, placing the centre of gravity more anteriorly compared with shorter-necked forms.

Based on teeth and stomach content preserved, elasmosaurids might have benefited more from hunting near the bottom of the ocean (McHenry *et al.*, 2005; Otero *et al.*, 2018), and shorter-necked forms would have the pelagic zone for themselves, suggesting a hunting diversity within the water column within the clade of plesiosaurs. Most plesiosaur specimens have been found in shallow marine environs of less than 200 m (Vincent *et al.*, 2011), and the Cretaceous created an expansion of the Atlantic Ocean and the break-up of the southern Gondwana, allowing open-sea plesiosaurs to spread out over large distances (Bardet *et al.*, 2014).

Henderson (2010) and Richards (2011) also found that high lung deflation would mean that plesiosaurs would sink, and in contrast float if lung deflation was low. Thus, plesiosaurs would likely have used gastroliths to counteract for sinking and being able to have a neutral buoyancy state even with low lung deflation. The use of gastroliths have been reported preserved within the stomach region of many excavated plesiosaurs (Brown, 1904; Shuler, 1950; Darby and Ojakangas, 1980; Martin and Kennedy, 1988; Everhart, 2000; Curimurri and Everhart, 2001), and has previously been hypothesised to help plesiosaur stay afloat and provide hydrostatic control (Taylor, 1994). Although, having a stable, floating equilibrium could have been done without the use of gastroliths according to Henderson (2006). Therefore, it is likely that plesiosaurs used buoyancy as a way of shifting in level within the pelagic zone to allow higher possibilities of capturing prey, compared to if plesiosaurs only hunted in the upper parts of the pelagic zone.

Some cetaceans socialise and hunt in relatively large groups (Baird and Dill, 1996), but whether this was the case for plesiosaurs has not yet been investigated, though they are often portrayed as top predators living somewhat social lives (Buckland, 1903; Shuler, 1950). Plesiosaurs could have benefitted living in a group by strengthening the possibility of capturing prey for each individual, e.g. like swimming in a pod (similar to cetaceans). Furthermore, by travelling in a group, plesiosaurs could have avoided larger aquatic predators such as sharks, mosasaurs and crocodilians (Forrest and Oliver, 2003; Everhart, 2005; Sato *et al.*, 2006; Einarsson *et al.*, 2010; Rothschild *et al.*, 2018). This is similar to what we see in migrating mammals (especially ungulates) and flocking birds. Another way to improve the possibility of capturing prey if living in a pod could have been done by communicating through the water, as we can observe from the echolocation in toothed whales. However, plesiosaurs would have used another way to communicate with fellow individuals as the structure of the plesiosaurian skull does not seem to allow space for the

melon which helps toothed whales to echolocate, and eye vision seem to have been restricted due to their relatively small eyes compared with e.g. ichthyosaurs (Humphries and Ruxton, 2002).

7.2.3 Evolution of the long neck in plesiosaurs – Body proportions

Illustrating the difference between the two plesiosaurian morphotypes through time can help us to identify what factors might have been selective for long necks in many plesiosaur genera. The ratio between neck length and trunk length can, according to Benson and colleagues (2012a), be used as representation for overall body proportions. The distribution of body proportions among plesiosaurs from the earliest to the latest forms have been studied (O'Keefe, 2002; Benson *et al.*, 2012a; Soul and Benson, 2017), and shown that the largest neck:trunk ratio is among elasmosaurids. A study by Knutsen *et al.* (2012a) suggested that, at least for pliosaurids, there is no relationship between limb size and skull or body length at interspecific level, which indicate that for this family the body proportions vary greatly. Neck length of plesiosaurs is diverse, and the longest are seen among plesiosauromorphs (Figure 128 and Figure 129), which include elasmosaurids. Neck variation in elasmosaurids has been suggested to have occurred at three stages during their evolution (Otero, 2016).

The second most dominant body proportion to change in plesiosaurians is the head size, with pliosauromorphs possessing the greatest skull size among plesiosaurians (Storrs, 1993; O'Keefe, 2002). Pliosaur species generally tend to possess shorter body parts (skull, scapula, coracoid, pubis, ischium, humerus and femur) compared with neck length than plesiosaur species (Figure 128). Similarly, pliosaurs have smaller neck length/trunk length ratios compared with plesiosaurs (Figure 129A), and these differences become more pronounced over time (Figure 129B). Late Cretaceous plesiosaurs had necks representing up to four times of their trunk length (Figure 129B), while pliosaurs had skulls up to about the same length as the neck (Figure 128A). Furthermore, Late Cretaceous plesiosaurs had up to 7 m in neck length, whereas pliosaurs only had a maximum neck length of 2 m in their total existence (Figure 129A-D). During the time plesiosaurians existed, the minimum trunk ratios of pliosaurs decreased, and the maximum of the trunk ratios of plesiosaurs increased (Figure 129B). The number of cervical vertebrae found in plesiosaurs are far greater than pliosaurs (cf. Chapter 3), though the number varies equally in neck length/cervical count ratio among plesiosaur and pliosaur species (Figure 129C), and the variation become more pronounced over time (Figure 129D). Ontogeny is known to affect morphology (Sato *et al.*, 2018), and the plesiosaur neck length is observed to vary greatly in juveniles as well as adult specimens,

and increases in both life stages over time (Figure 129E). Adult plesiosaur specimens possess a greater variety of neck length over time compared with adult pliosaur species (Figure 129E). Summarising all the data from Figure 128 and Figure 129, plesiosaurs are observed to evolve longer necks as well as neck:trunk ratios, whereas pliosaurs evolved shorter necks and larger trunks. The diversity seen in the plesiosaurian body size would allow various predatory lifestyles (Ferrón *et al.*, 2017), and the evolution of plesiosaurians as a whole seems to have had frequent and profound convergence in body plans (Fischer *et al.*, 2017) and ratios of anatomical body parts (O'Keefe and Carrano, 2005).

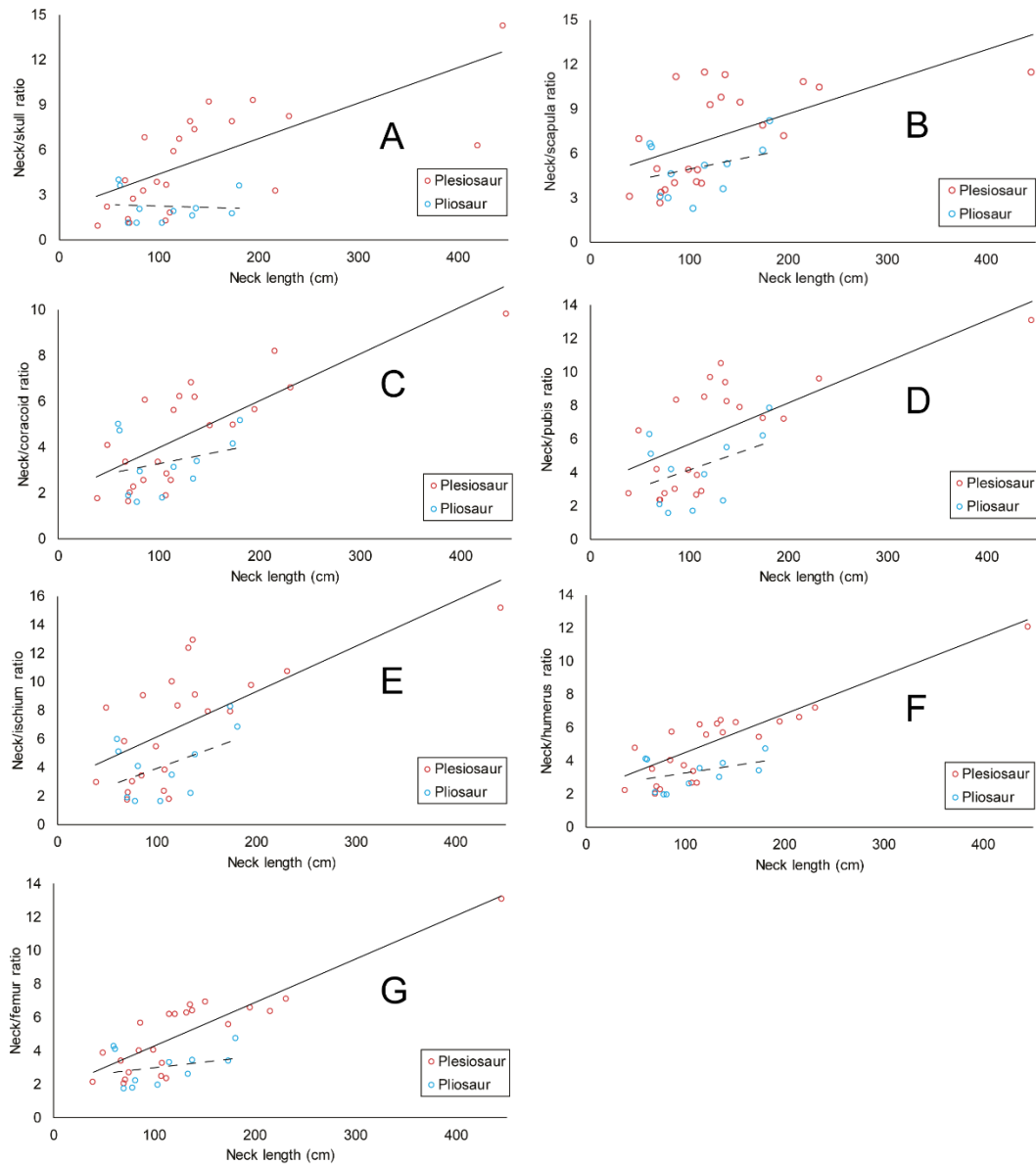


Figure 128: Ratios plotted against neck length (cm). A) Neck length/skull length ratio, B) neck length/scapula length ratio, C) neck length/coracoid length ratio, D) neck length/pubis length ratio, E) neck length/ischium length ratio, F) neck length/humerus length ratio, G) neck length/femur length ratio. Red indicate plesiosaur species and blue indicate pliosaur species. Trend lines indicated by black lines (plesiosaur) and stippled lines (pliosaur). Data from Conybeare (1824), Stutchbury (1846), Owen (1865), Cope (1869), Seeley (1874), Dames (1895), Williston (1904, 1906), Andrews (1910, 1913), Fraas (1910), Smellie (1917), Huene (1923), White (1940), Welles (1943, 1952, 1962), Welles and Bump (1949), Brown (1981), Sciau et al. (1990), Taylor (1992), Cruickshank (1994), Callaway and Nicholls (1997), Bardet et al. (1999), Carpenter (1999), O'Keefe (2001b, 2002, 2004), Cruickshank and Fordyce (2002), Sato (2002, 2003), Buchy et al. (2005), Everhart (2005), Druckenmiller and Russell (2006, 2008b), Sato et al. (2006), Smith (2007), Grossmann (2007), Smith and Dyke (2008), Ketchum and Smith (2010), Smith and Vincent (2010), Vincent and Taquet (2010), Benson et al. (2011, 2012a), Ketchum and Benson (2011), Vincent (2011), Evans (2012), Knutsen et al. (2012b), Kubo et al. (2012), Otero et al. (2014a, 2018), Sachs et al. (2016), Frey et al. (2017), Soul and Benson (2017), Vincent et al. (2017a), and Fischer et al. (2018).

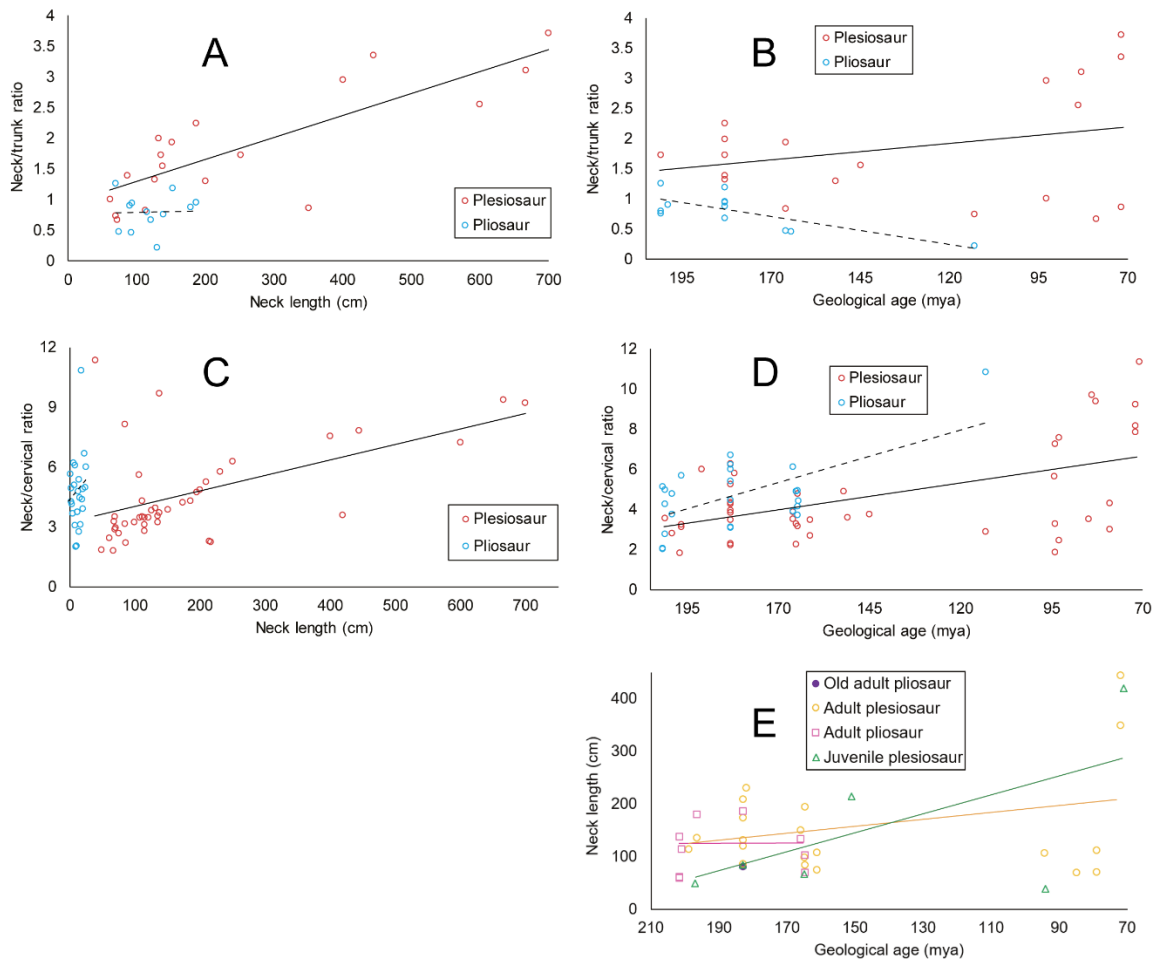


Figure 129: Ratios plotted against neck length (cm) and geological age (Mya). A+B neck length/trunk length ratio, C+D neck length/cervical count ratio, E neck length vs. geological age (Mya) for three life stages. Red indicate plesiosaur species, blue indicate pliosaur species, purple indicate old adult, orange indicate plesiosaur adults, pink indicate pliosaur adults, green indicate juvenile plesiosaurs. Trend lines indicated by black lines (plesiosaur), stippled lines (pliosaur), yellow line (adult plesiosaur), pink line (adult pliosaur), green line (juvenile plesiosaur).

Data from Conybeare (1824), Stutchbury (1846), Owen (1865), Cope (1869), Seeley (1874), Dames (1895), Williston (1904, 1906), Andrews (1910, 1913), Fraas (1910), Smellie (1917), Huene (1923), White (1940), Welles (1943, 1952, 1962), Welles and Bump (1949), Brown (1981), Sciau et al. (1990), Taylor (1992), Cruickshank (1994), Callaway and Nicholls (1997), Bardet et al. (1999), Carpenter (1999), O'Keefe (2001b, 2002, 2004), Cruickshank and Fordyce (2002), Sato (2002, 2003), Buchy et al. (2005), Everhart (2005), Druckenmiller and Russell (2006, 2008b), Sato et al. (2006), Smith (2007), Grossmann (2007), Smith and Dyke (2008), Ketchum and Smith (2010), Smith and Vincent (2010), Vincent and Taquet (2010), Benson et al. (2011, 2012a), Ketchum and Benson (2011), Vincent (2011), Evans (2012), Knutsen et al. (2012b), Kubo et al. (2012), Otero et al. (2014a, 2018), Sachs et al. (2016), Frey et al. (2017), Soul and Benson (2017), Vincent et al. (2017a), and Fischer et al. (2018).

7.3 CFD as a method for studying the hydrodynamics of plesiosaur necks

Computational fluid dynamics (CFD) as a method to study the hydrodynamics of plesiosaur necks is here discussed, by acknowledging the advantages and limitations of the method as well as mentioning other simulation software and experimental methods.

7.3.1 Advantages

For extinct animals, CFD can be useful to investigate aero- or hydrodynamic locomotion cases as well as feeding strategies, breathing or even soft tissue reconstructions (Bourke *et al.*, 2014; Rahman *et al.*, 2015a, 2015b; Darroch *et al.*, 2017; Lautenschlager, 2017; Rahman, 2017; Rahman and Lautenschlager, 2017; Gutarra *et al.*, 2019). In this thesis, CFD was used as a tool to investigate the hydrodynamic implication of the long neck in plesiosaurs, and from this we can predict to some extent how these extinct marine reptiles were moving in the water column millions of years ago. We are also able to test what would be the most reasonable neck thickness in plesiosaurs, and what would make sense in terms of hydrodynamics. By testing a variety of flow velocities based on previously calculated swimming speeds (Massare, 1988, 1994; Motani, 2002), the restrictions and benefits for long-necked plesiosaurs can be measured using CFD giving the drag force calculated by the software. The estimated drag force then allows us to compare with different models of plesiosaurs possessing a variety of neck lengths, thickness and degrees of curvature helping us understand plesiosaur ecology.

Another advantage to use CFD is the capability to share the raw data from the simulations. The reproductivity of the studies is therefore much easier to perform and it is recommended to publish as much of the details of the computational domain, fluid properties, boundary conditions and mesh as possible.

Compared to building a physical flow tank or wind tunnel, CFD is much quicker and simpler in its setup, only requiring a computer, and indeed has replaced flow tanks in many engineering applications (Evans and Harlow, 1957; Harlow and Welch, 1965; Rahman, 2017; Thorne and Blandford, 2017). CFD allows fine, precise and exclusive control over variables (Versteeg and Malalasekera, 1995; Kern and Koumoutsakos, 2006; Kambic *et al.*, 2014), and 3D simulations in general provide qualitative information regarding the kinematics of body motions (Kern and Koumoutsakos, 2006). Although, the computer and software might be expensive, many universities already possess such computers in engineering departments, and it is even possible to loan the capacity remotely from specific

companies and departments around the world. If we instead need to build a physical flow tank, all the materials needed for this construction takes up both great amounts of physical space as well as having an economic consequence following the construction of the setup. Additionally, the physical scale can be added to CFD and allows to study meter scale objects (like plesiosaurs) which would be effectively impossible to build with flume tanks. Thus, CFD can add a lot of value to science and engineering, by assembling data for unknown scenarios before they even occur or by predicting scenarios we think might occur.

7.3.2 Limitations

One of the major downsides to CFD is that the simulations made by the software only give us a predicted scenario and not reality itself. Therefore, depending on the study and questions needed to be answered, CFD (and similarly for physical flow tank experiments) only gives us a modelled indication of how reality could be. However, if the use of both CFD and physical flow tank experiments are performed well, we can, and should, trust the results, like the case of aeroplanes.

7.3.3 Other simulation software and experimental methods

The simulation software used in this thesis was Autodesk Simulation CFD, being among a wide range of CFD software available today, such as e.g. Abaqus, Ansys CFX, Ansys Fluent CFD, Strand 7, Adams, Opensim, OpenFOAM, Gaitsym, COMSOL (Davies *et al.*, 2017), and FlowLab (Munson *et al.*, 2009). The cost and level of expertise in order to use the software is the main difference for the various software. Autodesk Simulation CFD has a rather simple design and is user-friendly, as well as being free of use as long as the user is connected with an educational institution. In contrast, opensource CFD software is more complex than Autodesk Simulation CFD, as the level of building the codes involved is higher. In e.g. Autodesk Simulation CFD there are several commercial CFD codes employed into the software, making the process of solving much easier for people not familiar with coding, compared with opensource software. Ansys and COMSOL are very costly though more or less as simple in design as Autodesk Simulation CFD.

Unlike CFD, which can be thought of as a numerical experiment (Munson *et al.*, 2009), some studies might need a physical experiment by means of flow tanks to solve a problem. The difference between the two has previously been tested (Rahman and Lautenschlager, 2017). Specifically, in the case plesiosaur flipper locomotion, virtual simulations and physical experiments have both been applied previously (Muscutt *et al.*, 2017; Liu *et al.*, 2015).

Another experimental tool to visualise fluid flow is Digital Particle Image Velocimetry (DPIV), which is useful in association with e.g. animal movement. DPIV employs particles suspended in air or water that are illuminated by a laser light sheet and recorded with a high-speed video camera, and this way software tracks particle movement across a specified number of video frames, generating patterns of fluid flow through time (Ryerson and Schwenk, 2012). For most cases CFD appears steadier than DPIV, as parameters can be controlled more easily (Versteeg and Malalasekera, 1995; Munson *et al.*, 2009).

Chapter 8 - Conclusions and further work

8.1 Conclusions and significance of work undertaken

1. The effects of soft tissue on osteological range of motion were quantified. An ostrich neck complete with soft tissue is roughly three-times less flexible compared to only using the bones.
2. Plesiosaurs possessed a relatively high neck flexibility, mainly due to the number and morphology of successive cervical vertebrae. Dorsal flexion was restricted by the neural spine and ventral flexion by the cervical centra.
3. Lateral flexion appears to be predominant in plesiosaurs, which seems to be the case for most plesiosaur families.
4. Maximum osteological range of motion in the neck region of relatively long-necked plesiosaurs increased with increase in intervertebral distance. Soft tissue would have reduced range of motion more in live plesiosaurs.
5. Long necks held straight do not increase drag during forward motion. Swimming at 1 – 10 m/s pressure drag is predominant over friction drag for both short- and long-necked plesiosaurs.
6. Thick necks experience less drag compared with thin necks, but only at high velocities. Broader necks reduce the surface area normal or near normal to flow direction, helping to reduce drag. This suggests plesiosaurs swimming at high velocities would have been under selective pressure to evolve a thicker neck.
7. Bending a plesiosaur neck laterally, turning radius and drag would have been greatest in long-necked plesiosaurs and the least in short-necked plesiosaurs. Therefore, it was likely that short-necked plesiosaurs could turn the neck faster and with shorter turning radius than long-necked forms.

8.2 Future work

8.2.1 FEA

Finite Element Analysis (FEA) could be used to study plesiosaur necks, by means of bending stresses on the neck to explore further on hydrodynamics, turning performance and strength of the neck. This could be done both in 2D and 3D to test difference between them. Similar studies have been performed for plesiosaur skulls (Araújo and Polcyn, 2013; Foffa *et al.*, 2014).

8.2.2 Geometric morphometrics

The use of geometric morphometrics (GMM) could help explore shape changes throughout ontogeny in plesiosaurs. This way it would be possible to test for any visible changes in the neck of juvenile and adult specimens and observe if there would any significant changes over time between life stages. Regionalisation of the plesiosaurian neck could also be explored with the use of GMM, to look for changes within the neck in various species from different families.

8.2.3 Improvement of models

The models used in this thesis could be further improved, to test what the hydrodynamic implications would be with change in the surface of the plesiosaur models, by including a tail fin, changing of trunk to counteract for implications caused by volume and density change, or change of head size to include more pliosaur-like models. The results from Chapter 5 could be expanded by testing neck thickness for a short and long-neck plesiosaur model to look for trends between neck lengths with increase or decrease in the neck thickness. The transition from neck to body (especially the attachment of flippers) could also be changed to see what the hydrodynamic implications would be if the transition was more or less smooth compared with the models used in Chapter 5 and 6. Furthermore, calculation of e.g. cost-benefit analyses of bent necks would help to answer further questions regarding the biomechanical effect of turning plesiosaurs and the ecology of plesiosaurs in general.

8.2.4 Free body motion in CFD

The usage of free body motion in Autodesk Simulation CFD could be explored to test turning moments of different parts of the neck during turning motion. The study would be similar to the experiment from Chapter 6 within this thesis where bending distribution and location varies. The results from such a study can add valuable knowledge on turning performance during forward motion in plesiosaurs, and ultimately on plesiosaur ecology.

References

- Alexander, R. M. 1967. *Functional Design in Fishes*. London, Hutchinson, 160 pp.
- Alexander, R. M. 1989. *Dynamics of Dinosaurs and other Extinct Giants*. Columbia University Press, New York, 167 pp.
- Alexander, R. M. 2003. *Principles of Animal Locomotion*. Princeton University Press, Princeton and Oxford, 385 pp.
- Anderson, P. S., Bright, J. A., Gill, P. G., Palmer, C. and Rayfield, E. J. 2012. Models in palaeontological functional analysis. *Biology Letters*, 8(1), pp. 119-22.
- Andrews, C. W. 1910. *A Descriptive Catalogue of the Marine Reptiles of the Oxford Clay: Based on the Leeds Collection in the British Museum (Natural History)*. Order of the trustees, London, 173 pp.
- Andrews, C. W. 1913. *A Descriptive Catalogue of the Marine Reptiles of the Oxford Clay*. British Museum of Natural History, London, 292 pp.
- Anquetin, J., Tong, H. and Claude, J. 2017. A Jurassic stem pleurodire sheds light on the functional origin of neck retraction in turtles. *Scientific Reports*, 7, pp. 1-10.
- Apostolaki, N. E., Rayfield, E. J. and Barrett, P. M. 2015. Osteological and soft-tissue evidence for pneumatization in the cervical column of the ostrich (*Struthio camelus*) and observations on the vertebral columns of non-volant, semi-volant and semi-aquatic birds. *PLoS One*, 10(12), pp. 1-39.
- Araújo, R. and Correia, F. 2015. Soft-tissue anatomy of the plesiosaur pectoral girdle inferred from basal Eosauroptrygia taxa and the extant phylogenetic bracket. *Palaeontologia Electronica*, 18(1), pp. 1-32.
- Araújo, R. and Polcyn, M. J. 2013. A biomechanical analysis of the skull and adductor chamber muscles in the Late Cretaceous *Plesiosaur Libonectes*. *Palaeontologia Electronica*, 16(2), pp. 1-25.
- Arnold, P., Esteve-Altava, B. and Fischer, M. S. 2017. Musculoskeletal networks reveal topological disparity in mammalian neck evolution. *BMC Evolutionary Biology*, 17(251), pp. 1-18.
- Autodesk 2018a. *Learning Guide*. [online]. Available at: <https://knowledge.autodesk.com/support/cfd/learn-explore/caas/CloudHelp/cloudhelp/2014/ENU/SimCFD/files/GUID-A124B012-DFE2-4A01-8815-24CA229DE852-htm.html> [Accessed 7th Dec, 2018].

- Autodesk 2018b. *User's Guide*. [online]. Available at:
<https://knowledge.autodesk.com/support/cfd/learn-explore/caas/CloudHelp/cloudhelp/2014/ENU/SimCFD/files/GUID-B3B67A19-0CF3-424B-9C77-F474453C7C1B-htm.html> [Accessed 7th Dec, 2018].
- Baird, R. W. and Dill, L. M. 1996. Ecological and social determinants of group size in transient killer whales. *Behavioral Ecology*, 7(4), pp. 408-416.
- Bakker, R. T. 1993. Plesiosaur extinction cycles - events that mark the beginning, middle, and end of the Cretaceous. *Geological Association of Canada, Special Paper*, 39, pp. 641-664.
- Bardet, N., Falconnet, J., Fischer, V., Houssaye, A., Jouve, S., Suberbiola, X. P., Pérez-García, A., Rage, J. C. and Vincent, P. 2014. Mesozoic marine reptile palaeobiogeography in response to drifting plates. *Gondwana Research*, 26(3-4), pp. 869-887.
- Bardet, N., Godefroit, P. and Sciau, J. 1999. A new elasmosaurid plesiosaur from the Lower Jurassic of Southern France. *Palaeontology*, 42 (5), pp. 927-952.
- Bardet, N., Suberbiola, X. P. and Jalil, N. 2003. A new polycotyloid plesiosaur from the Late Cretaceous (Turonian) of Morocco. *Comptes Rendus Palevol*, 2(5), pp. 307-315.
- Bates, K. T., Benson, R. B. J. and Falkingham, P. L. 2012. A computational analysis of locomotor anatomy and body mass evolution in Allosauroidea (Dinosauria: Theropoda). *Paleobiology*, 38(3), pp. 486-507.
- Bates, K. T., Falkingham, P. L., Breithaupt, B. H., Hodgetts, D., Sellers, W. I. and Manning, P. L. 2009a. How big was 'Big Al'? Quantifying the effect of soft tissue and osteological unknowns on mass predictions for *Allosaurus* (Dinosauria:Theropoda). *Palaeontologia Electronica*, 12(3), pp. 1-33.
- Bates, K. T., Manning, P. L., Hodgetts, D. and Sellers, W. I. 2009b. Estimating mass properties of dinosaurs using laser imaging and 3D computer modelling. *PLoS ONE*, 4(2), pp. 1-26.
- Bateson, W. 1894. *Materials for the study of variation: treated with especial regard to discontinuity in the origin of species*. Macmillan and Co, London, 615 pp.
- Benson, R. B. 2013. Marine Reptiles. In: Grzimek, B., MacLeod, N., Archibald, J. B., and Levin, P. S. (eds.) *Grzimek's Animal Life Encyclopedia*. Gale/Cengage Learning, Detroit, pp. 267-279.

- Benson, R. B. and Druckenmiller, P. S. 2014. Faunal turnover of marine tetrapods during the Jurassic-Cretaceous transition. *Biological Reviews*, 89(1), pp. 1-23.
- Benson, R. B., Evans, M. and Druckenmiller, P. S. 2012a. High diversity, low disparity and small body size in plesiosaurs (Reptilia, Sauropterygia) from the Triassic-Jurassic boundary. *PLoS One*, 7(3), e31838.
- Benson, R. B., Ketchum, H. F., Noè, L. F. and Gómez-Pérez, M. 2011. New information on *Hauffiosaurus* (Reptilia, Plesiosauria) based on a new species from the Alum Shale Member (Lower Toarcian: Lower Jurassic) of Yorkshire, UK. *Palaeontology*, 54(3), pp. 547-571.
- Benson, R. B. J., Ketchum, H. F., Naish, D. and Turner, L. E. 2012b. A new leptocleidid (Sauropterygia, Plesiosauria) from the Vectis Formation (Early Barremian–Early Aptian; Early Cretaceous) of the Isle of Wight and the evolution of Leptocleididae, a controversial clade. *Journal of Systematic Palaeontology*, 11(2), pp. 233-250.
- Benton, M. J. and Taylor, M. A. 1984. Marine reptiles from the Upper Lias (Lower Toarcian, Lower Jurassic) of the Yorkshire coast. *Proceedings of the Yorkshire Geological Society*, 44(4), pp. 399-429.
- Berezin, A. Y. 2011. A new plesiosaur of the family Aristonectidae from the Early Cretaceous of the Center of the Russian Platform. *Paleontological Journal*, 45(6), pp. 648-660.
- Berta, A. and Ray, C. E. 1990. Skeletal morphology and locomotor capabilities of the archaic pinniped *Enaliarctos mealsi*. *Journal of Vertebrate Paleontology*, 10(2), pp. 141-157.
- Borazjani, I. and Sotiropoulos, F. 2010. On the role of form and kinematics on the hydrodynamics of self-propelled body/caudal fin swimming. *Journal of Experimental Biology*, 213(1), pp. 89-107.
- Boumans, M. L. L. M., Krings, M. and Wagner, H. 2015. Muscular arrangement and muscle attachment sites in the cervical region of the American barn owl (*Tyto furcata pratincola*). *PLoS One*, 10(7), pp. 1-29.
- Bourke, J. M., Porter, W. M. R., Ridgely, R. C., Lyson, T. R., Schachner, E. R., Bell, P. R. and Witmer, L. M. 2014. Breathing life into dinosaurs: Tackling challenges of soft-tissue restoration and nasal airflow in extinct species. *The Anatomical Record*, 297, pp. 2148-2186.

- Bradney, D. R., Davidson, A., Evans, S. P., Wueringer, B. E., Morgan, D. L. and Clausen, P. D. 2016. Sawfishes stealth revealed using computational fluid dynamics. *Journal of Fish Biology*, 90(4), pp. 1584-1596.
- Brainerd, E. L., Baier, D. B., Gatesy, S. M., Hedrick, T. L., Metzger, K. A., Gilbert, S. L. and Crisco, J. J. 2010. X-Ray reconstruction of moving morphology (XROMM): Precision, accuracy and applications in comparative biomechanics research. *Journal of Experimental Zoology*, 313A, pp. 1-18.
- Brown, B. 1904. Stomach stones and food of plesiosaurs. *Science*, 20(501), pp. 184-185.
- Brown, D., Vincent, P. and Bardet, N. 2013. Osteological redescription of the skull of *Microcleidus Homalospondylus* (Sauropterygia, Plesiosauria) from the Lower Jurassic of England. *Journal of paleontology*, 87(4), pp. 537-549.
- Brown, D. S. 1981. The English Upper Jurassic Plesiosauroidea (Reptilia) and a review of the phylogeny and classification of the Plesiosauria. *Bulletin of the British Museum of Natural History, Geology Series*, 35, pp. 253-347.
- Brown, D. S. and Cruickshank, A. R. I. 1994. The skull of the Callovian plesiosaur *Cryptoclidus eurymerus*, and the Sauropterygian cheek. *Palaeontology*, 37(4), pp. 941-953.
- Brown, D. S., Milner, A. C. and Taylor, M. A. 1986. New material of the plesiosaur *Kimmerosaurus langhami* Brown from the Kimmeridge Clay of Dorset. *Bulletin of the British Museum, Natural History. Geology*, 40(5), pp. 225-234.
- Buchholtz, E. A. and Schur, S. A. 2004. Vertebral osteology in Delphinidae (Cetacea). *Zoological Journal of the Linnean Society*, 140(3), pp. 383-401.
- Buchholtz, E. A. and Stepien, C. C. 2009. Anatomical transformation in mammals: developmental origin of aberrant cervical anatomy in tree sloths. *Evolution & development*, 11(1), pp. 69-79.
- Buchy, M. C., Métayer, F. and Frey, E. 2005. Osteology of *Manemergus anguirostris* n. gen. et so., a new plesiosaur (Reptilia, Sauropterygia) from the Upper Cretaceous of Morocco. *Palaeontographica Abteilung A*, 272, pp. 97-120.
- Buckland, F. T. 1903. *Curiosities of Natural History*. Macmillan and Co., New York, 411 pp.
- Burke, A. C., Nelson, C. E., Morgan, B. A. and Tabin, C. 1995. Hox genes and the evolution of vertebrae axial morphology. *Development*, 121(2), pp. 333-346.

- Böhmer, C. 2013. Correlation between vertebral Hox code and vertebral morphology in archosaurs: implications for vertebral evolution in sauropodomorph dinosaurs. MSc. thesis, Ludwig-Maximilians-Universität, München.
- Böhmer, C. 2017. Correlation between Hox code and vertebral morphology in the mouse: towards a universal model for Synapsida. *Zoological Letters*, 3(8), pp. 1-11.
- Böhmer, C., Amson, E., Arnold, P., Van Heteren, A. H. and Nyakatura, J. A. 2018. Homeotic transformations reflect departure from the mammalian ‘rule of seven’ cervical vertebrae in sloths: inferences on the Hox code and morphological modularity of the mammalian neck. *BMC Evolutionary Biology*, 18(84), pp. 1-11.
- Böhmer, C., Rauhaut, O. W. M. and Wörheide, G. 2015. Correlation between Hox code and vertebral morphology in archosaurs. *Proceedings of the Royal Society B*, 282(1810), 20150077.
- Böhmer, C. and Werneburg, I. 2017. Deep time perspective on turtle neck evolution: chasing the Hox code by vertebral morphology. *Scientific Reports*, 7(1), 8939.
- Caldwell, M. W. 2002. From fins to limbs to fins: Limb evolution in fossil marine reptiles. *American Journal of Medical Genetics*, 112(3), pp. 236-249.
- Callaway, J. M. and Nicholls, E. L. 1997. *Ancient Marine Reptiles*. Academic Press, San Diego, California, 501 pp.
- Carpenter, K. 1999. Revision of North American elasmosaurs from the Cretaceous of the Western Interior. *Paludicola*, 2(2), pp. 148-173.
- Carpenter, K., Sanders, F., Reed, B., Reed, J. and Larson, P. 2010. Plesiosaur swimming as interpreted from skeletal analysis and experimental results. *Transactions of the Kansas Academy of Science*, 113(1/2), pp. 1-34.
- Cerda, I. A. and Salgado, L. 2008. Gastrolitos en un plesiosaurio (Sauropterygia) de la Formación Allen (Campaniano-Maastrichtiano), provincial de Río Negro, Patagonia, Argentina. *Ameghiniana*, 45(3), pp. 529-536.
- Chang, B., Croson, M., Straker, L., Gart, S., Dove, C., Gerwin, J. and Jung, S. 2016. How seabirds plunge-dive without injuries. *Proceedings of the National Academy of Sciences*, 113(43), 12006-12011.
- Chatterjee, S. and Small, B. J. 1989. New plesiosaurs from the Upper Cretaceous of Antarctica. *Geological Society, London, Special Publications*, 47(1), pp. 197-215.
- Cheneval, O. 2005. Biomechanics of turning manoeuvres in steller sea lions (*Eumetopias jubatus*). MSc. thesis, University of British Columbia, Canada.

- Cheneval, O., Blake, R. W., Trites, A. W. and Chan, K. H. S. 2007. Turning maneuvers in Steller sea lions (*Eumatopias jubatus*). *Marine mammal science*, **23**(1), pp. 94-109.
- Cheng, Y., Wu, X. and Ju, Q. 2004. Triassic marine reptiles gave birth to live young. *Nature*, 432, pp. 383-386.
- Christian, A. and Dzemski, G. 2007. Reconstruction of the cervical skeleton posture of *Brachiosaurus brancai* Janensch, 1914 by an analysis of the intervertebral stress along the neck and a comparison with the results of different approaches. *Fossil Record*, 10(1), pp. 38-49.
- Clifton, G. T. and Biewener, A. A. 2018. Foot-propelled swimming kinematics and turning strategies in common loons. *The Journal of Experimental Biology*, 221(19), jeb168831.
- Clothier, C. R. 1950. A key to some souther california fishes: based on vertebral characters. *Fish Bulletin, California Department of Natural Resources, Diverse Fish and Game*, 79, pp. 1-83.
- Cobley, M. J., Rayfield, E. J. and Barrett, P. M. 2013. Inter-vertebral flexibility of the ostrich neck: implications for estimating sauropod neck flexibility. *PLoS One*, 8(8), e72187.
- Collin, R. and Janis, C. M. 1997. Morphological constraints on tetrapod feeding mechanisms: why were there no suspension-feeding marine reptiles? In: Callaway, J. M. and Nicholls, E. L. (eds). *Ancient Marine Reptiles*. Academic Press, San Diego, California, pp. 451-466.
- Conybeare, W. D. 1824. On the Discovery of an almost perfect Skeleton of the *Plesiosaurus*. *Transactions of the Geological Society of London*, 2(2), pp. 381-390.
- Cope, E. D. 1869. *Synopsis of the Extinct Batrachia and Reptilia of North America*. Transactions of the American Philosophical Society, Philadelphia, USA, 253 pp.
- Cope, E. D. 1872. On a species of Clidastes and on Plesiosaurus gulo Cope. *Proceedings of the Academy of Natural Sciences of Philadelphia*, 24, pp. 127-129.
- Cruickshank, A. R. I. 1994. A juvenile plesiosaur (Plesiosauria: Reptilia) from the Lower Lias (Hettangian: Lower Jurassic) of Lyme Regis, England: a pliosauroid-plesiosauroid intermediate? *Zoological Journal of the Linnean Society*, 112, pp. 151-178.
- Cruickshank, A. R. I. and Fordyce, R. E. 2002. A new marine reptile (Sauropterygia) from New Zealand: Further evidence for a Late Cretaceous Austral radiation of Cryptoclidid plesiosaurs. *The Palaeontological Association*, 45(3), pp. 557-575.

- Cruickshank, A. R. I., Small, P. G. and Taylor, M. A. 1991. Dorsal nostrils and hydrodynamically driven underwater olfaction in plesiosaurs. *Nature*, 352, pp. 62-64.
- Curimurri, D. J. and Everhart, M. J. 2001. An elasmosaur with stomach contents and gastroliths from the Pierre Shale (Late Cretaceous) of Kansas. *Transactions of the Kansas Academy of Science*, 104(3), pp. 129-143.
- Dames, W. 1895. Die Plesiosaurier der Süddeutschen Liasformation. *Abhandlungen der Königlich Preussischen Akademie der Wissenschaften zu Berlin 1985*, pp. 1-81.
- Darby, D. G. and Ojakangas, R. W. 1980. Gastroliths from an Upper Cretaceous plesiosaur. *Journal of Paleontology*, 54(3), pp. 548-556.
- Darroch, S. A. F., Rahman, I. A., Gibson, B., Racicot, R. A. and Laflamme, M. 2017. Inference of facultative mobility in the enigmatic Ediacaran organism *Parvancorina*. *Biology Letters*, 13, 20170033.
- Davenport, J., Fraher, J., Fitzgerald, E., McLaughlin, P., Doyle, T., Harman, L. and Cuffe, T. 2009. Fat head: an analysis of head and neck insulation in the leatherback turtle (*Dermochelys coriacea*). *The Journal of Experimental Biology*, 212, pp. 2753-2759.
- Davies, T. G., Rahman, I. A., Lautenschlager, S., Cunningham, J. A., Asher, R. J., Barrett, P. M., Bates, K. T., Bengtson, S., Benson, R. B., Boyer, D. M., Braga, J., Bright, J. A., Claessens, L. P. A. M., Cox, P. G., Dong, X., Evans, A. R., Falkingham, P. L., Friedman, M., Garwood, R. J., Goswami, A., Hutchinson, J. R., Jeffery, N. S., Johanson, Z., Lebrun, R., Martínez-Pérez, C., Marugán-Lobón, J., O'Higgins, P. M., Metscher, B., Orliac, M., Rowe, T. B., Rücklin, M., Sánchez-Villagra, M. R., Shubin, N. H., Smith, S. Y., Starck, J. M., Stringer, C., Summers, A. P., Sutton, M. D., Walsh, S. A., Weisbecker, V., Witmer, L. M., Wroe, S., Yin, Z., Rayfield, E. J. and Donoghue, P. C. J. 2017. Open data and digital morphology. *Proceedings of the Royal Society B: Biological Sciences*, 284(1852), 20170194.
- Deblois, M. C. 2013. Quantitative Reconstruction and Two-Dimensional, Steady Flow Hydrodynamics of the Plesiosaur Flipper. MSc. thesis, Marshall University, USA.
- Druckenmiller, P. S. 2002. Osteology of a new plesiosaur from the lower Cretaceous (Albian) Thermopolis Shale of Montana. *Journal of Vertebrate Paleontology*, 22(1), pp. 29-42.
- Druckenmiller, P. S. and Knutsen, E. M. 2012. Phylogenetic relationships of Upper Jurassic (Middle Volgian) plesiosaurians (Reptilia: Sauropterygia) from the

- Agardhfjellet Formation of central Spitsbergen, Norway. *Norwegian Journal of Geology*, 92, pp. 1-8.
- Druckenmiller, P. S. and Russell, A. P. 2006. A new elasmosaurid plesiosaur (Reptilia: Sauropterygia) from the Lower Cretaceous Clearwater Formation, Northeastern Alberta, Canada. *Paludicola*, 5(4), pp. 184-199.
- Druckenmiller, P. S. and Russell, A. P. 2008a. A phylogeny of Plesiosauria (Sauropterygia) and its bearing on the systematic status of *Leptocleidus* Andrews, 1922. *Zootaxa*, 1863, pp. 1-120.
- Druckenmiller, P. S. and Russell, A. P. 2008b. Skeletal anatomy of an exceptionally complete specimen of a new genus of plesiosaur from the Early Cretaceous (Early Albian) of northeastern Alberta, Canada. *Palaeontographica Abteilung A Band 283 Lieferung 1-3*, pp. 1-33.
- Drucker, E. G. and Lauder, G. V. 2001. Wake dynamics and fluid forces of turning maneuvers in Sunfish. *The Journal of Experimental Biology*, 204, pp. 431-442.
- Dudley, P. N., Bonazza, R., Jones, T. T., Wyneken, J. and Porter, W. P. 2014. Leatherbacks swimming *in silico*: modeling and verifying their momentum and heat balance using computational fluid dynamics. *PLoS One*, 9(10), e110701.
- Duellman, W. E. and Trueb, L. 1986. *Biology of Amphibians*. McGraw-Hill, New York, 670 pp.
- Dynowski, J. F., Nebelsick, J. H., Klein, A. and Roth-Nebelsick, A. 2016. Computational fluid dynamics analysis of the fossil Crinoid *Encrinus liliiformis* (Echinodermata: Crinoidea). *PLoS One*, 11(5), e0156408.
- Dzemeski, G. and Christian, A. 2007. Flexibility along the neck of the ostrich (*Struthio camelus*) and consequences for the reconstruction of dinosaurs with extreme neck length. *Journal of Morphology*, 268(8), pp. 701-714.
- Ellis, R. 2003. *Sea Dragons: Predators of the Prehistoric Oceans*. University Press of Kansas, Lawrence, USA, 326 pp.
- Einarsson, E., Lindgren, J., Kear, B. P. and Siverson, M. 2010. Mosasaur bite marks on a plesiosaur propodial from the Campanian (Late Cretaceous) of southern Sweden. *GFF*, 132(2), pp. 123-128.
- English, A. W. 1976. Limb movements and locomotor function in the California sea lion (*Zalophus californianus*). *Journal of Zoology*, 178, pp. 341-364.

- Evans, M. 1993. An investigation into the neck flexibility of two plesiosauroid plesiosaurs: *Cryptoclidus eurymerus* and *Muraenosaurus leedsii*. MSc. thesis, University College, London, UK.
- Evans, M. 1999. A new reconstruction of the skull of the Callovian elasmosaurid plesiosaur *Muraenosaurus leedsii* Seeley. *Mercian Geologist*, 14(4), pp. 191-198.
- Evans, M. 2012. A new genus of plesiosaur (Reptilia: Sauropterygia) from the Pliensbachian (Early Jurassic) of England, and a phylogeny of the Plesiosauria. Ph.D. thesis, University of Leicester, UK.
- Evans, M. W. and Harlow, F. H. 1957. The particle-in-cell method for hydrodynamic calculations. *Los Alamos Scientific Laboratory Report*, LA-2139, 76.
- Everhart, M. J. 2000. Gastroliths associated with plesiosaur remains in the Sharon Springs Member of the Pierre Shale (Late Cretaceous), Western Kansas. *Transactions of the Kansas Academy of Science*, 103(1/2), pp. 64-75.
- Everhart, M. J. 2005. Bite marks on an elasmosaur (Sauropterygia; Plesiosauria) paddle from the Niobrara Chalk (Upper Cretaceous) as probable evidence of feeding by the lamniform shark, *Cretoxyrhina mantelli*. *PalArch's Journal of Vertebrate Paleontology*, 2(2), pp. 14-24.
- Everhart, M. J. 2017. Captain Theophilus H. Turner and the unlikely discovery of *Elasmosaurus platyrurus*. *Transactions of the Kansas Academy of Science*, 120(3-4), pp. 233-246.
- Falkingham, P. L. 2011. Acquisition of high resolution three-dimensional models using free, open-source, photogrammetric software. *Palaeontologia Electronica*, 15(1), pp. 1T:15p.
- Falkingham, P. L., Finch, L., Marek, R. D. and Troelsen, P. V. 2017. *Annual meeting of the Society of Experimental Biology: Reconstructing moving morphology using RaspberryPi (PiROMM): Range of motion in ostrich cervical vertebrae at progressive stages of dissection*. Gothenburg: Sweden 2-6 July 2017.
- Faux, C. M. and Padian, K. 2007. The opisthotonic posture of vertebrate skeletons: postmortem contraction or death throes? *Paleobiology*, 33(2), pp. 201-226.
- Feldkamp, S. D. 1987. Swimming in the California sea lion: morphometrics, drag and energetics. *Journal of Experimental Biology*, 131(1), pp. 117-135.
- Ferrón, H. G., Martínez-Pérez, C. and Botella, H. 2017. The evolution of gigantism in active marine predators. *Historical Biology*, 30(5), pp. 712-716.

- Fischer, M. S., Benson, R. B. J., Druckenmiller, P. S., Ketchum, H. F. and Bardet, N. 2018. The evolutionary history of polycotyloid plesiosaurians. *Royal Society Open Science*, 5(3), 172177.
- Fischer, V., Benson, R. B., Zverkov, N. G., Soul, L. C., Arkhangelsky, M. S., Lambert, O., Stenshin, I. M., Uspensky, G. N. and Druckenmiller, P. S. 2017. Plasticity and convergence in the evolution of short-necked plesiosaurs. *Current Biology*, 27(11), pp. 1667-1676.
- Fish, F. E. 1993. Power output and propulsive efficiency of swimming Bottlenose Dolphins (*Tursiops truncatus*). *Journal of Experimental Biology*, 185, pp. 179-193.
- Fish, F. E. 2002. Balancing requirements for stability and maneuverability in cetaceans. *Integrative and Comparative Biology*, 42, pp. 85-93.
- Fish, F. E., Howle, L. E. and Murray, M. M. 2008. Hydrodynamic flow control in marine mammals. *Integrative and Comparative Biology*, 48(6), pp. 788-800.
- Fish, F. E., Hurley, J. and Costa, D. P. 2003. Maneuverability by the sea lion *Zalophus californianus*: turning performance of an unstable body design. *The Journal of Experimental Biology*, 206, pp. 667-674.
- Fish, F. E. and Lauder, G. V. 2017. Control surfaces of aquatic vertebrates: active and passive design and function. *Journal of Experimental Biology*, 220, pp. 4351-4363.
- Fish, F. E. and Rohr, J. J. 1999. *Review of Dolphin Hydrodynamics and Swimming Performance*. Space and naval warfare systems, San Diego, USA, 187 pp.
- Fitch, W. T. 2012. Evolutionary developmental biology and human language evolution: Constraints on adaptation. *Evolutionary Biology*, 39(4), pp. 613-637.
- Fleischle, C. V., Wintrich, T. and Sander, P. M. 2018. Quantitative histological models suggest endothermy in plesiosaurs. *PeerJ*, 6, e4955.
- Fletcher, T., Altringham, J., Peakall, J., Wignall, P. and Dorrell, R. 2014. Hydrodynamics of fossil fishes. *Proceedings of the Royal Society B: Biological Sciences*, 281(1788), 20140703.
- Foffa, D., Cuff, A. R., Sassoon, J., Rayfield, E. J., Mavrogordato, M. N. and Benton, M. J. 2014. Functional anatomy and feeding biomechanics of a giant Upper Jurassic pliosaur (Reptilia: Sauropterygia) from Weymouth Bay, Dorset, UK. *Journal of Anatomy*, 225(2), pp. 209-219.
- Forrest, R. 2003. Evidence for scavenging by the marine crocodile *Metriorhynchus* on the carcass of a plesiosaur. *Proceedings of the Geologist's Association*, 114, pp. 363-366.

- Forrest, R. and Oliver, N. 2003. Ichthyosaurs and plesiosaurs from the Lower Spilsby Sandstone Member (Upper Jurassic), north Lincolnshire. *Proceedings of the Yorkshire Geological Society*, 54(4), pp. 269-275.
- Fraas, E. 1910. Plesiosaurier aus dem oberen Lias von Holzmaden. *Palaeontographica (1846-1933) Band 57 Lieferung 3-4*, pp. 105-140.
- Frey, E., Mulder, E. W. A., Stinnesbeck, W., Rivera-Sylva, H. E., Padilla-Gutiérrez, J. M. and González-González, A. H. 2017. A new polycotyloid plesiosaur with extensive soft tissue preservation from the early Late Cretaceous of northeast Mexico. *Boletín de la Sociedad Geológica Mexicana*, 69(1), pp. 87-134.
- Friedman, C. and Leftwich, M. C. 2014. The kinematics of the California sea lion foreflipper during forward swimming. *Bioinspiration and biomimetics*, 9(4), 046010.
- Gadow, H. 1896. On the evolution of the vertebral column of Amphibia and Amniota. *Philosophical Transactions of the Royal Society of London. Series B, Containing Papers of a Biological Character*, 187, pp. 1-57.
- Galis, F. 1999. Why do almost all mammals have seven cervical vertebrae? Developmental constraints, How genes, and cancer. *Journal of Evolutionary Zoology*, 285(1), pp. 19-26.
- Galis, F., Van Alphen, J. J. M. and Metz, J. A. J. 2001. Why five fingers? Evolutionary constraints on digit numbers. *TRENDS in Ecology and Evolution*, 16(11), pp. 637-646.
- Galis, F., Van Dooren, T. J. M., Feuth, J. D., Metz, J. A. J., Witkam, A., Ruinard, S., Steigenga, M. J. and Wijnaendts, L. C. D. 2006. Extreme selection in humans against homeotic transformations of cervical vertebrae. *Evolution*, 60(12), pp. 2643-2654.
- Gasparini, Z. 2009. A new Oxfordian pliosaurid (Plesiosauria, Pliosauridae) in the Caribbean seaway. *Palaeontology*, 52(3), pp. 661-669.
- Gasparini, Z., Bardet, N., Martin, J. E. and Fernandez, M. 2003. The elasmosaurid plesiosaur *Aristonectes cabrera* from the Latest Cretaceous of South America and Antarctica. *Journal of Vertebrate Paleontology*, 23(1), pp. 104-115.
- Gatesy, S. M., Baier, D. B., Jenkins, F. A. and Dial, K. P. 2010. Scientific rotoscoping: A morphology-based method of 3-D motion analysis and visualization. *Journal of Experimental Zoology Part A: Ecological Genetics and Physiology*, 313(5), pp. 244-261.

- Gauthier, J., Kluge, A. G. and Rowe, T. 1988. Amniote phylogeny and the importance of fossils. *Cladistics*, 4(2), pp. 105-209.
- Glasgow, S., Troelsen, P. V., Falkingham, P. L. and Marek, R. D. 2019. *The Annual Meeting for the Society for Integrative and Comparative Biology. Stretching evolution: regionalisation aids neck elongation in plesiosaurs*. Tampa: USA 3-7 January 2019.
- Godfrey, S. J. 1985. Additional observations of subaqueous locomotion in the California Sea Lion (*Zalophus californianus*). *Aquatic Mammals*, 11(2), pp. 53-57.
- Graf, W., De Waele, C. and Vidal, P.-P. 1994. Biomechanics, movement strategies and the evolution of the head-neck system in mammals. In: Delgado-García, J. M., Godaux, E. and Vidal, P.-P. (eds.) *Information Processing Underlying Gaze Control*. Elsevier Science Ltd., Oxford, pp. 415-427.
- Grossmann, F. 2007. The taxonomic and phylogenetic position of the Plesiosauroidea from the Lower Jurassic Posidonia Shale of South-West Germany. *Palaeontology*, 50(3), pp. 545-564.
- Guinard, G., Marchand, D., Courant, F., Gauthier-Clerc, M. and Le Bohec, C. 2010. Morphology, ontogenesis and mechanics of cervical vertebrae in four species of penguins (Aves: Spheniscidae). *Polar biology*, 33(6), pp. 807-822.
- Gunji, M. and Endo, H. 2016. Functional cervicothoracic boundary modified by anatomical shifts in the neck of giraffes. *Royal Society Open Science*, 3(2), 150604.
- Gutarra, S., Moon, B. C., Rahman, I. A., Palmer, C., Lautenschlager, S., Brimacombe, A. J. and Benton, M. J. 2019. Effects of body plan evolution on the hydrodynamic drag and energy requirements of swimming in ichthyosaurs. *Proceedings of the Royal Society B*, 286: 20182786.
- Halstead, L. B. 1989. Plesiosaur locomotion. *Journal of the Geological Society*, 146(1), pp. 37-40.
- Harlow, F. H. and Welch, J. E. 1965. Numerical calculation of time-dependent viscous incompressible flow of fluid with free surface. *The physics of fluids*, 8(12), pp. 2182-2189.
- Heiss, E., Aerts, P. and Van Wassenbergh, S. 2018. Aquatic–terrestrial transitions of feeding systems in vertebrates: a mechanical perspective. *Journal of Experimental Biology*, 221(8), jeb154427.
- Henderson, D. 2006. Floating point: a computational study of buoyancy, equilibrium, and gastroliths in plesiosaurs. *Lethaia*, 39(3), pp. 227-244.

- Henderson, D. M. and Naish, D. 2010. Predicting the buoyancy, equilibrium and potential swimming ability of giraffes by computational analysis. *Journal of Theoretical Biology*, 265(2), pp. 151-159.
- Herrel, A., Van Damme, J. and Aerts, P. 2007. Cervical Anatomy and Function in Turtles. In: Wyneken, J., Godfrey, M. H. and Bels, V. (eds.) *Biology of Turtles*. Taylor & Francis Inc., Bosa Roca, USA, pp. 177-200.
- Hiller, N., Mannering, A. A., Jones, C. M. and Cruickshank, A. R. I. 2005. The nature of *Mauisaurus haasti* Hector 1874 (Reptilia: Plesiosauria). *Journal of Vertebrate Paleontology*, 25(3), pp. 588-601.
- Hocking, D. P., Marx, F. G., Park, T., Fitzgerald, E. M. G. and Evans, A. R. 2017. A behavioural framework for the evolution of feeding in predatory aquatic mammals. *Proceedings of the royal Society B*, 284(1850), 20162750.
- Hoerner, S. F. 1965. *Fluid Dynamic Drag*. Midland Park, New Jersey, 455 pp.
- Hone, D. W. E. and Benton, M. J. 2005. The evolution of large size: how does Cope's Rule work? *TRENDS in Ecology and Evolution*, 20(1), pp. 4-6.
- Huene, V. F. 1923. Ein Neuer Plesiosaurier aus dem oberen Lias Württembergs. *Jahreshefte des Vereins für vaterländische Naturkunde in Württemberg* 1923, pp. 3-23.
- Humphries, S. and Ruxton, G. D. 2002. Why did some ichthyosaurs have such large eyes? *Journal of Experimental Biology*, 205(4), pp. 439-441.
- Hutchinson, H. N. 1893. *Extinct Monsters: A Popular Account of Some of the Larger Forms of Ancient Animal Life*. Chapman and Hall, London, 362 pp.
- Hutchinson, J. R., Bates, K. T., Molnar, J., Allen, V. and Makovicky, P. J. 2011. A computational analysis of limb and body dimensions in *Tyrannosaurus rex* with implications for locomotion, ontogeny, and growth. *PLoS ONE*, 6(10), e26037.
- Jones, K. E., Angielczyk, K. D., Polly, P. D., Head, J. J., Fernandez, V., Lungmus, J. K., Tulga, S. and Pierce, S. E. 2018. Fossils reveal the complex evolutionary history of the mammalian regionalized spine. *Science*, 361(6408), pp. 1249-1252.
- Jones, M. E. H., Werneburg, I., Curtis, N., Penrose, R., O'Higgins, P., Fagan, M. J. and Evans, S. E. 2012. The head and neck anatomy of sea turtles (Cryptodira: Chelonioidae) and skull shape in testudines. *Plos One*, 7(11), e47852.
- Kambic, R. E., Biewener, A. A. and Pierce, S. E. 2017. Experimental determination of three-dimensional cervical joint mobility in the avian neck. *Frontiers in Zoology*, 14:37.

- Kambic, R. E., Roberts, T. J. and Gatesy, S. M. 2014. Long-axis rotation: a missing degree of freedom in avian bipedal locomotion. *Journal of Experimental Biology*, 217, jeb101428.
- Karakasiliotis, K., Thandiackal, R., Melo, K., Horvat, T., Mahabadi, N. K., Tsitkov, S., Cabelguyen, J. M. and Ijspeert, A. J. 2016. From cineradiography to biorobots: an approach for designing robots to emulate and study animal locomotion. *Journal of The Royal Society Interface*, 13(119), 20151089.
- Kardong, K. V. 2012. *Vertebrates: Comparative Anatomy, Function, Evolution*. McGraw-Hill, New York, 816 pp.
- Kear, B. P. 2004. Biogeographic and biostratigraphic implications of Australian Mesozoic marine reptiles. *Australian Biologist*, 17(1), pp. 4-22.
- Kear, B. P. 2006. Marine reptiles from the Lower Cretaceous of South Australia: Elements of a high-latitude cold-water assemblage. *Palaeontology*, 49(4), pp. 837-856.
- Kear, B. P., Larsson, D., Lindgren, J. and Kundrát, M. 2017. Exceptionally prolonged tooth formation in elasmosaurid plesiosaurosaurs. *PLoS One*, 12(2), e0172759.
- Kern, S. and Koumoutsakos, P. 2006. Simulations of optimized anguilliform swimming. *Journal of Experimental Biology*, 209(24), pp. 4841-4857.
- Ketchum, H. F. and Benson, R. B. 2010. Global interrelationships of Plesiosauria (Reptilia, Sauropterygia) and the pivotal role of taxon sampling in determining the outcome of phylogenetic analyses. *Biological Reviews*, 85(2), pp. 361-392.
- Ketchum, H. F. and Benson, R. B. J. 2011. A new pliosaurid (Sauropterygia, plesiosauria) from the Oxford Clay Formation (Middle Jurassic, Callovian) of England: Evidence for a gracile longirostrine grade of Early-Middle Jurassic pliosaurids. *Papers in Palaeontology*, 86, pp. 109-129.
- Ketchum, H. F. and Smith, A. S. 2010. The anatomy and taxonomy of *Macroplata tenuiceps* (Sauropterygia, Plesiosauria) from the Hettangian (Lower Jurassic) of Warwickshire, United Kingdom. *Journal of Vertebrate Paleontology*, 30(4), pp. 1069-1081.
- Khanna, D. R. 2004. *Biology of Reptiles*. Discovery Publishing House, Delhi, India, 410 pp.
- Klein, N. 2010. Long bone histology of Sauropterygia from the Lower Muschelkalk of the Germanic Basin provides unexpected implications for phylogeny. *PLoS One*, 5(7), e11613.

- Knutsen, E. M. 2012a. A taxonomic revision of the genus *Pliosaurus* (Owen, 1841a) Owen, 1841b. *Norwegian Journal of Geology*, 92, pp. 259-276.
- Knutsen, E. M. 2012b. Redescription and taxonomic clarification of ‘*Tricleidus*’ *svalbardensis* based on new material from the Agardhfjellet Formation (Middle Volgian). *Norwegian Journal of Geology*, 92, pp. 175-186.
- Knutsen, E. M., Druckenmiller, P. S. and Hurum, J. H. 2012a. A new species of *Pliosaurus* (Sauropterygia: Plesiosauria) from the Middle Volgian of central Spitsbergen, Norway. *Norwegian Journal of Geology*, 92, pp. 235-258.
- Knutsen, E. M., Druckenmiller, P. S. and Hurum, J. H. 2012b. Two new species of long-necked plesiosaurians (Reptilia: Sauropterygia) from the Upper Jurassic (Middle Volgian) Agardhfjellet Formation of central Spitsbergen. *Norwegian Journal of Geology*, 92, pp. 187-212.
- Knörlein, B. J., Baier, D. B., Gatesy, S. M., Laurence-Chasen, J. D. and Brainerd, E. L. 2016. Validation of XMALab software for marker-based XROMM. *Journal of Experimental Biology*, 219, jeb-145383.
- Kogan, I., Pacholak, S., Licht, M., Schneider, J. W., Brucker, C. and Brandt, S. 2015. The invisible fish: hydrodynamic constraints for predator-prey interaction in fossil fish *Saurichthys* compared to recent actinopterygians. *Biology Open*, bio-014720.
- Krings, M., Nyakatura, J. A., Fischer, M. S. and Wagner, H. 2014. The cervical spine of the American barn owl (*Tyto furcata pratincola*): I. Anatomy of the vertebrae and regionalization in their S-shaped arrangement. *PLoS One*, 9(3), e91653.
- Kubo, T., Mitchell, M. T. and Henderson, D. M. 2012. *Albertonectes vanderveldei*, a new elasmosaur (Reptilia, Sauropterygia) from the Upper Cretaceous of Alberta. *Journal of Vertebrate Paleontology*, 32(3), pp. 557-572.
- Kuroda, N. 1962. On the cervical muscles of birds. *Journal of the Yamashina Institute for Ornithology*, 3(3), pp. 189-211.
- Lamura, A., Gompper, G., Ihle, T. and Kroll, D. M. 2001. Multi-particle collision dynamics: Flow around a circular and a square cylinder. *Europhysics Letters*, 56(3), pp. 319-325.
- Landolt, R. and Zweers, G. 1985. Anatomy of the muscle-bone apparatus of the cervical system in the mallard (*Anas platyrhynchos* L.). *Netherlands Journal of Zoology*, 35(4), pp. 611-670.

- Lauder, G. V. and Madden, P. G. A. 2006. Learning from fish: kinematics and experimental hydrodynamics for roboticists. *International journal of automation and computing*, 3(4), pp. 325-335.
- Lautenschlager, S. 2017. Digital reconstruction of soft-tissue structures in fossils. *The Paleontological Society Papers*, 22, pp. 101-117.
- Leeuw, A. H. J., Bout, R. G. and Zweers, G. A. 2001. Evolutionary morphology of the neck system in ratites, fowl and waterfowl. *Netherlands Journal of Zoology*, 51(2), pp. 243-262.
- Lehmkuhl, O., Rodríguez, I., Borrell, R., Chiva, J. and Oliva, A. 2014. Unsteady forces on a circular cylinder at critical Reynolds numbers. *Physics of Fluids*, 26(12), 125110.
- Li, N., Liu, H. L. and Su, Y. 2017. Numerical study on the hydrodynamics of thunniform bio-inspired swimming under self-propulsion. *PLoS One*, 12(3), e0174740.
- Lingham-Soliar, T. 2013. The evolution of the feather: scales on the tail of *Sinosauropteryx* and an interpretation of the dinosaur's opisthotonic posture. *Journal of Ornithology*, 154(2), pp. 455-463.
- Liu, S., Smith, A. S., Gu, Y., Tan, J., Liu, C. K. and Turk, G. 2015. Computer simulations imply forelimb-dominated underwater flight in plesiosaurs. *PLoS Computational Biology*, 11(12), e1004605.
- Long, J. H., JR., Pabst, D. A., Shepherd, W. R. and McLellan, W. A. 1997. Locomotor design of dolphin vertebral columns: Bending mechanics and morphology of *Delphinus delphis*. *The Journal of Experimental Biology*, 200(1), pp. 65-81.
- Long, J. H., JR., Schumacher, J., Livingston, N. and Kemp, M. 2006. Four flippers or two? Tetrapodal swimming with an aquatic robot. *Bioinspiration & Biomimetics*, 1(1), pp. 20-29.
- Lovvorn, J. R. 2001. Upstroke thrust, drag effects, and stroke-glide cycles in wing-propelled swimming by birds. *American Zoologist*, 41(2), pp. 154-165.
- Lovvorn, J. R. and Liggins, G. A. 2002. Interactions of body shape, body size and stroke-acceleration patterns in costs of underwater swimming by birds. *Functional Ecology*, 16(1), pp. 106-122.
- Lovvorn, J. R., Liggins, G. A., Borstad, M. H., Calisal, S. M. and Mikkelsen, J. 2001. Hydrodynamic drag of diving birds: Effects of body size, body shape and feathers at steady speeds. *Journal of Experimental Biology*, 204(9), pp. 1547-1557.
- Mallison, H. and Wings, O. 2014. Photogrammetry in paleontology—a practical guide. *Journal of Paleontological Techniques*, 12, pp. 1-31.

- Manafzadeh, A. R. and Padian, K. 2018. ROM mapping of ligamentous constraints on avian hip mobility: implications for extinct ornithomirans. *Proceedings of the Royal Society B*, 285(1879), 20180727.
- Maresh, J. L., Fish, F. E., Nowacek, D. P., Nowacek, S. M. and Wells, R. S. 2004. High performance turning capabilities during foraging by bottlenose dolphins (*Tursiops truncatus*). *Marine mammal science*, 20(3), pp. 498-509.
- Martin, J. E., Frey, E. and Riess, J. 1986. Soft tissue preservation in ichthyosaurs and a stratigraphic review of the Lower Hettangian of Barrow-upon-Soar, Leicestershire. *Transactions of the Leicester Literary and Philosophical Society*, 80, pp. 58-72.
- Martin, J. E. and Kennedy, L. E. 1988. A plesiosaur with stomach contents from the Late Cretaceous (Campanian) Pierre Shale of South Dakota: A preliminary report. *Proceedings of the South Dakota Academy of Science*, 67, pp. 76-79.
- Martin, J. E., Sawyer, J. F., Reguero, M. and Case, J. A. 2007. Occurrence of a young elasmosaurid plesiosaur skeleton from the Late Cretaceous (Maastrichtian) of Antarctica. *U.S. Geological Survey and The National Academies; USGS OF-2007-1047*.
- Marzola, M., Mateus, O., Milàn, J. and Clemmensen, L. B. 2018. A review of Palaeozoic and Mesozoic tetrapods from Greenland. *Bulletin of the Geological Society of Denmark*, 66, pp. 21-46.
- Massare, J. A. 1987. Morphology and prey preference of Mesozoic marine reptiles. *Journal of Vertebrate Paleontology*, 7(2), pp. 121-137.
- Massare, J. A. 1988. Swimming capabilities of Mesozoic marine reptiles: implications for method of predation. *Paleobiology*, 14(2), pp. 187-205.
- Massare, J. A. 1994. Swimming capabilities of Mesozoic marine reptiles: a review. In: Maddock, L., Bone, Q. and Rayner, J. M. V. (eds). *Mechanics and Physiology of Animal Swimming*. Cambridge University Press, Cambridge, pp. 133-149.
- Massare, J. A. 1997. Faunas, behavior, and evolution. In: Callaway, J. M. and Nicholls, E. (eds.) *Ancient Marine Reptiles*. Academic Press, San Diego, USA, pp. 401-421.
- McGowan, C. 1999. *A Practical Guide to Vertebrate Mechanics*. Cambridge University Press, UK, 316 pp.
- McHenry, C. R., Cook, A. G. and Wroe, S. 2005. Bottom-feeding plesiosaurs. *Science*, 310(5745), pp. 75.

- McHenry, M. J., Anderson, P. S. L., Van Wassenbergh, S., Matthews, D. G., Summers, A. P. and Patek, S. N. 2016. The comparative hydrodynamics of rapid rotation by predatory appendages. *Journal of Experimental Biology*, 219(21), pp. 3399-3411.
- Molnar, J. L., Pierce, S. E., Bhullar, B. A., Turner, A. H. and Hutchinson, J. R. 2015. Morphological and functional changes in the vertebral column with increasing aquatic adaptation in crocodylomorphs. *Royal Society Open Science*, 2(11), 150439.
- Molnar, J. L., Pierce, S. E. and Hutchinson, J. R. 2014. An experimental and morphometric test of the relationship between vertebral morphology and joint stiffness in Nile crocodiles (*Crocodylus niloticus*). *Journal of Experimental Biology*, 217(5), pp. 758-768.
- Moodie, R. L. 1912. The stomach stones of reptiles. *Science*, 35(897), pp. 377-378.
- Motani, R. 2002. Swimming speed estimation of extinct marine reptiles: energetic approach revisited. *Paleobiology*, 28(2), pp. 251-262.
- Motani, R. 2009. The evolution of marine reptiles. *Evolution: Education and Outreach*, 2(2), pp. 224-235.
- Munson, B. R., Young, D. F., Okiishi, T. H. and Huebsch, W. W. 2009. *Fundamentals of Fluid Mechanics*. John Wiley & Sons, New Jersey USA, 776 pp.
- Murray, P. F. 1987. Plesiosaurs from Albian Aged Bathurst Island Formation Siltstones near Darwin, Northern Territory, Australia. *The Beagle: Records of the Museums and Art Galleries of the Northern Territory Museum of Arts and Sciences*, 4, pp. 95-102.
- Muscutt, L. E., Dyke, G. J., Weymouth, G. D., Naish, D., Palmer, C. and Ganapathisubramani, B. 2017. The four-flipper swimming method of plesiosaurs enabled efficient and effective locomotion. *Proceedings of the Royal Society B*, 284(1861), 20170951.
- Nagesan, R. S., Henderson, D. M. and Anderson, J. S. 2018. A method for deducing neck mobility in plesiosaurs, using the exceptionally preserved *Nichollssaura borealis*. *Royal Society Open Science*, 5(8), 172307.
- Naish, D. and Witton, M. P. 2017. Neck biomechanics indicate that giant Transylvanian azhdarchid pterosaurs were short-necked arch predators. *PeerJ*, 5, e2908.
- Narita, Y. and Kuratani, S. 2005. Evolution of the vertebral formulae in mammals: A perspective on developmental constraints. *Journal of Experimental Zoology*, 304(2), pp. 91-106.

- Neenan, J. M., Reich, T., Evers, S. W., Druckenmiller, P. S., Voeten, D. F. A. E., Choiniere, J. N., Barrett, P. M., Pierce, S. E. and Benson, R. B. J. 2017. Evolution of the sauropterygian labyrinth with increasingly pelagic lifestyles. *Current Biology*, 27(24), pp. 3852-3858.
- Neutens, C., De Dobbelaer, B., Claes, P. and Adriaens, D. 2017. Prehensile and non-prehensile tails among syngnathid fishes: what's the difference? *Zoology*, 120, pp. 62-72.
- Noè, L. 2006. The role of the plesiosaurian long neck - a new model. *Journal of Vertebrate Paleontology*, 26(3), 105A.
- Noè, L. F., Taylor, M. A. and Gómez-Pérez, M. 2017. An integrated approach to understanding the role of the long neck in plesiosaurs. *Acta Palaeontologica Polonica*, 62(1), pp. 137-162.
- O'Gorman, J. P., Coria, R. A., Reguero, M., Santillana, S., Mörs, T. and Cárdenas, M. 2018a. The first non-aristonectine elasmosaurid (Sauropterygia; Plesiosauria) cranial material from Antarctica: New data on the evolution of the elasmosaurid basicranium and palate. *Cretaceous Research*, 89, pp. 248-263.
- O'Gorman, J. P. and Fernandez, M. S. 2016. Neuroanatomy of the vertebral column of *Vegasaurus molyi* (Elasmosauridae) with comments on the scervico-dorsal limit in plesiosaurs. *Cretaceous Research*, 73, pp. 91-97.
- O'Gorman, J. P., Gasparini, Z. and Salgado, L. 2013. Postcranial morphology of *Aristonectes* (Plesiosauria, Elasmosauridae) from the Upper Cretaceous of Patagonia and Antarctica. *Antarctic Science*, 25(1), pp. 71-82.
- O'Gorman, J. P., Gasparini, Z. and Salgado, L. 2014. Reappraisal of *Tuarangisaurus? cabazai* (Elasmosauridae, Plesiosauria) from the Upper Maastrichtian of northern Patagonia, Argentina. *Cretaceous Research*, 47, pp. 39-47.
- O'Gorman, J. P., Gasparini, Z. and Spalletti, L. A. 2018b. A new *Pliosaurus* species (Sauropterygia, Plesiosauria) from the Upper Jurassic of Patagonia: new insights on the Tithonian morphological disparity of mandibular symphyseal morphology. *Journal of Paleontology*, 92(2), pp. 240-253.
- O'Gorman, J. P., Otero, R. A., Hiller, N., Simes, J. and Terezow, M. 2016a. Redescription of *Tuarangisaurus keyesi* (Sauropterygia; Elasmosauridae), a key species from the uppermost Cretaceous of the Weddellian Province: Internal skull anatomy and phylogenetic position. *Cretaceous Research*, 71, pp. 118-136.

- O'Gorman, J. P., Panzeri, K. M., Fernandez, M. S., Santillana, S., Moly, J. J. and Reguero, M. 2017. A new elasmosaurid from the upper Maastrichtian López de Bertodano Formation: new data on weddellonectian diversity. *Alcheringa: An Australasian Journal of Palaeontology*, 1-12.
- O'Gorman, J. P., Santillana, S., Reguero, M. and Moly, J. J. 2012. Primer registro de gastrolitos asociados a un specimen de *Aristonectes* sp (Plesiosauria, Elasmosauridae), Isla Seymour (Is. Marambio), Antártida. *Abriendo Ventanas al Pasado, Libro de Resúmenes III Simposio-Paleontología en Chile*, pp. 121-123.
- O'Gorman, J. P., Talevi, M. and Fernandez, M. S. 2016b. Osteology of a perinatal aristonectine (Plesiosauria; Elasmosauridae). *Antarctic Science*, 29(1), pp. 61-72.
- O'Keefe, F. R. 2001a. A cladistic analysis and taxonomic revision of the Plesiosauria (Reptilia: Sauropterygia). *Acta Zoologica Fennica*, 213, 1-63.
- O'Keefe, F. R. 2001b. Ecomorphology of plesiosaur flipper geometry. *Journal of Evolutionary Biology*, 14(6), pp. 987-991.
- O'Keefe, F. R. 2002. The evolution of plesiosaur and pliosaur morphotypes in the plesiosauria (Reptilia: Sauropterygia). *Paleobiology*, 28(1), pp. 101-112.
- O'Keefe, F. R. 2004. Preliminary description and phylogenetic position of a new plesiosaur (Reptilia: Sauropterygia). *Journal of Paleontology*, 78(5), pp. 973-988.
- O'Keefe, F. R. 2006. Neoteny and the plesiomorphic condition of the plesiosaur basicranium. In: Carrano, M. T., Gaudin, T. J., Blob, R. W. and Wible, J. R. (eds.) *Amniote Paleobiology: Perspectives on the Evolution of Mammals, Birds and Reptiles*. University of Chicago Press, Chicago, USA, 391-409 pp.
- O'Keefe, F. R. and Carrano, M. T. 2005. Correlated trends in the evolution of the plesiosaur locomotor system. *Paleobiology*, 31(4), pp. 656-675.
- O'Keefe, F. R. and Hiller, N. 2006. Morphologic and ontogenetic patterns in elasmosaur neck length, with comments on the taxonomic utility of neck length variables. *Paludicola*, 5, pp. 206-229.
- O'Keefe, F. R., Otero, R. A., Soto-Acuña, S., O'Gorman, J. P., Godfrey, S. J. and Chatterjee, S. 2017. Cranial anatomy of *Morturneria seymourensis* from Antarctica, and the evolution of filter feeding in plesiosaurs of the Austral Late Cretaceous. *Journal of Vertebrate Paleontology*, 37(4), e1347570.
- O'Keefe, F. R., Sander, P. M., Wintrich, T. and Werning, S. 2019. Ontogeny of polycotyloid long bone microanatomy and histology. *Integrative Organismal Biology*, 1(1), oby007.

- O'Keefe, F. R., Street, H. P., Cavigelli, J. P., Socha, J. J. and O'Keefe, R. D. 2009. A plesiosaur containing an ichthyosaur embryo as stomach contents from the Sundance Formation of the Bighorn Basin, Wyoming. *Journal of Vertebrate Paleontology*, 29(4), pp. 1306-1310.
- O'Keefe, F. R. and Wahl, W. 2003. Current taxonomic status of the plesiosaur *Pantasaurus striatus* from the Upper Jurassic Sundance Formation, Wyoming. *Paludicola*, 4(2), pp. 37-46.
- Orgeret, F., Weimerskirch, H. and Bost, C.-A. 2016. Early diving behaviour in juvenile penguins: improvement or selection processes. *Biology Letters*, 12(8), 20160490.
- Osborn, H. F. 1893. Recent researches upon the succession of the teeth in mammals. *The American Naturalist*, 27(318), pp. 493-508.
- Ossa-Fuentes, L., Otero, R. A. and Rubilar-Rogers, D. 2017. Microanatomy and osteohistology of a juvenile elasmosaurid plesiosaur from the Upper Maastrichtian of Marambio (=Seymour) Island, Antarctica. *Boletín del Museo Nacional de Historia Natural, Chile*, 66, pp. 149-160.
- Otero, R. A. 2016. Taxonomic reassessment of *Hydralmosaurus* as *Styxosaurus*: new insights on the elasmosaurid neck evolution throughout the Cretaceous. *PeerJ*, 4, e1777.
- Otero, R. A., O'Gorman, J. P., Moisley, W. L., Terezow, M. and McKee, J. 2017. A juvenile *Tuarangisaurus keyesi* Wiffen and Moisley 1986 (Plesiosauria, Elasmosauridae) from the Upper Cretaceous of New Zealand, with remarks on its skull ontogeny. *Cretaceous Research*, 85, pp. 214-231.
- Otero, R. A., Soto-Acuña, S. and O'Keefe, F. R. 2018. Osteology of *Aristonectes quiriquinensis* (Elasmosauridae, Aristonectinae) from the upper Maastrichtian of central Chile. *Journal of Vertebrate Paleontology*, 38(1), e1408638.
- Otero, R. A., Soto-Acuña, S. and O'Keefe, F. R., O'Gorman, J. P., Stinnesbeck, W., Suárez, M. E., Rubilar-Rogers, D., Salazar, C. and Quinzio-Sinn, L. A. 2014a. *Aristonectes quiriquinensis*, sp. nov., a new highly derived elasmosaurid from the upper Maastrichtian of central Chile. *Journal of Vertebrate Paleontology*, 34(1), pp. 100-125.
- Otero, R. A., Soto-Acuña, S. and Rubilar-Rogers, D. 2012. A postcranial skeleton of an elasmosaurid plesiosaur from the Maastrichtian of central Chile, with comments on the affinities of Late Cretaceous plesiosauroids from the Weddellian Biogeographic Province. *Cretaceous Research*, 37, pp. 89-99.

- Otero, R. A., Soto-Acuña, S., Vargas, A. O., Rubilar-Rogers, D., Yury-Yáñez, R. E. and Gutstein, C. S. 2014b. Additions to the diversity of elasmosaurid plesiosaurs from the Upper Cretaceous of Antarctica. *Gondwana Research*, 26(2), pp. 772-784.
- Owen, R. 1840. A description of a specimen of the *Plesiosaurus macrocephalus*, Conybeare, in the collection of Viscount Cole, M. P., D. C. L., F. G. S., & c. *Transactions of the Geological Society of London*, 2(3), pp. 515-535.
- Owen, R. 1865. *Monograph on the Fossil Reptilia of the Liassic Formations*. Palaeontographical Society, London, 73 pp.
- Park, S. G. and Sung, H. J. 2018. Hydrodynamics of flexible fins propelled in tandem, diagonal, triangular and diamond configurations. *Journal of Fluid Mechanics*, 840, pp. 154-189.
- Persson, P. O. 1959. Reptiles from the Senonian (U Cret.) of Scania (S. Sweden). *Arkiv för Mineralogi och Geologi*, 2(35), pp. 431-478.
- Pierce, S. E., Clack, J. A. and Hutchinson, J. R. 2011. Comparative axial morphology in pinnipeds and its correlation with aquatic locomotory behaviour. *Journal of Anatomy*, 219(4), pp. 502-514.
- Rahman, I. A. 2017. Computational fluid dynamics as a tool for testing functional and ecological hypotheses in fossil taxa. *Palaeontology*, 60(4), pp. 451-459.
- Rahman, I. A., Darroch, S. A. F., Racicot, R. A. and Laflamme, M. 2015a. Suspension feeding in the enigmatic Ediacaran organism *Tribrachidium* demonstrates complexity of Neoproterozoic ecosystems. *Science Advances*, 1(10), e1500800.
- Rahman, I. A. and Lautenschlager, S. 2017. Applications of three-dimensional box modeling to paleontological functional analysis. *The Paleontological Society Papers*, 22, pp. 119-132.
- Rahman, I. A., Zamora, S., Falkingham, P. L. and Phillips, J. C. 2015b. Cambrian cinctan echinoderms shed light on feeding in the ancestral deuterostome. *Proceedings of the Royal Society B*, 282(1818), 20151964.
- Randau, M., Cuff, A. R., Hutchinson, J. R., Pierce, S. E. and Goswami, A. 2017. Regional differentiation of felid vertebral column evolution: a study of 3D shape trajectories. *Organisms Diversity and Evolution*, 17(1), pp. 305-319.
- Ratnikov, V. Y. and Litvinchuk, S. N. 2007. Comparative morphology of trunk and sacral vertebrae of tailed amphibians of Russia and adjacent countries. *Russian Journal of Herpetology*, 14(3), pp. 177-190.

- Reisdorf, A. G. and Wuttke, M. 2012. Re-evaluating Moodie's opisthotonic-posture hypothesis in fossil vertebrates part I: Reptiles—the taphonomy of the bipedal dinosaurs *Compsognathus longipes* and *Juravenator starki* from the Solnhofen Archipelago (Jurassic, Germany). *Palaeobiodiversity and Palaeoenvironments*, 92(1), pp. 119-168.
- Richards, C. D. 2011. Plesiosaur Body Shape and its Impact on Hydrodynamic Properties. MSc. thesis. Marshall University.
- Riggs, E. S. 1939. A specimen of *Elasmosaurus serpentinus*. *Field Museum of Natural History*, 4, pp. 385-391.
- Rivera, G., Rivera, A. R. V., Dougherty, E. E. and Blob, R. W. 2006. Aquatic turning performance of painted turtles (*Chrysemys picta*) and functional consequences of a rigid body design. *The Journal of Experimental Biology*, 209(21), pp. 4203-4213.
- Robinson, J. A. 1975. The locomotion of plesiosaurs. *Neues Jahrbuch für Mineralogie Geologie und Paläontologie, Abhandlungen*, 149, pp. 286-332.
- Robinson, J. A. 1977. Intracorporal force transmission in plesiosaurs. *Neues Jahrbuch für Mineralogie Geologie und Paläontologie, Abhandlungen*, 153, pp. 86-128.
- Rockwell, H., Evans, F. G. and Pheasant, H. C. 1938. The comparative morphology of the vertebrate spinal column. Its form as related to function. *Journal of Morphology*, 63(1), pp. 87-117.
- Rodríguez, I., Lehmkuhl, O., Borrell, R., Paniagua, L. and Pérez-Segarra, C. D. 2013a. High performance computing of the flow past a circular cylinder at critical and supercritical Reynolds numbers. *Procedia Engineering*, 61, pp. 166-172.
- Rodríguez, I., Lehmkuhl, O., Chiva, J., Borrell, R. and Oliva, A. 2014. *6th European Conference on Computational Fluid Dynamics: On the wake transition in the flow past a circular cylinder at critical Reynolds numbers*. Barcelona: Spain 20-25 July 2014.
- Rodríguez, I., Lehmkuhl, O., Chiva, J. and Oliva, A. 2013b. *14th European Turbulence Conference: Unsteady forces on a circular cylinder at critical Reynolds numbers*. Lyon: France 1-4 September 2013.
- Root, R. B. 1967. The niche exploitation pattern of the Blue-gray gnatcatcher. *Ecological Monographs*, 37(4), pp. 317-350.
- Rothschild, B. M. 1982. *Rheumatology: A Primary Care Approach*. Yorke Medical Press, New York, 416 pp.

- Rothschild, B. M., Clark, N. D. L. and Clark, C. M. 2018. Evidence for survival in a Middle Jurassic plesiosaur with a humeral pathology: What can we infer of plesiosaur behaviour? *Palaeontologia Electronica*, 21(16), pp. 1-11.
- Rothschild, B. M. and Storrs, G. W. 2003. Decompression syndrome in plesiosaurs (Sauropterygia: Reptilia). *Journal of Vertebrate Paleontology*, 23(2), pp. 324-328.
- Rudwick, M. J. S. 2008. *Worlds Before Adam: The Reconstruction of Geohistory in the Age of Reform*. University of Chicago Press, Chicago and London, 639 pp.
- Russell, A. P. and Bentley, A. D. 2016. Opisthotonic head displacement in the domestic chicken and its bearing on the 'dead bird' posture of non-avian dinosaurs. *Journal of Zoology*, 298(1), pp. 20-29.
- Ryerson, W. G. and Schwenk, K. 2012. A simple, inexpensive system for digital particle image velocimetry (DPIV) in biomechanics. *Journal of Experimental Zoology: Part A - Ecological Genetics and Physiology*, 317(2), pp. 127-40.
- Sachs, S., Hornung, J. J. and Kear, B. P. 2016. Reappraisal of Europe's most complete Early Cretaceous plesiosaurian: *Brancaosaurus brancai* Wegner, 1914 from the "Wealden facies" of Germany. *PeerJ*, 4, e2813.
- Sachs, S., Hornung, J. J. and Kear, B. P. 2017. A new basal elasmosaurid (Sauropterygia: Plesiosauria) from the Lower Cretaceous of Germany. *Journal of Vertebrate Paleontology*, 37(4), e1301945.
- Sachs, S. and Kear, B. P. 2015. Fossil Focus: Elasmosaurs. *Palaeontology Online*, 5(2), pp. 1-8.
- Sachs, S. and Kear, B. P. 2017a. A rare new Pliensbachian plesiosaurian from the Amaltheenton Formation of Bielefeld in northwestern Germany. *Alcheringa: An Australasian Journal of Palaeontology*, 1-14.
- Sachs, S. and Kear, B. P. 2017b. Redescription of the elasmosaurid plesiosaurian *Libonectes atlasense* from the Upper Cretaceous of Morocco. *Cretaceous Research*, 74, pp. 205-222.
- Sachs, S., Kear, B. P. and Everhart, M. J. 2013. Revised vertebral count in the "longest-necked vertebrate" *Elasmosaurus platyurus* Cope 1868, and clarification of the cervical-dorsal transition in Plesiosauria. *PLoS One*, 8(8), e70877.
- Salisbury, S. W. and Frey, E. 2001. A biomechanical transformation model for the evolution of semi-spheroidal articulations between adjoining vertebral bodies in crocodylians. In: Franklin, C. and Grigg, G. C. (eds.) *Crocodylian Biology and Evolution*. Surrey Beatty & Sons, Australia, pp. 121-148.

- Samman, T. 2006. Craniocervical functional morphology of several North American coelurosaurian dinosaurs. Ph.D. thesis. University of Calgary.
- Sanderson, S. L. and Wassersug, R. 1993. Convergent and alternative design for vertebrate suspension feeding. In: Hanken, J. and Hall, B. K. (eds). *The Skull*. Chicago Press, Illinois, 37-112 pp.
- Sassoon, J. 2019. Congenital and late onset vertebral fusions in long necked plesiosaurs: The first report of spondylosis deformans in Sauropterygians. *Palaeontologia Electronica*, 22(1), pp. 1-15.
- Sassoon, J., Foffa, D. and Marek, R. 2015. Dental ontogeny and replacement in Pliosauridae. *Royal Society Open Science*, 2: 150384.
- Sato, T. 2002. Description of plesiosaurs (Reptilia Sauropterygia) from the Bearpaw Formation (Campanian-Maastrichtian) and a phylogenetic analysis of the Elasmosauridae. Ph.D. thesis. University of Calgary.
- Sato, T. 2003. *Terminonatator ponteixensis*, a new elasmosaur (Reptilia; Sauropterygia) from the Upper Cretaceous of Saskatchewan. *Journal of Vertebrate Paleontology*, 23(1), pp. 89-103.
- Sato, T., Hanai, T., Hayashi, S. and Nishimura, T. 2018. A Turonian polycotyloid plesiosaur (Reptilia: Sauropterygia) from Obira Town, Hokkaido, and its biostratigraphic and paleoecological significance. *Palaeontological Research*, 22(3), pp. 265-278.
- Sato, T., Hasegawa, Y. and Manabe, M. 2006. A new elasmosaurid plesiosaur from the Upper Cretaceous of Fukushima, Japan. *Palaeontology*, 49(3), pp. 467-484.
- Sato, T. and Tanabe, K. 1998. Cretaceous plesiosaurs ate ammonites. *Nature*, 394, pp. 629-630.
- Schlager, S., Profico, A., Di Vincenzo, F. and Manzi, G. 2018. Retrodeformation of fossil specimens based on 3D bilateral semi-landmarks: Implementation in the R package "Morpho". *PLoS One*, 13(3), e0194073.
- Schmeisser, R. L. and Gillette, D. D. 2009. Unusual occurrence of gastroliths in a polycotyloid plesiosaur from the Upper Cretaceous Tropic Shale, Southern Utah. *Palaios*, 24(7), pp. 453-459.
- Schnell, N. K. and Johnson, G. D. 2017. Evolution of a functional head joint in deep-sea fishes (Stomiidae). *PLoS One*, 12(2), e0170224.
- Schönberger, J. L. and Frahm, J.-M. 2016. Structure-from-Motion revisited. *Proceeding of the IEEE Conference on Computer Vision and Pattern Recognition*, pp. 4104-4113.

- Schönberger, J. L., Zheng, E., Pollyfeys, M. and Frahm, J.-M. 2016. Pixelwise view selection for unstructures multi-view stereo. *European Conference on Computer Vision (ECCV)*, pp. 501-518.
- Sciau, J., Crochet, J.-Y. and Mattei, J. 1990. Le premier squelette de plésiosaure de France sur le Causse du Larzac (Toarcien, Jurassique inférieur). *Géobios*, 23(1), pp. 111-116.
- Seddighi, M. and Allanson, D. 2017a. CFD - Lecture 8: Introduction to Turbulence (I). [online] Available at: <https://canvas.ljmu.ac.uk/> [Accessed 7th December, 2018]
- Seddighi, M. and Allanson, D. 2017b. CFD - Lecture 10: Introduction to Turbulence (II): Rans. [online] Available at: <https://canvas.ljmu.ac.uk/> [Accessed 7th December, 2018]
- Seddighi, M. and Allanson, D. 2017c. Verification and Validation (V & V) of CFD Results. [online] Available at: <https://canvas.ljmu.ac.uk/> [Accessed 7th December, 2018]
- Seeley, H. G. 1874. Note on some of generic modifications of the plesiosaurian pectoral arch. *Quarterly Journal of the Geological Society*, 30(1-4), pp. 436-449.
- Seeley, H. G. 1877. On *Mauisaurus gardneri* (Seeley), an elasmosaurian from the base of the gault of Folkestone. *Quarterly Journal of the Geological Society*, 33(1-4), pp. 541-547.
- Segre, P. S., Cade, D. E., Fish, F. E., Potvin, J., Allen, A. N., Calambokidis, J., Friedlaender, A. S. and Goldbogen, J. A. 2016. Hydrodynamic properties of fin whale flippers predict maximum rolling performance. *Journal of Experimental Biology*, 219(21), pp. 3315-3320.
- Sennikov, A. G. 2015. New data on the herpetofauna of the Early Triassic Donskaya Luka locality, Volgograd Region. *Paleontological Journal*, 49(11), pp. 1161-1173.
- Serratos, D. J., Druckenmiller, P. S. and Benson, R. B. J. 2017. A new elasmosaurid (Sauropterygia, Plesiosauria) from the Bearpaw Shale (Late Cretaceous, Maastrichtian) of Montana demonstrates multiple evolutionary reductions of neck length within Elasmosauridae. *Journal of Vertebrate Paleontology*, 37(2), e1278608.
- Shapiro, I. M. and Risbud, M. V. 2014. *The Intervertebral Disc: Molecular and Structural Studies of the Disc in Health and Disease*. Springer, Wien, 440 pp.
- Shuler, E. W. 1950. A new elasmosaur from the Eagle Ford Shale of Texas. *Fondren Science Series*, 1(2), pp. 1-33.

- Slijper, E. J. 1939. *Pseudorca crassidens* (Owen), ein Beitrag zur vergleichenden Anatomie der Cetaceen. *Zoologische Mededeelingen Rijksmuseum van Natuurlijke Historie Leiden*, 21, pp. 241-366.
- Smellie, W. R. 1917. *Apractocleidus teretipes*: A new Oxfordian plesiosaur in the Hunterian Museum, Glasgow University. *Transactions of the Royal Society of Edinburgh*, 51(3), pp. 609-629.
- Smith, A. S. 2007. Anatomy and systematics of the Rhomaleosauridae (Sauropterygia: Plesiosauria). Ph.D. thesis. University College Dublin.
- Smith, A. S. 2008. Plesiosaurs from the Pliensbachian (Lower Jurassic) of Bornholm, Denmark. *Journal of Vertebrate Paleontology*, 28(4), pp. 1213-1217.
- Smith, A. S. and Araújo, R. 2017. *Taumatodracon wiedenrothi*, a morphometrically and stratigraphically intermediate new rhomaleosaurid plesiosaurian from the Lower Jurassic (Sinemurian) of Lyme Regis. *Palaeontographica, Abt. A: Palaeozoology – Stratigraphy*, 308(4-6), pp. 89-125.
- Smith, A. S. and Benson, R. B. J. 2018. Osteology of *Rhomaleosaurus Thorntoni* (Sauropterygia: Rhomaleosauridae) from the Lower Jurassic (Toarcian) of Northamptonshire, England. *Monographs of the Palaeontographical Society*, 168(642), pp. 1-40.
- Smith, A. S. and Dyke, G. J. 2008. The skull of the giant predatory pliosaur *Rhomaleosaurus cramptoni*: implications for plesiosaur phylogenetics. *Naturwissenschaften*, 95(10), pp. 975-980.
- Smith, A. S. and Vincent, P. 2010. A new genus of pliosaur (Reptilia: Sauropterygia) from the Lower Jurassic of Holzmaden, Germany. *Palaeontology*, 53(5), pp. 1049-1063.
- Snively, E. and Russell, A. P. 2007. Functional morphology of neck musculature in the Tyrannosauridae (Dinosauria, Theropoda) as determined via a hierarchical inferential approach. *Zoological Journal of the Linnean Society*, 151(4), pp. 759-808.
- Sobral, G., Reisz, R., Neenan, J. M., Müller, J. and Scheyer, T. M. 2016. Basal Reptilians, Marine Diapsids, and Turtles: The Flowering of Reptile Diversity. In: Clack, J. A., Fay, R. R. and Popper, A. N. (eds.) *Evolution of the Vertebrate Ear*. Springer, Switzerland, pp. 207-243.
- Soul, L. C. and Benson, R. B. J. 2017. Developmental mechanisms of macroevolutionary change in the tetrapod axis: A case study of Sauropterygia. *Evolution*, 71(5), pp. 1164-1177.

- Starck, D. 1979. *Vergleichende Anatomie der Wirbeltiere*. Springer, Berlin, pp. 778.
- Stelle, L. L., Blake, R. W. and Trites, A. W. 2000. Hydrodynamic drag in steller sea lions (*Eumetopias jubatus*). *The Journal of Experimental Biology*, 203(12), pp. 1915-1923.
- Stephenson, N. G. 1951. Observations on the Development of the amphicoelous frogs, *Leiopelma* and *Ascaphus*. *Zoological Journal of the Linnean Society*, 42(283), pp. 18-28.
- Stevens, K. A. 2013. The articulation of sauropod necks: methodology and mythology. *PLoS One*, 8(10), e78572.
- Stevens, K. A. and Parrish, J. M. 1999. Neck posture and feeding habits of two Jurassic sauropod dinosaurs. *Science*, 284(5415), pp. 798-800.
- Stevens, K. A. and Parrish, J. M. 2005a. Digital Reconstructions of Sauropod Dinosaurs and Implications for Feeding. In: Rogers, K. A. C. and Wilson, J. A. (eds.) *The Sauropods: Evolution and Paleobiology*. University of California Press, Berkeley, USA, pp. 178-200.
- Stevens, K. A. and Parrish, J. M. 2005b. Neck posture, dentition, and feeding strategies in Jurassic sauropod dinosaurs. In: Tidwell, V. and Carpenter, K. (eds.) *Thunderlizards: The Sauropodomorph Dinosaurs*. Indiana University Press, Bloomington, pp. 212-232.
- Stevens, L. M., Blob, R. W. and Mayerl, C. J. 2018. Ontogeny, morphology and performance: changes in swimming stability and turning performance in the freshwater pleurodire turtle, *Emydura subglobosa*. *Biological Journal of the Linnean Society*, 125(4), pp. 718-729.
- Storrs, G. W. 1981. A review of occurrences of the Plesiosauria (Reptilia: Sauropterygia) in Texas, with description of new material. Ph.D. thesis. University of Texas.
- Storrs, G. W. 1993. Function and phylogeny in sauropterygian (Diapsida) evolution. *American Journal of Science*, 293(A), pp. 63-90.
- Stukely, W. 1717. An account of the impression of the almost entire sceleton of a large animal in a very hard stone, lately presented the Royal Society, from Nottinghamshire. *Philisophical Transactions*, 30(360), pp. 963-968.
- Stutchbury, S. 1846. A description of a new species of *Plesiosaurus* in the museum of the Bristol Institution. *Quarterly Journal of the Geological Society of London*, 2(1-2), pp. 411-417.

- Swinton, W. E. 1965. *Fossil Amphibians and Reptiles*. Trustees of the British Museum (Natural History). British Museum Press, Bristol, UK, 133 pp.
- Sørensen, A. M., Surlyk, F. and Lindgren, J. 2013. Food resources and habitat selection of a diverse vertebrate fauna from the upper lower Campanian of the Kristianstad Basin, southern Sweden. *Cretaceous Research*, 42, pp. 85-92.
- Taylor, M. A. 1981. Plesiosaurs - rigging and ballasting. *Nature*, 290, pp. 628-629.
- Taylor, M. A. 1986. Lifestyle of plesiosaurs. *Nature*, 319, pp. 179.
- Taylor, M. A. 1987. How tetrapods feed in water: a functional analysis by paradigm. *Zoological Journal of the Linnean Society*, 91(2), pp. 171-195.
- Taylor, M. A. 1992. Functional anatomy of the head of the large aquatic predator *Rhomaleosaurus zetlandicus* (Plesiosauria, Reptilia) from the Toarcian (Lower Jurassic) of Yorkshire, England. *Philosophical Transactions of the Royal Society of London B*, 335(1274), pp. 274-280.
- Taylor, M. A. 1994. Stone, bone or blubber? Buoyancy control strategies in aquatic tetrapods. In: Maddock, L., Bone, Q. and Rayner, J. M. V. (eds.) *Mechanics and Physiology of Animal Swimming*. Cambridge University Press, Cambridge, 151-161 pp.
- Taylor, M. A. and Cruickshank, A. R. I. 1993. A plesiosaur from the Linksfield erratic (Rhaetian, Upper Triassic) near Elgin, Morayshire. *Scottish Journal of Geology*, 29(2), pp. 191-196.
- Taylor, M. P. and Wedel, M. J. 2013a. The effect of intervertebral cartilage on neutral posture and range of motion in the necks of sauropod dinosaurs. *PLoS One*, 8(10), e78214.
- Taylor, M. P. and Wedel, M. J. 2013b. Why sauropods had long necks; and why giraffes have short necks. *PeerJ*, 1, e36.
- Taylor, M. P., Wedel, M. J. and Naish, D. 2009. Head and neck posture in sauropod dinosaurs inferred from extant animals. *Acta Palaeontologica Polonica*, 54(2), pp. 213-220.
- Thompson, W. A., Martin, J. E. and Reguero, M. 2007. Comparison of gastroliths within plesiosaurs (Elasmosauridae) from the Late Cretaceous marine deposits of Vega Island, Antarctic Peninsula, and the Missouri River area, South Dakota. *Geological Society of America Special Paper*, 427, pp. 147-153.

- Thorne, K. S. and Blandford, R. D. 2017. *Modern Classical Physics: Optics, Fluids, Plasmas, Elasticity, Relativity, and Statistical Physics*. Princeton University Press, New Jersey, 1552 pp.
- Tihen, J. A. 1965. Evolutionary trends in frogs. *American Zoologist*, 5(2), pp. 309-318.
- Torrens, H. 1995. Presidential address: Mary Anning (1799-1847) of Lyme: 'The greatest fossilist the world ever knew'. *The British Journal for the History of Science*, 28(3), pp. 257-284.
- Tsuihiji, T. 2004. The ligament system in the neck of *Rhea americana* and its implication for the bifurcated neural spines of sauropod dinosaurs. *Journal of Vertebrate Paleontology*, 24(1), pp. 165-172.
- Tsuihiji, T. 2005. Homologies of the transversospinalis muscles in the anterior presacral region of Sauria (crown Diapsida). *Journal of Morphology*, 263(2), pp. 151-178.
- Tutin, S. L. and Butler, R. J. 2017. The completeness of the fossil record of plesiosaurs, marine reptiles from the Mesozoic. *Acta Palaeontologica Polonica*, 62(3), pp. 563-573.
- Van Wassenbergh, S., Potes, N. Z. and Adriaens, D. 2015. Hydrodynamic drag constrains head enlargement for mouthbrooding in cichlids. *Journal of the Royal Society Interface*, 12(109), 20150461.
- Van Wassenbergh, S., Van Manen, K., Marcroft, T. A., Alafaro, M. E. and Stamhuis, E. J. 2014. Boxfish swimming paradox resolved: forces by the flow of water around the body promote manoeuvrability. *Journal of The Royal Society Interface*, 12(103), 20141146.
- VanBuren, C. S. and Evans, D. C. 2016. Evolution and function of anterior cervical vertebral fusion in tetrapods. *Biological Reviews*, 92(1), pp. 608-626.
- Varela-Lasheras, I., Bakker, A. J., Van Der Mije, S. D., Metz, J. A., Van Alphen, J. and Galis, F. 2011. Breaking evolutionary and pleiotropic constraints in mammals: on sloths, manatees and homeotic mutations. *EvoDevo*, 2(11).
- Vaughan, T. A., Ryan, J. M. and Czaplewski, N. J. 2015. *Mammalogy*. Jones & Bartlett Learning, Massachusetts, 750 pp.
- Versteeg, H. K. and Malalasekera, W. 1995. *An Introduction to Computational Fluid Dynamics - The Finite Volume Method*. Longman Scientific & Technical, Harlow, 267 pp.

- Vidal, D. and Díaz, V. D. 2017. Reconstructing hypothetical sauropod tails by means of 3D digitization: *Lirainosaurus astibiae* as case study. *Journal of Iberian Geology*, 43(2), pp. 293-305.
- Vincent, P. 2011. A re-examination of *Hauffiosaurus zanoni*, a pliosauroid from the Toarcian (Early Jurassic) of Germany. *Journal of Vertebrate Paleontology*, 31(2), pp. 340-351.
- Vincent, P., Allemand, R., Taylor, P. D., Suan, G. and Maxwell, E. E. 2017a. New insights on the systematics, palaeoecology and palaeobiology of a plesiosaurian with soft tissue preservation from the Toarcian of Holzmaden, Germany. *The Science of Nature*, 104(51).
- Vincent, P., Bardet, N., Pereda Suberbiola, X., Bouya, B., Amaghazaz, M. and Meslouh, S. 2011. *Zarafasaura oceanis*, a new elasmosaurid (Reptilia: Sauropterygia) from the Maastrichtian Phosphates of Morocco and the palaeobiogeography of latest Cretaceous plesiosaurs. *Gondwana Research*, 19(4), pp. 1062-1073.
- Vincent, P. and Taquet, P. 2010. A plesiosaur specimen from the Lias of Lyme Regis: the second ever discovered plesiosaur by Mary Anning. *Geodiversitas*, 32(3), pp. 377-390.
- Vincent, P., Weis, R., Kronz, G. and Delsate, D. 2017b. *Microcleidus melusinae*, a new plesiosaurian (Reptilia, Plesiosauria) from the Toarcian of Luxembourg. *Geological Magazine*, pp. 1-18.
- Vogel, S. 1989. *Life in Moving Fluids: The Physical Biology of Flow*. Princeton University Press, Princeton, 352 pp.
- Vogel, S. 2013. *Comparative Biomechanics: Life's Physical World*. Princeton University Press, Princeton, 640 pp.
- Walker, J. A. 2000. Does a rigid body limit maneuverability? *Journal of Experimental Biology*, 203(22), pp. 3391-3396.
- Ward, A. B. and Mehta, R. S. 2014. Differential occupation of axial morphospace. *Zoology*, 117(1), pp. 70-76.
- Ward, L., Pang, A. S. W., Evans, S. E. and Stern, C. D. 2018. The role of the notochord in amniote vertebral column segmentation. *Developmental Biology*, 439(1), pp. 3-18.
- Watson, D. M. S. 1924. The elasmosaurid shoulder-girdle and fore-limb. *Proceedings of the Zoological Society of London*, 94(3), pp. 885-917.
- Weihs, D. 2002. Stability versus maneuverability in aquatic locomotion. *Integrative and Comparative Biology*, 42(1), pp. 127-134.

- Welles, S. P. 1943. Elasmosaurid plesiosaurs with description of new material from California and Colorado. *Memoirs of the University of California*, 13, pp. 125-134.
- Welles, S. P. 1952. A review of the North American Cretaceous elasmosaurs. *University of California Publications in Geological Sciences*, 29, pp. 47-144.
- Welles, S. P. 1962. A new species of elasmosaur from the Aptian of Colombia and a review of the Cretaceous plesiosaurs. *University of California publications in the Geological sciences*, 44, pp. 1-96.
- Welles, S. P. and Bump, J. D. 1949. *Alzadasaurus pembertoni*, a new elasmosaur from the Upper Cretaceous of South Dakota. *Journal of Vertebrate Paleontology*, 23, pp. 521-535.
- Welles, S. P. and Gregg, D. R. 1971. Late Cretaceous marine reptiles of New Zealand. *Records of the Canterbury Museum*, 9, pp. 1-111.
- Werneburg, I., Hinz, J. K., Gumpenberger, M., Volpato, V., Natchev, N. and Joyce, W. G. 2015. Modeling neck mobility in fossil turtles. *Journal of Experimental Zoology Part B: Molecular and Developmental Evolution*, 324(3), pp. 230-243.
- Werneburg, I., Wilson, L. A. B., Parr, W. C. H. and Joyce, W. G. 2014. Evolution of neck vertebral shape and neck retraction at the transition to modern turtles: an integrated geometric morphometric approach. *Systematic Biology*, 64(2), pp. 187-204.
- White, F. M. 2010. *Fluid Mechanics*. McGraw-Hill, New York, 885 pp.
- White, T. E. 1940. Holotype of *Plesiosaurus longirostris* Blake and classification of the plesiosaurs. *Journal of Paleontology*, 14(5), pp. 451-467.
- Wilkinson, D. M. and Ruxton, G. D. 2012. Understanding selection for long necks in different taxa. *Biological Reviews*, 87(3), pp. 616-30.
- Williams, T. M. 1999. The evolution of cost efficient swimming in marine mammals: limits to energetic optimization. *Philosophical Transactions of the Royal Society of London B: Biological Sciences*, 354(1380), pp. 193-201.
- Williston, S. W. 1889. A new plesiosaur from the Niobrara Cretaceous of Kansas. *Transactions of the Annual Meetings of the Kansas Academy of Science*, 12, pp. 174-178.
- Williston, S. W. 1893. An interesting food habit of the plesiosaurs. *Transactions of the Annual Meetings of the Kansas Academy of Science*, 13, pp. 121-122.
- Williston, S. W. 1904. The stomach stones of the plesiosaurs. *Science*, 20(513), pp. 565.
- Williston, S. W. 1906. North American plesiosaurs; *Cimoliasaurus*, and *Polycotylus*. *American Journal of Science*, 21(123), pp. 221-236.

- Williston, S. W. 1907. The skull of *Brachauchenius*, with observations on the relationships of the plesiosaurs. *Proceedings of the United States National Museum*, 32, 477-489.
- Wilson, D. E. and Mittermeier, R. A. 2014. *Handbook of Mammals of the World, 4: Sea Mammals*. Lynx Edicions, Barcelona, 614 pp.
- Wilson, R. P., Gómez-Laich, A., Sala, J.-E., Dell’Omo, G., Holton, M. D. and Quintana, F. 2017. Long necks enhance and constrain foraging capacity in aquatic vertebrates. *Proceedings of the Royal Society B*, 284(1867), 20172072.
- Wintrich, T., Hayashi, S., Houssaye, A., Nakajima, Y. and Sander, P. M. 2017a. A Triassic plesiosaurian skeleton and bone histology inform on evolution of a unique body plan. *Science Advances*, 3(12), e1701144.
- Wintrich, T., Scaal, M. and Sander, P. M. 2017b. Foramina in plesiosaur cervical centra indicate a specialized vascular system. *Fossil Record*, 20(2), pp. 279-290.
- Witmer, L. M. 1995. The extant phylogenetic bracket and the importance of reconstructing soft tissues in fossils. In: Thomason, J. J. (eds.) *Functional Morphology in Vertebrate Paleontology*. Cambridge University Press, New York, 19-33 pp.
- Zammit, M., Daniels, C. B. and Kear, B. P. 2008. Elasmosaur (Reptilia: Sauropterygia) neck flexibility: implications for feeding strategies. *Comparative Biochemistry and Physiology Part A: Molecular & Integrative Physiology*, 150(2), pp. 124-30.
- Zarnik, B. 1925. K etologiji plesiosaurija, sa primosima mehanici kralježnice u recentnih sauropsida. *Glasnik Nauč. Casopis Prirod. Društvo*, 38(39), pp. 424-479.
- Zweers, G. A., Vanden Berge, J. C. and Koppendraier, R. 1987. Avian cranio-cervical systems. Part I: Anatomy of the cervical column in the chicken (*Gallus gallus* L.). *Acta Morphologica Neerlando-Scandinavica*, 25(3), pp. 131-155.